NONLINEAR SYSTEM IDENTIFICATION AND NONLINEAR EXPERIMENTAL MODAL ANALYSIS BY USING RESPONSE CONTROLLED STEPPED SINE TESTING

A THESIS SUBMITTED TO
THE GRADUATE SCHOOL OF NATURAL AND APPLIED SCIENCES
OF
MIDDLE EAST TECHNICAL UNIVERSITY

BY

TAYLAN KARAAĞAÇLI

IN PARTIAL FULFILLMENT OF THE REQUIREMENTS
FOR
THE DEGREE OF DOCTOR OF PHILOSOPHY
IN
MECHANICAL ENGINEERING

DECEMBER 2020

Approval of the thesis:

NONLINEAR SYSTEM IDENTIFICATION AND NONLINEAR EXPERIMENTAL MODAL ANALYSIS BY USING RESPONSE CONTROLLED STEPPED SINE TESTING

submitted by **TAYLAN KARAAĞAÇLI** in partial fulfillment of the requirements for the degree of **Doctor of Philosophy** i**n Mechanical Engineering, Middle East Technical University** by,

Prof. Dr. Halil Kalıpçılar
Dean, Graduate School of **Natural and Applied Sciences** _____

Prof. Dr. M. A. Sahir Arıkan
Head of the Department, **Mechanical Engineering** _____

Prof. Dr. H. Nevzat Özgüven
Supervisor, **Mechanical Engineering Dept., METU** _____

Examining Committee Members:

Assoc. Prof. Dr. M. Bülent Özer
Mechanical Engineering Dept., METU _____

Prof. Dr. H. Nevzat Özgüven
Mechanical Engineering Dept., METU _____

Assoc. Prof. Dr. Melin Şahin
Aerospace Engineering Dept., METU _____

Prof. Dr. Erhan Budak
Faculty of Eng. And Natural Sciences, Sabancı University _____

Prof. Dr. Kenan Yüce Şanlıtürk
Mechanical Engineering Dept., ITU _____

Date: 24.12.2020

I hereby declare that all information in this document has been obtained and presented in accordance with academic rules and ethical conduct. I also declare that, as required by these rules and conduct, I have fully cited and referenced all material and results that are not original to this work.

Name, Last name: Taylan KARAAĞAÇLI

Signature:

ABSTRACT

NONLINEAR SYSTEM IDENTIFICATION AND NONLINEAR EXPERIMENTAL MODAL ANALYSIS BY USING RESPONSE CONTROLLED STEPPED SINE TESTING

Karaağaçlı, Taylan
Doctor of Philosophy, Mechanical Engineering
Supervisor: Prof. Dr. H. Nevzat Özgüven

December 2020, 226 pages

In this work, two novel nonlinear system identification methods are proposed in both the modal and spatial domains, respectively, based on response-controlled stepped-sine testing (RCT) where the displacement amplitude of the excitation point is kept constant throughout the frequency sweep.

The proposed nonlinear modal identification method, which is also a nonlinear experimental modal analysis technique, applies to systems with several nonlinearities at different (and even unknown) locations (e.g. joint nonlinearities) and/or with continuously distributed (geometrical) nonlinearities, provided that no internal resonance occurs. This method identifies nonlinear modal parameters as functions of modal amplitude by applying standard linear modal analysis techniques to measured frequency response functions (FRFs) which come out in quasi-linear form by RCT. In the case of multiple sensors, nonlinear normal modes can be determined from the identified modal constants. Furthermore, near-resonant constant-force FRFs can be calculated from the identified modal parameters or can be directly extracted from the experiment by using a novel concept proposed in this

work, namely the harmonic force surface (HFS). The key feature of the HFS is its ability to accurately extract the unstable branches and the turning points of constant-force FRFs, which makes it possible to extract the backbone curves of strongly nonlinear systems as well. Coming to the proposed nonlinear spatial identification method, it extends the classical describing function method to make the identification of localized nonlinearities nonparametric and to determine the frequency dependence of nonlinearity.

The validation of the proposed methods is demonstrated with various numerical and experimental case studies including complex engineering systems such as a real missile structure with considerable damping nonlinearity due to bolted joints and a real control fin actuation mechanism with complex and strong nonlinearity due to backlash and friction.

Keywords: Nonlinear Experimental Modal Analysis, Nonlinear System Identification, Response Controlled Stepped Sine Testing, Harmonic Force Surface, Nonlinear Mode, Describing Surface Method

ÖZ

CEVAP KONTROLLÜ KADEMELİ SİNÜS TESTİ KULLANARAK DOĞRUSAL OLMAYAN SİSTEM TANILAMA VE DOĞRUSAL OLMAYAN DENEYSEL MODAL ANALİZ

Karaağaçlı, Taylan
Doktora, Makina Mühendisliği
Tez Yöneticisi: Prof. Dr. H. Nevzat Özgüven

Aralık 2020, 226 sayfa

Bu çalışmada, sırasıyla modal ve uzaysal alanlarda iki yeni doğrusal olmayan sistem tanılama yöntemi önerilmiştir. Her iki yöntem, frekans taraması boyunca tahrik noktasının yer değiştirme genliğinin sabit tutulduğu cevap kontrollü kademeli sinüs tarama testine (CKT) dayanmaktadır.

Önerilen modal tanılama yöntemi, ki aynı zamanda doğrusal olmayan bir modal analiz tekniğidir, içsel rezonans olmaması koşuluyla, faklı (ve hatta bilinmeyen) noktalara dağılmış çok sayıda doğrusalsızlık içeren (örn. cıvata bağlantıları) sistemlere ve doğrusalsızlığın sürekli (geometrik) olduğu sistemlere uygulanabilir. Bu yöntem, CKT yardımıyla doğrusal formda ölçülen frekans tepki fonksiyonlarına (FTF) standart doğrusal modal analiz yöntemlerini uygulayarak, doğrusal olmayan modal parametreleri modal genliğin fonkisyonu şeklinde tanılamaktadır. Çoklu duyarga (sensör) kullanılması durumunda, doğrusal olmayan normal modlar, tanılanan modal sabitlerden deneysel olarak elde edilebilmektedir. Dahası, rezonans civarındaki sabit-kuvvet FTF'leri, tanılanan modal parametrelerden hesaplanabilmekte veya bu çalışmada önerilen yeni bir kavram olan harmonik kuvvet yüzeyi (HKY) ile doğrudan deneysel yolla tespit edilebilmektedir. HKY'nin

öne çıkan özelliği, sabit kuvvet FTF'lerindeki karasız bölgeleri ve dönüş noktalarını hassas biçimde saptaması ve bu sayede yüksek doğrusalsızlık içeren sistemlerin bile omurga eğrilerini çıkarabilmesidir. Önerilerin doğrusal olmayan uzaysal tanılama yöntemi ise, klasik tanımlayıcı fonkisyon metodunu daha da geliştirerek yerel doğrusalsızlıkların tanılanmasını parametrik olmayacak şekilde ve frekansa bağlılığı hesaba katacak şekilde yapabilmeyi sağlamaktadır.

Önerilen yöntemlerin doğrulaması, cıvata bağlantılarından ötürü önemli ölçüde sönüm doğrusalsızlığı içeren gerçek bir füze sistemi ve boşluk ve sürtünmelerden ötürü karmaşık ve yüksek doğrusalsızlık içeren gerçek bir kontrol kanatçığı gibi kompleks mühendislik sistemlerinin dahil olduğu deneysel uygalamalar ve nümerik uygulamalarla yapılmıştır.

Anahtar Kelimeler: Doğrusal Olmayan Deneysel Modal Analiz, Doğrusal Olmayan Sistem Tanılama, Cevap Kontrollü Kademeli Sinüs Testi, Harmonik Kuvvet Yüzeyi, Doğrusal Olmayan Mod, Tanımlayıcı Yüzey Metodu

To My Lovely Wife Seval and My Precious Daughter İpek

ACKNOWLEDGMENTS

I would like to express my deepest gratitude to Prof. Dr. H. Nevzat Özgüven, for his enormous support, patience, continuous enthusiasm, and excellent supervision throughout this thesis work. Without his inspiring advice and his outstanding scientific work previously published, this thesis work would not have been possible at all. I hope that this is not the end but a brand new beginning for a long-lasting collaboration in many future projects.

I would like to express special thanks to Dr. Ümit Ceyhan for his continuous moral and technical support throughout this thesis work. He provided me the opportunity to build up all the experimental setups studied in this thesis and gave me unlimited access to the testing capabilities of TÜBİTAK-SAGE.

No words are sufficient to express my gratitude to my dear mom Ceyhan who made me the man who I am today, and to my lovely grandmom Mevlüde who has always taken care of me more than I.

I am especially grateful to my lovely wife Seval for her love, care, patience, and enormous support. She was the only one who believed me and who encouraged me to start from scratch. Her genuine curiosity in my work was amazing. She has always asked about the developments and has closely shared all my defeats and glories throughout this thesis work. Without her, this thesis would have never been completed. Last but not least, I thank my precious daughter İpek for her love and wonderful smile that has been my fuel at times I felt exhausted.

TABLE OF CONTENTS

LIST OF TABLES

TABLES

LIST OF FIGURES

FIGURES

LIST OF ABBREVIATIONS

ABBREVIATIONS

CBC	Control based continuation
DFM	Describing function method
DSM	Describing surface method
ECL	Ecole centrale de Lyon
EMD	Empirical mode decomposition
FNSI	Frequency domain nonlinear subspace identification
FRF	Frequency response function
HBM	Harmonic balance method
HFS	Harmonic force surface
HVD	Hilbert vibration decomposition
INTL	Identification of nonlinearity by time series based linearity plots
LCO	Limit cycle oscillation
MDOF	Multi degree of freedom
NARMAX	Nonlinear autoregressive moving average with exogenous input
NLRDM	Nonlinear resonant decay method
NNM	Nonlinear normal mode
PLL	Phase locked loop
RCT	Response controlled stepped sine testing
RFS	Restoring force surface
SDOF	Single degree of freedom
TNSI	Time domain nonlinear subspace identification

LIST OF SYMBOLS

SYMBOLS

$\bar{A}$	Modal constant
$[C]$	Viscous damping matrix
c	Viscous damping
c_f	Coulomb friction
[D]	Structural damping matrix
$\{f\}$	External excitation force vector
$\{F\}$	External excitation force amplitude vector
F	External excitation force amplitude
$\{F_N\},\{G\}$	Complex nonlinear internal force amplitude vector
[H]	Receptance matrix
h	Harmonic multiplier
$\bar{h}$	Modal structural damping
i	Unit imaginary number
$[K]$	Stiffness matrix
k	Stiffness
k^*	Cubic stiffness
$\bar{k}$	Modal stiffness
$[M]$	Mass matrix
m	Mass

$\bar{m}$	Modal mass
$\{N\}$	Nonlinear internal force vector
q	Modal amplitude
t	Time
$\{x\}$	Displacement vector
$\{\dot{x}\}$	Velocity vector
$\{\ddot{x}\}$	Acceleration vector
$\{X\}$	Complex displacement amplitude vector
$[Z]$	Dynamic stiffness matrix
α	Receptance
$[\Delta]$	Complex nonlinearity matrix
$[\Delta]_{re}$	Real part of the nonlinearity matrix
$[\Delta]_{im}$	Imaginary part of the nonlinearity matrix
$\bar{\eta}$	Modal structural damping ratio
$\bar{\xi}$	Modal viscous damping ratio
υ	Describing function of nonlinearity
$\{\bar{\phi}\}$	Mass normalized nonlinear normal mode vector
$\{\bar{\psi}\}$	Nonlinear normal mode vector
ω	Excitation frequency
$\bar{\omega}$	Natural frequency
∂	Partial derivative operator

Subscripts

h	Harmonic number
j, k, p, r, s	Coordinate
r	Mode number

Superscripts

k	Displacement amplitude level
L	Linear
NL	Nonlinear

CHAPTER 1

INTRODUCTION

1.1 Motivation

In the 20th century, the *flutter* problem in the aircraft industry and the *chatter* problem in the machine tool industry acted as a catalyst in the commercialization of sensor and data acquisition technologies, which started the modern era of experimental modal analysis in the mid-1960s [1]. In the 21st century, these two self-excited vibration problems are still hot research topics investigated by various research groups in different countries including Turkey, with a shift of emphasis toward structural nonlinearities.

TÜBİTAK-SAGE (shortly SAGE) is the leading institution of Turkey in the aeroelastic qualification of military aircraft (e.g. the F-16 fighter aircraft) with external stores and is heavily involved in the aeroelastic research and the problem of flutter in connection with the Turkish Air Force, which constitutes the major motivation of this thesis study.

Today, the aeroelastic qualification of aircraft is a well-established procedure that consists of four main stages requiring considerable expertise and investment: 1) Ground Vibration Testing, 2) Finite Element Model Updating 3) Aeroelastic Analysis, and 4) Flight Flutter Testing.

The classical aeroelastic flutter is defined as a catastrophically divergent structural oscillation at a definite frequency where energy is extracted from the airstream by the oscillation itself. Another important aeroelastic problem frequently encountered in military aircraft is called *Limit Cycle Oscillation* (LCO). The term LCO has been widely used since the mid-1970s [2] to describe the sustained, periodic but not

catastrophically divergent oscillation of military aircraft with external store configurations within the flight envelope.

The F-16 fighter aircraft (Figure 1-1), which is widely used by many countries around the world including Turkey, is well known for its persistent LCO problem [2-3]. LCO may adversely affect ride comfort, control quality as well as weapon aiming. Furthermore, it may also lead to the vibration fatigue of aircraft components. Consequently, LCO is a serious problem that must be investigated thoroughly during the aeroelastic qualification campaign of military aircraft with external stores.

Figure 1-1. The F-16 aircraft with external stores

Norton's work [4] and SAGE's own experience showed that the LCO behavior of a fighter aircraft is very sensitive to external store configuration. In the case of the F-16 aircraft, there are nine external store stations: two on the wingtips, six underwing, and one on the centerline, which leads to a tremendous number of sub-configurations (due to possible ejections) for a specific take-off configuration. Accordingly, the LCO clearance of the F-16 aircraft for a specific take-off

configuration usually requires the careful investigation of hundreds of sub-configurations, which makes it practically impossible to carry out flight flutter testing for all possible configurations. Consequently, the development of realistic and accurate aeroelastic analysis tools becomes a matter of vital importance.

LCO of the F-16 aircraft is a highly nonlinear phenomenon both due to nonlinear aerodynamics and structural nonlinearities. Although the computational prediction of the F-16 LCO has been the subject of an extensive body of research covering the last three decades (e.g. [5-9]), none of them has proved to be successful in accurately predicting the LCO onset velocity and LCO amplitudes measured by flight testing. Most of the studies were focusing on modeling nonlinear aerodynamics with high fidelity computational fluid dynamics tools by overlooking structural nonlinearities. Among them, the work of Dowell et al. [9], which uses a Navier-Stokes solver, came into prominence to produce F-16 LCO solutions being very similar to what is observed in flight-flutter testing. In that work, the structural model of the aircraft was a linear modal model, and the authors concluded by suggesting that modeling structural nonlinearities may improve computational results. In the same year, Chen et al. [10] proposed a time-domain aeroelastic solution with nonlinear damping, which showed that nonlinear structural damping is a viable mechanism to suppress flutter and produce LCO. Finally, two very recent studies [11-12] showed that nonlinear structural damping plays a crucial role in the accurate prediction of the LCO onset velocity and LCO amplitudes of the F-16 aircraft. Denegri et al. [11] proposed several different nonlinear modal viscous damping profiles (parabolic, cubic, etc.) defined as functions of the response amplitude of a selected reference point and compared their computational results for a specific F-16 configuration. Later, Chen et al. [12] proposed a nonlinear structural damping model based on a simple Maxwell viscoelastic formula. In that model, a single parameter, γ, is tuned in a manner to match the computational LCO results with those of flight test data. By using γ values tuned for several selected aircraft/store configurations, Chen et al. [12] developed an "estimator" formula which is closely related to the LCO frequency and which can be used for the

nonlinear structural damping model of untested aircraft/store configurations. Although the application of the method has given promising results for a specific configuration, it requires further validation on a sufficiently large number of aircraft/store configurations, which is a long-term research issue.

As discussed above, the methods proposed in [11-12] are essentially empirical approaches that are based on tuning the parameters of some theoretical nonlinear structural damping model. This issue naturally results from the lack of practical techniques for directly measuring nonlinear structural damping, which brings us to the major motivation of this thesis work.

Over the last two decades, a vast and rich literature has accumulated about nonlinear system identification in structural dynamics. Despite the significant progress in the state-of-the-art, the identification of structural nonlinearities in complex engineering systems such as aircraft with external stores or missile systems is still a difficult problem if not impossible. Any commercial modal testing equipment is restricted to linear system identification. Furthermore, some recently developed promising experimental modal analysis techniques for nonlinear structures require the design of sophisticated control algorithms which have not been commercialized yet and the use of which is currently confined to few research laboratories. More importantly, these techniques were not validated in complex engineering structures. All these issues are discussed in detail in Sections 1.2 and 1.4.

Following the discussion given above, the major motivation of this thesis work is to develop *innovative* nonlinear system identification methodologies for complex engineering structures based on currently available industrial modal testing equipment.

1.2 Literature Survey

With the increasing interest of academia in the field of nonlinear system identification in structural dynamics, a vast and rich literature has accumulated in this field over the last two decades. In this section, the most important developments in the state-of-the-art are overviewed by emphasizing well-established powerful techniques as well as recently developed promising approaches. An interested reader may refer to the review papers of Kerschen et al. [13] and Noel and Kerschen [14] to gain a more profound insight into the state-of-the-art.

Even though different classifications can be employed, most of the nonlinear system identification techniques developed so far can be classified under two main categories: Spatial and modal approaches. The first part of this section is dedicated to an overview of spatial methods that accomplish nonlinear system identification in physical coordinates. Modal methods, which provide a more successful framework compared to spatial methods in handling multiple discrete (e.g. joint nonlinearities) and continuously distributed (geometrical) nonlinearities, are thoroughly discussed in the second part of this section.

It is important to note that this thesis work proposes two versatile nonlinear system identification techniques in both the spatial and modal categories as discussed in Section 1.3.

1.2.1 Nonlinear System Identification in the Spatial Domain

One of the most widely used nonlinear system identification methodologies in structural dynamics is the well-known *Restoring Force Surface* (RFS) method proposed by Masri and Caughey [15]. A similar approach named force-state mapping was also independently developed by Crawley and Aubert [16]. The popularity of the RFS method stems from its simplicity and its nonparametric nature. This time-domain technique identifies the internal restoring force of a

single-degree-of-freedom (SDOF) nonlinear system as a nonparametric function of displacement and velocity amplitudes by just processing measured acceleration data. Although the RFS method was theoretically extended to multi-degree-of-freedom (MDOF) systems [17], its application to general nonlinear MDOF systems showed to be difficult and time-consuming [18]. Early applications of the RFS approach were the characterization and identification of automobile shock absorbers [19-21]. More recent applications focusing on the identification of nonlinear stiffness mechanisms include [22-26]. There are also several important studies investigating complex damping nonlinearities. For example, an automotive damper is identified by the RFS in [27]. In that work, the inability of the RFS method to capture the frequency dependence of nonlinear damping is reported as an important drawback. In another interesting study [28], the hysteretic behavior of the frictional contact support of a cantilever beam was identified by the force-state mapping approach. Due to its simplicity and efficiency, the RFS method is also preferred for the qualitative identification of nonlinearity in complex MDOF engineering structures. For example, the stiffness and damping nonlinearities at the mounting interface of a payload in an F-16 fighter aircraft were recently characterized by the RFS method in [29].

Another versatile time-domain approach is the *Nonlinear Auto-Regressive Moving Average with Exogenous Input* (NARMAX) method proposed by Leontaritis and Billings [30-31]. This method constructs a black-box model that expresses the future outputs of a system as functions of the past values of its inputs, outputs, and noise, where input and output variables are usually physical quantities like force and displacement response. Although the NARMAX made important progress by several improving works in the late 1980s [32-36] and its structure compatible with the neural network architecture has good potential to cope with challenging problems including chaos and bifurcations, the method could not achieve widespread use in the upcoming years. One reason for the infrequent use of the NARMAX may be its black-box nature which does not give insight into the physics of a system. Another reason stated in [14] is that as the number of system's

degrees-of-freedom to be considered increases, the number of parameters to be identified grows exponentially even in the case of systems with reasonable DOFs. Several recent applications of the NARMAX can be found in [37-40].

The third technique worth mentioning is the Hilbert transform, which can be applied in both the frequency and time domains to identify nonlinear structures. Early published work focused primarily on the frequency-domain Hilbert transform [41, 42], which diagnoses nonlinearity based on the deviation of the original measured frequency response function (FRF) from its Hilbert transform. Since FRFs of linear systems are invariant under the Hilbert transform, a significant deviation is assessed to be an indication of considerable structural nonlinearity. An important practical problem of the method is that the Hilbert integration requires FRF data to be measured over all frequencies from zero to infinity, which is practically impossible and which results in truncation errors. Although corrective formulas have been proposed in [41] to solve this issue, they are restricted to lightly damped systems. In the mid-1990s, the application of the Hilbert transform in the time domain to identify nonlinear SDOF systems was first proposed by Feldman based on free-vibration data [43] and then based on forced vibration data [44]. These approaches combine the time signal and its Hilbert transform to build up an analytic signal which is processed to determine backbone and damping curves, in other words, variations of the instantaneous frequency and damping of nonlinear systems with respect to the vibration amplitude. However, an important limitation of the methods proposed in [43, 44] is that they are only applicable to monocomponent signals. In the early 2000s, two new techniques similar to each other in spirit and capable of decomposing multicomponent signals into elemental signals have been developed, namely the *Empirical Mode Decomposition* (EMD) [45] and the *Hilbert Vibration Decomposition* (HVD) [46]. Some studies investigating the implementation of the EMD in nonlinear structural dynamics are [47, 48]. The HVD also enjoyed some progress in recent years on the identification of simple nonlinear systems [49], but it has not yet been applied to large-scale structures. Although these techniques gave some thrust to the ongoing research

about the application of the Hilbert transform in nonlinear system identification, they still require exhaustive data filtering and smoothing effort to obtain the backbone and damping curves of nonlinear systems at an acceptable accuracy.

Wavelet transform [50] is another well-established technique, which provides a convenient framework especially for interpreting higher harmonic components in vibration responses of nonlinear systems. By virtue of the kernels, i.e. basis functions, which decay quickly, the wavelet transform is capable of capturing non-stationary effects in a time signal, contrary to the classical Fourier transform. This key feature is very crucial to detect and characterize structural nonlinearities. Some interesting application examples of the wavelet transform in nonlinear system identification can be found in [51-52].

In the new millennium, a promising parametric nonlinear system identification technique in the frequency domain, namely the *Describing Function Method* (DFM), emerged as an important contribution to the nonlinear structural dynamicist's toolbox. The initial motivation of the DFM, which dates back to the early 1990s, was to calculate harmonic vibration responses of nonlinear MDOF systems [53]. In essence, the DFM is mathematically equivalent to the classical *Harmonic Balance Method* (HBM). The major difference between both techniques relies on the interpretation of nonlinear internal forces. The HBM expresses nonlinear internal forces as a single force vector, whereas in the DFM they are written as a multiplication of the displacement vector with the so-called *nonlinearity matrix* which has an important physical meaning. The real and imaginary parts of this matrix essentially correspond to the equivalent nonlinear stiffness and damping matrices at a given response level, respectively. The concept of using the nonlinearity matrix approach in nonlinear system identification was first suggested by Özer and Özgüven [54], and a method was developed to identify the type and parametric values of a nonlinear element between the ground and a single coordinate in an MDOF system, which is later extended to identify a single nonlinear element between any two coordinates of the system [55]. It was further improved by Aykan and Özgüven [56] by using incomplete FRF data, which makes

the method applicable to large systems with localized nonlinearity. The proposed method basically takes the inverse of measured constant-force FRF based on the SDOF assumption to determine the describing function of a localized nonlinearity. In this current thesis work, by virtue of a new technique called the *Describing Surface Method* (DSM), the DFM is further improved in a manner to identify localized nonlinearities nonparametrically and to quantify the frequency dependence of nonlinearity.

In addition to the previously mentioned well-established techniques, there are also some recently proposed promising identification methods worth mentioning. Two interesting examples are the *Time-Domain* and the *Frequency-Domain Nonlinear Subspace Identification* methods abbreviated as TNSI [57] and FNSI [58], respectively. These approaches treat nonlinear internal forces as external feedback forces applied to the underlying linear system. Nonlinear structures are excited with periodic random input and the coefficients of nonlinearities are determined based on a state-space representation of the equation of motion. The TNSI method, which was originally proposed in the control literature [59], was implemented in nonlinear structural dynamics by Marchesiello and Garibaldi in 2008 [57]. A few years later, its frequency-domain counterpart FNSI was proposed by Noel and Kerschen in [58]. Although both techniques were successfully applied to identify the strong nonlinearity at the mounting interface of an inertia wheel system in a spacecraft structure in [60], the number of applications up to today remained rather scarce. Among possible reasons for the infrequent use of these methods may be the complexity of their algorithms and the considerable data processing effort required to avoid ill-conditioning especially in the case of large structures with many degrees-of-freedom.

This section is concluded by referring to two very recent publications that propose two new frequency domain identification techniques specifically focusing on the frequency dependence of nonlinearity [61, 62]. The method proposed in [61] achieves the parametric identification of nonlinear rubber rings by using constant-response FRFs regenerated from a series of open-loop, constant-frequency, and

variable-excitation sinusoidal tests. The most important limitation of that technique is that it does not apply to strongly nonlinear systems which exhibit the *jump phenomenon* in their frequency responses. The other technique proposed in [62] relies on nonlinear frequency responses measured during open-loop stepped-sine testing and yields the mathematical model of a nonlinear structural element as functions of frequency and response amplitude by using the equivalent dynamic stiffness concept. The method is validated on a metal mesh damper which exhibits frequency-dependent nonlinear damping. Two important advantages of this method are its nonparametric merit and its applicability to strongly nonlinear systems. The method is nonparametric in the sense that it does not demand an a priori form of nonlinearity, but it still requires polynomial surface fit which may be an important issue especially in the case of complex nonlinearities. Furthermore, although the method can simulate the jump phenomenon in harmonic analysis, it is not capable of capturing the actual cause of the jump, i.e. the unstable branches of nonlinear frequency responses.

1.2.2 Nonlinear System Identification in the Modal Domain

The well-established and powerful spatial nonlinear system identification methods overviewed in the previous section can also be called the *nonmodal* methods. These techniques proved to be successful in the identification of simple structures with localized nonlinearity, either weak or strong. However, none of them could achieve widespread use in the case of general MDOF structures mostly due to the mathematical complexity and the computational burden.

The identification of multiple nonlinearities coexisting at different locations is still a challenge, especially if these nonlinearities are strong. There are still difficult problems such as joint nonlinearities (multiple and discrete) or geometrical (i.e. continuously distributed) nonlinearities due to large amplitude oscillations. Since there are generally several joints in engineering structures, it would be very difficult, if not impossible, to identify each joint nonlinearity separately. On the

other hand, in the case of geometrical nonlinearities, the concept of discrete nonlinear elements cannot be used. Consequently, the right identification strategy in these complex problems is to quantify the resultant effect of all nonlinearities, instead of focusing on individual nonlinear elements. Fortunately, the concept of nonlinear normal modes (NNM), which dates back to Rosenberg [63,64] (the 1960s), provides a rigorous theoretical framework to study the overall effect of several nonlinearities in a structure. Analogous to linear normal modes, Rosenberg defined an NNM as a *vibration in unison* of the system, i.e. synchronous periodic motion. Later, in 1979, Szemplinska-Stupnicka proposed a novel technique called the *single nonlinear mode method* [65] to study the effect of nonlinearities on the resonant vibrations of MDOF systems. The method showed that if the modes are well separated and no pronounced modal coupling occurs in the energy range of interest, near-resonant frequency responses of a nonlinear system can be represented accurately by a single NNM and its corresponding natural frequency which are functions of the modal amplitude. This pioneering work of Szemplinska-Stupnicka led to the development of various nonlinear modal identification techniques. For example, in the early 1990s, Setio et al. [66] proposed to extract nonlinear modal parameters by minimizing the error function between frequency responses measured by force-controlled sine-sweep testing and analytical frequency responses represented by the superposition of NNMs, which gives satisfactory results if the modes are well separated and no internal resonance occurs. The method was validated on a real cantilever beam supported at its free end by a string that creates a cubic stiffness effect. Another nonlinear modal identification method from the early 1990s is the one proposed by Lin [67]. In this method, two frequency points that correspond to the same response amplitude on either side of the resonance peak of a measured constant-force FRF are used to identify nonlinear modal parameters corresponding to that response amplitude. Different frequency pairs are processed successively to determine nonlinear modal parameters as functions of the response amplitude. This nonlinear modal analysis method is then combined with describing function in order to determine the real

and imaginary parts of amplitude-dependent nonlinear complex stiffness. In his PhD thesis, Lin introduced also the stiffness error matrix due to nonlinearity concept to find the location and the describing function coefficients of a localized nonlinearity in nonlinear structures. Lin applied these techniques to FRF data generated by analog circuits simulating SDOF nonlinear systems and to simple MDOF structures with local nonlinearity. Later, in the early 2000s, Gibert [68] proposed a modal identification algorithm based on the minimization of the error function between measured and analytical frequency responses similar to Setio's method [66] and showed that the superposition of NNMs gives satisfactory results for the synthesis of frequency responses of the Ecole-Centrale-de-Lyon (ECL) benchmark [69] over the frequency range including the first three elastic modes.

The early 2000s witnessed other promising nonlinear modal identification strategies. For example, Göge et al. [70] proposed a novel method called the *Identification of Nonlinearity by Time-Series-Based Linearity* plots (INTL) which is based on the application of the RFS method [15] in the modal space. The test strategy used in the INTL approach is the normal mode force appropriation which is also known as phase resonance testing, where the nonlinear system is harmonically excited at its resonance frequency using an excitation force pattern appropriated to a single mode of interest. Nonlinear modal stiffness and damping parameters can then be determined by curve fitting to the measured nonlinear restoring force in the modal space. The application of the method was demonstrated on a real space structure. Platten et al. [71] also proposed another RFS-based technique called the *Nonlinear Resonant Decay Method* (NLRDM). This method differs from the INTL approach in that it can take also the cross-coupling of nonlinear modes into account by virtue of its excitation strategy which consists of a burst sine at the resonance frequency of the mode of interest. The NLRDM technique was validated on a wing-like structure with hardening stiffness at the pylon connections [72] and on a real transport aircraft [73].

In 2008 Arslan and Özgüven [74] proposed a nonlinear modal identification method for structures that exhibit local nonlinearity between the excitation point

and the ground based on the quasi-linearization of measured FRFs by keeping the displacement amplitude constant. They identified nonlinear modal parameters of a beam structure with a local nonlinearity as functions of the response amplitude in [75]. In 2010 Link et al. [76] applied constant-acceleration base excitation testing to extract modal parameters of a weakly-nonlinear satellite structure as a function of the acceleration-load level from measured transmissibility data. In 2011 Carrella and Ewins published an application paper [77] of Lin's method [67] and reported that this method does not give acceptable accuracy especially in the case of strongly nonlinear structures because of the missing frequency points of the measured FRFs due to the jump phenomenon and can only provide a qualitative assessment of nonlinearity.

The major difference between the new generation techniques developed in the last decade and the afore-mentioned ones is that in the new generation algorithms, the computational effort is minimized at the cost of experimental effort. Most of the recently developed nonlinear modal identification methods are inspired by the phase resonance testing approach and they focus on the direct parameter estimation, which reduces the computational effort considerably. For example, in the method proposed by Peeters et al. [78] in 2011, the phase lag quadrature criterion was generalized to nonlinear structures to locate a single NNM during the experiment. Once the NNM appropriation is achieved, the frequency-energy dependence of that nonlinear mode can be determined by applying time-frequency analysis to the free decay response data. The proposed methodology was demonstrated on numerical examples [78] and a real nonlinear beam structure [79]. However, an important drawback of this early version of the nonlinear phase resonance testing was the manual tuning process of the phase lag between response and excitation. By virtue of the recently proposed control algorithms [80, 81], the tuning of the phase lag was automated throughout the entire NNM backbone curve. The control technique proposed by Peter and Leine in [80] is called the *Phase-Locked-Loop* (PLL) control which provides a robust and fast way of tracing out the backbone curves as well as stabilizing the unstable branches of near-resonant

frequency response curves. The PLL control strategy was validated on a benchmark beam structure in [80] and a circular plate, a Chinese gong, and a piezoelectric cantilever beam in [82]. In accordance with the single nonlinear mode assumption [65], the synthesis of the near-resonant frequency response curve of a nonlinear cantilever beam from a single NNM measured by the PLL technique was also demonstrated in [83]. Another interesting application of the PLL technique is the identification of the nonlinear dissipation at a bolted joint [84]. The control approach proposed by Renson et al. in [81], called the *Control-Based Continuation* (CBC), is similar to the PLL method, and also enables the backbone curve identification of nonlinear structures. The application of the CBC method was demonstrated on a real SDOF oscillator in [81].

All of the nonlinear modal identification techniques mentioned above have their advantages and limitations. The early identification methods [66-68] which rely on simple frequency response data measured by standard force-controlled sine sweep testing involve considerable computational cost. On the other hand, the INLT method and the NLRDM require considerable effort both in computation and experiment, and they apply to weakly nonlinear systems. In the nonlinear phase resonance testing method [78], the computational effort is considerably reduced, but the manual tuning of the phase lag between response and excitation requires careful and time-consuming experimentation. Although recently developed PLL and CBC control strategies automated the tuning of the phase lag as well as the determination of the backbone curve, they cannot make use of the available standard equipment. Furthermore, although the experimental extraction of natural frequencies and deflection shapes at resonance is straightforward in the methods based on the phase resonance testing approach, the determination of nonlinear modal damping and mass normalized NNMs is still an important issue.

1.3 Objective and Scope of the Thesis

From the literature survey, it can be deduced that no general technique applicable to a wide range of nonlinear MDOF systems has been developed so far, and consequently, nonlinear system identification in structural dynamics has retained its toolbox philosophy up to today. Spatial-domain methods, which accomplish nonlinear system identification in physical coordinates, are restricted, in practice, to the identification of local nonlinearities. Although modal-domain approaches provide a more successful framework compared to spatial methods in handling multiple discrete (e.g. joint nonlinearities) and continuously distributed (geometrical) nonlinearities, well-established modal methods require considerable experimental and computational effort, and recently proposed promising modal-domain methods necessitate the design of sophisticated control algorithms, have difficulties in identifying nonlinear modal damping as well as mass normalized NNMs and could not be validated on real complex engineering structures yet.

The objective of this thesis work is to develop a general nonlinear system identification framework that can be applied to a wide range of nonlinear structures including strongly nonlinear real engineering systems by *innovatively* using currently available industrial modal testing equipment. To achieve this objective, two novel nonlinear system identification methods are proposed in both the modal and spatial domains, respectively. These two methods are essentially based on the *Response-Controlled Stepped-Sine Testing* (RCT) strategy where the *displacement amplitude* of the driving point is kept constant throughout the frequency sweep. At one end, the proposed nonlinear modal identification approach, which is also a nonlinear experimental modal analysis technique, provides a very useful framework to quantify the overall effect of multiple discrete nonlinearities at several different (and even unknown) locations and/or continuously distributed (geometrical) nonlinearities, which cannot be achieved by the proposed spatial approach. On the other hand, the proposed nonlinear spatial identification approach may be very useful, for example, if individually identified nonlinear elements have

to be integrated into large finite element models where the representation of nonlinearity requires being in physical coordinates instead of modal coordinates and/or the frequency dependence of nonlinearity has to be considered. Consequently, both methods, which compensate limitations of each other, have the potential to build up a general system identification framework that can be applied to a wide range of nonlinear structures including strongly nonlinear real engineering systems. In the context of this thesis, the strong nonlinearity terminology is used to refer to nonlinear systems with overhanging unstable branches in frequency response curves, which result in the jump phenomenon in standard constant-force stepped-sine testing. This does not necessarily imply a significant effect of higher harmonics, as illustrated in the numerical and experimental case studies. Within the scope of this thesis work, the effects of higher harmonics are assumed to be negligible.

The first method proposed in this thesis work is the *Experimental Modal Analysis with RCT* [85], which belongs to the category of nonlinear system identification in the modal domain. The method is based on the quasi-linearization of measured FRFs by keeping the displacement amplitude of the excitation point constant, which was proposed by Arslan and Özgüven in [74] and experimentally validated on a beam structure with a localized nonlinearity in [75]. In these studies, it is shown that nonlinear modal parameters can be extracted as functions of the displacement amplitude by applying standard linear modal analysis techniques to measured quasi-linear FRFs. However, the method proposed in [74] is restricted to simple structures that exhibit a single nonlinear element specifically localized between the excitation point and the ground and is not capable of identifying unstable frequency responses, backbone curves, and NNMs of nonlinear structures. In this thesis study, this method is extended to nonlinear MDOF systems which exhibit several nonlinearities at different (and even unknown) locations as well as to MDOF systems with continuously distributed (geometrical) nonlinearities, provided that modes are well separated and no internal resonance occurs. This extension is based on the single nonlinear mode assumption of Szemplinska-

Stupnicka [65], where the near-resonant frequency responses of a nonlinear system can be represented accurately by a single NNM and its corresponding natural frequency which are functions of a single modal amplitude. The extended method hypothesizes that if the modal amplitude is kept constant with the RCT strategy during modal testing, the measured FRFs of nonlinear MDOF systems come out in the quasi-linear form. In this thesis work, it is shown that in the case of a single point excitation, keeping the modal amplitude constant is equivalent to keeping the displacement amplitude of the excitation point constant. It is also shown that standard linear modal analysis tools can be used to extract all modal parameters as functions of the modal amplitude. The identified modal parameters can then be employed to synthesize near-resonant frequency response curves including unstable branches, if there is any, for various untested harmonic forcing scenarios. Furthermore, in the case of multiple sensors, NNMs can also be determined from the identified modal constants. Therefore, the contribution of the proposed method to the state-of-the-art is threefold. Firstly, it relies on standard controllers (available in commercial modal testing hardware and driven by commercial software) which makes it very attractive especially for industrial applications. Secondly, the identification of modal damping and of the mass normalized NNMs, which are necessary for the prediction of the frequency responses of untested harmonic forcing scenarios, is straightforward with the proposed method, by applying linear modal analysis methods available in commercial software packages to the measured constant-response FRFs of nonlinear structures. Finally, the proposed approach provides two different ways of determining near-resonant frequency response curves for untested constant-amplitude harmonic forcing scenarios; either computationally by using the nonlinear modal parameters identified during RCT, or experimentally by directly extracting isocurves of constant-amplitude forcing from the measured *Harmonic Force Surface* (HFS), a new concept proposed in this thesis. The HFS leads to constant-force frequency response curves with accurately measured turning points and unstable branches (if there are any), which makes it possible to identify the backbone curves of strongly nonlinear structures

experimentally. This feature of the HFS concept, which is an outcome of this thesis work, is studied in detail in [86].

Within the scope of this thesis work, the proposed nonlinear experimental modal analysis method is validated with various numerical and experimental case studies. Experimental case studies are as follows:

- A cantilever beam with a localized strong stiffening nonlinearity,
- A beam which exhibits continuously distributed strong geometrical nonlinearity due to large deformations,
- A real missile structure which exhibits considerable damping nonlinearity mostly due to several bolted joints on the structure,
- A control fin actuation mechanism which exhibits very complex and strong nonlinearity due to backlash and friction.

The second method proposed in this thesis work is the *Describing Surface Method (DSM)* [87], which belongs to the category of nonlinear system identification in the spatial domain. This method applies to structures with a single nonlinearity localized between the excitation point and the ground and it yields the describing surface of nonlinearity, real and imaginary parts of which correspond to the equivalent nonlinear stiffness and nonlinear damping of that nonlinearity. The harmonic response of a nonlinear system to any harmonic force, including any existing unstable branch, can then be calculated iteratively by using the describing surface representing the nonlinearity together with Newton's method and the arclength continuation algorithm. Similar to the nonlinear experimental modal analysis method mentioned above, the DSM also relies on the FRFs measured with the RCT strategy by using a standard data acquisition hardware and software (e.g. LMS SCADAS Mobile and LMS Test Lab.). Consequently, it can be easily used by practicing engineers. More importantly, the method determines nonlinearity as a function of not only the displacement amplitude but also the frequency, which is not addressed by many of the state-of-the-art techniques. Furthermore, the identification is purely nonparametric in the sense that it determines a describing

surface of nonlinearity which can be used as a look-up table without necessitating any surface fitting.

Within the scope of this thesis work, the DSM is validated with various numerical and experimental case studies. Experimental case studies are as follows:

- A cantilever beam with a localized strong stiffening nonlinearity,
- A dummy mass on elastomeric vibration isolators,
- A control fin actuation mechanism which exhibits very complex and strong nonlinearity due to backlash and friction.

1.4 Contribution of the Thesis

The important limitations of the state-of-the-art methods and the contributions of this thesis work to the literature are discussed to some extent in Sections 1.2 and 1.3, respectively. In order to fully inform the reader about these issues, this section is dedicated to a more comprehensive discussion of the novelties of this thesis work by making comparisons with the state-of-the-art techniques. Firstly, the contributions of this thesis work are summarized below:

- An experimental methodology based on RCT is proposed for the accurate identification of nonlinear modal parameters of strongly nonlinear MDOF systems and is successfully applied to real structures that exhibit several nonlinearities at different (and even unknown) locations and/or continuously distributed (geometrical) nonlinearities, which are challenging problems for the-state-of-the-art.
- The frequency responses of nonlinear MDOF systems including unstable branches, if there are any, for unmeasured forcing scenarios are accurately predicted from the identified nonlinear modal parameters by combining Newton's method with the arc-length continuation algorithm.
- It is proposed to determine mass normalized NNMs of nonlinear MDOF systems from the identified nonlinear modal constants and this method is

successfully applied on a geometrically nonlinear structure, which is a challenging problem for the state-of-the-art.

- A simple and accurate way of experimental identification of nonlinear modal damping ratio is proposed and demonstrated on several different structures including a real control fin actuation mechanism which exhibits very high and nonlinear damping, which is also a challenge for the state-of-the-art.
- A novel concept called *Harmonic Force Surface (HFS)* is proposed for the robust and accurate identification of unstable branches and turning points of constant-force FRFs as well as NNM backbone curves directly from the experiment.
- The proposed RCT technique and the HFS concept build up a self-validation framework.
- Contrary to the general preconception, it is shown that response-controlled sine testing is considerably fast compared to the classical force-controlled sine testing by virtue of the quasi-linearization which renders the test structure more predictable and so easily controllable.
- The *Describing Surface Method* (DSM) is proposed to extend the classical describing function method to make the identification of localized nonlinearities nonparametric and to determine the frequency dependence of nonlinearity.

The rest of this section is dedicated to a comparative discussion of the above contributions with the state-of-the-art.

An early example of nonlinear system identification techniques worth mentioning is the one proposed by Setio et al. [66] in the early 1990s as discussed in Section 1.2. Although Setio's method and the nonlinear modal identification method proposed in this thesis work both rely on the single nonlinear mode theory [65], they differ in the control strategy, which brings important advantages to the latter. Setio's iterative algorithm based on constat-force sine testing assumes no damping

nonlinearity and leads to a considerable computational cost in the case of SIMO testing, which restricts it to simple structures that exhibit local conservative nonlinearities. However, the modal identification technique proposed in this thesis work introduces a simple general framework that is capable of handling a wide range of nonlinear structures including real and complex engineering systems such as a real missile structure and a control fin actuation mechanism.

Another nonlinear modal identification method from the early 1990s is the one proposed by Lin [67]. This method allows processing only a single FRF at a time, which makes it a SISO method. So, it cannot identify the NNMs of nonlinear MDOF systems. Furthermore, it does not provide any numerical or experimental scheme for the determination of unstable branches and backbone curves of nonlinear systems. More importantly, it does not achieve an unacceptable accuracy in the identified modal parameters especially in the case of strongly nonlinear structures as reported by Carrella and Ewins [77], which limits the method to the qualitative assessment of nonlinearity.

As previously discussed in Section 1.2 and 1.3, the method proposed by Arslan and Özgüven [74] is restricted to simple structures that exhibit a single nonlinear element specifically localized between the excitation point and the ground and is not capable of identifying unstable frequency responses, backbone curves and NNMs of nonlinear structures.

Link et al. [76] apply constant-acceleration base excitation testing to extract modal parameters of a weakly-nonlinear satellite structure as a function of the acceleration-load level from measured transmissibility data. However, this study does not provide a solid theoretical framework for the quasi-linearization of nonlinear MDOF systems in the case of constant-acceleration testing and consequently remains as an empirical work that mainly resides on the observation of a weakly nonlinear structure. It is important to note that constant-acceleration sine testing does not guarantee the quasi-linearization of measured FRFs especially in the case of strongly nonlinear structures due to the change of the displacement

amplitude. An important contribution of this thesis work is to show that keeping the displacement amplitude constant throughout the frequency-sweep guarantees the quasi-linearization of a wide range of nonlinear structures including real engineering systems with strong and complex nonlinearities.

Considering the literature review covering the last three decades as given above, it can be concluded that the actual potential of the response-controlled stepped-sine testing in nonlinear system identification has been overlooked or underestimated due to the lack of a general theoretical framework and due to the general preconception which assumes that constant-displacement sine testing is difficult and time-consuming until this present work. The main contribution of this thesis study, which has the potential to create a paradigm shift in the field of nonlinear system identification, is to build up the RCT approach on a solid theoretical framework and to show that this framework can be applied to a wide range of strongly nonlinear engineering structures including real and complex engineering systems such as a real missile and a control fin actuation mechanism. The other important contribution of this thesis work is to show that contrary to the general preconception, constant-displacement sine testing is very fast and accurate even in the case of strongly nonlinear structures. For example, in the T-beam problem, it is shown that RCT is three times faster than the classical constant-force testing due to the quasi-linear behavior of the system, which is more predictable and so controllable. This thesis work also shows that constant-displacement closed-loop control can be achieved easily by using the accelerometer, the most popular sensor used in modal testing, by defining an appropriate acceleration profile as a reference.

So far, the advantages of the RCT approach against early techniques have been discussed. To fully inform the reader about the potential of the RCT approach, it is also important to compare it with recently developed promising state-of-the-art methods. Two such promising techniques worth mentioning are PLL [80] and CBC [81] methods that were discussed previously in Section 1.2.

An advantage of the CBC technique is that it provides a non-invasive control strategy which becomes important in the case of the internal resonance where the effects of higher harmonics cannot be neglected. In such a situation, non-invasive control makes sure that the steady-state solution of the controlled system is the same as the steady-state solution of the open-loop system. Internal resonance can be a problem in the case of conservatively nonlinear systems with very low damping. However, as illustrated in the experimental case studies of this thesis work, real-life structures (including complex engineering systems such as a real missile and a control fin actuation mechanism) exhibit in general moderate to high damping which suppresses the effects of higher harmonics and, so the internal resonance. Accordingly, within the scope of this thesis work, non-invasive control is not required and the RCT approach is successfully implemented with standard commercial modal test equipment. The implementation of the RCT strategy with non-invasive control in the case of internal resonance will be studied in the future as discussed in Chapter 6 (Future Directions).

On the other hand, the RCT approach proposed in this thesis work has several important advantages compared to the CBC method:

- CBC is essentially an amplitude sweep technique conducted at constant forcing frequency. This procedure results in displacement amplitude versus force amplitude curves which come out typically in S-shape at a fixed frequency. An important drawback of this approach is that these S-shaped curves also include unstable regions similar to the case of the constant force sweep. So, in order to stabilize these unstable regions, the control gain must be adequately chosen to avoid the jump phenomenon, which requires trial and error effort and so, time-consuming experimentation. In contrast to the CBC method, RCT is a frequency sweep technique at constant amplitude, which results in frequency versus force amplitude curves (i.e. harmonic force spectra) being typically in V-shape at fixed displacement amplitude. An important advantage of the RCT approach is that these V-shaped curves

do not include any instability because initial conditions (displacement and velocity) are nearly constant (the displacement amplitude is kept constant, yet the velocity amplitude changes slightly due to the frequency change) and avoid the competition of multiple stable orbits and so the jump phenomenon.

- Another drawback of the CBC technique is that although the S-curves can be combined to create a manifold similar to the HFS, they constitute a difficult topology that requires advanced post-processing tools such as Gaussian process regression [81] to obtain a smooth surface. This issue may lead to difficulties in the accurate extraction of turning points and unstable branches of constant force-frequency response curves from that surface. Another important contribution of the RCT approach is that the topology of the measured V-shaped harmonic force spectra makes it very easy to obtain a smooth HFS by simply using linear interpolation.
- CBC can trace out the backbone curve and determine the NNM of nonlinear structures by searching the resonance point which satisfies the phase quadrature condition, i.e. 90^o phase difference between the response and the excitation. Phase quadrature is a valid assumption for conservatively nonlinear systems with low damping. However, in the case of high and non-proportional damping, the phase lag at resonance may considerably deviate from 90^o, which requires time-consuming iterations to determine actual resonance peaks and so backbone curves and NNMs. The RCT approach does not need to search for the exact resonance locations to determine NNMs. It simply processes multiple quasi-linear FRFs measured from SIMO testing simultaneously by standard linear modal analysis to determine modal constants which turn out to be complex values in the case of high and non-proportional damping. Mass normalized NNMs can then be determined easily from these modal constants as functions of the response amplitude.

- CBC cannot determine NNMs in the mass normalized form. However, the nonlinear experimental modal analysis method proposed in this thesis work determines NNMs directly and accurately in the mass normalized form by virtue of the modal constants identified from quasi-linear constant-response FRFs measured by RCT. Mass normalized NNMs are crucial to synthesize constant-force FRFs corresponding to unmeasured forcing scenarios by using the single nonlinear mode theory.
- CBC does not provide any way of determining the nonlinear modal damping ratio. However, the nonlinear experimental modal analysis technique proposed in this thesis identifies the nonlinear modal damping ratio easily by applying standard linear modal analysis to quasi-linear constant-response FRFs measured by RCT.

Coming to the PLL technique, it is essentially the extension of the classical linear phase resonance testing, which is also called normal mode testing, to nonlinear structures. In this approach, the backbone curves of nonlinear structures are traced out by satisfying the phase quadrature condition, i.e. 90^o phase difference between the response and the excitation with phase control. Phase resonance testing is a time-consuming process even in the case of linear experimental modal analysis and is not a preferable tool especially for the modal identification of complex engineering systems (e.g. aircraft). The important advantages of the RCT approach compared to the PLL technique are given as follows:

- PLL technique can trace out the unstable branches of constant-force FRFs [83]. However, using this procedure to determine FRFs at different force levels would be very time consuming and would not be practical. The HFS concept proposed in this thesis work, on the other hand, is a very practical tool to experimentally extract various constant-force FRFs with accurately identified turning points and unstable branches.
- In the case of the PLL technique, the determination of actual resonance peaks and so backbone curves and NNMs of highly and non-proportionally

damped structures can be very time-consuming similar to the CBC. However, as previously mentioned, the RCT approach does not need to search for resonance peaks because it determines NNMs practically from the identified nonlinear modal constants.

- Similar to the CBC, the mass normalization of the experimentally extracted NNMs is also a considerable issue in the case of the PLL technique. PLL normalizes NNMs via an experimental estimate of the mass matrix obtained by taking the generalized (pseudo) inverse of the experimentally extracted (and so truncated) modal matrix of the underlying linear system [83]. This is a very intricate procedure that brings many practical problems. Firstly, it requires placing many sensors at different locations that physically may not be possible. Secondly, the measurement of linear FRFs requires low-level excitation which may give poor results especially in the case of friction type of nonlinearity which is dominant at low vibration levels and which is widely encountered in practice due to the mechanical joints. Thirdly, the generalized inverse of a truncated experimental matrix may lead to unacceptable accuracy in the estimation of the mass matrix. However, the identification of the mass normalized NNMs by the RCT approach is very simple and accurate as discussed above.
- In the PLL technique, the nonlinear modal damping ratio is estimated by the balance of the excitation power and dissipated power. The estimation of the modal amplitude that appears in the formulation of the modal damping ratio is accomplished based on the experimental estimate of the mass matrix mentioned above. Accordingly, the inaccuracy of the mass normalization may lead to considerable inaccuracy in the estimation of the modal damping ratio as well. Furthermore, this procedure does not guarantee the consistency of the modal damping with other modal parameters. However, in the case of the RCT approach, the modal damping ratio is determined by fitting a linear modal model to the multiple quasi-linear FRFs measured at

different locations simultaneously, which gives the best damping estimate consistent with the modal model.

Concluding this section, it is important to note that three promising and competitive nonlinear system identification techniques have been developed recently, namely CBC, PLL, and RCT. As discussed above, RCT has seemingly important advantages compared to the two other techniques. So far, CBC and PLL have been applied to simple benchmark structures that exhibit conservative nonlinearities. PLL technique has also been challenged very recently with a cantilever beam that exhibits high and nonlinear damping due to a localized friction element [88]. However, this is a special setup that exhibits full stick at low vibration levels, which may allow the accurate estimation of linear modes and which does not challenge the experimental estimation of the mass matrix, mass normalized NNMs, and the modal damping ratio. Moreover, the constant-force FRFs synthesized from the identified nonlinear modal parameters considerably deviate from the actual measured FRFs. On the other hand, in this thesis work, the proposed nonlinear experimental methodology based on RCT has been successfully applied in the modal identification of a wide range of structures including a clamped-clamped beam with strong distributed (geometrical) nonlinearity, a control fin actuation mechanism with strong non-smooth stiffness nonlinearity as well as high and nonlinear damping and a real missile structure with considerable damping nonlinearity.

1.5 Outline of the Thesis

Chapter 2 presents the *Experimental Modal Analysis with RCT and the HFS Concept* as a new approach for the experimental modal analysis of strongly nonlinear complex engineering structures that exhibit several nonlinearities at different (and even unknown) locations and/or which exhibit continuously distributed (geometrical) nonlinearities. Firstly, the theoretical background, which consists of the *nonlinearity matrix* concept and the *single nonlinear mode theory*, is

explained in detail. Next, the proposed experimental methodology is summarized in a flow-chart followed by a comprehensive study of its key features: 1) Measurement of constant-response FRFs in quasi-linear form, 2) Excitation strategy, 3) Response control strategy, 4) Identification of nonlinear modal parameters, 5) Synthesis of nonlinear frequency responses, including any existing unstable branch, from the identified modal parameters for untested constant amplitude harmonic forcing scenarios. As a part of the methodology, a new concept called the *Harmonic Force Surface* (HFS) is also proposed to experimentally extract the constant-force frequency response curves with unstable branches (if there are any) and the backbone curves of nonlinear systems. Finally, the application of the method is demonstrated in a numerical example.

Chapter 3 presents the *Describing Surface Method* (DSM) as a novel frequency-domain nonparametric identification method for nonlinear structures. First of all, the theoretical background of the classical *Describing Function Method* is introduced. Next, the proposed DSM, which extends the classical approach by including frequency dependence of nonlinearity in addition to response amplitude dependence and by determining nonlinearity in nonparametric form as a lookup table, is explained in detail. Finally, the application of the method is demonstrated in numerical examples.

Chapter 4 is dedicated to the experimental validation of the proposed nonlinear experimental modal analysis method and the DSM. The nonlinear experimental modal analysis technique is validated on the T-beam benchmark which exhibits strong localized cubic stiffness nonlinearity, on a thin metal beam which exhibits continuously distributed strong geometrical nonlinearity due to large amplitude oscillations, on a real missile structure which exhibits considerable damping nonlinearity mostly due to several bolted joints and on a control fin actuation mechanism which exhibits very complex and strong nonlinearity due to backlash and friction. In all of these applications, frequency response curves for constant amplitude harmonic forcing are accurately predicted (including any existing unstable branch) from the identified nonlinear modal parameters. Furthermore,

frequency response curves with unstable branches (if there are any) and backbone curves are experimentally extracted from the HFS. On the other hand, the DSM is validated by using three experimental case studies: the T-beam benchmark, a dummy mass on elastomeric vibration isolators, and a control fin actuation mechanism of a real missile structure. In each case, nonlinear FRFs calculated by using the identified describing surface agree very well with measured FRFs at various force levels.

Chapter 5 gives a summary of this thesis study and specifies key conclusions.

Chapter 6 discusses future directions.

CHAPTER 2

NONLINEAR EXPERIMENTAL MODAL ANALYSIS BY USING RESPONSE-CONTROLLED STEPPED-SINE TESTING AND THE HARMONIC FORCE SURFACE CONCEPT

2.1 The Nonlinearity Matrix Concept

Equation of motion of a nonlinear n degrees-of-freedom system with structural damping subjected to a harmonic excitation force of frequency ω, neglecting all the sub- and super-harmonic terms, can be written in the form of a nonlinear complex algebraic equation in the frequency domain as follows

$$-\omega^2[M]\{X\} + i[D]\{X\} + [K]\{X\} + \{F_N\} = \{F\}, \tag{2.1}$$

where $[M]$, $[D]$ and $[K]$ are the mass, hysteretic (structural) damping and stiffness matrices of the underlying linear system, respectively. $\{X\}$, $\{F_N\}$ and $\{F\}$ are the complex vectors of displacement amplitude, nonlinear internal force amplitude, and external excitation force amplitude, respectively.

According to the Describing Function Method (DFM) [53], the complex vector of nonlinear internal force amplitude can be expressed as

$$\{F_N\} = [\Delta]\{X\}, \tag{2.2}$$

where $[\Delta]$ is the displacement level-dependent complex and symmetric *nonlinearity matrix*. Real and imaginary parts of this matrix correspond to the displacement level-dependent nonlinear stiffness and nonlinear damping matrices, respectively.

Substituting Eq. (2.2) into Eq. (2.1) yields

$$(-\omega^2[M] + i[D] + [K] + [\Delta])\{X\} = \{F\}. \tag{2.3}$$

It should be noted that the DFM is mathematically equivalent to the classical Harmonic Balance Method (HBM). The major difference between the DFM and the HBM relies on the expression of nonlinear internal forces. The HBM expresses nonlinear internal forces as a single force vector, whereas in the DFM they are written as a multiplication of the so-called nonlinearity matrix with the displacement amplitude vector as shown in Eq. (2.2). The second representation allows one to treat a nonlinear system, mathematically, as a linear system at a given displacement amplitude level, which makes it possible to extend some of the methods developed for linear systems to nonlinear systems by using iterative solutions.

2.2 The Nonlinear Eigenvalue Problem

According to the single nonlinear mode theory [65], nonlinear normal modes (NNMs) are found by solving the nonlinear eigenvalue problem associated with the *conservative* part of Eq. (2.3) as follows

$$([K] + [\Delta]_{re})\{\bar{\psi}(q_r)\}_r = \bar{\omega}_r^2(q_r)[M]\{\bar{\psi}(q_r)\}_r. \tag{2.4}$$

Here, q_r is the r^{th} modal amplitude, $\{\bar{\psi}(q_r)\}_r$ and $\bar{\omega}_r(q_r)$ are the r^{th} real-valued NNM and its corresponding natural frequency, which are functions of q_r. $[\Delta]_{re}$ represents the real part of the nonlinearity matrix, which corresponds to the nonlinear stiffness matrix. It should be noted that $[\Delta]_{re}$ depends on the displacement response level of the system, which is equivalent to the product $q_r\{\bar{\psi}(q_r)\}_r$ as discussed in Section 2.3. Accordingly,

$$[\Delta]_{re} = [\Delta\ (q_r\{\bar{\psi}(q_r)\}_r)]_{re}. \tag{2.5}$$

Consequently, Eq. (2.4) is a nonlinear eigenvalue problem which requires an iterative solution procedure. Starting from the corresponding normal mode of the underlying linear system, Eq. (2.4) can be solved for $\{\bar{\psi}(q_r)\}_r$ and $\bar{\omega}_r(q_r)$ by using various iterative solution techniques (e.g. Newton-Raphson Method [66]).

2.3 The Single Nonlinear Mode Method

If the modes are well separated and no pronounced modal coupling occurs in the energy range of interest, the near-resonant solution of Eq. (2.3) around an r^{th} mode can be approximated by a single NNM calculated from Eq. (2.4) as follows [65]

$$\{X\} = q_r\{\bar{\psi}(q_r)\}_r. \tag{2.6}$$

Substituting Eq. (2.6) into Eq. (2.3) and premultiplying by $\{\bar{\psi}(q_r)\}_r^T$ yields

$$(-\omega^2\bar{m}_r(q_r) + \bar{k}_r(q_r) + i\bar{h}_r(q_r))q_r = \{\bar{\psi}(q_r)\}_r^T\{F\}, \tag{2.7}$$

where

$$\bar{m}_r(q_r) = \{\bar{\psi}(q_r)\}_r^T[M]\{\bar{\psi}(q_r)\}_r, \quad \bar{k}_r(q_r) = \{\bar{\psi}(q_r)\}_r^T([K] + [\Delta]_{re})\{\bar{\psi}(q_r)\}_r,$$

$$\bar{h}_r(q_r) = \{\bar{\psi}(q_r)\}_r^T([D] + [\Delta]_{im})\{\bar{\psi}(q_r)\}_r. \tag{2.8}$$

Here, $\bar{m}_r(q_r)$, $\bar{k}_r(q_r)$ and $\bar{h}_r(q_r)$ are the modal mass, modal stiffness, and modal hysteretic damping, respectively. $[\Delta]_{im}$ represents the imaginary part of the nonlinearity matrix, which corresponds to the displacement response level-dependent nonlinear damping matrix.

Eqn. (2.7) can be alternatively written as

$$\bar{m}_r(q_r)(-\omega^2 + \bar{\omega}_r^2(q_r) + i\bar{\eta}_r(q_r)\bar{\omega}_r^2(q_r))q_r = \{\bar{\psi}(q_r)\}_r^T\{F\}, \tag{2.9}$$

where

$$\bar{\omega}_r^2(q_r) = \bar{k}_r(q_r)/\bar{m}_r(q_r), \qquad \bar{\eta}_r(q_r) = \bar{h}_r(q_r)/(\bar{m}_r(q_r)\bar{\omega}_r^2(q_r)). \tag{2.10}$$

Modal amplitude q_r can be solved from Eq. (2.9) as follows

$$q_r = \frac{\{\bar{\psi}(q_r)\}_r^T\{F\}}{\bar{m}_r(q_r)\left(\bar{\omega}_r^2(q_r) - \omega^2 + i\bar{\eta}_r(q_r)\bar{\omega}_r^2(q_r)\right)}. \tag{2.11}$$

Inserting Eq. (2.11) into Eq. (2.6) yields

$$\{X\} = \frac{\{\bar{\psi}(q_r)\}_r \{\bar{\psi}(q_r)\}_r^T \{F\}}{\bar{m}_r(q_r)\left(\bar{\omega}_r^2(q_r) - \omega^2 + i\bar{\eta}_r(q_r)\bar{\omega}_r^2(q_r)\right)}. \tag{2.12}$$

Here, NNM can be normalized with respect to modal mass as follows

$$\{\bar{\phi}(q_r)\}_r = \{\bar{\psi}(q_r)\}_r / \sqrt{\bar{m}_r(q_r)}. \tag{2.13}$$

Substituting Eq. (2.13) into Eq. (2.12) yields

$$\{X\} = \frac{\{\bar{\phi}(q_r)\}_r \{\bar{\phi}(q_r)\}_r^T \{F\}}{\bar{\omega}_r^2(q_r) - \omega^2 + i\bar{\eta}_r(q_r)\bar{\omega}_r^2(q_r)}. \tag{2.14}$$

Near-resonant receptance α_{jk} at point j for a given excitation at point k can be deduced from Eq. (2.14) as follows

$$\alpha_{jk}(\omega, q_r) = \frac{\bar{\phi}_{jr}(q_r)\bar{\phi}_{kr}(q_r)}{\bar{\omega}_r^2(q_r) - \omega^2 + i\bar{\eta}_r(q_r)\bar{\omega}_r^2(q_r)}. \tag{2.15}$$

In Eq. (2.15), the nonlinear hysteretic modal damping model can be replaced by an equivalent nonlinear viscous damping model as well. Accordingly, an alternative form of Eq. (2.15) can be written as follows

$$\alpha_{jk}(\omega, q_r) = \frac{\bar{\phi}_{jr}(q_r)\bar{\phi}_{kr}(q_r)}{\bar{\omega}_r^2(q_r) - \omega^2 + i2\bar{\xi}_r(q_r)\omega\bar{\omega}_r(q_r)}. \tag{2.16}$$

where $\bar{\xi}_r(q_r)$ is the nonlinear viscous modal damping ratio.

The experimental methodology proposed to identify nonlinear modal parameters that can be used for the synthesis of near-resonant frequency response curves for untested constant-amplitude harmonic forcing scenarios is explained in the next section.

2.4 Nonlinear Experimental Modal Analysis Methodology with RCT and the HFS Concept

Since a graphical summary may help the reader to see the global picture much better, before jumping into the details, the flowchart of the proposed nonlinear experimental modal analysis methodology with *Response-Controlled Stepped-Sine Testing* (RCT) and the *Harmonic Force Surface* (HFS) concept is given in Figure 2-1.

The first step consists of measuring quasi-linear frequency response functions (FRFs) and harmonic excitation force spectra at several different constant displacement amplitude levels. The quasi-linearization of constant-response FRFs stems from the key formulations given in Eqs. (2.15) and (2.16). These formulations clearly indicate that if the modal amplitude is kept constant throughout the stepped-sine testing, the measured FRFs turn out to be quasi-linear. In the case of a single point excitation, the constant modal amplitude can be achieved by keeping the displacement amplitude of the excitation point constant. The displacement amplitude can be kept constant indirectly by defining an accelerometer as the control sensor and by feeding the closed-loop controller with an appropriate acceleration profile. The good thing is that in the absence of internal resonance, this control strategy can easily be achieved via standard equipment (e.g. LMS Test Lab).

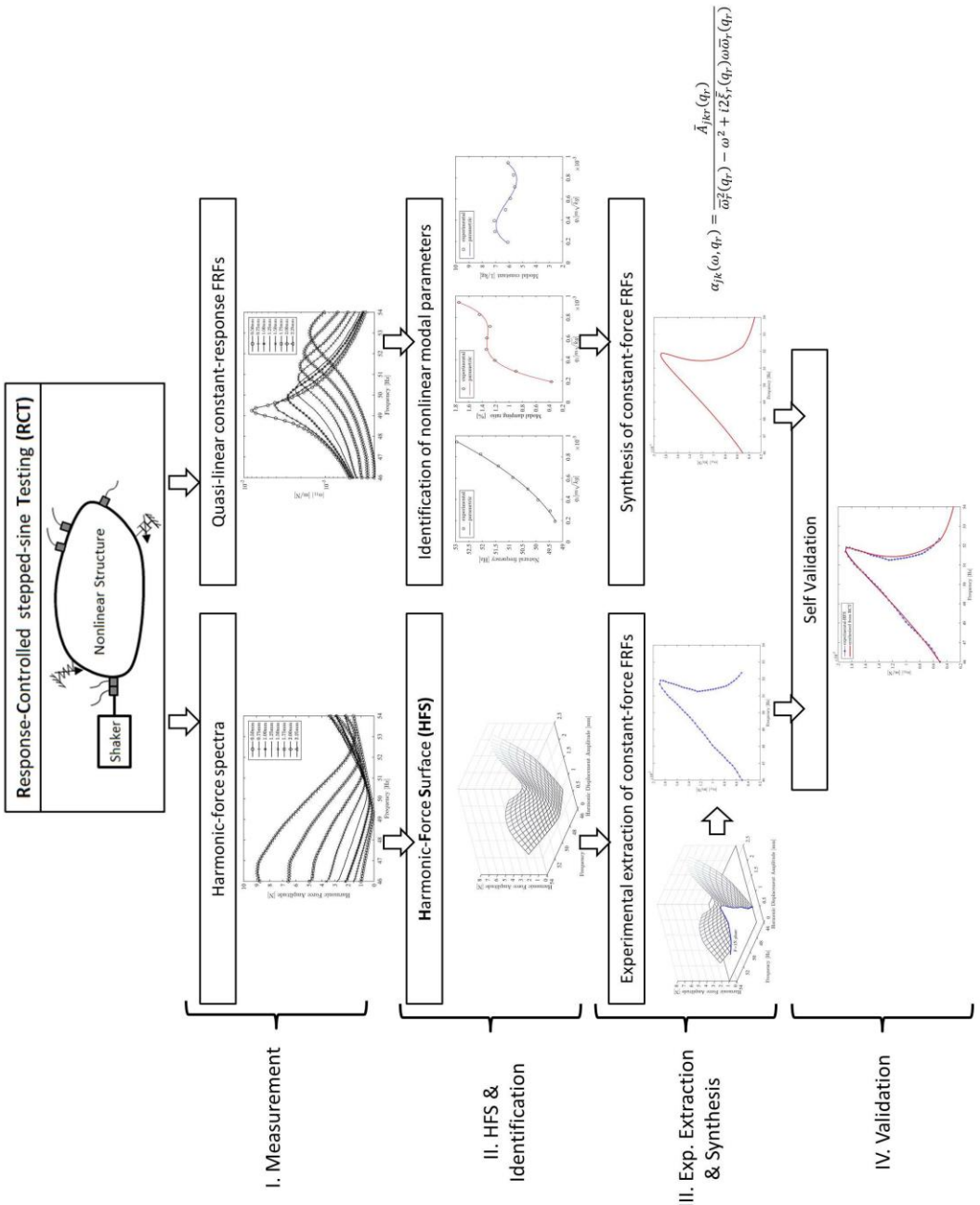

Figure 2-1. Nonlinear experimental modal analysis with RCT and the HFS concept

The second step of the proposed methodology consists of processing the measured experimental data. Quasi-linear FRFs corresponding to different constant displacement amplitude levels can easily be processed by using standard linear modal analysis techniques to extract modal parameters. This procedure is very familiar to practicing engineers in the industry. Repeating the same procedure at different amplitude levels ultimately gives modal parameters as functions of the displacement (or equivalently modal) amplitude. In parallel, harmonic excitation spectra measured at different displacement amplitude levels are collected together to build up the so-called HFS.

In the third step, constant-force FRFs corresponding to untested forcing levels can be independently obtained by two different approaches. They can either be synthesized by using the identified nonlinear modal parameters in a Newton-Raphson scheme with the arc-length continuation algorithm, or they can directly be extracted by cutting the HFS, which is purely experimental data, with constant force planes. Ideally, the synthesized and extracted constant-force FRFs must match perfectly, which constitutes the self-validation measure of the proposed experimental methodology as shown in the fourth step.

The flow chart given in Figure 2-1 and the summary given above are supported with detailed explanations in the following sections to help the reader develop a profound understanding of the proposed experimental methodology.

2.4.1 Measurement of Constant-Response FRFs in Quasi-Linear Form

The modal parameters in Eqs. (2.15)-(2.16) are functions of a single parameter; the modal amplitude. Here, it is proposed to measure *constant-response* FRFs of nonlinear systems by keeping the displacement amplitude of the driving (excitation) point constant with the RCT strategy. According to the single nonlinear mode assumption, these constant-response FRFs are expected to come out in the quasi-linear form. Consequently, modal parameters can be extracted from

measured constant-response FRFs by using standard linear modal analysis methods available in commercial software packages. As discussed in Section 1.3, this approach essentially extends the method proposed by Arslan and Özgüven [74], which is restricted to structures where the nonlinearity is localized between a single DOF and the ground, to complex engineering structures with multiple nonlinearities connecting internal coordinates and spread over the structure (e.g., structures with several bolted joints or geometrical nonlinearities continuously distributed over structures).

Although the single nonlinear mode theory [65] completely discards higher harmonics in the derivation of the nonlinear receptance model given in Eqs. (2.15)-(2.16), the quasi-linearization of FRFs with RCT strategy can still be achieved under the effects of higher harmonics if these effects are not pronounced. In Section 2.5, this is demonstrated on the RCT simulation of a lumped MDOF system with strong conservative nonlinearity, where the system is excited at a single DOF and the fundamental harmonic displacement of the driving point is kept constant. Firstly, the frequency responses of the fundamental and higher harmonics, as well as the excitation force spectrum are calculated by using the multi-harmonics version of the DFM [89]. Secondly, the constant-response FRFs that correspond to the fundamental harmonic are determined by dividing the fundamental harmonic displacement with the harmonic excitation force. Eventually, it is shown that the FRFs determined by using multiple harmonics are also quasi-linear.

2.4.2 Excitation Strategy

Several experimental studies have shown that in the absence of internal resonances; single point, single harmonic excitation is sufficient to isolate nonlinear modes to a satisfying accuracy [78, 83]. Furthermore, in the case of a single point excitation, keeping the modal amplitude constant is equivalent to keeping the displacement amplitude of the driving point constant. Due to these practical benefits, in the

proposed method, a single input stepped-sine test strategy is used to identify modal parameters. Theoretically, the RCT approach can also be applied by using multi-point excitation. In that case, the adjustment of the amplitude ratios of excitation signals would be necessary, as in the case of NNM force appropriation, to keep the modal amplitude at a constant level. This adjustment can be achieved with the help of a preliminary single-point excitation test.

2.4.3 Response Control Strategy

The displacement amplitude of the driving point can be kept constant either directly or indirectly depending on the type of sensor used during RCT. Since the accelerometer is the most widely used sensor in experimental modal analysis, it was chosen as the control sensor in the proposed method. The acceleration profile corresponding to a constant displacement amplitude over the frequency range of interest is calculated and input to the *closed-loop* controller as a reference profile, which is an available option in standard modal testing software packages (e.g. LMS Test Lab©).

2.4.4 Identification of Nonlinear Modal Parameters and Experimental Extraction of Mass Normalized NNMs

The determination of near-resonant frequency response curves for various unmeasured harmonic forcing scenarios is an important task to understand the complex dynamics of engineering structures and eventually to satisfy critical design requirements. If one could experimentally extract the nonlinear modal parameters used in Eqs. (2.15)-(2.16), these identified modal parameters can then be used to synthesize near-resonant frequency responses corresponding to various constant-amplitude harmonic forcing scenarios.

In the proposed method, in order to identify the nonlinear modal parameters, constant-response FRFs at several different displacement amplitude levels are

measured by conducting a series of modal tests with the RCT strategy. Then, the modal identification is achieved by fitting the following analytical model to the measured constant-response FRFs with an appropriate linear modal analysis method

$$\alpha_{jk}(\omega, q_r) = \frac{\bar{A}_{jkr}(q_r)}{\bar{\omega}_r^2(q_r) - \omega^2 + i\bar{\eta}_r(q_r)\bar{\omega}_r^2(q_r)}, \tag{2.17}$$

where $\bar{A}_{jkr}(q_r)$ is a complex-valued modal constant. The nonlinear hysteretic modal damping model used in Eq. (2.17) can be replaced by an equivalent nonlinear viscous modal damping model as follows

$$\alpha_{jk}(\omega, q_r) = \frac{\bar{A}_{jkr}(q_r)}{\bar{\omega}_r^2(q_r) - \omega^2 + i2\bar{\xi}_r(q_r)\omega\bar{\omega}_r(q_r)}. \tag{2.18}$$

Once $\bar{A}_{jkr}(q_r)$, $\bar{\omega}_r(q_r)$ and $\bar{\xi}_r(q_r)$ (or $\bar{\eta}_r(q_r)$) are experimentally extracted, they can be plotted with respect to modal amplitude. These plots can either be used in parametric form by fitting polynomials, if possible, or directly as look-up tables in the synthesis of near-resonant frequency response curves for untested harmonic forcing scenarios (see the right column of Figure 2-1).

In the case of a single input and multiple outputs modal testing, the mass normalized NNMs can be determined from the experiment by using the following procedure.

First of all, the identified modal constants can be collected into a vector as follows

$$\{\bar{A}(q_r)\}_r^T = \{\bar{A}_{11r}(q_r) \quad \bar{A}_{21r}(q_r) \quad \cdots \quad \bar{A}_{m1r}(q_r)\}^T, \tag{2.19}$$

where m indicates the total number of measurement points.

Comparison of Eqs. (2.17)-(2.18) with Eqs. (2.15)-(2.16) reveals that the experimentally extracted modal constants are closely related to the mass normalized NNMs with the following relation

$$\bar{A}_{jkr}(q_r) = \bar{\phi}_{jr}(q_r)\bar{\phi}_{kr}(q_r). \tag{2.20}$$

Substituting Eq. (2.20) into Eq. (2.19) yields

$$\{\bar{A}(q_r)\}_r = \{\bar{\phi}_{1r}(q_r)\bar{\phi}_{1r}(q_r) \quad \bar{\phi}_{1r}(q_r)\bar{\phi}_{2r}(q_r) \quad \cdots \quad \bar{\phi}_{1r}(q_r)\bar{\phi}_{mr}(q_r)\}^T. \tag{2.21}$$

It can be easily noticed that all the terms of the vector given in Eq. (2.21) have a common multiplier which is $\bar{\phi}_{1r}(q_r)$. This multiplier can be determined by taking the square root of the identified modal constant of the driving point FRF as follows

$$\bar{\phi}_{1r}(q_r) = \sqrt{\bar{A}_{11r}(q_r)}. \tag{2.22}$$

Finally, dividing Eq. (2.21) by the square root term given in Eq. (2.22), the NNM of interest can be identified in mass normalized form as follows

$$\{\bar{\phi}(q_r)\}_r = \frac{1}{\sqrt{\bar{A}_{11r}(q_r)}}\{\bar{A}(q_r)\}_r. \tag{2.23}$$

The nonlinear modal damping ratio and the mass normalized NNMs are the essential elements required in the synthesis of frequency response curves for untested harmonic forcing scenarios. Obviously, if one is interested in the synthesis of the frequency response curves of a single point, the identification of the modal constant corresponding to that point will be sufficient.

In concluding this section, it is important to note that the NNMs used in Eqs. (2.15)-(2.16) are assumed to be the NNMs of the underlying conservative system, whereas those extracted from experimental data by using Eq. (2.23) are the NNMs of the actual damped system, which may seem paradoxical. However, the damped NNMs of a nonlinear system can be approximated by the NNMs of the underlying undamped system, and vice versa, under the assumption of moderate damping as discussed in [79, 90]. On the other hand, in this thesis work, the applicability of the method in the case of very high damping is also validated on the control fin action mechanism of a real missile in Section 4.1.4.

2.4.5 Synthesis of Frequency Responses for Untested Constant-Amplitude Harmonic Forcing Scenarios

The nonlinear modal parameters identified from constant-response FRFs can be employed in the following equation to calculate the near-resonant frequency responses for untested constant-amplitude harmonic forcing scenarios

$$X_j(q_r) = \frac{\bar{A}_{jkr}(q_r)F_k}{\bar{\omega}_r^2(q_r) - \omega^2 + i2\bar{\xi}_r(q_r)\omega\bar{\omega}_r(q_r)}. \tag{2.24}$$

where $X_j(q_r)$ is the displacement amplitude at point j for a given constant-amplitude force F_k at point k.

In this study, Eq. (2.24) is solved iteratively by using Newton's Method with the arc-length continuation algorithm which is capable of capturing any unstable branch which might occur in strongly nonlinear systems (see the right column of Figure 2-1).

2.4.6 The HFS Concept

As an alternative to the computational approach given in Eq. (2.24), the HFS concept is capable of deriving frequency response curves, experimentally, at constant force levels including unstable branches, if there is any, by using harmonic force spectra measured at constant vibration levels during RCT without any extra experimental effort.

In the linear experimental modal analysis, the standard closed-loop stepped sine test with force control starts with a linear system identification which determines a rough initial estimate of the plant, i.e. the transfer function of the structure under test. In the case of nonlinear structures, this procedure may lead to a very poor estimate of the structure's actual dynamic behavior. Consequently, the controller may need to make many corrective iterations to keep the force within the tolerance

limits of the reference profile, which may become very time-consuming. Furthermore, in the case of nonlinear structures with strong stiffening or softening character, multiple steady-state vibration responses may co-exist for the same excitation frequency, which results in an overhanging unstable branch in the frequency response curve. Standard force-control algorithms available in commercial software can only measure nonlinear frequency responses until the turning points of the stable branches, at the cost of multiple runs with different sweep directions. When a turning point is reached, the standard force-controller cannot avoid jumping from one stable branch to another, passing over the unstable region as shown in Figure 2-2(a). Even worse, in some cases, the small corrective force perturbations of the controller to capture the reference signal in the vicinity of the turning points may lead to a *premature jump* before reaching the actual turning point as shown in Figure 2-2(b). These drawbacks of the standard techniques paved the way for the development of sophisticated control algorithms such as PLL and CBC. The primary advantage of these two control strategies over the classical force-control approach is the ability to measure the backbone curves and the unstable branches of nonlinear frequency responses. However, these control strategies could not be validated on real and complex engineering systems yet, the experimental extraction of nonlinear modal damping ratio and mass normalized NNMs is still an important issue and available standard equipment cannot be used in these approaches which require the design of sophisticated control algorithms.

As an alternative to the new generation control strategies mentioned above, the Harmonic Force Surface (HFS) concept proposed in this thesis can be used as described below, in order to determine the unstable branches of nonlinear frequency response curves by using standard controllers available in commercial modal testing hardware and driven by commercial software together with the RCT strategy.

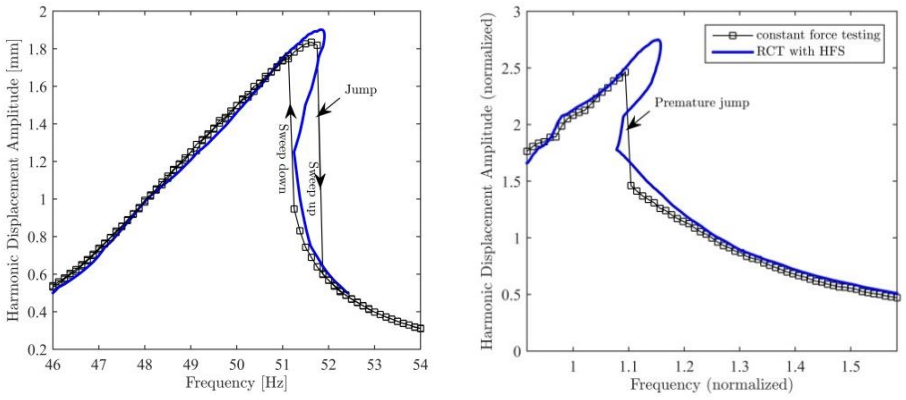

(a) (b)

Figure 2-2. Frequency response curves measured in constant-force stepped-sine testing compared to the ones measured by RCT with HFS: (a) the jump phenomenon (b) the premature jump

In the case of strong stiffness nonlinearity where multiple steady-state vibration responses co-exist for the same excitation frequency, the response level of the structure highly depends on initial conditions. In the case of the force-control test strategy, there is no control over the vibration response which may exhibit drastic changes around resonance even if very small frequency steps are used. Since a gradual change in the vibration response and eventually in the initial conditions is not guaranteed, the experimental continuation of the unstable branch cannot be achieved. In the RCT approach, this problem is solved by keeping the displacement amplitude constant, which results in a smooth response spectrum incorporating the points of the unstable branch as well. This is somewhat different from the PLL and CBC algorithms which aim at tracing the points of the unstable branch consecutively. In the RCT strategy, the points of the unstable branch are visited at different times during stepped-sine tests carried out at different vibration amplitude levels. Then they are collected together on the HFS. The determination of the nonlinear frequency response with an unstable branch by using RCT and the HFS concept consists of the following steps (see the left column of Figure 2-1):

1. An RCT is carried out by keeping the displacement amplitude of the driving point constant. The test is repeated at several different displacement amplitude levels (in general, repeating the test at 10-15 different levels may be sufficient to obtain satisfactory results), and the corresponding harmonic force spectra of the driving point are measured.
2. The Harmonic Force Surface, HFS, is constructed by collecting the measured harmonic force spectra and using linear interpolation.
3. The contour plot obtained by cutting the HFS with a constant force plane gives the harmonic response spectrum corresponding to that force level, including any unstable branch if there is any.

The HFS procedure given above is demonstrated with numerical and experimental case studies in the subsequent sections.

2.5 Numerical Validation: 5 DOF Lumped System with Cubic Stiffness Elements

In this section, the modal identification method proposed in the previous section is validated on the 5 DOF nonlinear lumped system with 5 cubic stiffness elements, which is shown in Figure 2-3. The parameters of the system are as follows: $m = 1\ kg, k = 10000\ N/m, c = 5\ Ns/m, k^* = 10^{\,7}\ N/m^3$.

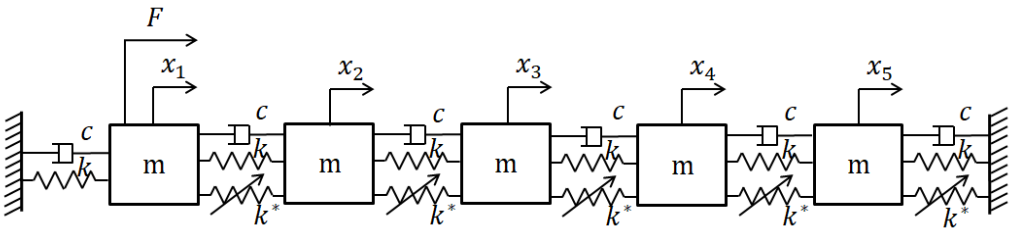

Figure 2-3. 5 DOF system with cubic stiffness nonlinearity

Standard force-control and RCT simulations carried out in this section are achieved by solving the following equation of motion which includes multiple harmonics [89]

$$\left(\begin{bmatrix} [Z]_{11} & 0 & \cdots & 0 \\ 0 & [Z]_{22} & \cdots & 0 \\ \vdots & \vdots & \vdots & \vdots \\ 0 & 0 & \cdots & [Z]_{hh} \end{bmatrix} + \begin{bmatrix} [\Delta]_{11} & [\Delta]_{12} & \cdots & [\Delta]_{1h} \\ [\Delta]_{21} & [\Delta]_{22} & \cdots & [\Delta]_{2h} \\ \vdots & \vdots & \vdots & \vdots \\ [\Delta]_{h1} & [\Delta]_{h2} & \cdots & [\Delta]_{hh} \end{bmatrix}\right) \begin{Bmatrix} \{X\}_1 \\ \{X\}_2 \\ \vdots \\ \{X\}_h \end{Bmatrix} = \begin{Bmatrix} \{F\} \\ 0 \\ \vdots \\ 0 \end{Bmatrix}, \tag{2.25}$$

where $\{X\}_h$ and $[Z]_{hh}$ are the complex displacement amplitude vector and the dynamic stiffness matrix corresponding to the h^{th} harmonic, respectively. $\{F\}$ denotes the vector of external excitation force amplitude. $[\Delta]_{11}, [\Delta]_{12}$ etc. are the components of the complex nonlinearity matrix, where the off-diagonal matrices represent the coupling terms between different harmonics (e.g., $[\Delta]_{12}$ is the coupling matrix between 1st and 2nd harmonics). In the paper where the DFM was first introduced [53], only a single harmonic was considered, which corresponds to taking $[Z]_{11}$ and $[\Delta]_{11}$ matrices into account and neglecting all other sub-matrices in Eq. (2.25). $[Z]_{hh}$ can be explicitly written as follows

$$[Z]_{hh} = -(h\omega)^2[M] + i[H] + [K]. \tag{2.26}$$

In the force-control simulations, a single point, single harmonic excitation force is applied to the 1st DOF which is the driving point, and Eq. (2.25) is solved for the displacement amplitudes of the fundamental and higher harmonics by keeping the amplitude of the excitation force constant. On the other hand, in the RCT simulations, the displacement amplitude corresponding to the first harmonic of the 1st DOF is kept constant and Eq. (2.25) is solved for the displacement amplitudes of all the other DOFs (including higher harmonics) as well as the amplitude of the excitation force. In both simulations, the equation of motion is solved numerically by using Newton's Method with the arc-length continuation algorithm. In this case study, it is found sufficient to consider only the first and the third harmonics in the

solution. The effect of the third harmonic on the FRFs in the first mode is illustrated in Figure 2-4. It should be noted that throughout the thesis, the FRF term is used to refer to the frequency response function between the fundamental harmonic response and the excitation force. Since the FRFs of nonlinear systems are not invariant to the excitation force, the normalization of the frequency response with the amplitude of the excitation force may seem to be unnecessary. However, the normalization process, which is very commonly used even for nonlinear systems in literature, helps to suppress the effect of the excitation force on the amplitude of the frequency response curve and to emphasize the effect of nonlinear stiffness and damping on the shape change of the frequency response curve.

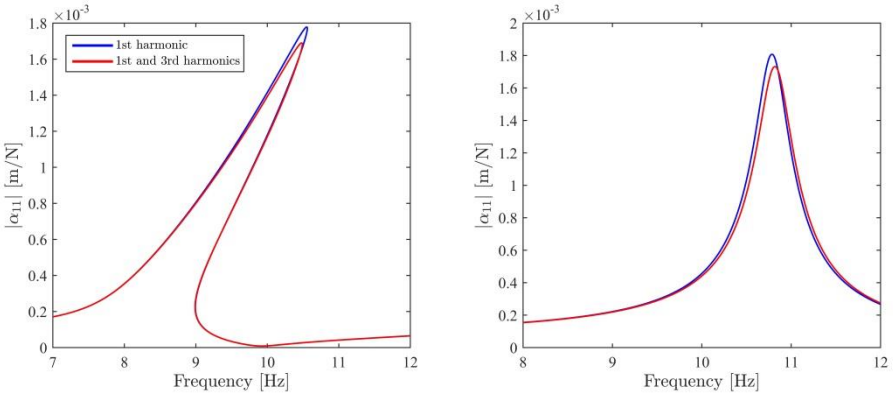

(a) (b)

Figure 2-4. Effect of the 3rd harmonic on the FRFs (a) constant-force driving point FRF at 50 N (b) constant-response driving point FRF at 0.10 m

2.5.1 Results of Standard Force-Control Simulations

The classical approach for measuring the frequency responses of a nonlinear system is to apply force-controlled stepped-sine testing by keeping the amplitude of the harmonic forcing constant throughout the frequency sweep. Accordingly, a series of force-control simulations were carried out on the 5 DOF nonlinear system shown in Figure 2-3. The constant-force FRFs determined around the first mode of the system at different forcing levels ranging from 1 N to 50 N are shown in Figure 2-5. The strong stiffness nonlinearity of the system changes the shape of each FRF considerably with increasing forcing level and results in overhanging unstable branches. By virtue of the arc-length continuation algorithm, the computer simulation made it possible to capture these unstable branches and consequently, to determine the exact locations of the resonance points which constitute the NNM backbone curves. However, in real experimental applications, this cannot be achieved by using standard force control testing due to the jump phenomenon as explained in Section 2.4.6. In the following section, it is shown that by just switching the control strategy from the force control to the response control, the jump phenomenon can be avoided, and consequently, standard equipment can still be used for the modal identification of nonlinear systems.

2.5.2 Determination of Constant-Response FRFs by Using RCT Simulations

The harmonic excitation force spectra of the driving point (1^{st} DOF) determined from the RCT simulations at different displacement amplitude levels are shown in Figure 2-6. By dividing the displacement amplitude spectrum of each DOF with the harmonic excitation force spectrum, the constant-response FRFs (corresponding to the first harmonic) were determined around the first mode of the system at different displacement amplitude levels ranging from 0.01 m to 0.1 m as shown in Figure 2-7. It should be noted that not only the constant-response FRFs of the 1^{st} DOF but

also the constant-response FRFs of all the other DOFs turned out to be quasi-linear. Of course, the visual inspection is not sufficient, and the solid proof is given in the next section by fitting linear analytical models to the constant-response FRFs. This outcome validates the fundamental hypothesis of the proposed method, i.e. if the modal amplitude is kept constant, the FRFs that are represented by Eqs. (2.15)-(2.16) turn out to be quasi-linear. It should be noted that in the case of a single point excitation, the modal amplitude can be kept constant by just keeping the displacement amplitude of the driving point constant.

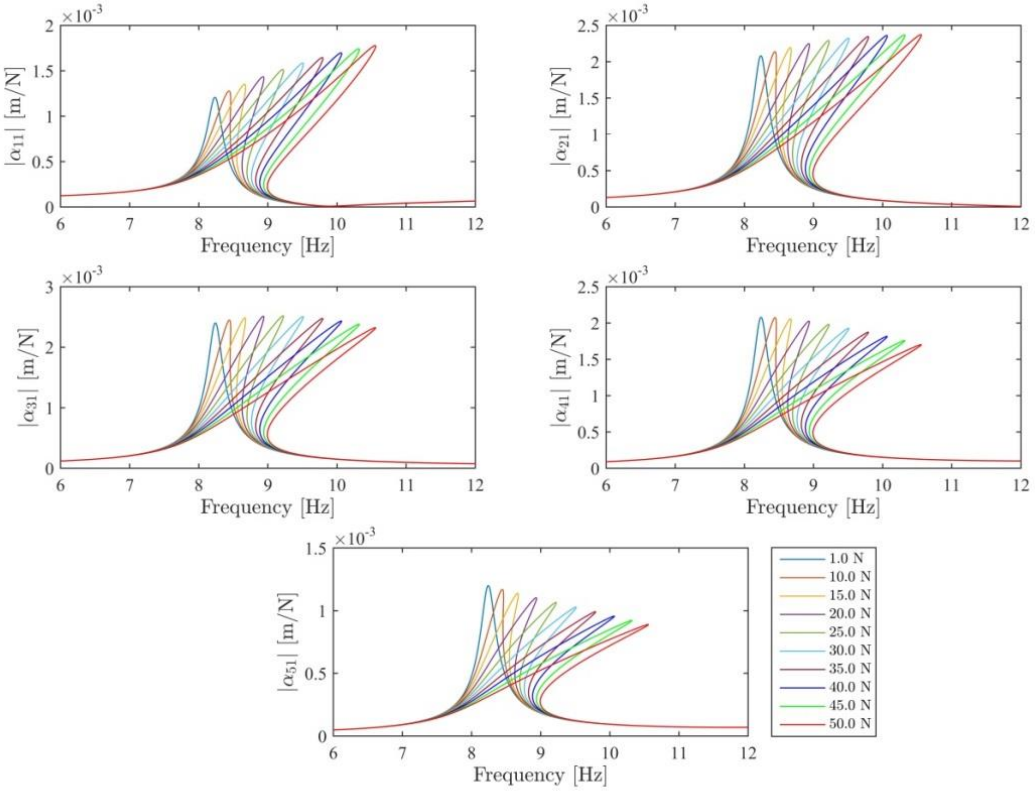

Figure 2-5. Constant-force FRFs of the 5 DOF system with cubic stiffness, obtained by the force-controlled stepped-sine testing simulations

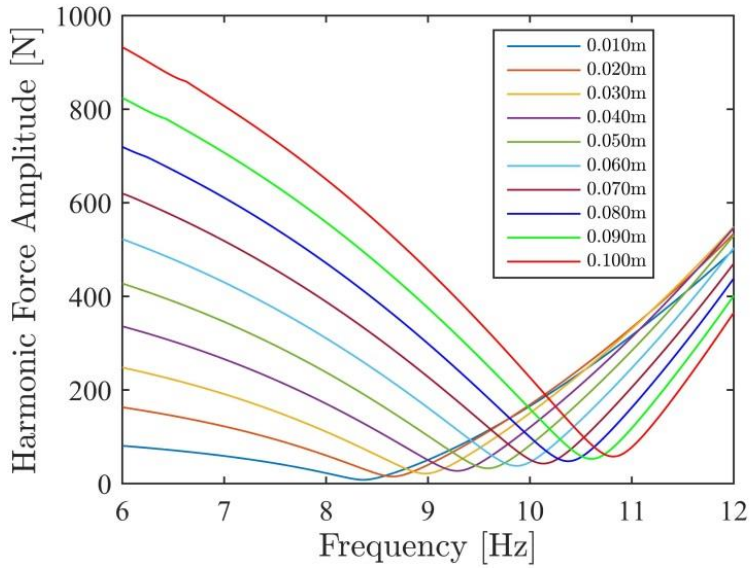

Figure 2-6. Harmonic force spectra of the driving point (1st DOF) of the 5 DOF nonlinear system obtained from the RCT simulations

The physics behind the quasi-linearization phenomenon is essentially very simple. When the displacement amplitude of the driving point is kept constant, if the NNM of interest is well separated from the other modes and no internal resonances occur, then the near-resonant deflection shape of the system can be approximated by the product of that single NNM with the modal amplitude. If the modal amplitude is kept constant, the deflection shape and so the energy level of the system is *frozen* throughout the frequency sweep in the vicinity of the resonant region. Accordingly, if this *frozen* deflection shape is fed into the nonlinearity matrix given in Eq. (2.3), this matrix remains also constant, which quasi-linearizes the equation of motion.

Even though the displacement level is kept constant through the frequency sweep, the resonant peaks are observed in the constant-response FRFs shown in Figure 2-7. These peaks result from the dip of the excitation force spectrum at the resonant point as shown in Figure 2-6.

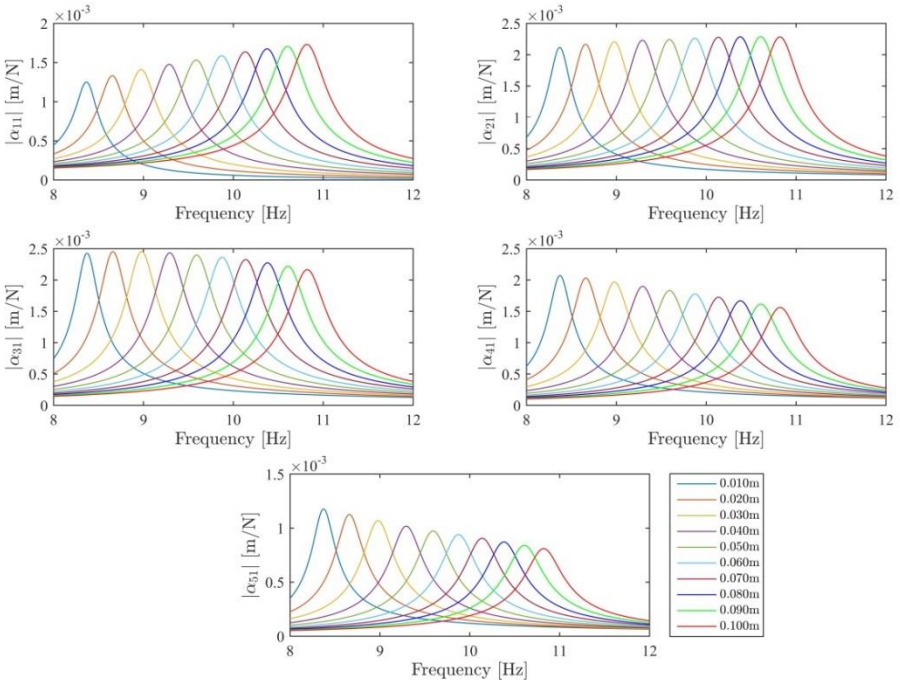

Figure 2-7. Constant-response FRFs of the 5 DOF system with cubic stiffness, obtained from the RCT simulations

It is important to note that the quasi-linearization holds true even when the shape of the NNM strongly depends on the response level as shown in Figure 2-8. The shape of the 1st NNM of the 5 DOF nonlinear system considered in this study deviates from a symmetric shape toward an asymmetric shape with increasing displacement amplitude level due to the missing cubic stiffness element between the 1st DOF and the ground as shown in Figure 2-3. Yet, the constant-response FRFs given in Figure 2-7 are still quasi-linear.

A final important observation made from Figure 2-7 is that the constant-response FRFs do not exhibit unstable branches although they cover the excitation forcing levels (1N to 50 N) studied in Section 2.5.1. As explained in Section 2.4.6, the points on the unstable branches are visited at different times during RCT carried out at different displacement amplitude levels. In other words, the points on the

unstable branch of a constant-force FRF given in Figure 2-5 are stabilized and shared among several different constant-response FRFs given in Figure 2-7. This point is explained further in Section 2.5.5 by using the HFS concept.

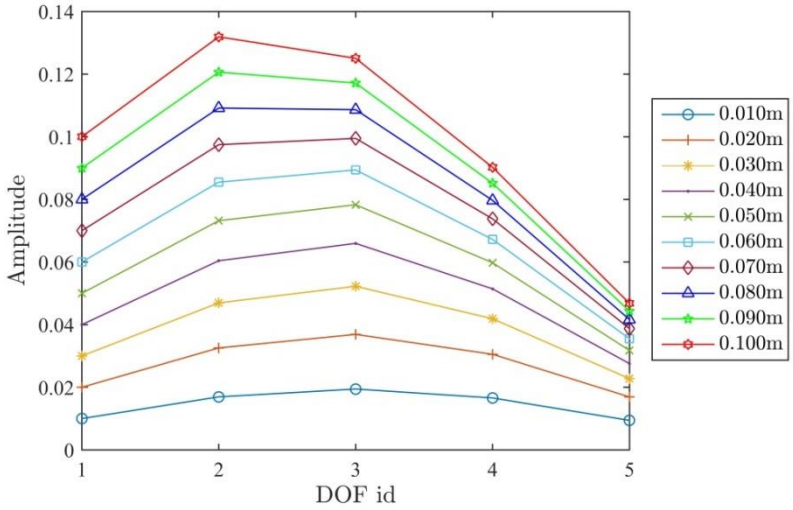

Figure 2-8. The shape change of the 1st NNM of the 5 DOF nonlinear system with the increasing displacement amplitude level

2.5.3 Identification of Nonlinear Modal Parameters from Quasi-Linear Constant-Response FRFs

Once the constant-response FRFs are determined by using the RCT simulations as shown in Figure 2-7, modal identification methods for linear systems can then be used to extract the nonlinear modal parameters as functions of the modal amplitude. In this study, the well-known peak-picking method is used to determine the modal parameters at each displacement amplitude level. As an example, the constant-response FRFs corresponding to the highest displacement amplitude level, i.e. 0.10 m, obtained by the RCT simulation are compared with the corresponding FRFs synthesized by using the modal parameters identified from the peak-picking

technique in Figure 2-9. The good match between the results of the simulated experiment and the corresponding linear analytical models shows that the constant-response FRFs are really quasi-linear.

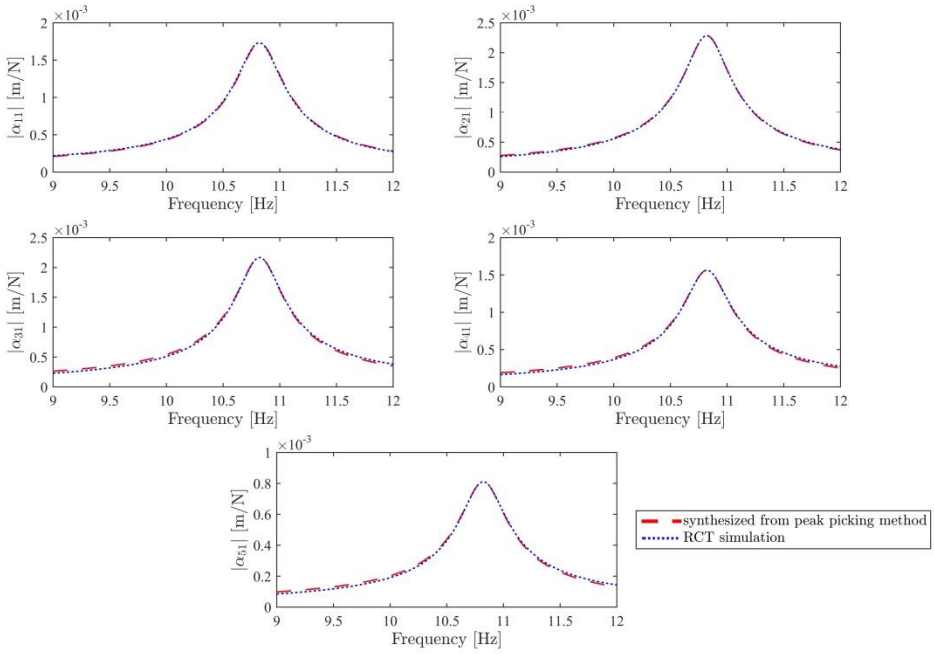

Figure 2-9. Comparison of the constant-response FRFs obtained from the RCT simulation, with the FRFs synthesized by using the modal parameters identified from the pick-peaking method at the 0.10 mm amplitude level

By processing each set of FRFs corresponding to each displacement amplitude level (see Figure 2-7) and collecting the modal parameters of the 1st mode; the variations of the natural frequency, the nonlinear modal damping ratio, and the modal constants with respect to the modal amplitude can be determined as shown in Figure 2-10 and Figure 2-11. Substituting these modal parameters into Eq. (2.24), one can predict the frequency responses of the system to various forcing scenarios without making any force-controlled test, which is very useful for the design and analysis of engineering structures. It should be noted that the modal

constants $\bar{A}_{jkr}$ given in Figure 2-11 are closely related with the mass normalized NNMs as shown in Eq. (2.23) and explained in Section 2.4.4. So, the RCT approach makes it possible to experimentally extract the mass normalized NNM from the identified modal constants given in Figure 2-11.

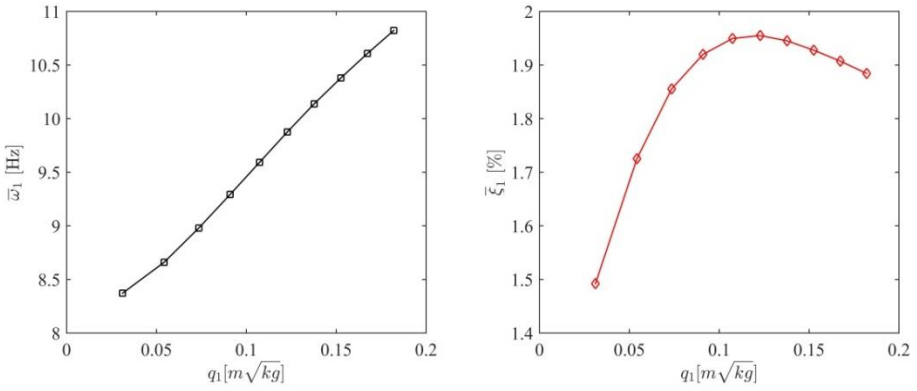

(a) (b)

Figure 2-10. Variation of the modal parameters corresponding to the 1st mode of the 5 DOF nonlinear system with the modal response level (a) natural frequency (b) viscous modal damping ratio

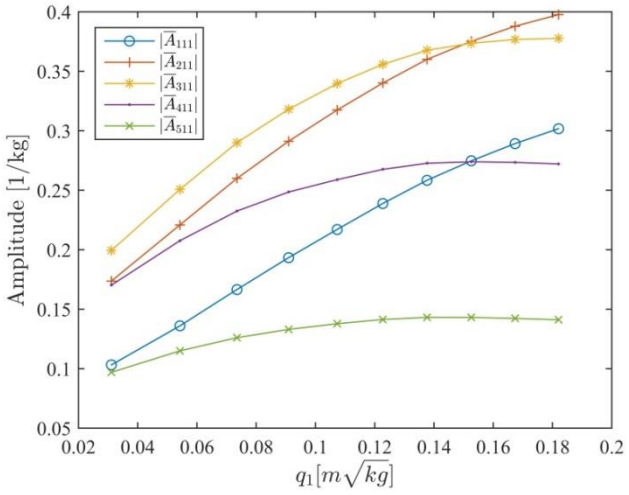

Figure 2-11. Variation of the modal constants corresponding to the 1st mode of the 5 DOF nonlinear system with the modal response level

2.5.4 Synthesis of Constant-Force FRFs by Using Nonlinear Modal Parameters Identified with RCT

The identified modal parameters that are given in Figure 2-10 and Figure 2-11 can be employed in Eq. (2.24) to synthesize frequency responses for various harmonic forcing scenarios. For validation, the frequency responses of all 5 dofs were synthesized at 50 N using Eq. (2.24) iteratively by applying Newton's Method with the arc-length continuation algorithm. These frequency responses were then normalized with 50 N and were compared with the results of the constant-force simulations as shown in Figure 2-12. The comparison was also made at different force levels as shown in Figure 2-13. The match between the computational results and the simulated experimental results is found to be satisfactory. It is important to note that the modal parameters given in Figure 2-10 and Figure 2-11 were used as look-up tables without necessitating any polynomial fit.

2.5.5 Experimental Extraction of Constant-Force FRFs by Using HFS

As an alternative to the analytical model based on the identified modal parameters, untested constant-force FRFs can also be determined directly from the experimental data by using the HFS concept. To do so, first of all, the harmonic force spectra already obtained from the RCT simulations at 10 different displacement amplitude levels were combined to construct the HFS as shown in Figure 2-14. Then, the surface was cut with the 50 N constant-amplitude plane as illustrated in Figure 2-15(a). The curve intersecting this plane and the HFS is nothing but the frequency response curve of the 1^{st} DOF corresponding to the 50 N forcing level. Finally, the receptance curve for the 1^{st} DOF was obtained by normalizing the frequency response curve with the amplitude of the excitation force. The comparison of the receptances obtained from the HFS approach with the ones synthesized by using the identified modal parameters, as well as with the

original receptances obtained from the simulated force-control experiment is shown in Figure 2-15(b).

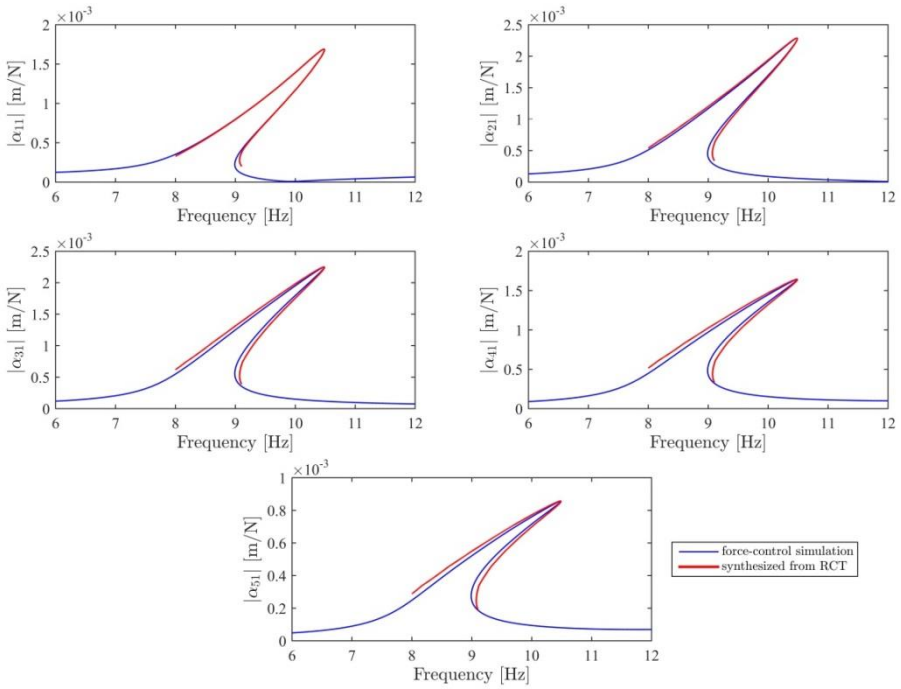

Figure 2-12. Comparison of the constant-force FRFs obtained from the simulated experiment, with the FRFs synthesized by using the nonlinear modal parameters of the 5 DOF nonlinear system at 50 N forcing amplitude level

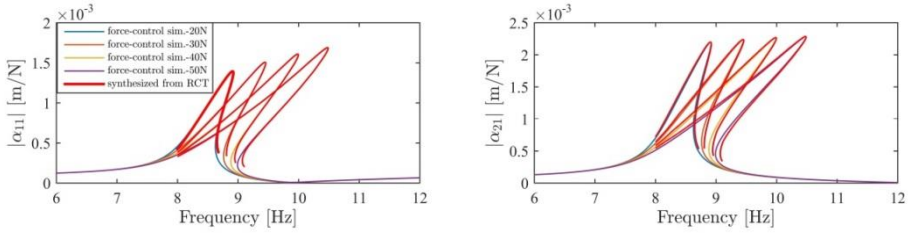

Figure 2-13. Comparison of the constant-force FRFs obtained from the simulated experiment, with the FRFs synthesized by using the nonlinear modal parameters of the 5 DOF nonlinear system at several different forcing amplitude levels

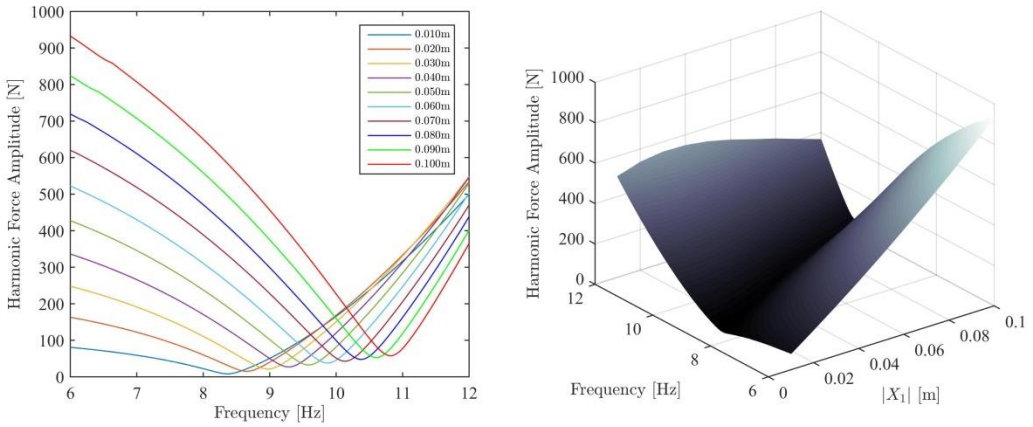

(a) (b)

Figure 2-14. Construction of the HFS corresponding to the 1st DOF by combining the harmonic force spectra with linear interpolation (a) harmonic excitation force spectra (b) HFS of the 1st DOF

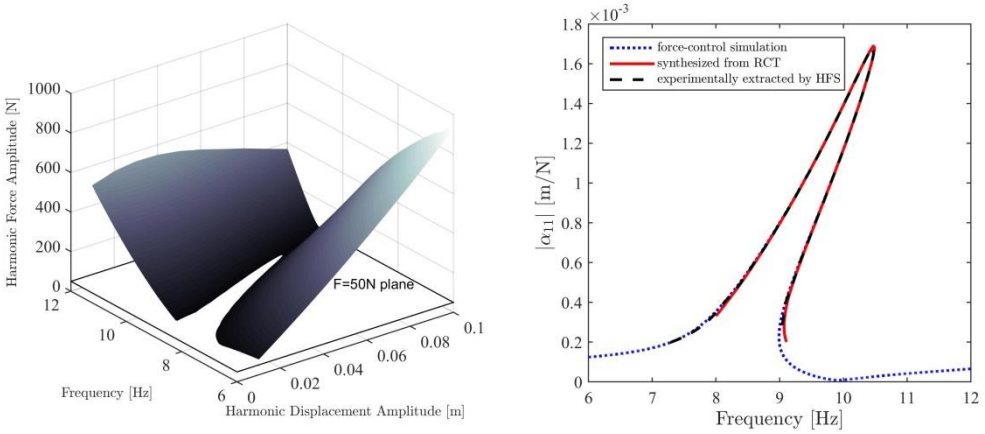

(a) (b)

Figure 2-15. (a) HFS of the 5 DOF nonlinear system (b) comparison of the receptances extracted by using the HFS approach, with the ones synthesized by using the nonlinear modal parameters identified from RCT, and with the original receptances obtained from the simulated force-control experiment at 50 N

2.5.6 Determination of Backbone Curves by Using Constant-Force Simulations

The frequency response curves of the 1st and 5th DOFs obtained from the constant-force simulations at force levels ranging from 10 N to 50 N and corresponding to the first mode are illustrated in Figure 2-16. In Figure 2-4, it is shown that the effect of higher harmonics is negligible for the force and displacement levels of interest. However, the stiffness nonlinearity is still strong in the sense that it leads to the overhanging unstable branches as shown in Figure 2-16. Although in a simulated experiment resonance peaks can accurately be determined with the help of the arc length continuation algorithm, in a real experiment this may not be possible due to a jump or, even worse, due to a premature jump as explained in Section 2.4.6. In the next section, it is demonstrated that by just using RCT and the HFS concept, the inaccuracies due to the jump can be avoided, which makes it possible to identify the backbone curve more accurately.

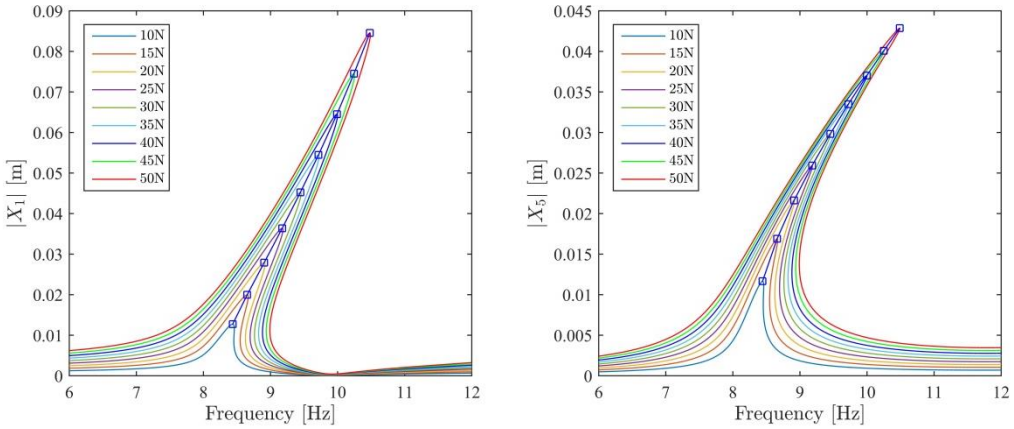

Figure 2-16. Determination of the backbone curves (blue square markers) of the 5 DOF nonlinear system corresponding to the 1st and 5th DOFs by using constant-force stepped-sine testing

2.5.7 Determination of Backbone Curves by Using HFS

The harmonic excitation force spectra of the driving point (1st DOF) obtained from the RCT simulations at several constant displacement amplitude levels ranging from 0.01 m to 0.1 m in the first mode are already illustrated in Figure 2-14(a). As explained in Section 2.5.5, the HFS corresponding to the 1st DOF is constructed by combining the harmonic excitation force spectra and using linear interpolation as shown in Figure 2-14(b).

By cutting the HFS with the constant force planes ranging from 10 N to 50 N (with 5 N increments) as shown in Figure 2-17(a), the constant-force frequency response curves of the 1st DOF are successfully extracted with the accurate resonance turning points and the unstable branches as demonstrated in Figure 2-17(b). Finally, the backbone curve of the 1st DOF is determined by combining the resonance peaks of the extracted frequency response curves as shown in the same figure.

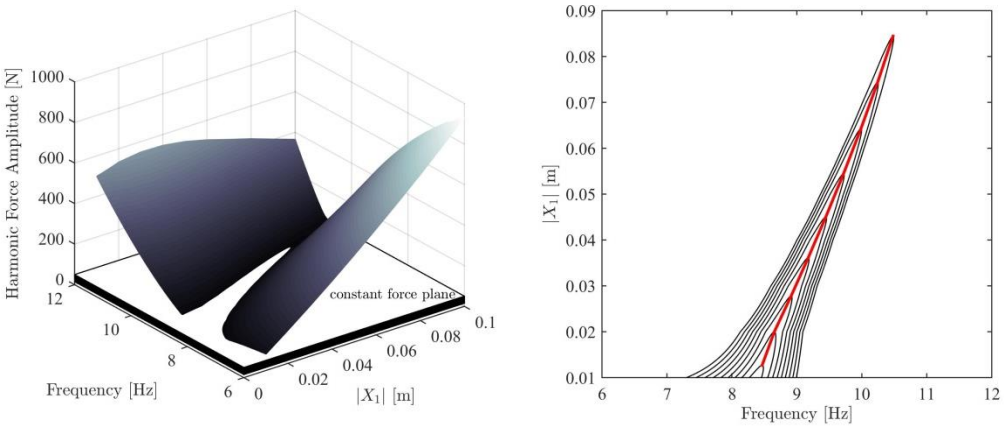

(a) (b)

Figure 2-17. (a) HFS of the 1st DOF cut with constant force planes (b) extraction of constant-force frequency response curves (black-ranging from 10N to 50N with 5N increments) and identification of the backbone curve (red) of the 1st DOF from HFS

In the case of a real experiment, the measurements of the unstable branches together with the smooth turning points shown in Figure 2-17(b) would not be possible with conventional constant-force testing due to the jump (or even worse, the premature jump) phenomenon, which eventually led the development of advanced experimental continuation techniques in the last decade to determine the backbone curves of structures exhibiting strong conservative nonlinearity. Alternatively, the RCT strategy combined with the HFS concept reveals that standard equipment can still do a good job in the experimental extraction of unstable branches and backbone curves. In the RCT-HFS approach, instead of consecutively tracing out the points on an unstable branch or a backbone curve, these points are measured at different times during stepped-sine tests carried out at different constant amplitude levels and then merged into the HFS.

It is important to note that the HFS given in Figure 2-17(a) was constructed by considering the displacement amplitudes of the 1st DOF, i.e. $|X_1|$, as can be seen from the label of the displacement axis. So, this surface specifically belongs to the 1st DOF, and can only be used to obtain the constant-force frequency response curves of the 1st DOF. In order to obtain the frequency responses of another DOF, the HFS needs to be reconstructed by considering the displacement amplitudes of that specific DOF. As an example, the HFS corresponding to the 5th DOF is illustrated in Figure 2-18(a). Once again, the constant-force frequency response curves and the backbone curve corresponding to the 5th DOF are successfully determined as shown in Figure 2-18(b).

Finally, the backbone curves determined from the HFS approach are compared with those obtained from the constant-force simulations for the 1st and 5th DOFs as shown in Figure 2-19. The excellent match indicates that the HFS is a very promising concept to extract the backbone curves of strongly nonlinear systems directly from experimental measurements. It is interesting to note that once the backbone curves corresponding to several different measurement points are experimentally identified as illustrated in Figure 2-19, collecting the points on these backbone curves corresponding to the same resonance frequency (or

equivalently energy level) into a vector gives the NNM of the structure at that energy level. This is an alternative way of obtaining NNMs of a nonlinear structure directly from experimental measurements to the one proposed in Section 2.4.4, where the experimentally identified nonlinear modal constants are used to calculate NNMs.

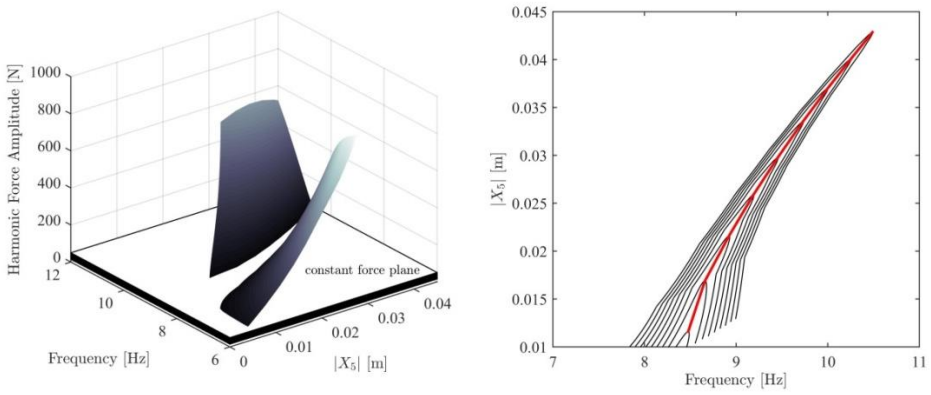

(a) (b)

Figure 2-18. (a) HFS of the 5th DOF cut with constant force planes (b) extraction of constant-force frequency response curves (black-ranging from 10 N to 50 N with 5 N increments) and backbone curve (red) of the 5th DOF from HFS

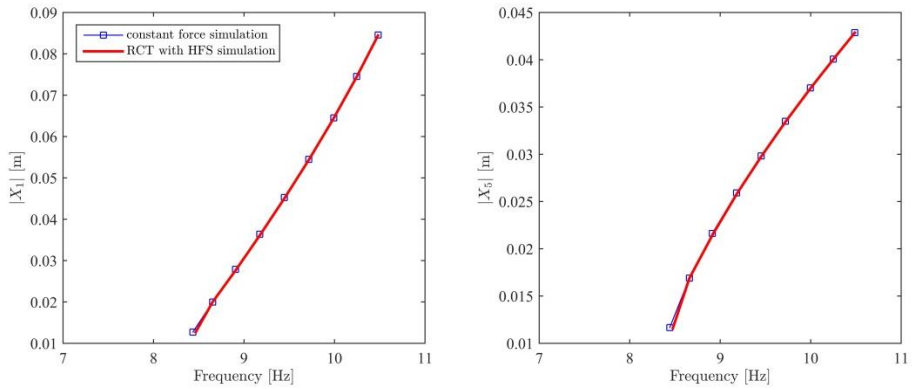

(a) (b)

Figure 2-19. Comparison of the backbone curves obtained from RCT with HFS simulations with those obtained from constant force simulations (a) backbone curve of the 1st DOF (b) backbone curve of the 5th DOF

CHAPTER 3

NONPARAMETRIC IDENTIFICATION OF NONLINEARITIES IN THE SPATIAL DOMAIN BY USING RESPONSE-CONTROLLED STEPPED-SINE TESTING: THE DESCRIBING SURFACE METHOD

The Describing Function Method (DFM), which was essentially developed for the harmonic vibration analysis of nonlinear systems, was proposed in [53] in the early 1990s. It is mathematically equivalent to the classical Harmonic Balance Method (HBM). The major difference between the DFM and the HBM relies on the interpretation of nonlinear internal forces. The HBM expresses nonlinear internal forces as a single force vector, whereas in the DFM they are written as a multiplication of the displacement vector with the so-called nonlinearity matrix which has an important physical meaning. The real and imaginary parts of this matrix essentially correspond to the equivalent nonlinear stiffness and damping matrices at a given response level, respectively. This simple but innovative idea was first prosed by Budak and Özgüven [91, 92] in their studies investigating the harmonic vibration responses of nonlinear MDOF systems. Later, the method was generalized for any type of nonlinearity by Tanrıkulu et al. [53] by using describing functions [93], after which this approach is named the DFM.

The concept of using the nonlinearity matrix approach in nonlinear system identification was first suggested by Özer and Özgüven [54], and a method was developed to identify the type and parametric values of a nonlinear element between the ground and a single coordinate in an MDOF system, which is later extended to identify a single nonlinear element between any two coordinates of the system [55]. It was further improved by Aykan and Özgüven [56] by using incomplete FRF data which makes the method applicable to large systems with localized nonlinearity. These parametric identification methods based on the

classical DFM are restricted to the cases where nonlinearity is not a function of frequency.

This thesis work proposes a novel frequency-domain nonparametric identification technique, namely the *Describing Surface Method* (DSM), which extends the methods mentioned above to the identification of nonlinearities which can be functions of both displacement amplitude and frequency. Moreover, since nonlinearity does not need to be mathematically expressible in terms of response amplitude and frequency, in the proposed method, complex nonlinearities can easily be identified nonparametrically contrary to the DFM-based identification methods which are restricted to the parametric representation of nonlinearity.

It is important to note that the current formulation of the DSM restricts its application to structures where a single nonlinear element is localized between the excitation point and the ground. Currently, the DSM does not apply in the case of a nonlinearity localized between two internal coordinates or in the case of multiple nonlinearities spread over the structure of interest. In such cases, the reader is recommended to use the experimental modal analysis approach introduced in Chapter 2.

For the sake of completeness, the theoretical bases of the DFM [53] and the nonlinearity matrix concept are summarized below before introducing the so-called DSM.

3.1 The Classical Describing Function Method

The equation of motion for a nonlinear MDOF system under harmonic excitation can be written as

$$[M]\{\ddot{x}\} + [C]\{\dot{x}\} + [K]\{x\} + \{N(x, \dot{x})\} = \{f\}, \tag{3.1}$$

where $[M]$, $[C]$ and $[K]$ are the mass, viscous damping, and stiffness matrices of the underlying linear system, respectively. Here, the vectors $\{x\}$ and $\{f\}$ represent

the response of the system and the external force applied to it, respectively. $\{N\}$ is the nonlinear internal force in the system.

Consider a harmonic excitation of

$$\{f\} = \{F\}e^{i\omega t}, \tag{3.2}$$

where $\{F\}$ denotes the amplitude of forcing, ω represents the excitation frequency. "i" shows the unit imaginary number. The response is assumed to be harmonic with a response amplitude of $\{X\}$. Neglecting all the sub- and super-harmonic terms, the internal nonlinear forces can be written as

$$\{N\} = \{G\}e^{i\omega t}, \tag{3.3}$$

where the amplitude of the internal nonlinear forcing vector can be expressed [53] as

$$\{G\} = [\Delta]\{X\}. \tag{3.4}$$

Here $[\Delta]$ is called the nonlinearity matrix, and it is response level dependent.

Tanrıkulu et al. [53] proposed the use of describing functions for the evaluation of the nonlinearity matrix, $[\Delta]$. The elements of $[\Delta]$ are obtained as follows

$$\Delta_{rr} = \upsilon_{rr} + \sum_{\substack{s=1 \\ s\neq r}}^{n} \upsilon_{rs}, \tag{3.5}$$

$$\Delta_{rs} = -\upsilon_{rs}. \tag{3.6}$$

Here, n is the total degrees of freedom of the system and υ_{rs} is the harmonic describing function representation of the nonlinear internal force which can be obtained as

$$\upsilon_{rs} = \frac{i}{\pi Y_{rs}} \int_0^{2\pi} N_{rs} e^{i\psi}\, d\psi, \tag{3.7}$$

where N_{rs} and Y_{rs} are, respectively, the amplitudes of the nonlinear internal force and the relative displacement between coordinates r and s for $r \neq s$, and between r^{th} coordinate and the ground for $r = s$.

$$Y_{rs} = \begin{Bmatrix} if\ r \neq s, & X_r - X_s \\ if\ r = s, & X_r \end{Bmatrix} \tag{3.8}$$

and

$$\psi = \omega t. \tag{3.9}$$

Then, the response vector $\{X\}$ can be written as

$$\{X\} = [H^{NL}]\{F\}, \tag{3.10}$$

where $[H^{NL}]$ is the nonlinear receptance matrix and it can be evaluated as

$$[H^{NL}] = (-\omega^2[M] + i\omega[C] + [K] + [\Delta])^{-1}. \tag{3.11}$$

As the elements of the nonlinearity matrix $[\Delta]$ are functions of the response itself, an iterative procedure is to be applied to calculate the response amplitude $\{X\}$ from Eq. (3.10). Details of the DFM can be found in [53].

3.2 The Describing Surface Method

Inverting the nonlinear receptance matrix given by Eq. (3.11) yields

$$-\omega^2[M] + i\omega[C] + [K] + [\Delta] = [H^{NL}]^{-1}. \tag{3.12}$$

Similarly, the inverse of the receptance matrix of the underlying linear system can be written as

$$-\omega^2[M] + i\omega[C] + [K] = [H^{L}]^{-1}. \tag{3.13}$$

Subtracting Eq. (3.13) from Eq. (3.12) yields

$$[\Delta] = [H^{NL}]^{-1} - [H^{L}]^{-1}. \tag{3.14}$$

Consider an MDOF system with localized nonlinearity at a single coordinate, say a nonlinear element between coordinate p and the ground. Then the nonlinearity matrix $[\Delta]$ will include only a single nonzero element Δ_{pp} as follows

$$[\Delta] = \begin{bmatrix} 0 & \cdots & 0 \\ \vdots & \Delta_{pp} & \vdots \\ 0 & \cdots & 0 \end{bmatrix}. \tag{3.15}$$

Since there is a single nonlinear element in the system, Eq. (3.15) yields

$$\Delta_{pp} = \upsilon_{pp}, \tag{3.16}$$

where υ_{pp} is the describing function of nonlinearity between coordinate p and the ground.

Substituting Eqs. (3.15)-(3.16) into Eq. (3.14) and using the single-degree-of-freedom (SDOF) assumption at coordinate p yields

$$\upsilon_{pp}\left(|X_p|, \omega\right) = 1/H_{pp}^{NL} - 1/H_{pp}^{L}. \tag{3.17}$$

where $|X_p|$ denotes the displacement amplitude at coordinate p and ω is the excitation frequency. Here, H_{pp}^{L} and H_{pp}^{NL} represent point FRFs of the underlying linear and nonlinear MDOF systems at p^{th} coordinate, respectively.

For the sake of simplicity, subscript p will be dropped out hereafter. Displacement amplitudes $|X_p|$ will be referred to generically by $|X|$. Similarly, the H_{pp}^{L} and H_{pp}^{NL} terms will be represented generically by H^{L} and H^{NL}, respectively.

If the nonlinear system has multiple nonlinearities at the same location (with potentially hysteretic terms), nonlinear internal forces may not be negligible at very low or very high vibration levels. Consequently, the receptance of the underlying linear system H^{L} may not be measured accurately. An alternative solution could be to eliminate H^{L} from Eq. (3.17) as explained below.

Consider that response controlled stepped-sine tests (RCT) were conducted successively by keeping the displacement amplitude constant at levels $|X^{k}|$ and

$|X^{k+1}|$ with closed-loop control. Then, the describing function of nonlinearity at these vibration levels can be written as

$$v(|X^k|,\omega) = 1/H^{NL}_{|X^k|} - 1/H^L, \tag{3.18}$$

$$v(|X^{k+1}|,\omega) = 1/H^{NL}_{|X^{k+1}|} - 1/H^L. \tag{3.19}$$

where superscripts $k,\ k+1$ denote successive amplitude levels.

Subtracting Eq. (3.18) from Eq. (3.19) yields

$$v(|X^{k+1}|,\omega) - v(|X^k|,\omega) = 1/H^{NL}_{|X^{k+1}|} - 1/H^{NL}_{|X^k|}. \tag{3.20}$$

Dividing Eq. (3.20) by $\delta X = |X^{k+1}| - |X^k|$ yields a finite difference approximation to the partial derivative of $v(|X|,\omega)$ with respect to $|X|$ within the interval $[|X^k|, |X^{k+1}|]$ as follows:

$$\partial v/\partial |X| \approx \left(1/H^{NL}_{|X^{k+1}|} - 1/H^{NL}_{|X^k|}\right)/(|X^{k+1}| - |X^k|),\ \ |X| \in [|X^k|, |X^{k+1}|]. \tag{3.21}$$

By using the above formulation, the main algorithm of the DSM can be given as follows:

1. A stepped-sine test is conducted at a constant displacement amplitude level $|X^1|$ and the corresponding nonlinear receptance H^{NL} is measured (within the frequency range of interest). The same procedure is repeated at successive vibration levels $|X^2|, \dots, |X^k|, |X^{k+1}|, \dots |X^n|$.

2. The right-hand side of Eq. (3.21) is calculated as a nonparametric function of $|X|$ at each interval $[|X_k|, |X_{k+1}|]$ by using the measured nonlinear FRFs.

3. Differential Eq. (3.21) is solved numerically for $v(|X|,\omega_1), v(|X|,\omega_2)$, etc., i.e. for each frequency point separately. Then the describing functions determined at all frequency points are combined to construct the describing function surface $v(|X|,\omega)$. In this study, Eq. (3.21) is solved by using the finite element method.

4. The estimate of the FRF of the underlying linear system, then, can be obtained as follows

$$H^L = 1/\left(1/H^{NL}_{|X^k|} - \upsilon(|X^k|, \omega)\right). \quad (3.22)$$

Since H^L is unique, $|X^k|$ can be any of the constant displacement amplitude levels tested, i.e. $|X^1|$ or $|X^2|$, etc.

5. Finally, the response of the nonlinear system to any harmonic forcing can be determined iteratively by applying Newton's Method and the arc-length continuation algorithm to the following equation

$$X = F/\left(1/H^L + \upsilon(|X|, \omega)\right). \quad (3.23)$$

Important clues for a successful application of the DSM are as follows:

- Describing surface of nonlinearity $\upsilon(|X|, \omega)$ is actually a complex function. Its real and imaginary parts stand for the equivalent nonlinear stiffness and nonlinear damping terms, respectively. Consequently, equation (3.21) has to be evaluated for the real and imaginary parts separately.

- Eq. (3.21) is a first-order differential equation and needs a specific boundary value for a unique solution. If the measured FRF converges to a linear FRF at a low vibration level, then the appropriate boundary values for the real and imaginary parts of $\upsilon(|X|, \omega)$ are $Re\left(\upsilon(0, \omega)\right) = 0$ and $Im\left(\upsilon(0, \omega)\right) = 0$, respectively. On the other hand, if the measured FRF converges to a linear FRF at high vibration levels, then the appropriate boundary values for the real and imaginary parts of $\upsilon(|X|, \omega)$ are $Re\left(\upsilon(\infty, \omega)\right) = 0$ and $Im\left(\upsilon(\infty, \omega)\right) = 0$, respectively.

- As another example, if a structure includes cubic stiffness and Coulomb friction, the appropriate boundary values for the real and imaginary parts of $\upsilon(|X|,\omega)$ would be $Re\big(\upsilon(0,\omega)\big)=0$ and $Im\big(\upsilon(\infty,\omega)\big)=0$, respectively.

- In structures with complex nonlinear behavior, deciding on the appropriate boundary value and consequently determining the absolute value of the describing surface of the nonlinearity may be difficult. In such cases, Eq. (3.18) can be substituted into Eq. (3.23) to obtain

$$X = F/\Big(1/H^{NL}_{|X^s|}+\upsilon(|X|,\omega)-\upsilon(|X^s|,\omega)\Big). \qquad (3.24)$$

  which is an alternative form of Eq. (3.23), and it takes the nonlinear FRF measured at displacement level $|X^s|$ as the reference, instead of the linear FRF.

- In the most general case, different displacement levels can be chosen as the reference values for the real and imaginary parts of the complex dynamic stiffness, which puts Eq. (3.24) into the following form

$$X = F/\Big(Re\left(1/H^{NL}_{|X^s|}+\upsilon(|X|,\omega)-\upsilon(|X^s|,\omega)\right)+Im\left(1/H^{NL}_{|X^r|}+\upsilon(|X|,\omega)-\upsilon(|X^r|,\omega)\right)\Big). \qquad (3.25)$$

  where $|X^s|\neq|X^r|$.

- In solving Eq. (3.21) numerically, it is usually a good practice to start with the assumption that $\upsilon(|X|,\omega)$ is C^o continuous, which means that the partial derivative value calculated using the right-hand side of Eq. (3.21) is assumed to be constant for each interval $[|X^k|,|X^{k+1}|]$. In all of the experimental case studies given in this thesis work (see Section 4), $\upsilon(|X|,\omega)$ is assumed to be C^o continuous.

- Since the nonlinear FRF at absolute zero vibration level cannot be measured, the partial derivative within the interval $[0,|X^1|]$ cannot be obtained directly from measurements. In that case, the missing information can be obtained by linear extrapolation. So, if $\upsilon(|X|,\omega)$ is assumed to be C^o continuous, linear

extrapolation corresponds to taking the partial derivative within the interval $[0, |X^1|]$ to be equal to the one calculated in the interval $[|X^1|, |X^2|]$.

As discussed at the beginning of this chapter, in the case of a structure where a single nonlinear element is localized between the excitation point and the ground, the application of the DSM is straightforward. However, in the case of structures with several localized nonlinearities at different locations, the application of the DSM requires that each nonlinearity is isolated from the structure and identified separately. For example, if it is desired to identify the equivalent nonlinear stiffness and damping at the mounting interface of an aircraft pylon and its payload by using the DSM, the pylon has to be isolated from the aircraft and rigidly fixed to the ground. On the other hand, the main wings of an aircraft which include many riveted and bolted connections as well as wide contacting surfaces are examples of structures with distributed nonlinearities. The application of the DSM to such distributed nonlinearities requires the direct implementation of Eq. (3.14) which is not so straightforward as there are several critical issues such as missing elements of the linear and nonlinear receptance matrices which may not be measured due to physical limitations and sensitivity of matrix inversions to measurement error. In the case of such distributed nonlinearities, it is recommended to apply the experimental modal analysis methodology based on response-controlled stepped-sine testing (RCT) and the harmonic force surface (HFS) concept as introduced in Chapter 2.

3.3 Numerical Case Studies

3.3.1 SDOF System with Cubic Stiffness Element

The first case study consists of an SDOF system with a cubic stiffness element as shown in Figure 3-1. System parameters are as follows: $m = 0.2\,kg,\ k =$

$12633\ N/m,\ \ c = 5\ Ns/m,\ \ k^* = 2.667 \cdot 10^8\ N/m^3$. The linear stiffness was adjusted such that the natural frequency of the underlying linear system is exactly at 40 Hz.

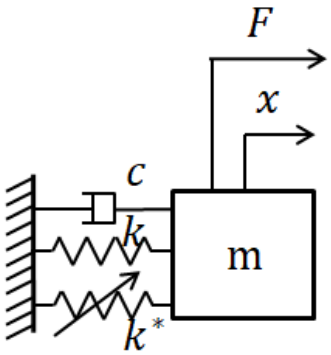

Figure 3-1. SDOF system with cubic stiffness nonlinearity

In this study, a series of stepped-sine test simulations were conducted at 6 different constant displacement amplitude levels ranging from 2.5 mm to 4.5 mm. Response and force signals calculated in the time domain were polluted with noise generated by using the randn() function of Matlab. In order to demonstrate the robustness of the proposed technique, the noise level was taken to be about 20%-30% of the original signal amplitude, which is an excessively exaggerated level that cannot be encountered in real life. The resulting frequency response functions obtained from the virtual experiment are shown in Figure 3-2 in comparison with the frequency response function of the underlying linear system.

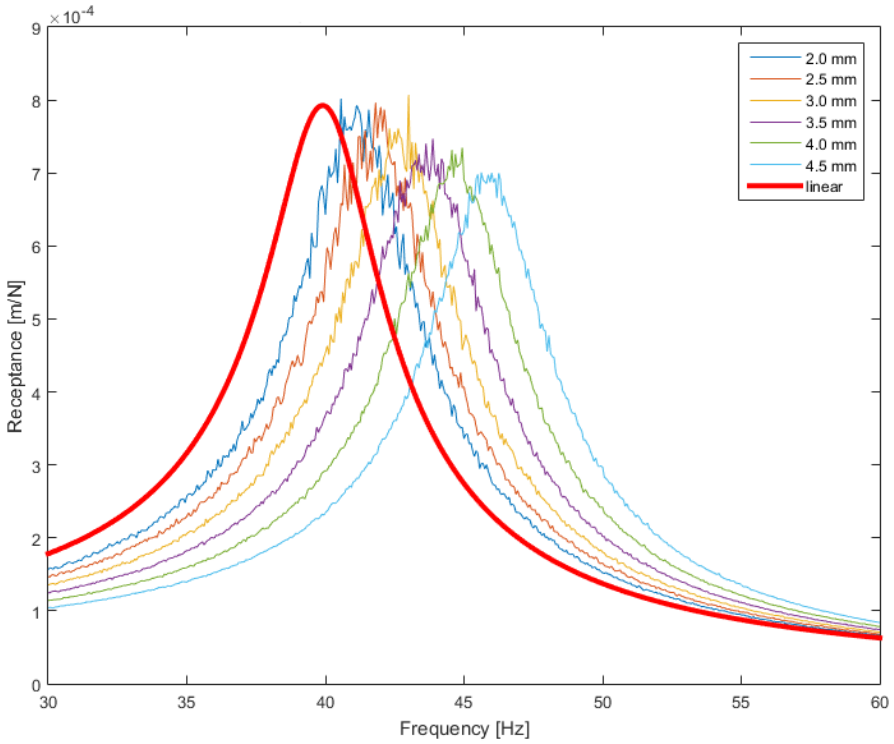

Figure 3-2. Constant-response FRFs of the SDOF system with cubic stiffness nonlinearity obtained from virtual response-controlled stepped-sine testing

By applying Eq. (3.21) to the virtual experimental FRF data given in Figure 3-2, the real and imaginary parts of the partial derivative of the describing surface of nonlinearity are obtained as shown in Figure 3-3 and Figure 3-4, respectively. Due to excessive noise, the partial derivatives turn out to be considerably scattered. However, the best polynomial surface fits give very good estimates of the partial derivatives as illustrated in the same figures, which demonstrates the robustness of the DSM.

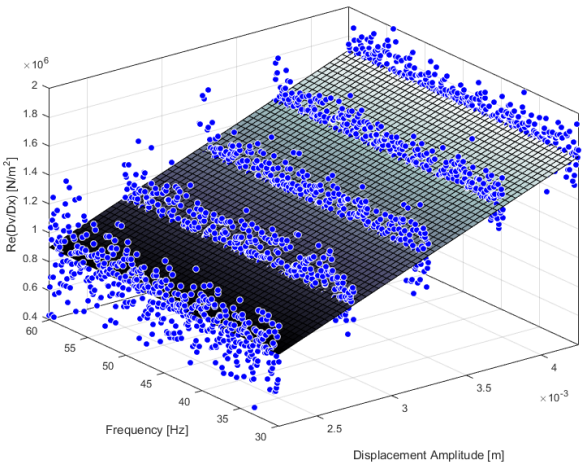

Figure 3-3. The real part of the partial derivative of the describing surface of nonlinearity of the SDOF system with cubic stiffness element

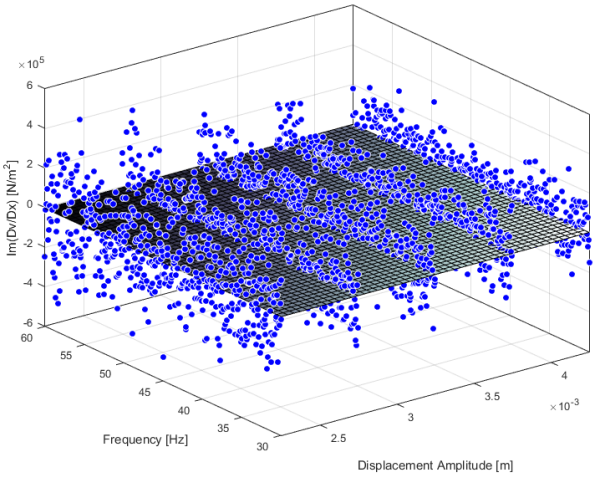

Figure 3-4. The imaginary part of the partial derivative of the describing surface of nonlinearity of the SDOF system with cubic stiffness element

By integrating the partial derivative surfaces, the real and imaginary parts of the describing surface of nonlinearity are determined as shown in Figure 3-5 and Figure 3-6.

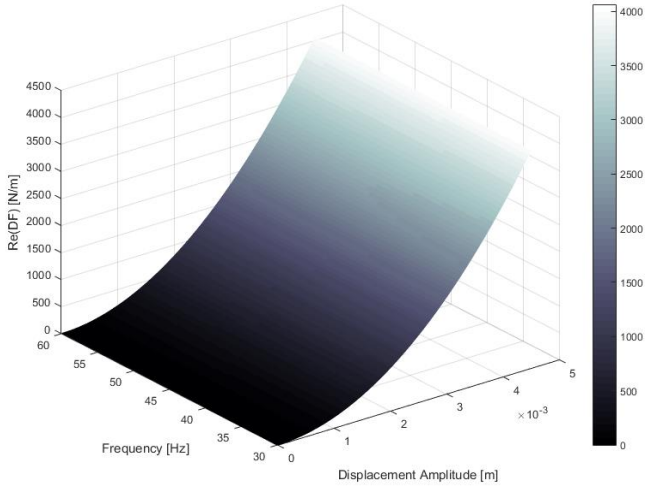

Figure 3-5. The real part of the describing surface of nonlinearity of the SDOF system with cubic stiffness element

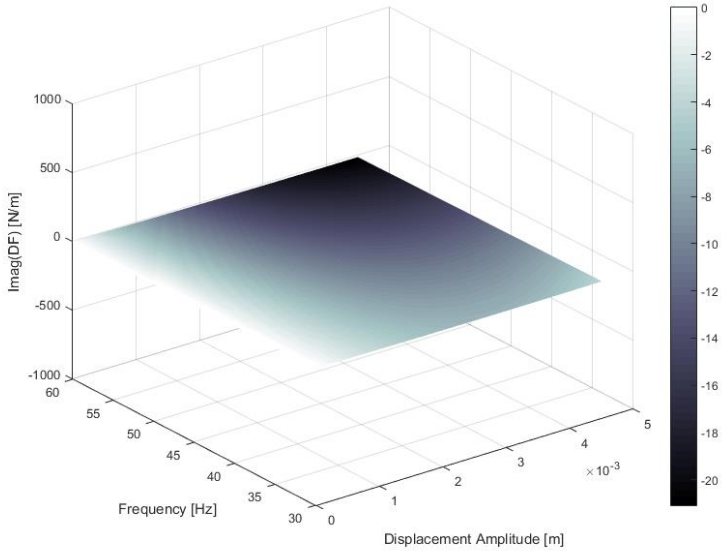

Figure 3-6. The imaginary part of the describing surface of nonlinearity of the SDOF system with cubic stiffness element

The real part of the identified describing surface of nonlinearity shown in Figure 3-5 indicates nothing but the stiffness nonlinearity of the system in physical, i.e. spatial, coordinates. The comparison of the surface with the theoretical model of

the cubic stiffness nonlinearity is illustrated in Figure 3-7. As can be observed from the figure, the match between the identified surface and the theoretical cubic stiffness model, $\nu = \frac{3}{4}(2.667 \cdot 10^8)X^2$, is perfect, which validates the DSM.

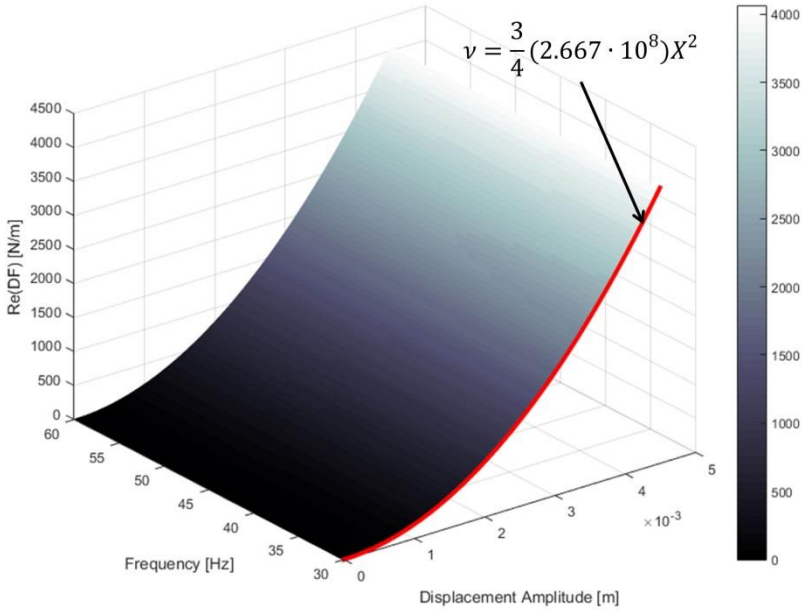

Figure 3-7. Comparison of the real part of the identified describing surface of nonlinearity with the theoretical model of the cubic stiffness element

Another important observation that can be made from Figure 3-7 is that the describing surface of stiffness nonlinearity does not exhibit any frequency dependence. In other words, the cut of the surface with a vertical plane at each constant frequency point gives exactly the same curve, which is naturally expected because the theoretical formulation of the cubic stiffness nonlinearity, $\nu = \frac{3}{4}(2.667 \cdot 10^8)X^2$, only depends on the vibration amplitude and does not involve any frequency term.

Coming to the imaginary part of the describing surface of nonlinearity shown in Figure 3-6, this surface definitely indicates zero damping nonlinearity. This is exactly what is expected because the mathematical model of the SDOF system exhibits only some amount of linear viscous damping but does not involve any damping nonlinearity.

Finally, the FRF of the underlying linear system is estimated by plugging the identified describing surface of nonlinearity into Eq. (3.22). It should be noted that in this formulation, FRF measured at any displacement amplitude level can be used. Theoretically, all the estimates of the linear FRF obtained from the FRFs measured at different displacement amplitude levels must be exactly the same as demonstrated in Figure 3-8. As observed from the figure, the match between the estimated linear FRF and the exact theoretical FRF is perfect.

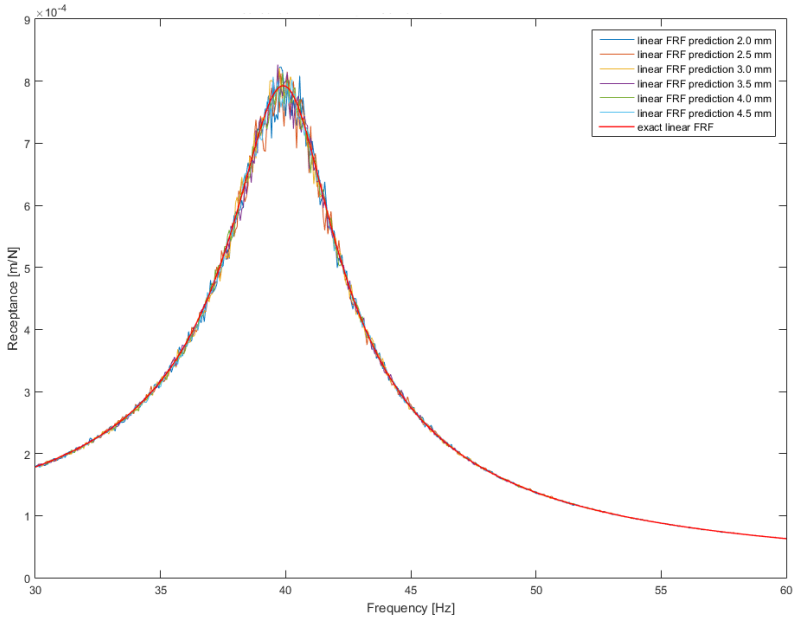

Figure 3-8. FRF of the underlying linear system that is estimated by using identified describing surface of nonlinearity of the SDOF system with cubic stiffness

3.3.2 SDOF System with Cubic Stiffness and Coulomb Friction Elements

The second case study consists of an SDOF system with a cubic stiffness element and a Coulomb friction element as shown in Figure 3-9. System parameters are as follows: $m = 0.2\,kg$, $k = 12633\,N/m$, $c = 5\,Ns/m$, $k^* = 2.667 \cdot 10^8\,N/m^3$, $c_f = 0.25\,N$.

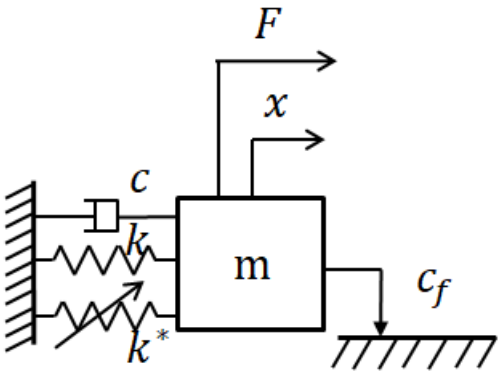

Figure 3-9. SDOF system with cubic stiffness and Coulomb friction nonlinearities

Similar to the previous case study, a series of stepped-sine test simulations were conducted at 9 different constant displacement amplitude levels ranging from 0.5 mm to 4.5 mm. Once again, response and force signals calculated in the time domain were polluted with noise whose level is around 20%-30% of the original signal amplitude. The resulting frequency response functions obtained from the virtual experiment are illustrated in Figure 3-10.

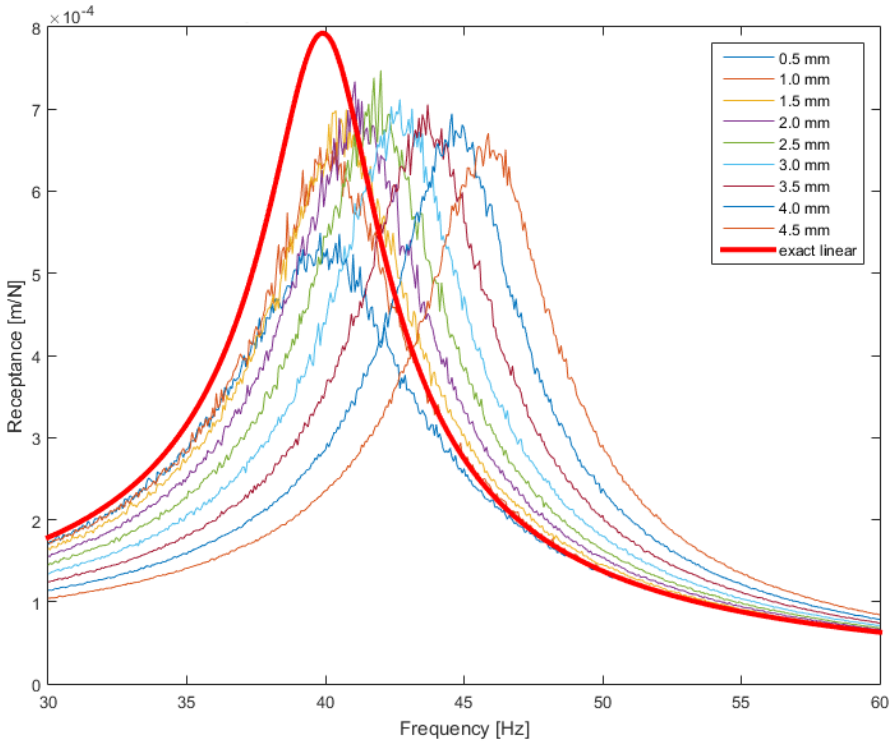

Figure 3-10. Constant-response FRFs of the SDOF system with cubic stiffness and Coulomb friction elements obtained from virtual response-controlled stepped-sine testing

By applying Eq. (3.21) to the virtual experimental FRF data given in Figure 3-10, the real and imaginary parts of the partial derivative of the describing surface of nonlinearity are obtained as shown in Figure 3-11 and Figure 3-12, respectively. Due to the excessive noise, the partial derivatives turn out to be considerably scattered. However, the best polynomial surface fits give very good estimates of the partial derivatives as illustrated in the same figures, which demonstrates the robustness of the proposed DSM.

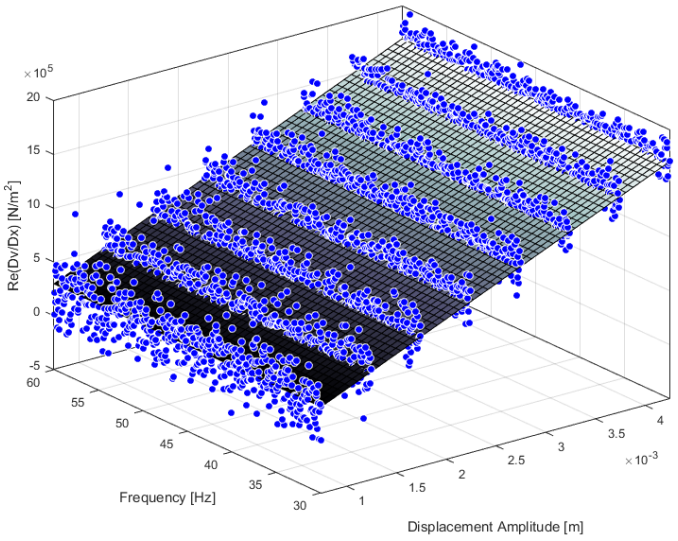

Figure 3-11. The real part of the partial derivative of the describing surface of nonlinearity of the SDOF system with cubic stiffness and Coulomb friction elements

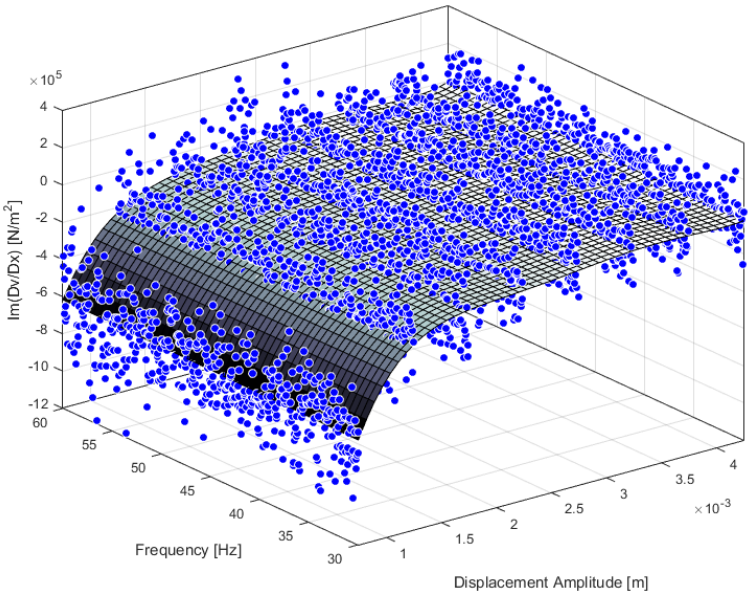

Figure 3-12. The imaginary part of the partial derivative of the describing surface of nonlinearity of the SDOF system with cubic stiffness and Coulomb friction elements

By integrating the partial derivative surfaces, the real and imaginary parts of the describing surface of nonlinearity are determined as shown in Figure 3-13 and Figure 3-14.

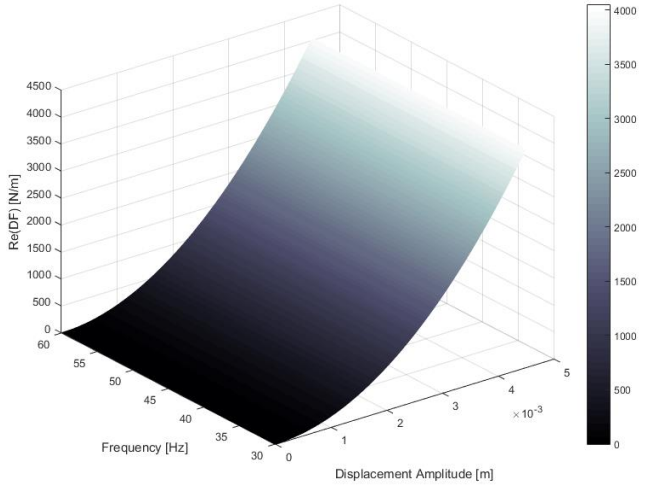

Figure 3-13. The real part of the describing surface of nonlinearity of the SDOF system with cubic stiffness and Coulomb friction elements

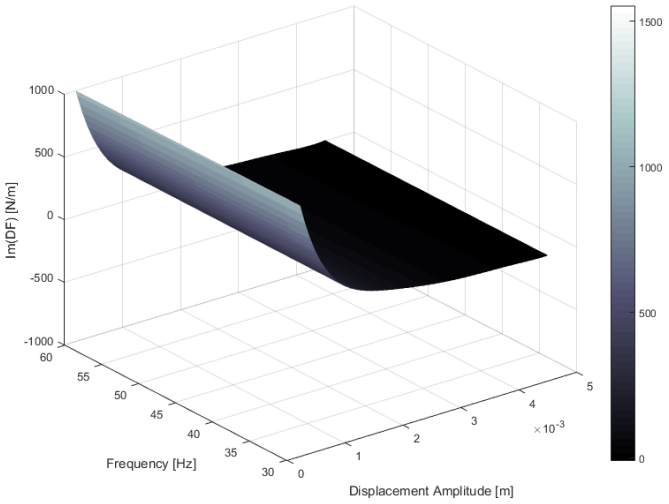

Figure 3-14. The imaginary part of the describing surface of nonlinearity of the SDOF system with cubic stiffness and Coulomb friction elements

The real and imaginary parts of the identified describing surface of nonlinearity shown in Figure 3-13 and Figure 3-14 correspond to the stiffness nonlinearity and the damping nonlinearity of the system in spatial coordinates, respectively. Comparisons of these surfaces with corresponding theoretical models are given Figure 3-15 and Figure 3-16.

As can be seen from Figure 3-15, the match between the real part of the describing surface and the theoretical cubic stiffness model, $\nu = \frac{3}{4}(2.667 \cdot 10^8)X^2$, is perfect once again.

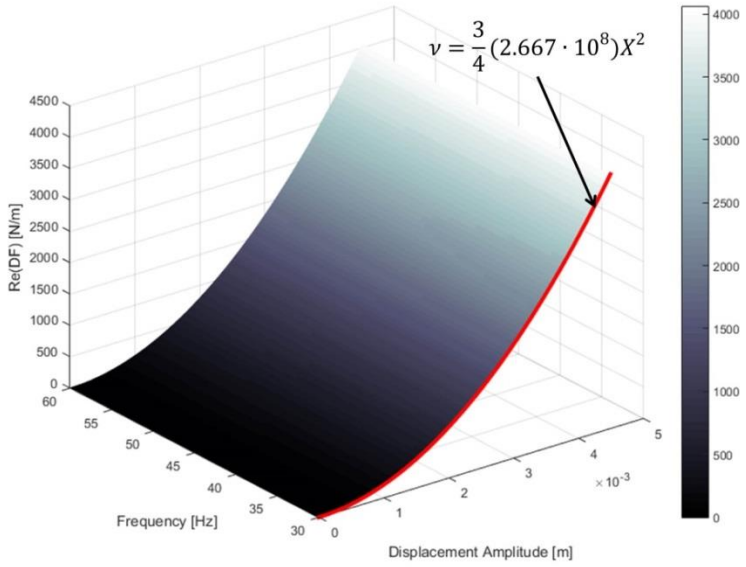

Figure 3-15. Comparison of the real part of the identified describing surface of nonlinearity with the theoretical model of the cubic stiffness nonlinearity

On the other hand, the imaginary part of the describing surface does not match perfectly with the Coulomb friction model but agrees with it at an acceptable accuracy as illustrated in Figure 3-16. The main reason for the discrepancy results from the mathematical model of the Coulomb friction, $\frac{4 \cdot (0.25)}{\pi X}$, which cannot be

represented by ordinary polynomials. In the application of the DSM, it is assumed that apriori knowledge of the nonlinearity type is not available. Accordingly, ordinary polynomial surfaces are fit to the real and imaginary parts of the derivatives of the describing surface. Since the cubic stiffness model can be represented by a second-order polynomial, its estimate based on the polynomial surface fit gives a perfect match with the actual theoretical model, which is not true for the case of the Coulomb friction model. Consequently, the polynomial surface fitted to the imaginary part of the describing function derivative and the succeeding integration process result in some discrepancy between the estimated surface and the actual theoretical model of the Coulomb friction as shown in Figure 3-16.

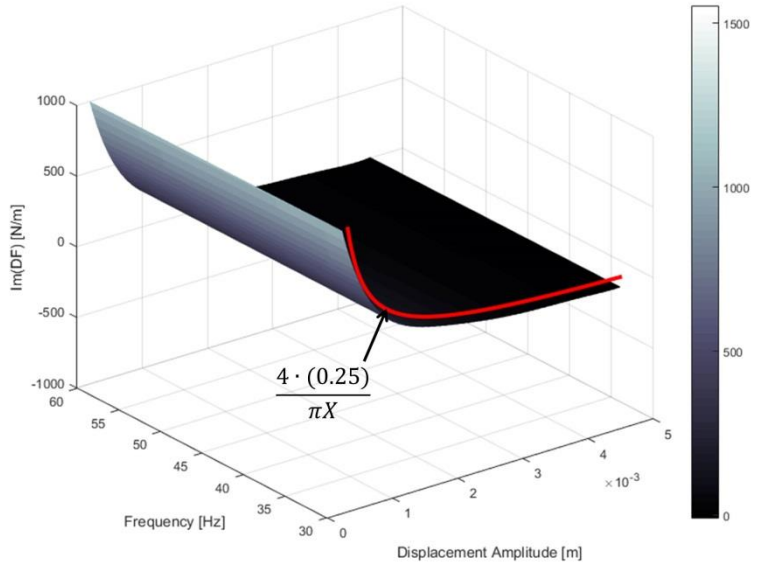

Figure 3-16. Comparison of the imaginary part of the identified describing surface of nonlinearity with the theoretical model of the Coulomb friction nonlinearity

Finally, the FRF of the underlying linear system is estimated by plugging the identified describing surface of nonlinearity into Eq. (3.22). As can be deduced from Figure 3-17, the match between the estimated linear FRF and the exact theoretical FRF is quite satisfactory.

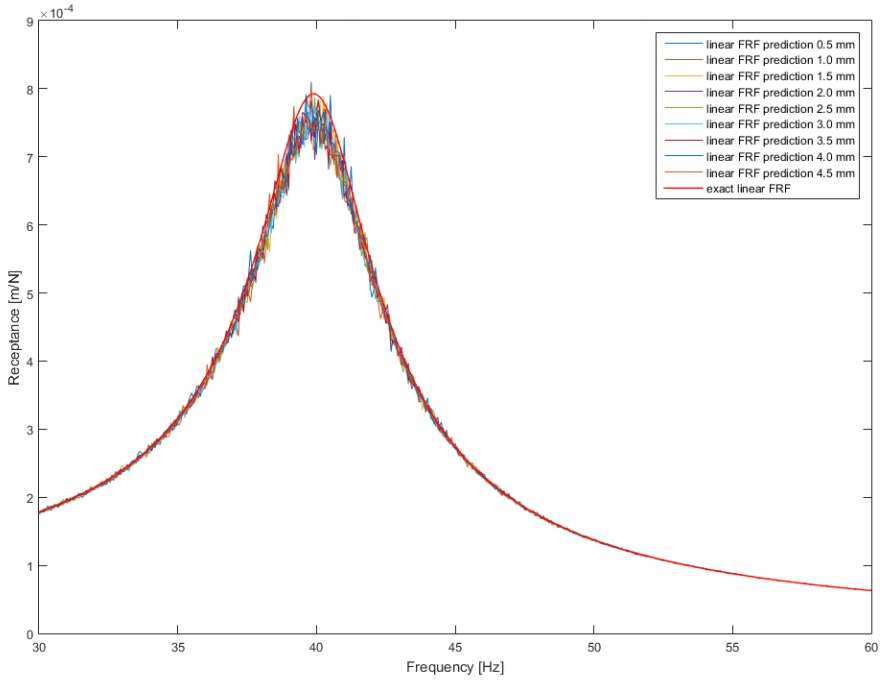

Figure 3-17. FRF of the underlying linear system of the SDOF system with cubic stiffness and Coulomb friction elements estimated by using the identified describing surface of nonlinearity

CHAPTER 4

EXPERIMENTAL APPLICATIONS

This chapter is dedicated to the experimental validation of the modal domain nonlinear system identification technique which also constitutes the major part of the nonlinear experimental modal analysis method proposed in Chapter 2 and of the spatial domain nonlinear system identification technique, namely the Describing Surface Method, proposed in Chapter 3.

4.1 Experimental Validation of the Proposed Nonlinear Experimental Modal Analysis Method Based on RCT and the HFS Concept

4.1.1 The T-Beam Benchmark

The first experimental setup used to validate the proposed nonlinear experimental modal analysis method is shown in Figure 4-1. The test rig consists of a cantilever beam supported at its free end by two metal strips which create cubic stiffness nonlinearity. The dimensions of the rig are shown in Figure 4-2. This experimental study focuses on the frequency responses around the first nonlinear mode of the structure where a strong stiffening nonlinearity is observed.

The system is excited with a B&K shaker at the intersection of the cantilever beam and thin metal strips by using a push-rod as shown in Figure 4-1. The excitation force is measured with a Dytran 1022V force transducer attached to the push-rod. The vibration response data is collected via a miniature accelerometer (Dytran 3225M23) placed above the force transducer. All measurements and closed-loop control tasks are achieved by the LMS SCADAS Mobile data acquisition system and the LMS Test Lab. software package. The upper and lower frequency limits of the stepped-sine tests covering the first elastic mode of the structure are determined

based on preliminary broadband random testing. The frequency step used during stepped-sine tests is 0.125 Hz. In stepped-sine testing, the controller first puts the control signal between the tolerance limits of the reference signal. Then, it waits for several delay cycles and switches to the next frequency point.

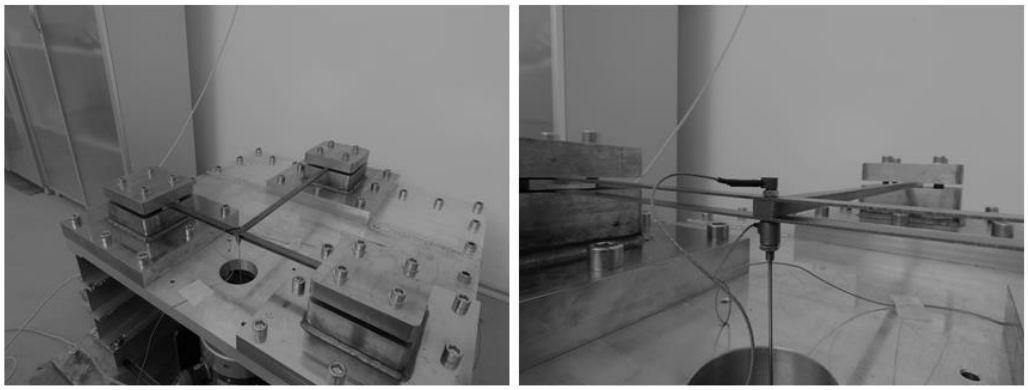

Figure 4-1. The T-beam experimental setup

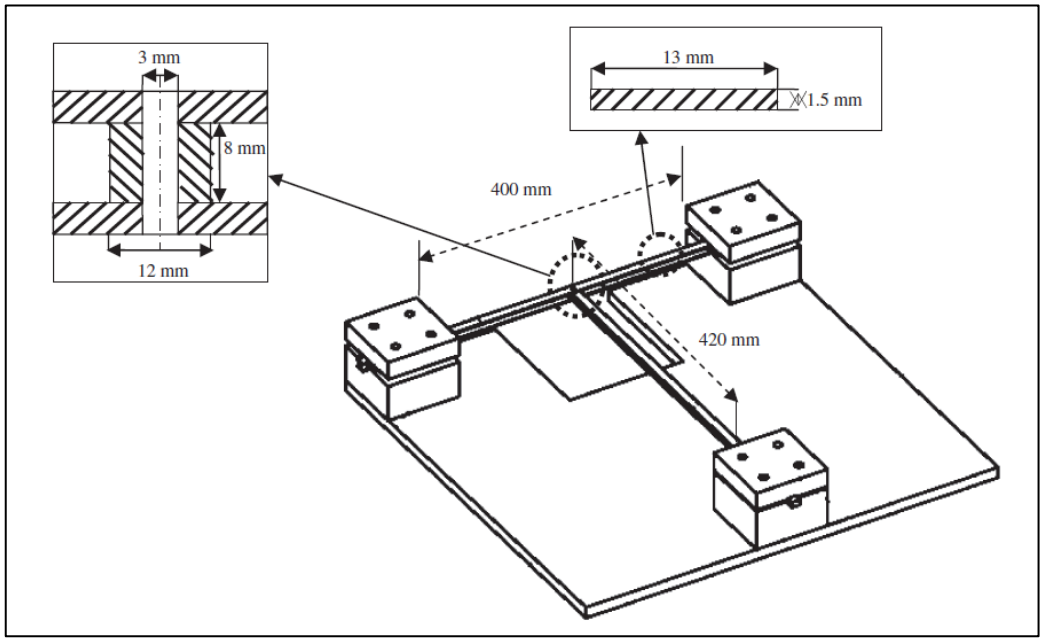

Figure 4-2. Dimensions of the T-beam test rig

The test campaign starts with a series of constant-force stepped-sine tests based on the classical force-control strategy. The constant-force FRFs measured at 3 different excitation levels are shown in Figure 4-3(a). As can be seen from the figure, the resonance peak shifts toward higher frequencies with increasing excitation level, and the jump phenomenon occurs at the highest level, which clearly indicates strong hardening nonlinearity.

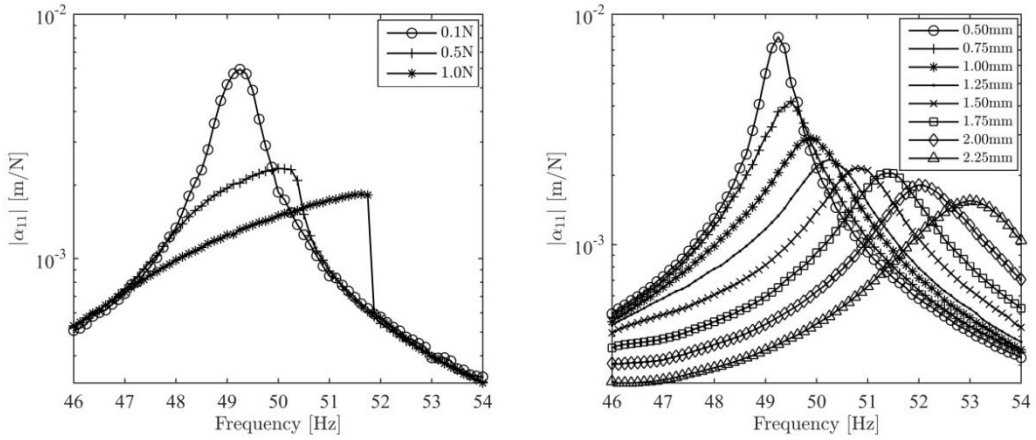

(a) (b)

Figure 4-3. (a) Constant-force FRFs of the T-beam measured by the classical force-control approach (b) constant-response FRFs of the T-beam measured by the RCT approach

Force-control tests are followed by a series of stepped-sine tests with the RCT strategy. The constant-response FRFs of the T-beam measured at 8 different constant displacement amplitude levels, ranging from 0.50 mm to 2.25 mm, are shown in Figure 4-3(b). It can be argued that the RCT approach requires collecting more data compared to some other state-of-the-art techniques and this may be time-consuming. However, the total experimental effort does not increase, at least compared to force-control testing. Actually, the response control is easier than the force control due to the quasi-linear behavior of the system, which is more

predictable. Consequently, response-controlled testing is much faster. In the T-beam case, single response-controlled testing is about 3 times faster than single force-controlled testing.

The fast-Fourier-transforms (FFTs) of time data samples recorded during response-controlled and force-controlled stepped-sine tests of the T-beam around the resonance region are shown in Figure 4-4. In both situations, the higher harmonic term is negligible compared to the fundamental harmonic, which validates the fundamental assumption of the proposed nonlinear experimental modal analysis method.

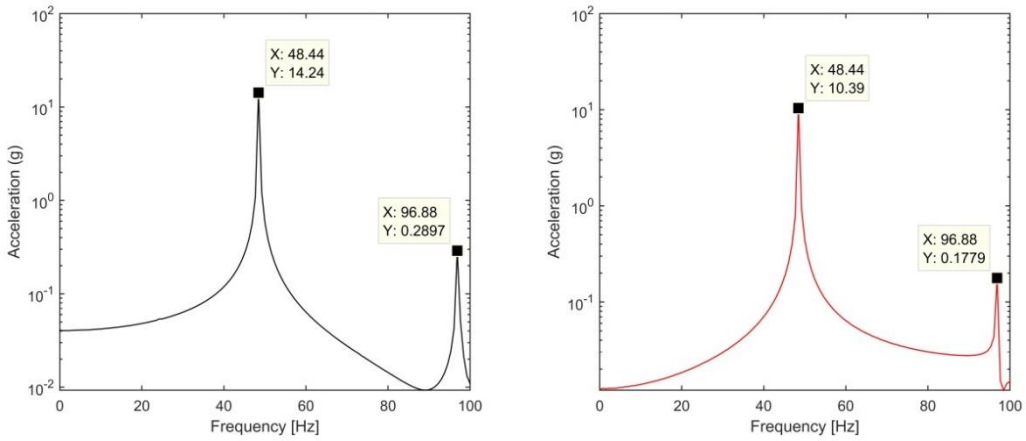

(a) (b)

Figure 4-4. Typical FFTs of time data samples collected during stepped-sine testing of the T-beam: (a) response-controlled test (1.50 mm amplitude level) (b) force-controlled test (1.0 N amplitude level)

In Figure 4-5 and Figure 4-6, the graphics show the variations of the nonlinear modal parameters (corresponding to the 1st mode of the T-beam) with respect to modal amplitude. These parameters were identified from the constant-response FRFs given in Figure 4-3(b) by using the linear modal analysis module of the LMS Test Lab., namely the PolyMAX. Figure 4-5 and Figure 4-6 show also the

parametric models which consist of the smooth polynomials fitted to the experimental data.

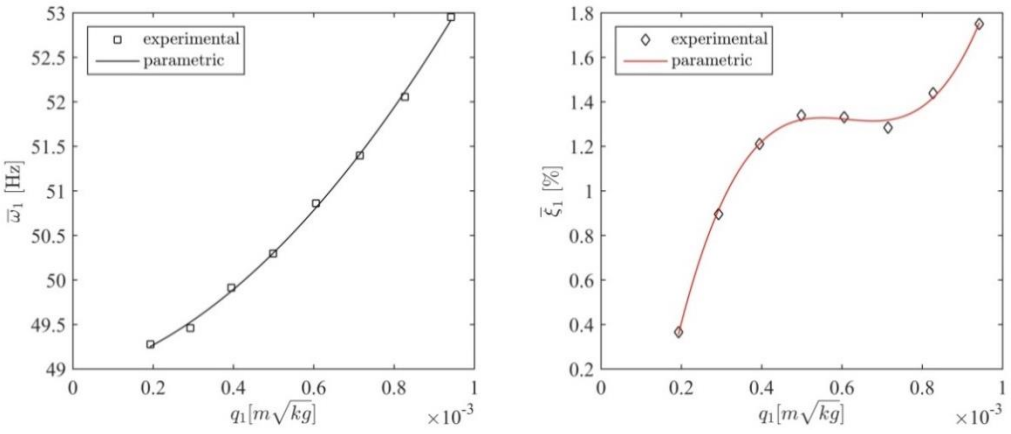

(a) (b)

Figure 4-5. Variation of the modal parameters corresponding to the 1st mode of the T-beam with modal response level (a) natural frequency (b) viscous modal damping ratio

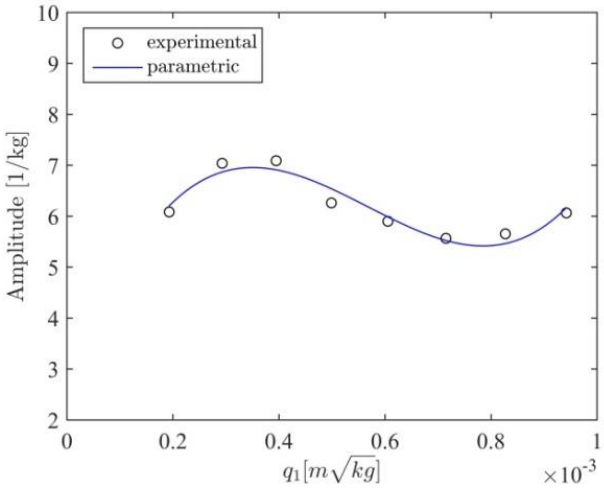

Figure 4-6. Variation of the modal constant corresponding to the 1st mode of the T-beam with modal response level

Figure 4-7 gives the comparison of the constant-force FRFs synthesized by using the identified nonlinear modal parameters in Eq. (2.24), with the ones directly measured during constant-force stepped sine tests. The match between the computational and experimental results is very satisfactory. It is important to note that constant-force testing cannot capture the unstable branch. However, the mathematical model constructed by the identified nonlinear modal parameters determines the unstable branch by virtue of the arc-length continuation algorithm used in solving Eq. (2.24).

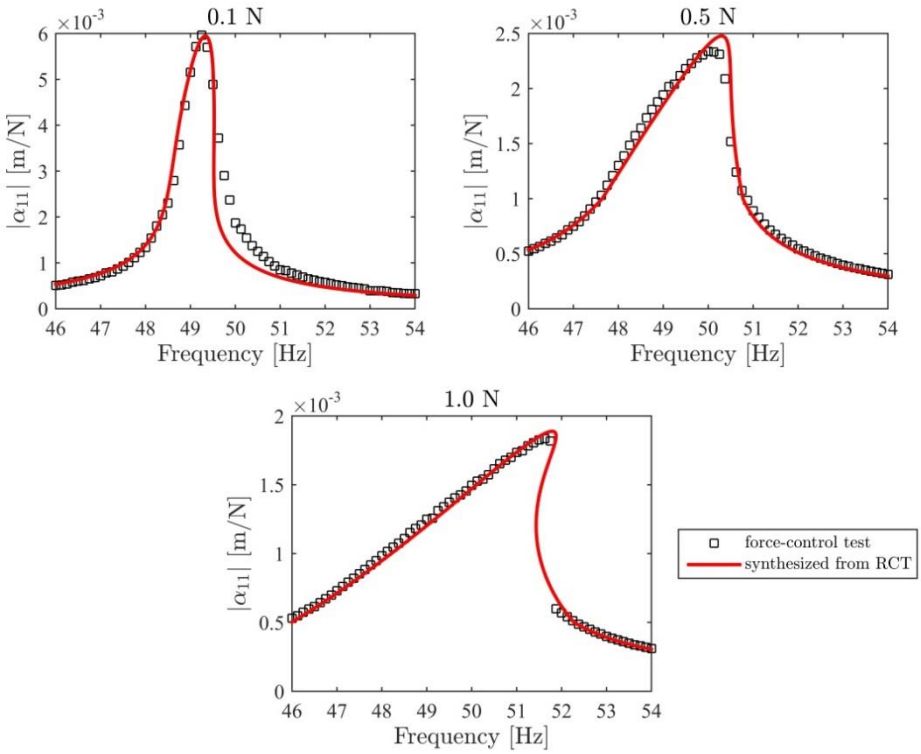

Figure 4-7. Comparison of the constant-force FRFs obtained from the force-control test with the FRFs synthesized by using the nonlinear modal parameters of the T-beam

Figure 4-8(a) gives the harmonic force spectra measured at different constant displacement amplitude levels during response-controlled tests. The HFS of the T-beam is built up by merging these force spectra via linear interpolation as shown in Figure 4-8(b).

The frequency response curve corresponding to the 1N excitation force level is extracted by cutting the HFS with the 1N constant-amplitude plane as shown in Figure 4-9(a). The comparison of this frequency response curve with the one directly measured during the constant-force stepped-sine test is given in Figure 4-9(b). Although the HFS is capable of capturing the unstable branch completely, classical force-controlled testing can only capture it until the turning points at the cost of multiple runs with different sweep directions.

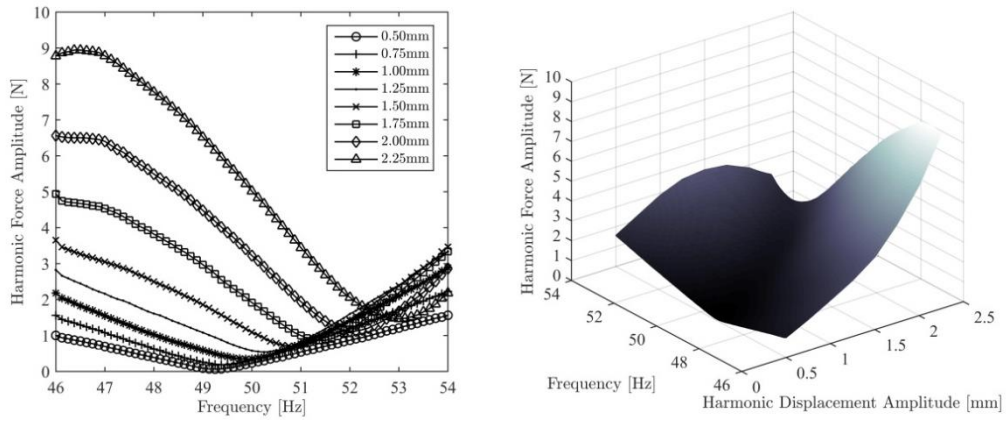

(a) (b)

Figure 4-8. (a) Harmonic force spectra of the T-beam measured during RCT (b) HFS of the T-beam constructed by collecting harmonic force spectra and using linear interpolation

Finally, the constant-force FRF synthesized at the 1 N excitation level from the nonlinear modal parameters identified by RCT is compared to the one extracted from the HFS and to the one directly measured from the classical constant-force

stepped-sine testing in Figure 4-10. The match between all three approaches is very good.

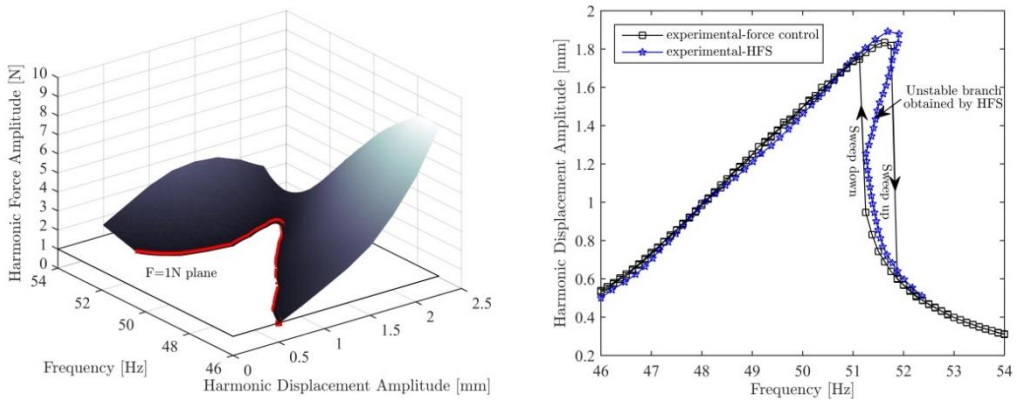

(a) (b)

Figure 4-9. (a) Determination of the harmonic response spectrum with any existing unstable branch by cutting the HFS with a constant force plane (b) Comparison of the response spectrum obtained from the HFS with the one obtained by force-controlled testing

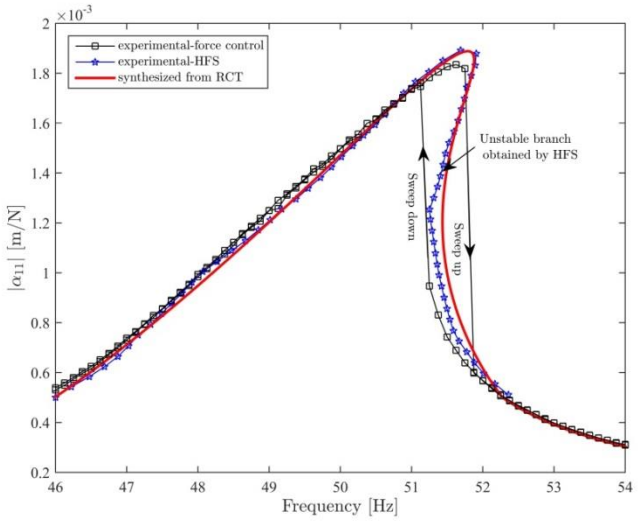

Figure 4-10. Comparison of the receptances of the T-beam extracted by using the HFS approach with the ones synthesized by using the nonlinear modal parameters identified from RCT, and with the original receptances obtained from the force-control experiment at 1 N

To conclude this experimental study, nonlinear frequency response curves corresponding to various constant force levels ranging from 0.1 N to 1.4 N with 0.05 N increments are extracted by cutting the HFS with corresponding constant force planes as shown in Figure 4-11. Finally, the backbone curve is identified by combining the resonance peaks of these frequency response curves, as shown in the same figure. Figure 4-11 clearly proves that the HFS technique can successfully extract the turning points of overhanging frequency response curves, which cannot be obtained accurately by conventional constant-force testing because of the jump phenomenon and which is still a difficult task even for the state-of-the-art experimental continuation algorithms.

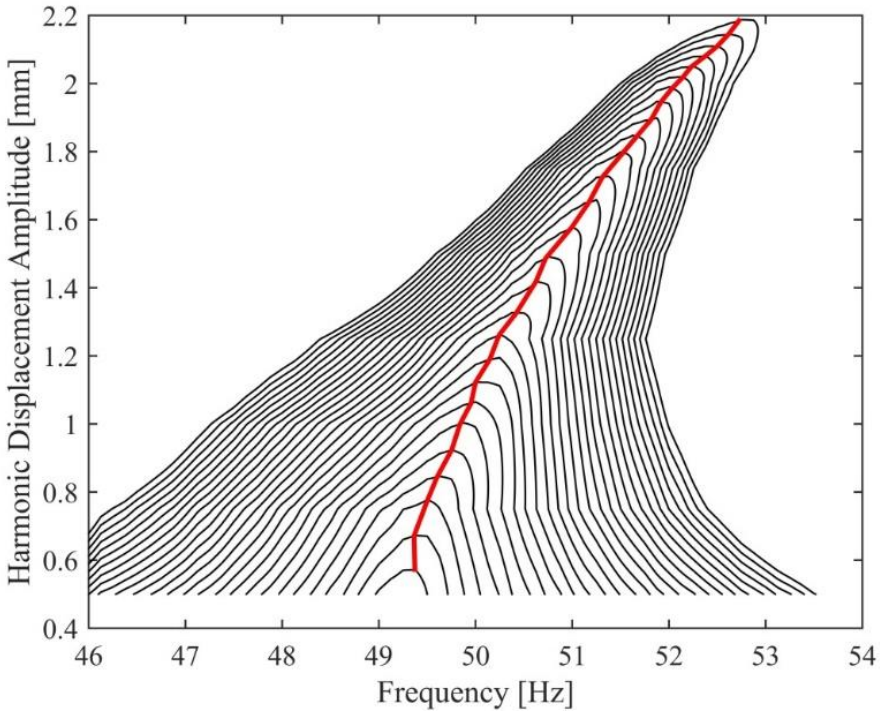

Figure 4-11. Constant-force frequency response curves (0.1 N-1.4N) and the backbone curve of the T-beam at the T-junction obtained by cutting the HFS with various constant force planes

4.1.2 Geometrically Nonlinear Clamped-Clamped Beam

In this second application study, the proposed nonlinear experimental modal analysis technique is validated on a geometrically nonlinear structure shown in Figure 4-12. The test setup consists of a very thin clamped-clamped metal strip (thin beam) with distributed nonlinearity due to large amplitude oscillations. The strip is made of stainless steel and its dimensions are 502x19x0.8 mm.

In total 7 miniature accelerometers (Dytran 3225M23) are placed along the length of the beam from left to right as illustrated in Figure 4-12. The sensor positions starting from the left end of the beam are given in Table 4-1. The structure is excited at the location of the 1st accelerometer via a push-rod attached to a B&K shaker as shown in Figure 4-12. The harmonic excitation spectrum is measured via a Dytran 1022V force transducer attached to the push-rod.

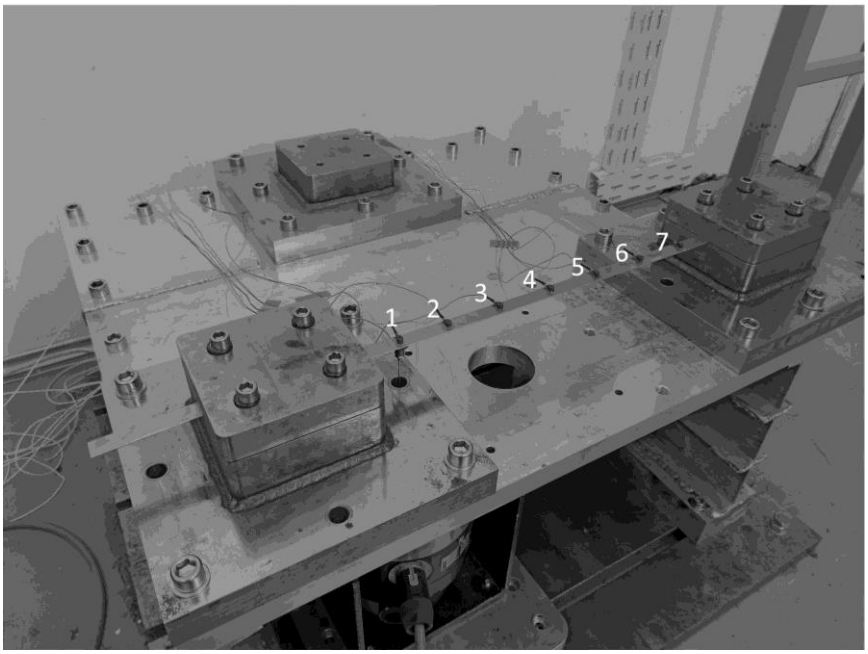

Figure 4-12. Geometrically nonlinear clamped-clamped beam experimental setup

Table 4-1. Positions of the accelerometers from the left end of the beam

Accelerometer#	**1**	**2**	**3**	**4**	**5**	**6**	**7**
Position (mm)	50	110	180	250	320	390	460

Similar to the previous application, the equipment used for data acquisition and closed-loop control in this case study is the LMS SCADAS Mobile data acquisition system and the LMS Test Lab. software package. The mode of interest is the first elastic mode of the clamped-clamped metal strip which exhibits strong stiffening nonlinearity. The upper and lower frequency limits of the stepped-sine tests covering the first mode of the structure were determined based on FRF data measured with preliminary broadband random excitation. The frequency step was taken to be 0.125 Hz.

The results of the force-controlled and response-controlled stepped sine tests are compared in Figure 4-13. The constant-force FRFs obtained by the classical force-control technique in the sweep-up direction at excitation levels 0.125N, 0.150N, and 0.175N are shown in Figure 4-13(a). Since the frequency response curves of all the accelerometers are very similar in shape, only the FRFs of accelerometers 1, 4, and 6 are shared for illustrative purposes in the figure from top to bottom. As a clear indication of the hardening nonlinearity, the resonance peak shifts toward higher frequencies with increasing excitation levels. Furthermore, the jump phenomenon occurs at all excitation levels, which shows the strong nonlinear behavior.

The constant-response FRFs measured at 9 constant displacement amplitude levels of the driving point (i.e. accelerometer 1 in Figure 4-12) by using the RCT strategy are given in Figure 4-13(b). It is important to note that the constant-response FRFs turn out to be quasi-linear. Accordingly, the classical linear experimental modal analysis is applied at each displacement amplitude level to extract modal parameters. Another important notice is that although the constant-response FRFs shown in Figure 4-13(b) cover the excitation levels shown in Figure 4-13(a), they

do not show the jump phenomenon. This is related to the fact that the points which would appear on the unstable branches of constant-force FRFs are visited at different times during response-controlled stepped-sine tests conducted at different displacement amplitude levels.

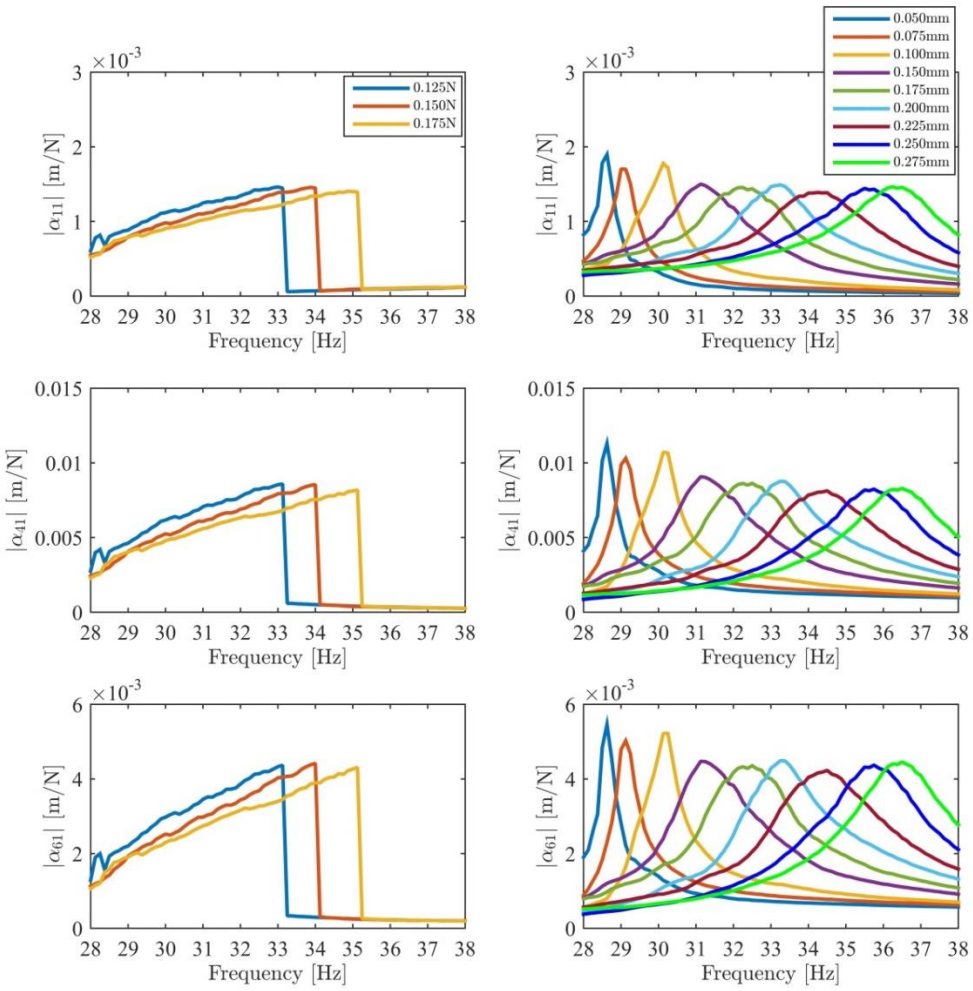

Figure 4-13. Frequency response functions of the geometrically nonlinear clamped-clamped beam: (a) Constant-force FRFs measured by the classical constant-force testing (b) quasi-linear constant-response FRFs measured with RCT

In Figure 4-13(b) the shift of the FRF peaks toward higher frequencies with increasing displacement amplitude level confirms the hardening nonlinear behavior detected from the constant-force FRFs. As a final notice, the separation of the half-power points with increasing displacement amplitude level points out the increase of damping.

At this stage, it is important to check the single harmonic assumption of the proposed nonlinear experimental modal analysis technique. Accordingly, the typical fast-Fourier transforms (FFTs) of time data samples collected at the driving point during constant-force and constant-response stepped-sine tests of the geometrically nonlinear metal strip around the resonance region are demonstrated in Figure 4-14. Obviously, in both cases, the fundamental harmonic is an order of magnitude greater than higher harmonics, which validates the single harmonic assumption for this case study.

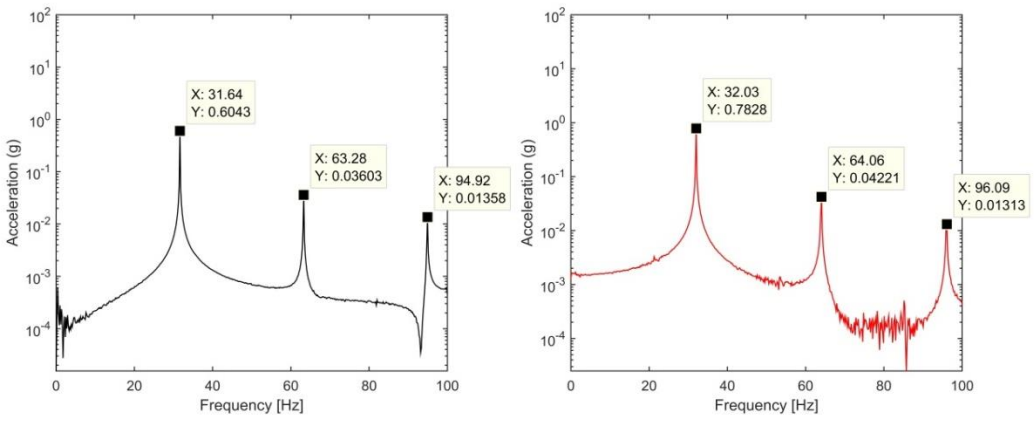

(a) (b)

Figure 4-14. FFTs of time data recorded at the driving point of the geometrically nonlinear beam (a) Response-controlled test (0.150 mm amplitude level) (b) force-controlled test (0.175 N amplitude level)

After making sure that no internal resonance occurs in the energy range of interest, linear experimental modal analysis is applied to the constant-response FRFs measured during RCT by using the PolyMAX module of the LMS Test Lab. Accordingly, the variation of the identified modal parameters measured at 9 different displacement amplitude levels ranging from 0.05 mm to 0.275 mm with respect to the modal amplitude are shown in Figure 4-15 and Figure 4-16. The parametric models shown in these figures are obtained by fitting 3rd order polynomials to the experimentally extracted nonlinear modal parameters. The first important observation made from Figure 4-15 is the considerable increase of the natural frequency with increasing modal amplitude, which indicates the hardening stiffness nonlinearity of the structure. Secondly, the modal damping ratio exhibits an order of magnitude increase from about 0.5% up to 4% with increasing modal amplitude. So, it is concluded that the geometrically nonlinear clamped-clamped metal strip does not only show conservative nonlinearity but also considerable damping nonlinearity mostly due to joint interfaces at the boundaries.

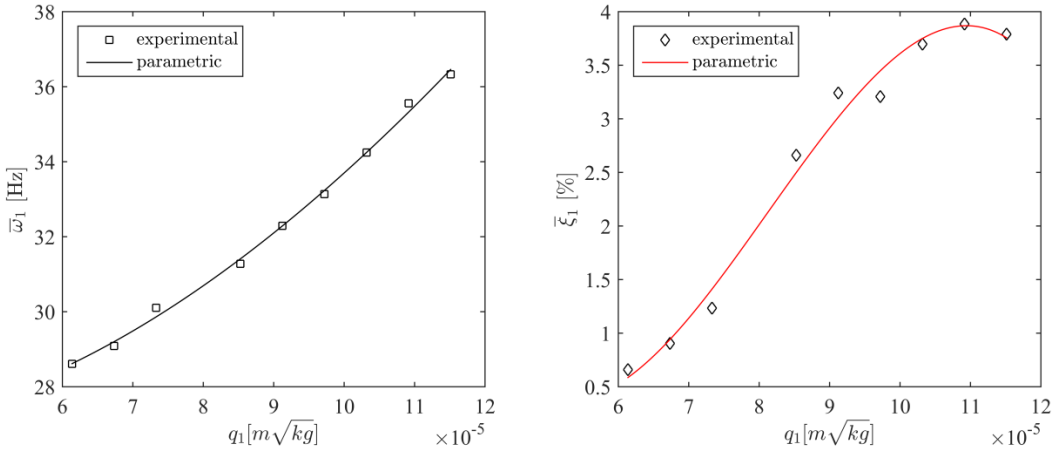

(a) (b)

Figure 4-15. Variation of the modal parameters corresponding to the 1st mode of the geometrically nonlinear beam with modal response level: (a) Natural frequency (b) viscous modal damping ratio

The NNM of the geometrically nonlinear beam obtained by substituting the identified modal constants given in Figure 4-16 into Eq. (2.23) is also shown in Figure 4-17. As can be clearly seen from the figure, the shape of the NNM changes considerably with increasing vibration amplitude.

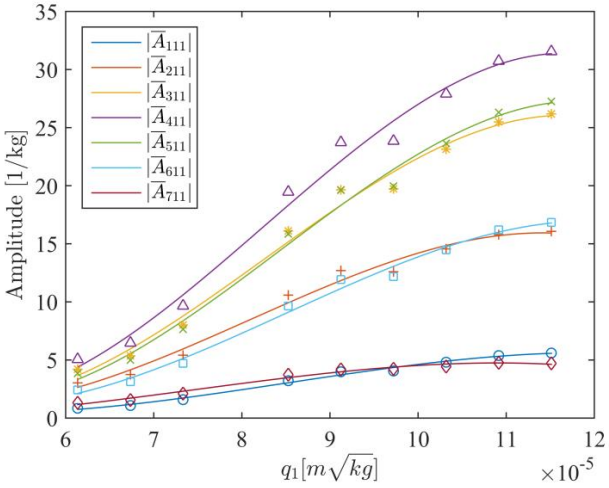

Figure 4-16. Variation of the modal constants corresponding to the 1st mode of the geometrically nonlinear beam with modal response level

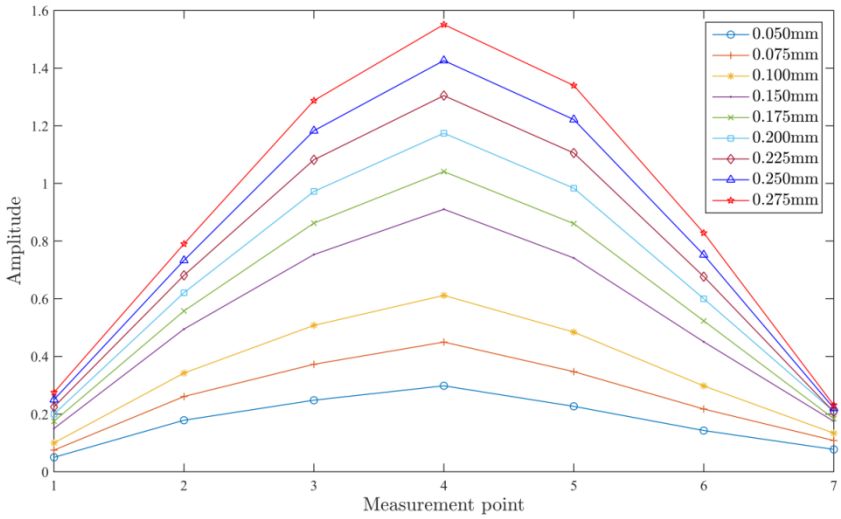

Figure 4-17. Variation of the 1st NNM of the geometrically nonlinear beam with response level

In order to validate the nonlinear modal parameters of the geometrically nonlinear beam structure identified from RCT, the constant-force frequency response curves synthesized from the identified nonlinear modal parameters by using Newton's method and the arc-length continuation algorithm are compared with the constant-force stepped-sine test results between Figures 4-18 and 4-20.

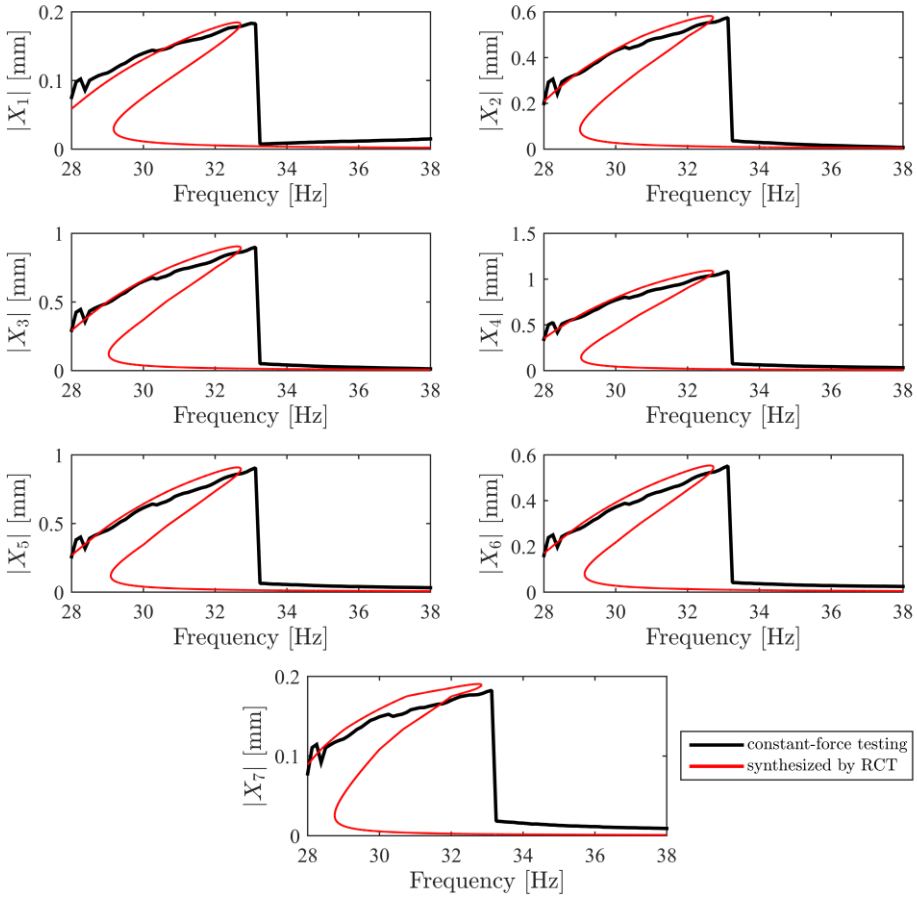

Figure 4-18. Comparison of the constant-force frequency response curves synthesized by using the identified nonlinear modal parameters of the geometrically nonlinear beam with the ones obtained from classical force-control testing at F=0.125 N force level

Despite the very strong nonlinear behavior, the match between the computational and experimental results is quite satisfactory. The match between the synthesized and experimental frequency response curves is almost perfect at moderate and high force levels (0.150 N and 0.175). The discrepancy between some of the FRF pairs (mostly at the lowest force level 0.125 N) is mainly related to the variability of the nonlinear dynamics (which might be due to the variation in support conditions in time) between the RCT and constant-force test campaigns.

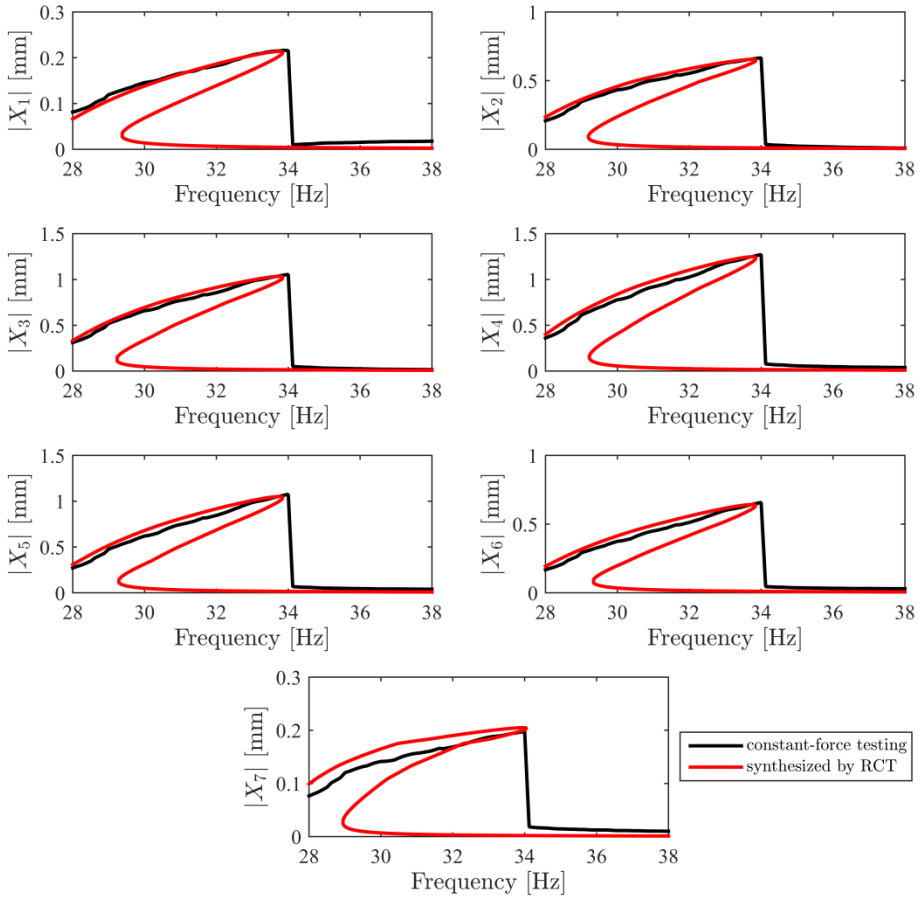

Figure 4-19. Comparison of the constant-force frequency response curves synthesized by using the identified nonlinear modal parameters of the geometrically nonlinear beam with the ones obtained from classical force-control testing at F=0.150 N force level

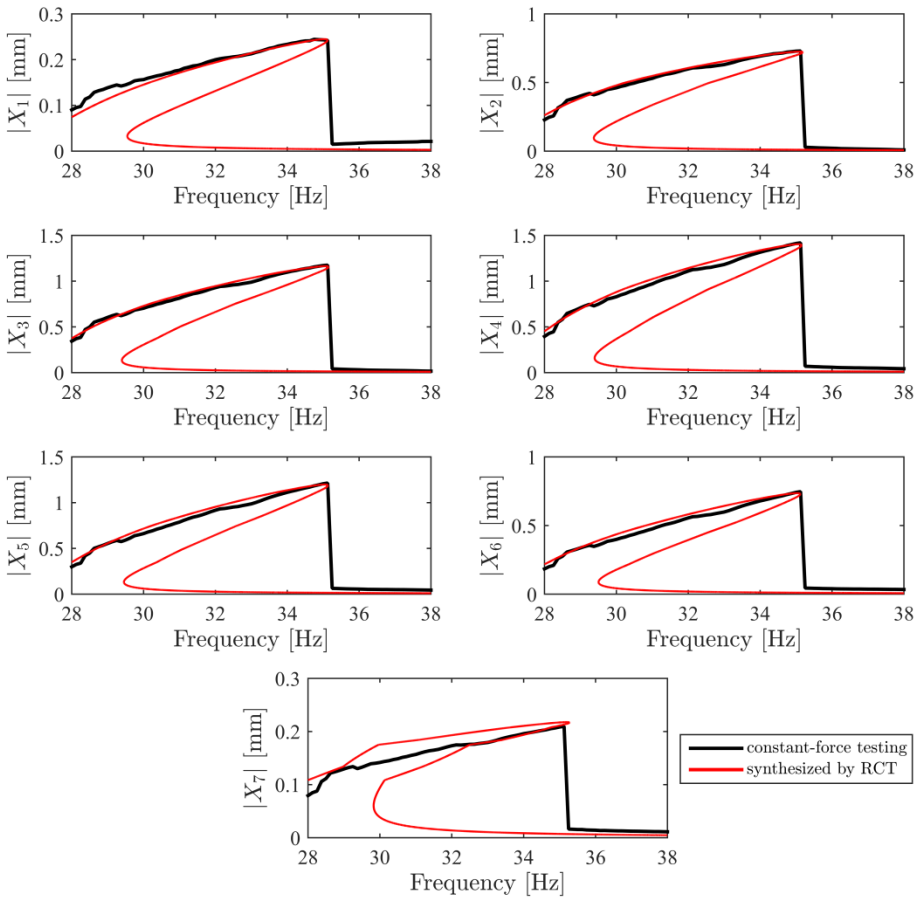

Figure 4-20. Comparison of the constant-force frequency response curves synthesized by using the identified nonlinear modal parameters of the geometrically nonlinear beam with the ones obtained from classical force-control testing at F=0.175 N force level

As can be seen from Figures 4-18 to 4-20, the arc-length continuation algorithm helps the constructed mathematical model to capture the unstable branches. However, the frequency response curves measured during constant-force tests exhibit the jump phenomenon, i.e. they cannot capture the unstable branches. This is a very typical drawback of the classical force-control approach encountered in the case of strongly nonlinear systems. In the context of this thesis work, the strong nonlinearity concept is used to refer to nonlinear systems with overhanging

unstable branches in the frequency response curves. This does not necessarily imply internal resonance as illustrated in this study (see Figure 4-14).

The unstable branches calculated by using the identified nonlinear modal parameters as shown between Figures 4-18 to 4-20 can be validated experimentally by using the HFS concept. The HFS is simply built up by merging the harmonic excitation force spectra measured during RCT with linear interpolation as shown in Figure 4-21. Cutting the HFS with a constant-force plane gives the frequency response curve corresponding to that force level with accurately identified turning points and unstable branches. In Figure 4-22, the frequency response curves computed by using the identified nonlinear modal parameters are compared with the ones extracted from the HFS. It should be emphasized that the HFS is purely experimental data. Figure 4-22 indicates that the turning points and the unstable branches obtained from simulations agree very well with the ones extracted from the HFS. The accurate identification of the turning points and unstable branches of frequency response curves, which is a considerable issue even for the new generation experimental continuation techniques, is the prominent feature of the HFS technique. This feature was successfully used in [86] to experimentally determine the backbone curves of strongly nonlinear structures.

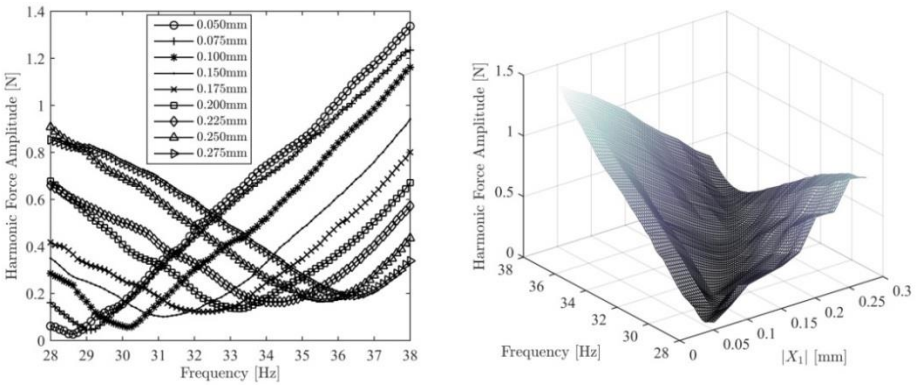

(a) (b)

Figure 4-21. (a) Harmonic excitation force spectra of the geometrically nonlinear beam measured during RCT (b) HFS of the driving point constructed by combining harmonic force spectra with linear interpolation

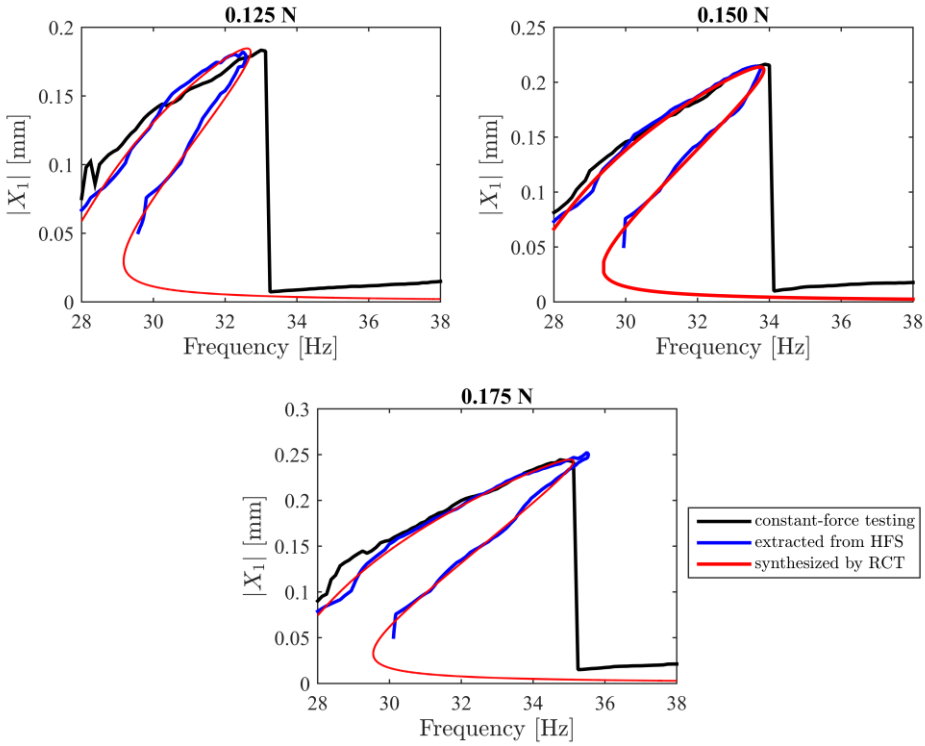

Figure 4-22. Comparison of the frequency response curves of the geometrically nonlinear beam extracted from the HFS with the ones synthesized by using nonlinear modal parameters and with the ones measured by classical constant force stepped-sine testing

Finally, nonlinear frequency response curves corresponding to various constant force levels ranging from 0.08 N to 0.175 N with 0.005 N increments are extracted by cutting the HFS with corresponding constant force planes as shown in Figure 4-23. Then, the backbone curve is identified by combining the resonance peaks of these frequency response curves, as shown in the same figure. Figure 4-23 clearly proves that the HFS technique can successfully extract the turning points of overhanging frequency response curves.

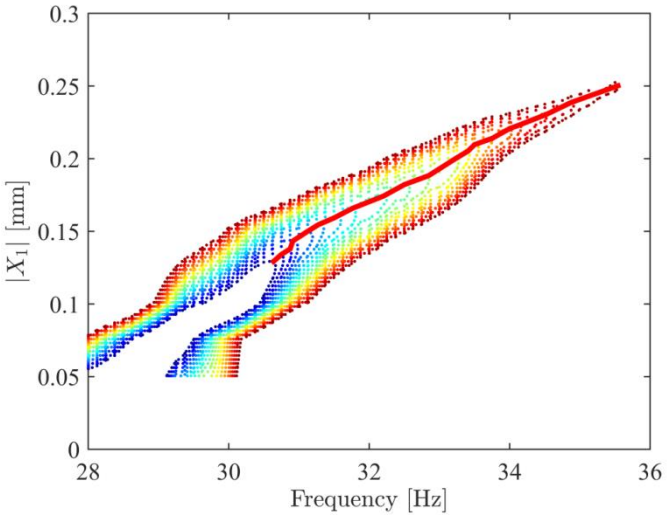

Figure 4-23. Constant-force frequency response curves and the backbone curve of the geometrically nonlinear beam at the driving point obtained by cutting the HFS with various constant force planes

4.1.3 Real Missile

The third experimental study is dedicated to the application of the proposed nonlinear experimental modal analysis method on a real missile structure which exhibits considerable damping nonlinearity mostly due to several bolted joints.

The test setup of the real missile structure is shown in Figure 4-24. As shown in the figure, the structure is suspended with bungees to get close to free-free boundary conditions, and so to keep the rigid body modes of the missile far away from its elastic modes. The missile body is instrumented with 8 miniature accelerometers (Dytran 3225M23) along its length as illustrated in Figure 4-24.

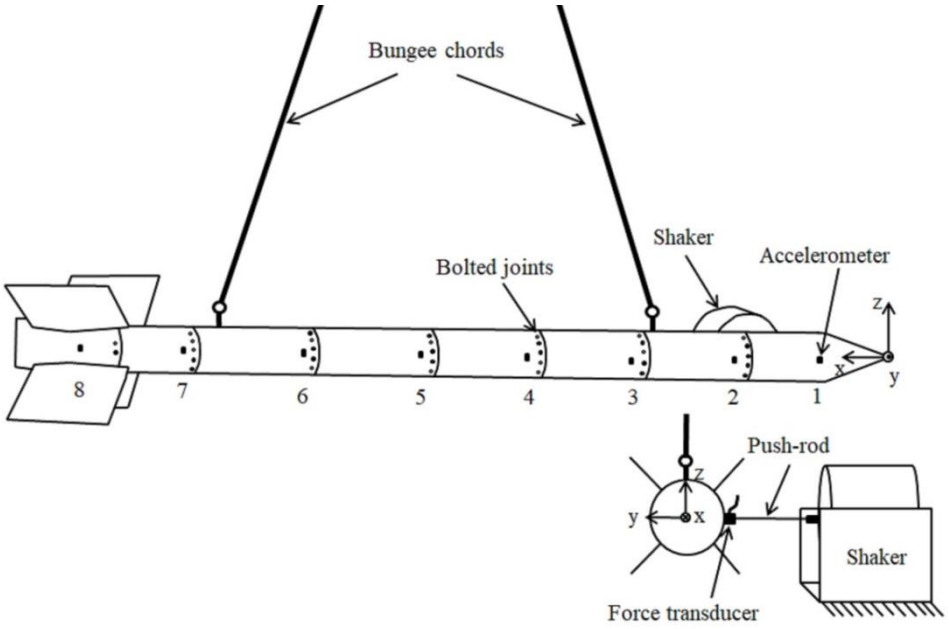

Figure 4-24. Sketch of the experimental setup of the real missile

Similar to the two previous case studies, the mode of interest is once again the first elastic mode of the structure. Accordingly, the system is excited with a single shaker at point 1 in the y-direction by using a push rod attached to an electrodynamic shaker (MB Dynamics Modal 110). The harmonic excitation signal is measured via a Dytran 1051V4 force transducer attached to the tip of the push-rod. Measurement and control are achieved by the LMS SCADAS Mobile data acquisition system and the LMS Test Lab. software package.

As seen from Figure 4-24, the missile consists of a considerable number of sub-assemblies attached together with many bolts. All these bolts are identical and they are tightened at the same toque level.

The test campaign starts with a series of stepped-sine tests by using the classical force-control approach. The constant-force FRFs measured at excitation levels F, 2F, and 3F are given in Figure 4-25(a). Since the frequency response curves of all the accelerometers are very similar in shape, only the FRFs of accelerometers 1, 5,

and 8 are illustrated in the figure from top to bottom. The shift of the resonance peak toward lower frequencies and the decrease in the FRF peak amplitude with increasing excitation level indicate softening nonlinear behavior with increasing nonlinear damping.

The constant-force tests were followed by a series of stepped-sine tests with RCT strategy. The constant-response FRFs of the missile structure are measured at 14 different constant displacement amplitude levels, ranging from D to 20D. For the sake of readability, the constant-response FRFs corresponding to six selected displacement amplitude levels are shown in Figure 4-25(b).

Figure 4-26 and Figure 4-27 show the variations of the modal parameters identified from the quasi-linear constant-response FRFs by using the LMS PolyMAX which is a standard linear modal analysis tool. The confidence intervals are determined with repeated tests at the same displacement level during the test campaign. In Figure 4-26, it is clearly seen that the nonlinear modal damping ratio exhibits an order of magnitude change. However, the change of the natural frequency is very small. So, it is concluded that the system exhibits considerable damping nonlinearity but weak stiffness nonlinearity. It is also interesting that in the transition region (between 0.2 and 0.4), the nominal damping exhibits a sharp increase, and the confidence intervals get considerably large. This transition region may be an indication of the stick to slip transition (slipping means more friction and damping). On the other hand, large confidence intervals may result from combined effects of several different environmental conditions such as the temperature change and changes of contact conditions due to vibration at the joint interfaces.

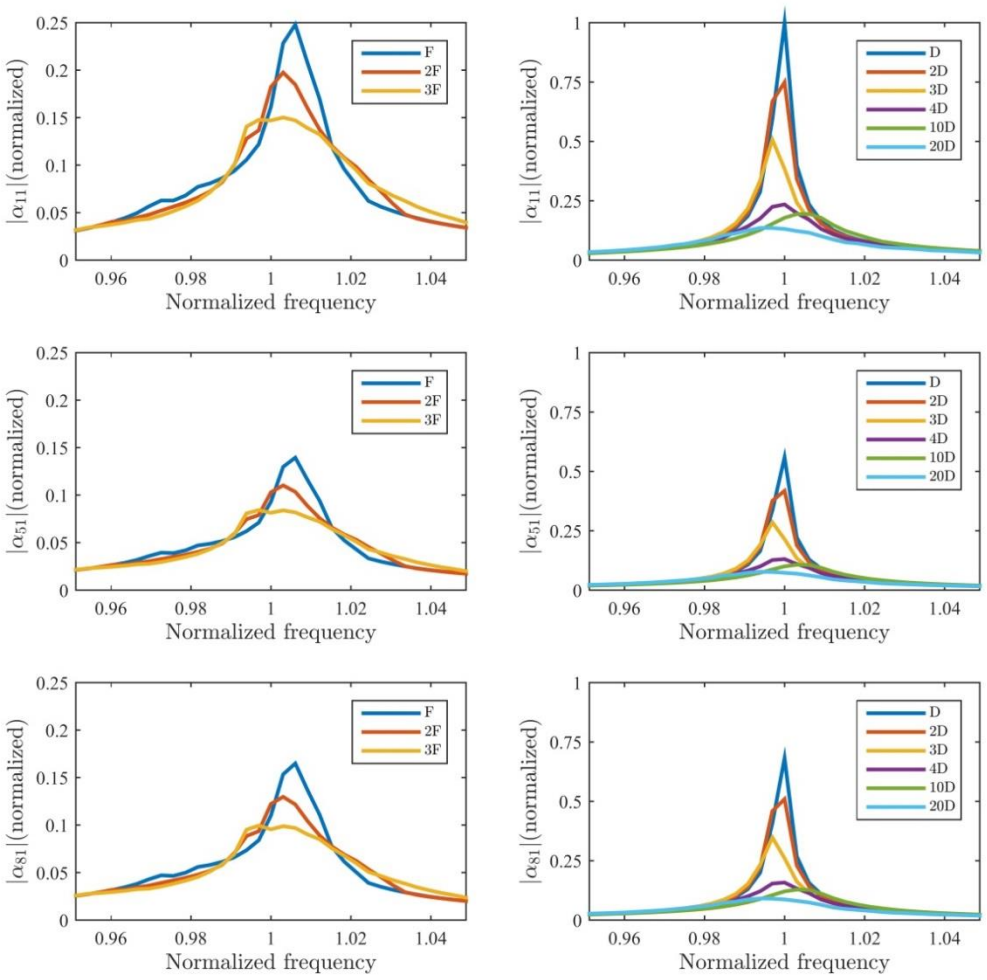

(a) (b)

Figure 4-25. (a) Constant-force FRFs of the missile structure measured by the classical force-control approach (b) constant-response FRFs of the missile structure measured by the RCT approach

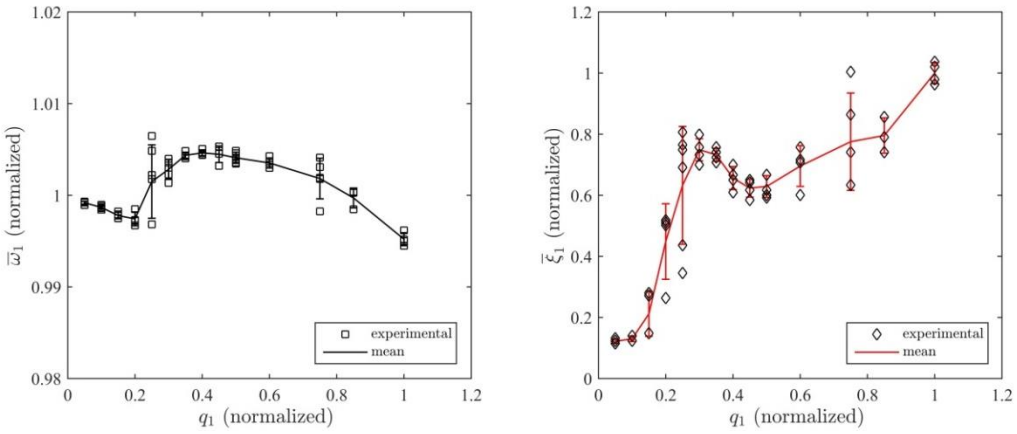

(a) (b)

Figure 4-26. Variation of the modal parameters corresponding to the 1st mode of the missile structure with modal response level (a) natural frequency (b) viscous modal damping ratio

Figure 4-27 indicates that the variation of the identified modal constants with respect to vibration amplitude is negligible. Consequently, the shape changes in the NNM which is closely related to modal constants through Eq. (2.23) are also negligible as can be seen in Figure 4-28.

This section is concluded by comparing the constant-force FRFs calculated by using the identified nonlinear modal parameters (see Figure 4-26 and Figure 4-27) in Eq. (2.24), with the experimental data directly obtained from constant-force stepped sine tests, as shown in Figure 4-29. The match between the computational and experimental results is found to be quite satisfactory at moderate and high excitation levels (i.e. at 2F and 3F). At the lowest excitation level, repeatability of the measured constant-force FRFs is poor, which is the cause of large confidence intervals observed in the nonlinear modal damping ratio shown in Figure 4-26(b). Consequently, the agreement between the computational and experimental FRFs at the lowest excitation level is not as good as the ones obtained at moderate and high excitation levels.

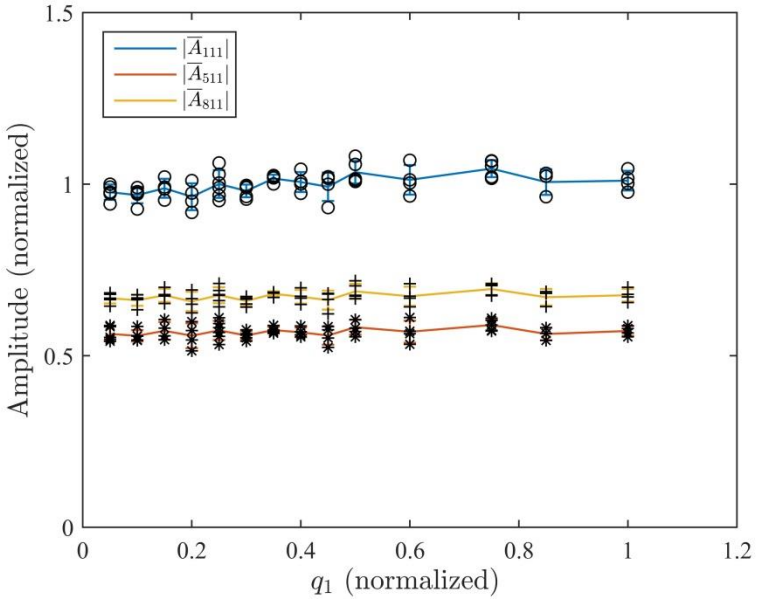

Figure 4-27. Variation of the modal constants corresponding to the 1st mode of the missile structure with modal response level

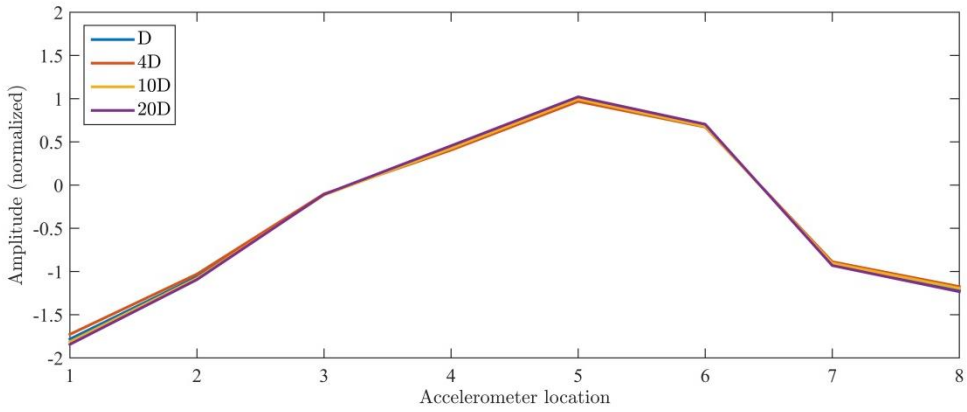

Figure 4-28. 1st NNM of the missile structure experimentally extracted by using the modal constants identified from RCT

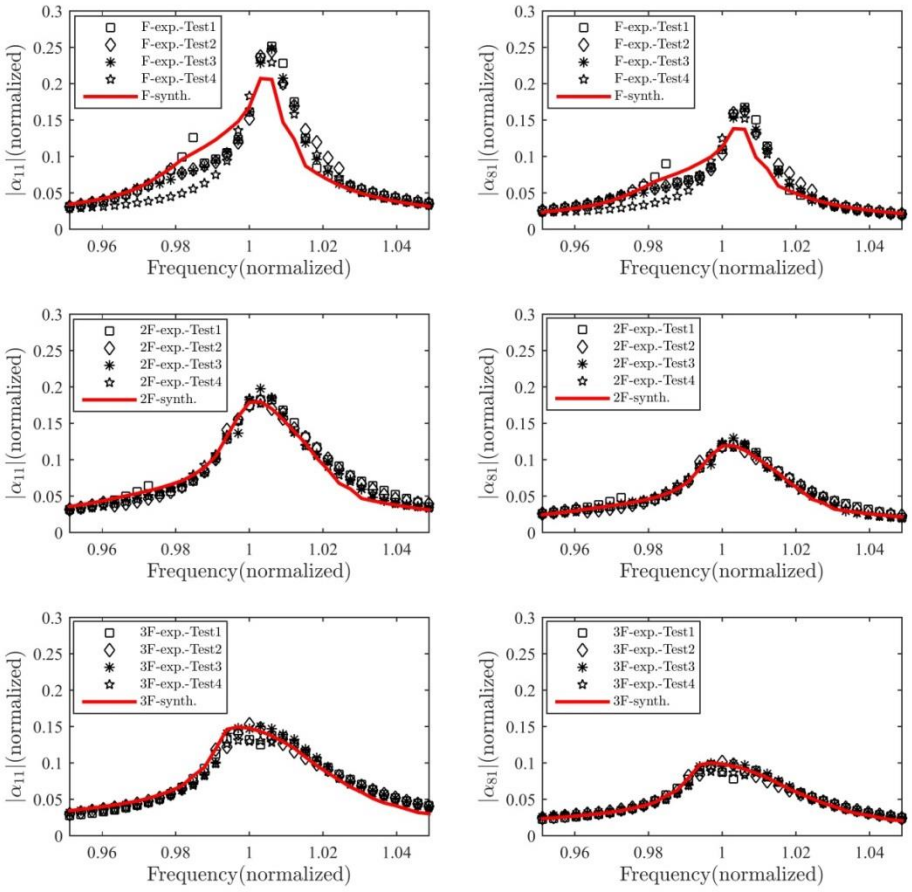

(a) (b)

Figure 4-29. Comparison of the constant-force FRFs obtained from force-controlled testing, with the FRFs synthesized by using the nonlinear modal parameters of the missile structure: (a) driving point FRF (point1 in Figure 4-24) (b) FRF between tail point (point 8 in Figure 4-24) and driving point

The nonlinear modal parameters shown in Figure 4-26 correspond to the bolt tightening torque level T1 of the bolts illustrated in Figure 4-24. To see the effects of bolt preload on the modal parameters, response-controlled stepped-sine tests were also conducted for a lower torque level of 0.77 T1. The modal parameters obtained at these two different torque levels are compared in Figure 4-30.

Figure 4-30(a) indicates that the reduction of bolt preload results in the decrease of the natural frequency. In other words, the structure becomes more flexible. Besides, since less preload means more sliding (i.e. more friction and damping), nonlinear damping at the joints is enhanced when the preload is reduced as shown in Figure 4-30(b). It is also worth mentioning that the percentage increase in the modal damping ratio exceeds 50% at various displacement levels, while the decrease in the natural frequency is limited to 3-5%. Therefore, it is deduced that modal damping, compared to the natural frequency, is much more sensitive to bolt preload. In other words, stiffness is affected much less than damping. To know the amount of increase that can be achieved in modal damping by decreasing bold preload may be an important parameter in designing such structures from the aeroelastic perspective.

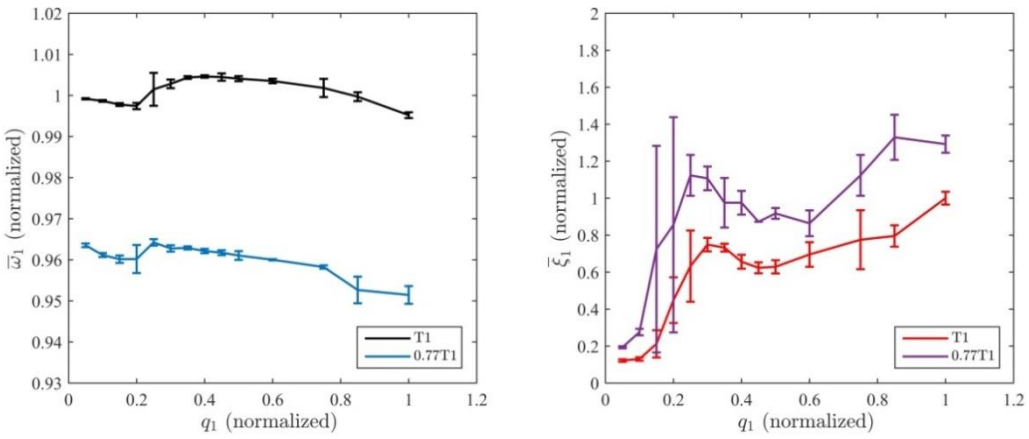

(a) (b)

Figure 4-30. Effect of bolt preload on the modal parameters (a) natural frequency (b) viscous modal damping ratio

4.1.4 Control Fin Actuation Mechanism of a Real Missile

So far the proposed nonlinear experimental modal analysis method was validated on a cantilever beam with a smooth localized nonlinearity (T-beam), on a clamped-clamped metal strip with continuously distributed (geometrical) nonlinearity, and on a real missile structure with joint nonlinearities (multiple and discrete). Finally, in this case study, the proposed technique is applied to a control fin actuation mechanism that exhibits non-smooth nonlinearities due to backlash and friction. The diversity among all these applications clearly proves that the developed technique can be applied to a wide range of nonlinear system identification problems.

Control fins have a key role in the aeroelastic behavior of the guided missiles [94, 95]. The actuation mechanism of a control fin involves many moving components that exhibit various types of nonlinearity such as backlash and friction. This may result in strongly nonlinear behavior with the jump phenomenon around the first torsional mode of the system. The identification of such a nonlinear behavior is quite a challenge for the current state-of-the-art techniques. In this study, this difficult identification problem is systematically solved by the proposed nonlinear experimental modal analysis technique based on RCT and HFS.

The sketch of the experimental setup is illustrated in Figure 4-31. The casing of the mechanism is rigidly fixed to the ground. The control fin is instrumented with 10 miniature accelerometers (Dytran 3225M23), as shown in Figure 4-31. The structure is excited at point 1 in the z-direction with a push-rod attached to an electrodynamic shaker (B&K). The excitation force is measured with a force transducer (Dytran 1022V) attached to the tip of the push-rod.

Similar to the previous experimental studies, the data acquisition and closed-loop control tasks are accomplished by using the LMS SCADAS Mobile data acquisition system and the LMS Test Lab. software package. A frequency resolution of 0.125 Hz is used. The mode of interest is once again the first elastic

mode of the structure which is the torsional mode. It should be noted that the deformation of the fin surface does not contribute to this mode as confirmed by the mode shape simulation obtained from preliminary tests. This mode simply results from the torsional stiffness created by the actuation mechanism. Accordingly, the system can be treated as an SDOF rotational system. So, the nonlinear system identification can be accomplished simply by using the driving point FRFs of the system.

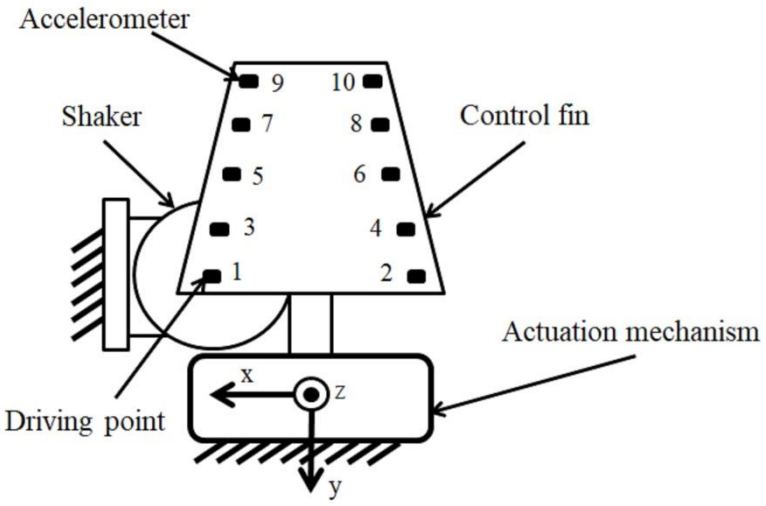

Figure 4-31. Sketch of the experimental setup for the control fin actuation mechanism

As the reader is familiar with previous case studies, the test campaign consists of a series of force-controlled and response-controlled stepped sine tests, results of which are shown in Figure 4-32. The constant-force FRFs measured at the driving point by the classical force-control strategy in the sweep-up direction at excitation levels ranging from F1 to F4 are given in Figure 4-32(a). Here, the excitation level increases from F1 to F4. An important observation made from Figure 4-32(a) is that the resonance peak first decreases and then increases with increasing excitation

level, which clearly indicates the complex nonlinear behavior of the actuation mechanism. The second important observation is the jump phenomenon occurring in the measured FRFs at levels F2, F3, and F4, which shows that the system exhibits strong nonlinearity.

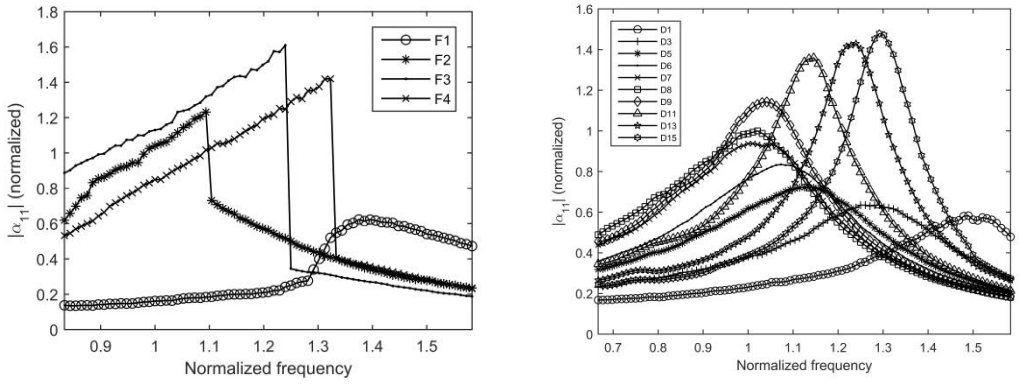

(a) (b)

Figure 4-32. Frequency response functions of the control fin actuation mechanism at the driving point: (a) Constant-force FRFs measured by the classical constant-force testing (b) constant-response FRFs measured with RCT

The constant-response FRFs of the system are measured at 15 different constant displacement amplitude levels (labeled D1 to D15) of the driving point (i.e. accelerometer 1 in Figure 4-31) by using the RCT strategy. For clarity, the receptances corresponding to only 10 different constant displacement amplitude levels are shown in Figure 4-32(b). It can be clearly seen from the figure that the constant-response FRFs turn out to be quasi-linear as in the case of previous experimental studies. Accordingly, classical linear experimental modal analysis techniques can be applied at each displacement amplitude level to extract the modal parameters. It is important to note that although the constant-response FRFs shown in Figure 4-32(b) cover the excitation levels shown in Figure 4-32(a), they do not exhibit the jump phenomenon. In other words, although two equilibrium

states coexist on a constant-force FRF at a specific frequency depending on the initial conditions, which gives rise to an unstable branch, there is a one-to-one correspondence between amplitude and frequency in the case of a constant-response FRF. This makes sense because during response-controlled stepped-sine testing, the displacement amplitude is kept constant and consequently, there is not much deviation from the initial equilibrium state. This is the key feature of the RCT strategy. At this point, one may ask the following question: What exactly happens to the consecutive points on the unstable branch of a constant-force FRF when switched to constant-response testing? The answer is very simple: Each of these consecutive points shows up on a different constant-response FRF.

As a final step before passing to the identification of nonlinear modal parameters, the fundamental assumption of the proposed method is checked based on the FFTs of time data samples collected during stepped sine tests as illustrated in Figure 4-33. As can be seen from the figure, the higher harmonic term is negligible compared to the fundamental harmonic, which proves that the single harmonic assumption holds for this system as well.

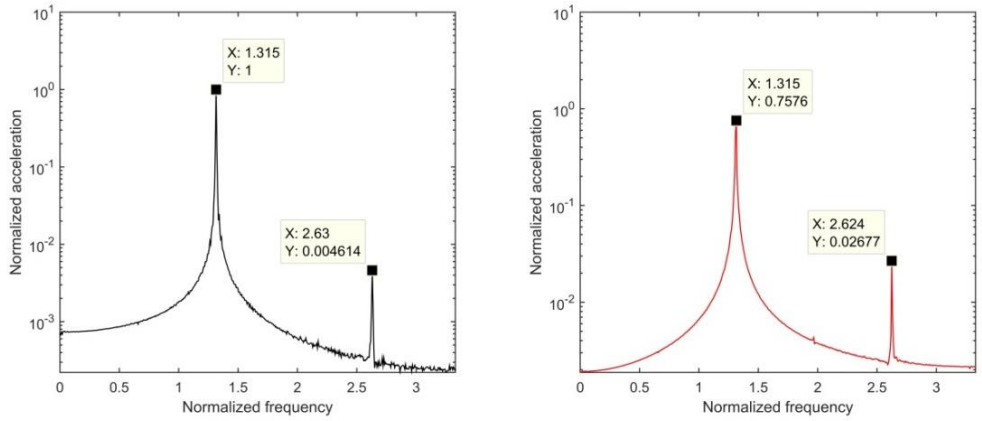

(a) (b)

Figure 4-33. Typical FFTs of time data samples collected during stepped-sine testing of the control fin actuation mechanism: (a) response-controlled test (D15 amplitude level) (b) force-controlled test (F4 amplitude level)

After making sure that no internal resonance occurs in the energy range of interest, linear experimental modal analysis is applied to the constant-response FRFs measured during RCT by using the PolyMAX module of the LMS Test Lab. Accordingly, the variation of identified modal parameters with respect to the modal amplitude is shown in Figure 4-34 and Figure 4-35.

The first important observation made from Figure 4-34 is that the natural frequency of the torsional mode decreases down to a minimum value, after which it keeps a monotonic increase. It is highly probable that the initial softening behavior is an indication of the stick-to-slip transition and the succeeding hardening behavior is related to backlash. It is also important to note that the value of the natural frequency exhibits an extreme change which is about 50%. The ability to cope with systems involving such huge stiffness nonlinearity definitely demonstrates the power of the proposed method.

The second important observation made from Figure 4-34 is that the nonlinear modal damping ratio first increases up to a certain value, after which it exhibits a monotonic decrease. This is an indication of a very complex damping mechanism. More importantly, even though the values of the modal damping ratio given in Figure 4-34 are in normalized form due to the confidentiality issue, the actual values of the modal damping ratio are considerably high. This proves that the proposed method applies to systems with high damping. Furthermore, the value of the damping ratio drops from 1 to about 0.3 which corresponds to a 70% change as shown in Figure 4-34. This indicates that the proposed method is not only applicable in the case of high damping but also the case of high nonlinearity in damping.

Before getting into the validation of the identified nonlinear modal parameters, the harmonic force spectra measured at the driving point during RCT are merged into the HFS by using linear interpolation as shown in Figure 4-36. Cutting the HFS with a constant-force plane gives the frequency response curve corresponding to

that force level with accurately identified turning points and unstable branches. Once again, it is important to emphasize that the HFS is purely experimental data.

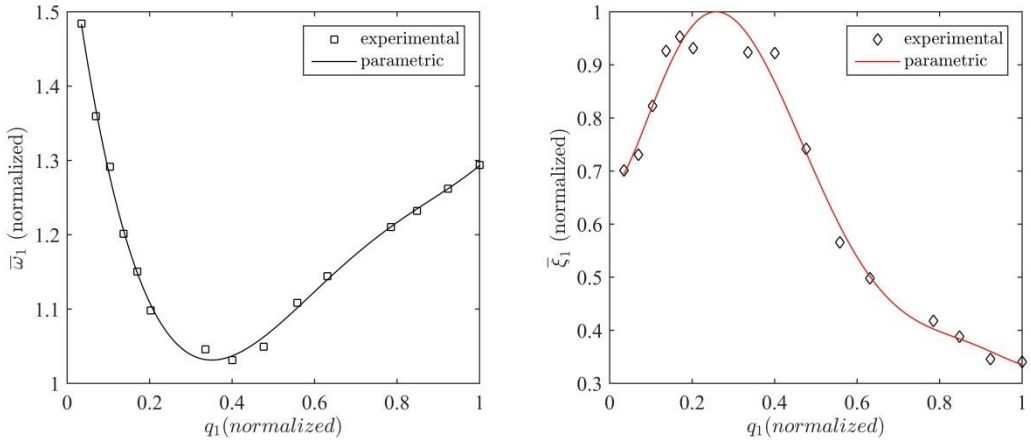

(a) (b)

Figure 4-34. Variation of the modal parameters corresponding to the 1st mode of the control fin actuation mechanism with modal response level (a) natural frequency (b) viscous modal damping ratio

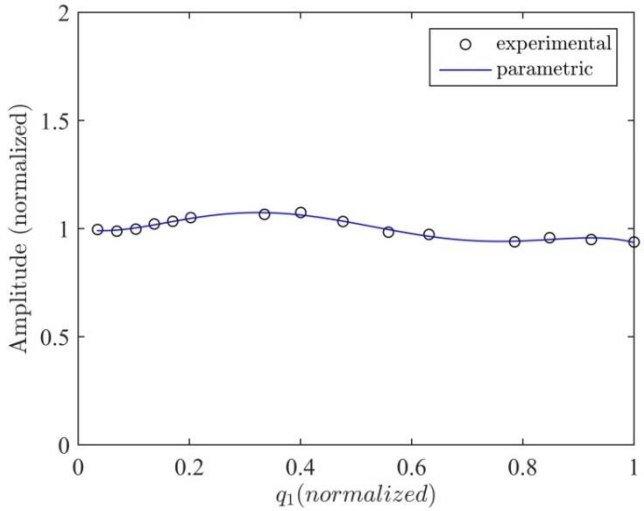

Figure 4-35. Variation of the modal constant corresponding to the 1st mode of the control fin actuation mechanism with modal response level

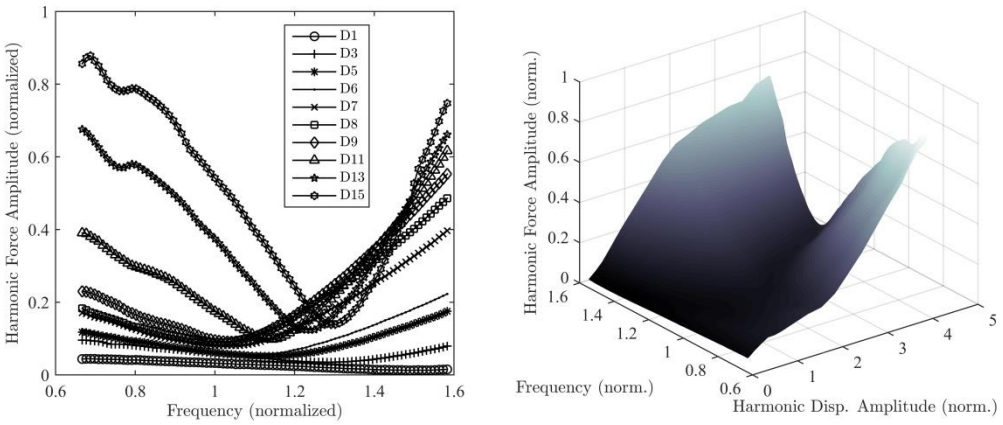

(a) (b)

Figure 4-36. (a) Harmonic force spectra of the control fin actuation mechanism measured by RCT (b) HFS of the control fin actuation mechanism at the driving point, constructed by combining harmonic force spectra

Finally, in order to validate the nonlinear modal model obtained from the proposed nonlinear experimental modal analysis technique based on RCT, the constant-force FRFs synthesized (computed) by using the identified nonlinear modal parameters are compared with the purely experimental data in Figure 4-37. First of all, as can be seen from the figure, the match between the synthesized FRFs and the ones extracted from the HFS is perfect. On the other hand, even though the agreement between the synthesized FRFs and the ones measured from constant-force testing is quite satisfactory, there exists some discrepancy that deserves an explanation. The perfect match between the synthesized FRFs and the FRFs extracted from the HFS, which is purely experimental data, proves that the nonlinear modal model works properly and there cannot be an error in this model. This brings us to the question of why the constant-force FRFs directly measured from force-controlled testing do not match perfectly with the FRFs extracted from the HFS, even though both data are purely experimental? Two suspects of this issue can be the effects of higher harmonics or the relatively poor repeatability of the experimental data. As shown in Figure 4-33, the effect of higher harmonics is not significant and consequently, it

cannot be the main reason for the discrepancy between the two types of tests. The main reason for the discrepancy is seemingly poor repeatability, i.e. the variability of the repeated tests. During the tests, it was observed that repeating the same (response-controlled or force-controlled) test does not give exactly the same frequency response curve.

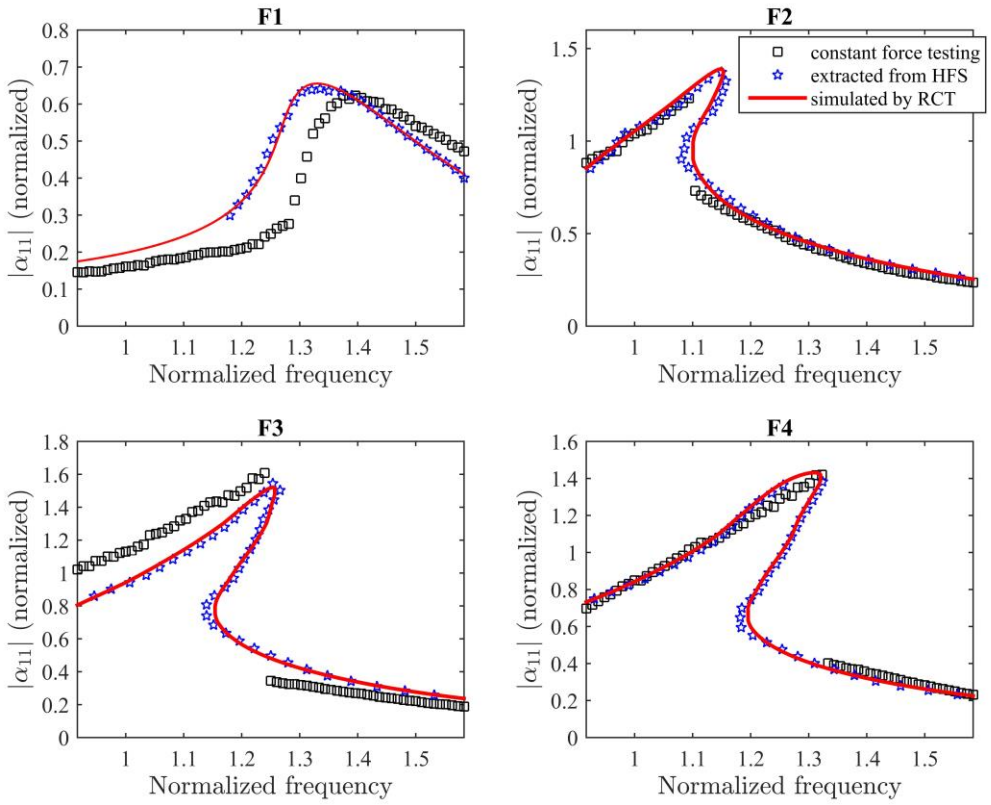

Figure 4-37. Comparison of the driving point receptances of the control fin actuation mechanism synthesized from the identified nonlinear modal parameters with the receptances directly measured from constant-force testing and with the receptances extracted from HFS

It is highly probable that the relatively poor repeatability is closely related to gaps and friction surfaces between moving parts, as well as with the sensitivity of the lubricants to environmental conditions such as temperature. At the end of a specific test, the reconfiguration of gaps and contact surfaces in a random manner due to excessive vibration, and the significant temperature change due to heat generation may result in some changes in the nonlinear dynamics of the system.

A final question that can be asked is why the computed FRFs match perfectly with the experimental data extracted from the HFS but not with the experimental data measured from the constant-force testing. The answer is simple: Identification of the nonlinear modal parameters and the construction of the HFS rely on the same experimental data set collected during response-controlled stepped-sine testing. However, the FRFs obtained from constant-force testing represent another experimental data set which is not used in the identification of nonlinear modal parameters.

To conclude this experimental study, nonlinear frequency response curves corresponding to various constant force levels are extracted by cutting the HFS with corresponding constant force planes as shown in Figure 4-38. Finally, the backbone curve is identified by combining the resonance peaks of these frequency response curves, as shown in the same figure. Figure 4-38 clearly proves that the HFS technique can successfully extract the turning points of overhanging frequency response curves.

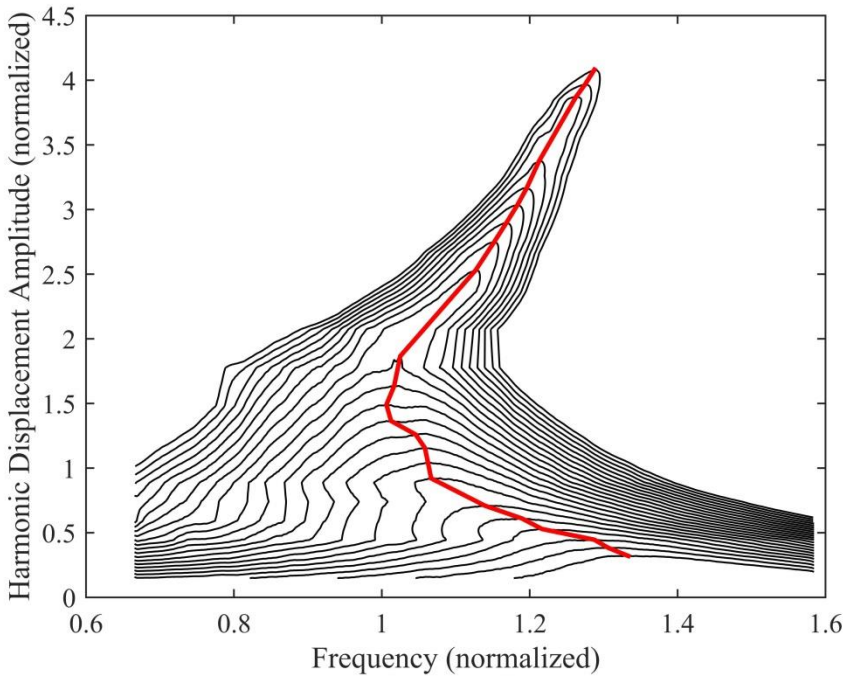

Figure 4-38. Constant-force frequency response curves and the backbone curve of the real control fin actuation mechanism at the driving point, obtained by cutting the HFS with various constant force planes

4.2 Experimental Validation of the Proposed Nonparametric Identification Technique in the Spatial Domain: The Describing Surface Method

4.2.1 The T-Beam Benchmark

The T-beam benchmark experimental setup was previously studied in Section 4.1.1 to validate the nonlinear modal identification technique proposed in Chapter 2. In this study, the same test rig is used to validate the Describing Surface Method (DSM) proposed in Chapter 3.

The nonlinearity introduced by the metal strips shown in Figure 4-1 is treated in this application as a localized nonlinearity between the free end of the cantilever

beam and the ground. Accordingly, the equivalent stiffness and damping nonlinearities are identified in physical (spatial) coordinates.

The experimental data used in the DSM is the same constant-response FRF data measured by RCT as shown in Figure 4-3(b). In this figure, it can be clearly seen that the resonance frequency increases with increasing vibration amplitude, which indicates hardening stiffness behavior. On the other hand, the decreasing FRF amplitude with increasing vibration amplitude shows that the nonlinear damping increases. Since nonlinearities can be neglected at low vibration levels in the T-beam case, the appropriate boundary condition in solving Eq. (3.21) is $\upsilon(0,\omega) = 0$.

The partial derivatives of the describing surface of nonlinearity can be calculated as illustrated in Figure 4-39 by substituting the constant-response receptances given in Figure 4-3(b) into Eq. (3.21). As suggested in Section 3.2, the partial derivative value between two successive displacement amplitude levels is taken to be constant, i.e. $\upsilon(|X|,\omega)$ is assumed to be C^o continuous. Then, Eq. (3.21) is solved numerically, which yields the describing surface of nonlinearity as shown in Figure 4-40. Fitting a mathematical model to such surfaces usually requires considerable effort and sometimes may not be possible at all. Accordingly, in constructing the mathematical model represented by Eq (3.23), the identified describing surface of nonlinearity is preferably used in its nonparametric form, i.e. as a look-up table. However, it is always an option to fit a parametric model to the identified surface whenever it is possible.

As can be seen from the above discussion, the receptances measured at several different 'constant displacement amplitude' levels (see Figure 4-3(b)) are the only necessary input required for the nonlinear system identification by using the DSM. These receptances are simply measured by using the RCT strategy, which is based on the closed-loop control of the displacement amplitude corresponding to the fundamental harmonic throughout the frequency sweep. An initial estimate of the transfer function between the drive voltage and the control channel obtained from

preliminary system identification (by using broadband random or sine sweep testing) is fed into the controller. This transfer function is updated in real-time during the actual response-controlled stepped-sine testing in order to keep the control channel value within the tolerance limits of the reference profile.

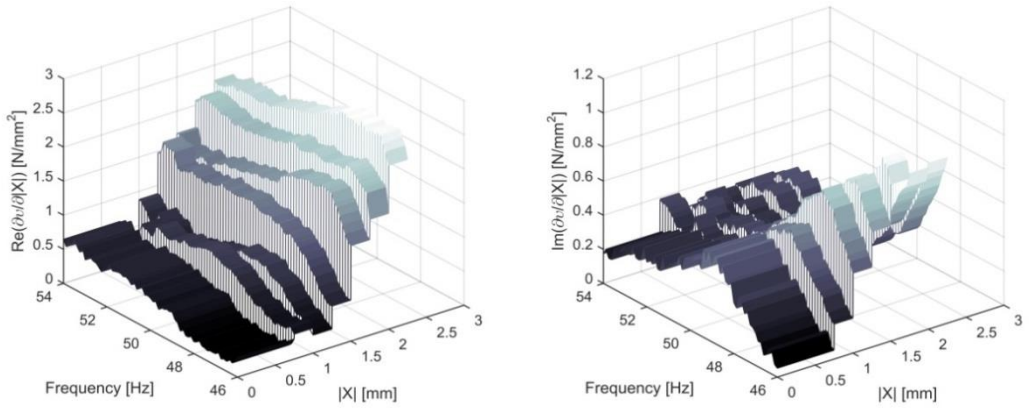

(a) (b)

Figure 4-39. Real (left) and imaginary (right) parts of the partial derivative of the describing surface of nonlinearity for the T-beam

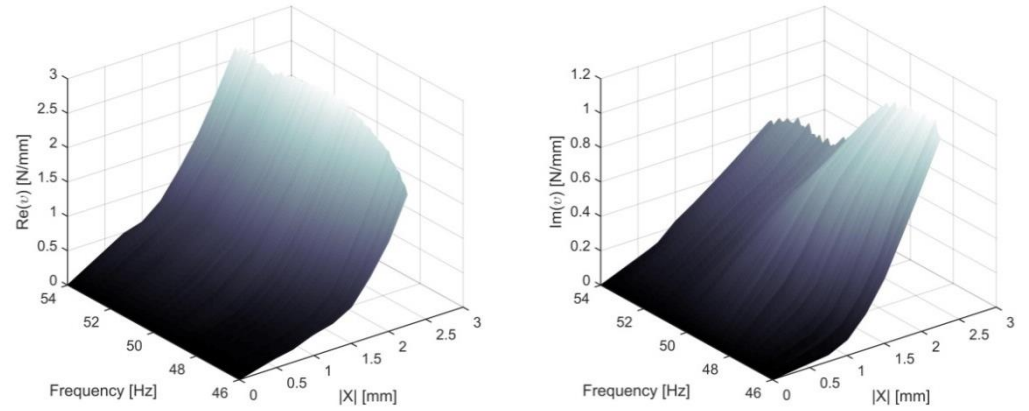

Figure 4-40. Real (left) and imaginary (right) parts of the describing surface of nonlinearity for the T-beam

In Figure 4-40, the real and imaginary parts of the describing surface represent the equivalent nonlinear stiffness and the equivalent nonlinear damping of the structure in the spatial domain, i.e. in physical coordinates, respectively. The first observation made from the figure is the increase of the real part with increasing vibration amplitude, which indicates hardening stiffness behavior. Secondly, the increase of the imaginary part with increasing vibration amplitude shows that the system exhibits an increasing damping nonlinearity. However, the most interesting observation that can be made from Figure 4-40 is that although the frequency dependence of the nonlinear stiffness is negligible, the nonlinear damping significantly depends on frequency especially at relatively high vibration levels, which can be seen from the imaginary part given on the right of the figure. It is important to note that most of the well-established state-of-the-art techniques such as the classical DFM or the well-known restoring force surface (RFS) method are not capable of identifying the frequency dependence of nonlinearity.

Once the describing surface of nonlinearity is determined, the FRF of the underlying linear system can be estimated by using Eq. (3.22). The result is shown in Figure 4-41.

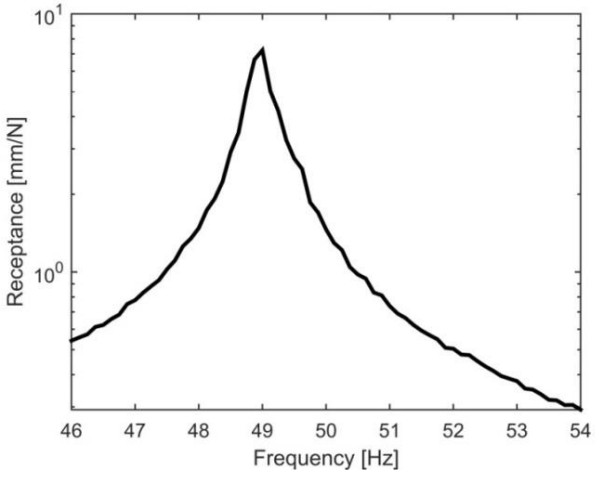

Figure 4-41. Receptance of the underlying linear system of the T-beam estimated by using the DSM

At this stage, it would be a good practice to evaluate the performance of the DSM in comparison with the classical DFM [55, 56]. To do so, the identification of the T-beam is also accomplished by using the latter approach. In the DFM, the describing function of nonlinearity is determined by using the constant-force FRFs measured by the classical force-controlled steppe-sine tests and shown in Figure 4-3(a). The variations of the real and imaginary parts of the describing function of nonlinearity with displacement amplitude are shown in Figure 4-42. The best parametric model fitted to the real part of the describing function is a second-order polynomial, which reveals the cubic stiffness behavior of the T-beam. On the other hand, a polynomial of order 5 is fitted to the imaginary part which represents the equivalent nonlinear damping.

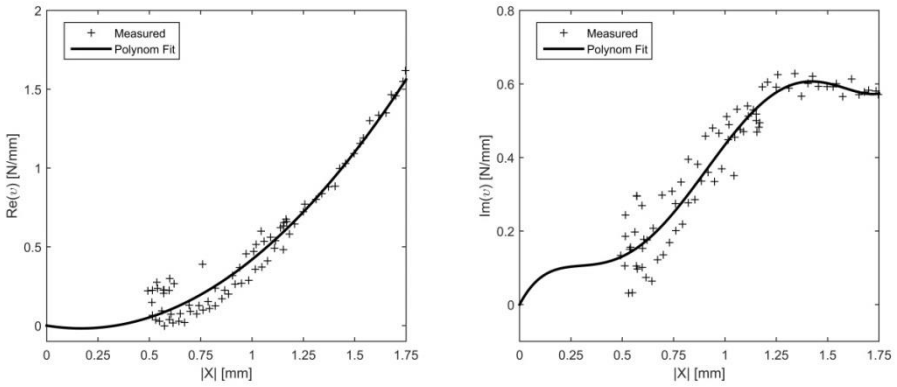

Figure 4-42. Real (left) and imaginary (right) parts of the describing function of nonlinearity of the T-beam

The main objective of the DSM (or the DFM) is to construct a reliable mathematical model that accurately estimates the nonlinear response of the system to prescribed harmonic forcing. In order to validate the DSM and to compare its accuracy with that of the DFM, the driving point receptances of the T-beam are calculated by using the DSM and the DFM at forcing levels 0.1, 0.5, and 1.0 N. The comparison of these computational results with the real experimental data is

given in Figure 4-43. As can be seen from the figure, the simulation results of the DSM match perfectly with the measured constant-force receptances, which is not the case for the DFM simulation results.

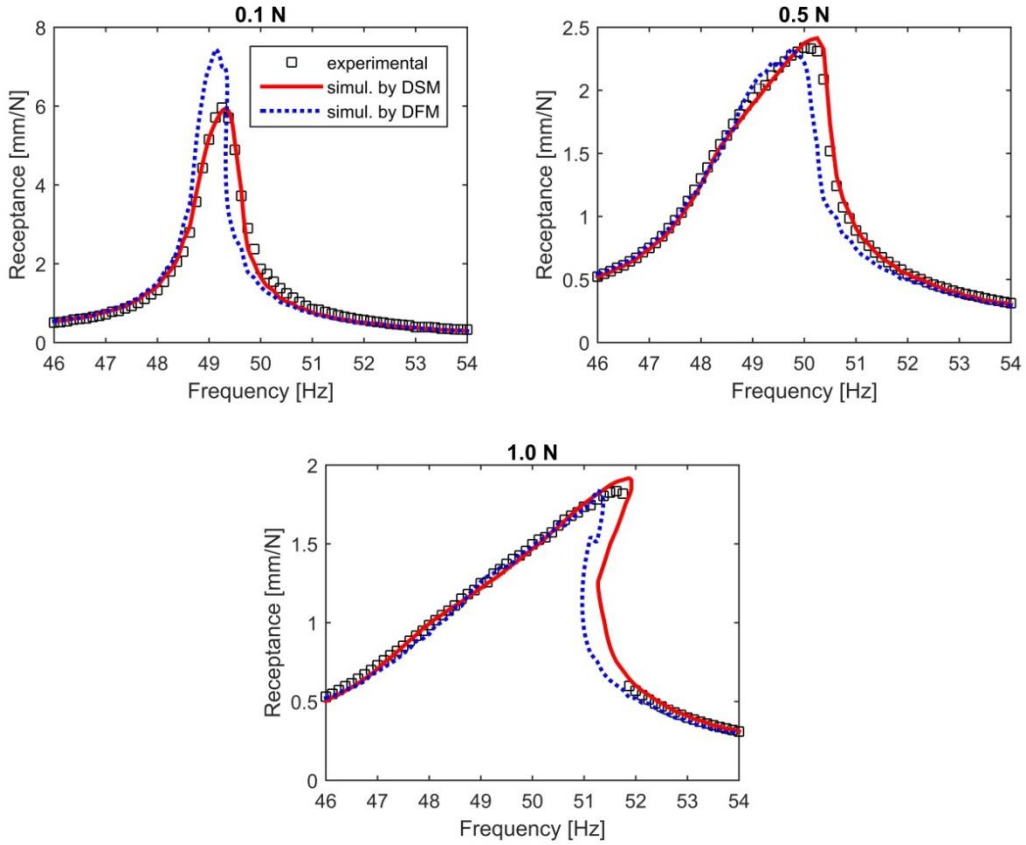

Figure 4-43. Comparison of the simulation results obtained by the DSM and the DFM with the experimental data of the T-beam obtained from force-controlled stepped-sine testing

It is important to note that the RCT strategy used by the DSM has several important advantages over the classical constant-force testing employed by the DFM and by many other state-of-the-art identification techniques. There exist at most two frequency points (before and after resonance) corresponding to the same

displacement amplitude on a near resonant-frequency response curve measured by the constant-force stepped-sine testing. In this circumstance, the describing function of nonlinearity may not be accurately identified. Most importantly, the frequency dependence of nonlinearity cannot be fully assessed. However, these drawbacks of the constant-force testing (i.e. the force-control approach) are avoided by the RCT strategy which collects as much data as the frequency points at a constant displacement amplitude level. Furthermore, in contrast to the common preconception, in sine testing of nonlinear structures, it is much easier for the closed-loop controller to keep a constant response profile within the tolerance limits than a constant force profile. Any closed-loop stepped sine test carried out with standard (commercial) equipment is preceded by a linear system identification process to obtain a rough initial estimate of the transfer function of the test subject. In the case of constant-force testing, switching from one frequency point to another causes the response amplitude to change drastically especially around resonance. Consequently, the actual transfer function considerably deviates from its approximate initial estimate due to nonlinear effects, and eventually the controller needs to make many corrective iterations to keep the force within the tolerance limits. However, in the case of the response-controlled tests, since the response amplitude (upon which the nonlinear stiffness and damping depend the most) is kept constant, the deviation from the approximate transfer function is minimized, which results in very fast and smooth stepped sine testing compared to the force-control approach.

This section is concluded by validating the receptance curve estimated by the DSM at the constant force level of F=1N (see Figure 4-43) with the experimental data as shown in Figure 4-44. As can be seen from the figure, the simulation result agrees very well with the experimental results including the unstable region. It is important to note that the unstable branch extracted from the HFS is purely experimental and its perfect match with the simulation result validates the accuracy of the DSM.

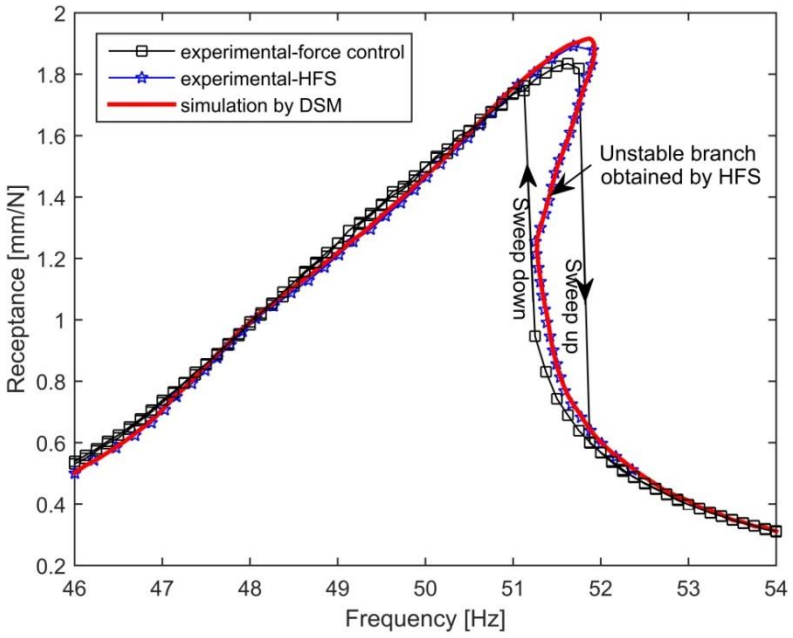

Figure 4-44. Comparison of the receptances measured by the HFS of the T-beam at F=1N with the DSM simulation results and the receptances measured by using force-controlled stepped-sine testing

4.2.2 Dummy Mass on Elastomeric Vibration Isolators

In this second experimental study, the DSM is validated by using a dummy mass on elastomeric vibration isolators as illustrated in Figure 4-45. The test setup is composed of four identical AM-002-7 series LORD elastomeric vibration isolators attached to a round dummy mass of 6.4 kg. Vibration isolators are placed symmetrically with respect to the centerline of the dummy mass so that the structure can be modeled as an SDOF system.

The test rig is excited with an electrodynamic shaker (B&K) attached to the centerline of the dummy mass via a push-rod as shown in Figure 4-45. The excitation force is measured by using a force transducer (Dytran 1022V) attached

to the push-rod. The vibration response data is recorded by using a miniature (Dytran 3225M23) accelerometer placed at the top of the dummy mass.

The test campaign consists of a series of force-controlled and response-controlled stepped-sine tests. The constant-response receptances of the system measured by RCT at 8 different constant displacement amplitude levels, ranging from 0.01 mm to 0.08 mm, are given in Figure 4-46. A frequency resolution of 0.125 Hz is used. Figure 4-47 shows the typical FFTs of time data samples recorded during the response-controlled and force-controlled stepped-sine tests of the system. The higher harmonic term turns out to be negligible compared to the fundamental harmonic, which validates the single harmonic assumption of the DSM.

In this study, it is observed that the nonlinearity of the vibration isolators diminishes as the vibration amplitude increases. Accordingly, the appropriate boundary condition would be $\upsilon(\infty, \omega) = 0$. Due to the difficulty of applying an asymptotic boundary condition in numerical analysis, the relative describing surface definition represented by Eq. (3.24) is used in this study by taking the receptance measured at the highest vibration level, i.e. 0.080 mm, as the reference value, as shown in Figure 4-46. The relative describing surface of nonlinearity determined by the DSM is shown in Figure 4-48.

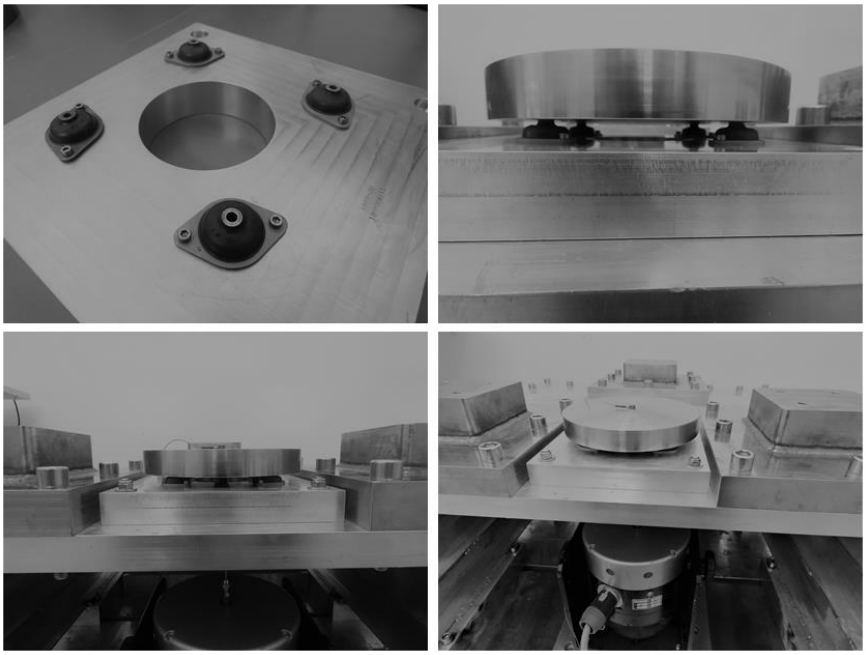

Figure 4-45. Experimental setup of the dummy mass on elastomeric vibration isolators

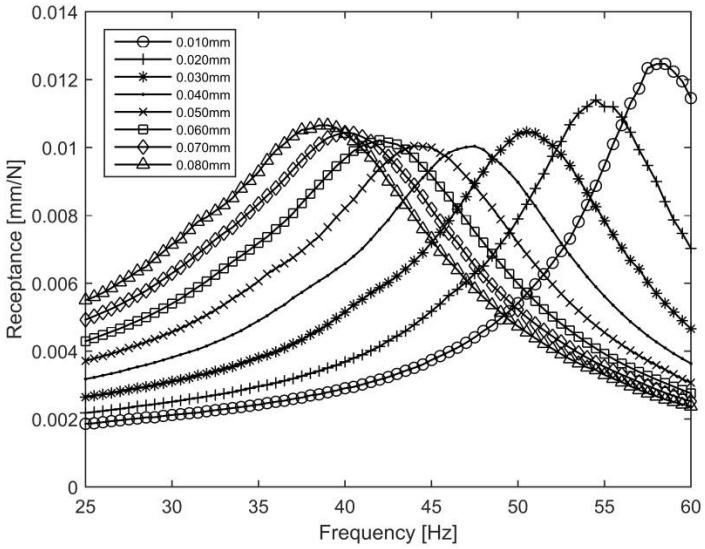

Figure 4-46. Receptances of the dummy mass on elastomeric vibration isolators measured by response-controlled stepped sine tests at various constant displacement amplitudes

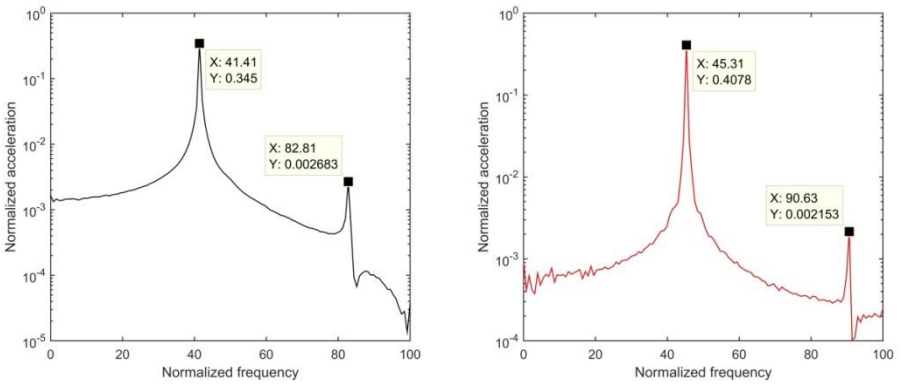

(a) (b)

Figure 4-47. Typical FFTs of time data samples collected during stepped-sine testing of the dummy mass on elastomeric vibration isolators: (a) response-controlled test (0.05 mm amplitude level) (b) force-controlled test (5.0 N amplitude level)

In Figure 4-48, it is clearly seen that the nonlinear damping considerably depends on frequency as in the case of the T-beam. On the other hand, the frequency dependence of the stiffness nonlinearity is, once again, negligible.

To validate the DSM and to compare its performance with the DFM, first of all, the constant-force FRFs are measured at three different force levels as shown in Figure 4-49. Then, these FRFs are used in the DFM, which gives the relative describing function of nonlinearity as shown in Figure 4-50. The constant-force receptances calculated by the DSM and the DFM are compared with the experimental data in Figure 4-51. It is observed once again that the simulation results of the DSM match perfectly with the real experimental data and do a better job than the DFM, especially around resonance.

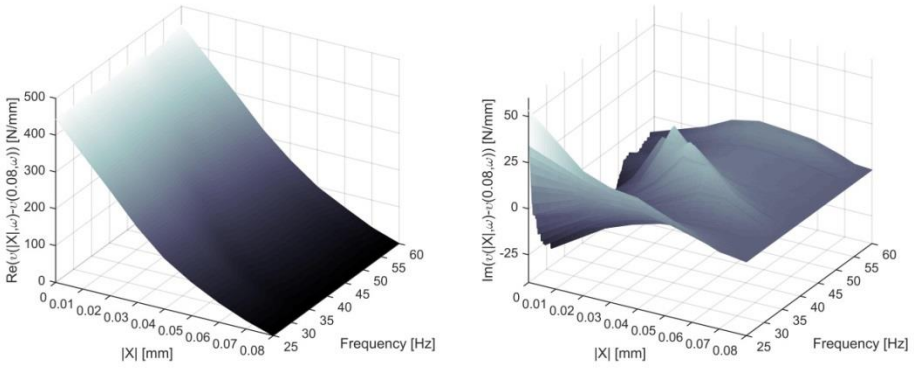

Figure 4-48. Real (left) and imaginary (right) parts of the relative describing surface of the nonlinearity of the elastomeric vibration isolators

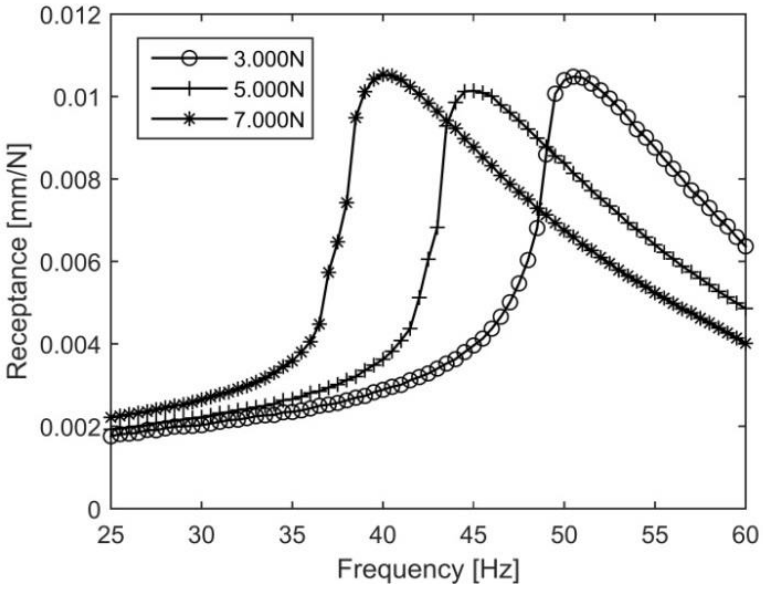

Figure 4-49. Receptance curves of the dummy mass on elastomeric vibration isolators measured by the force-controlled stepped sine tests at three different force amplitudes

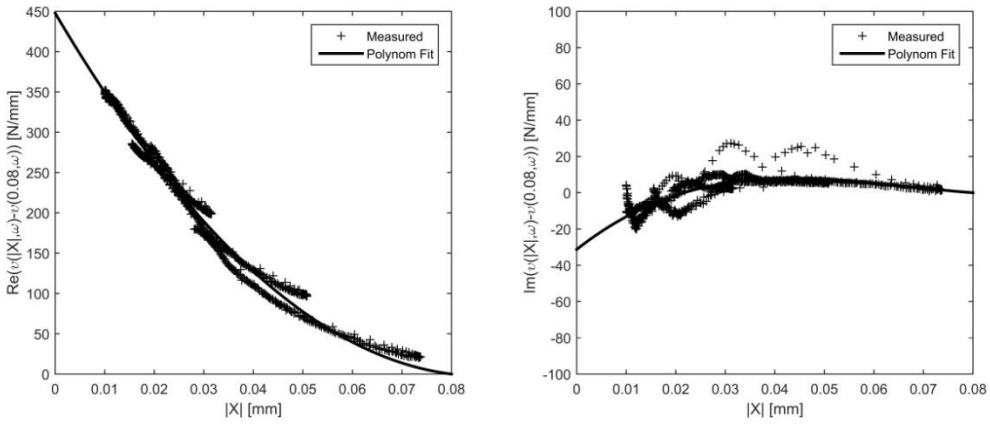

Figure 4-50. Real (left) and imaginary (right) parts of the relative describing function of nonlinearity of the dummy mass on elastomeric vibration isolators

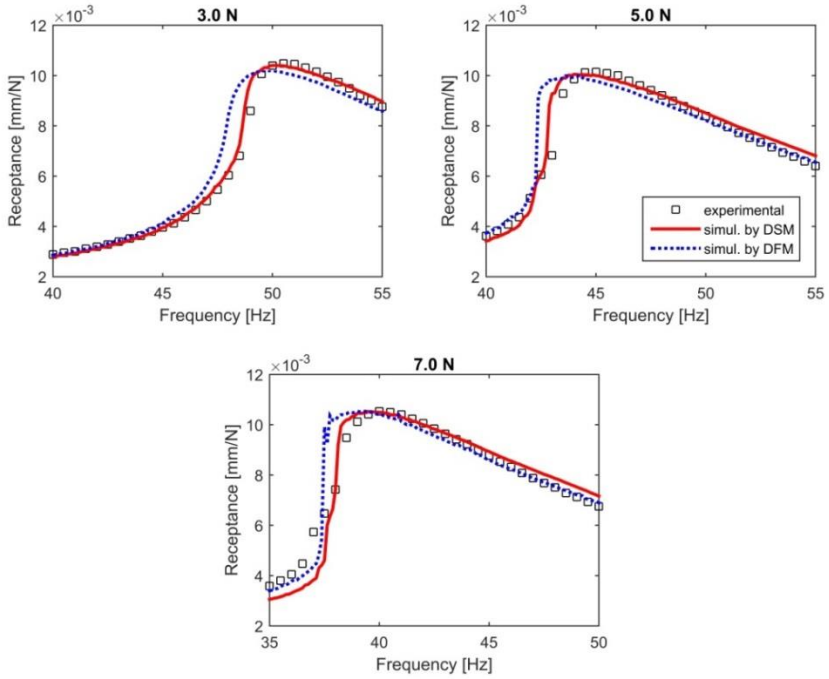

Figure 4-51. Comparison of the simulation results obtained by the DSM and the DFM, with the experimental data of the dummy mass on elastomeric vibration isolators obtained from force-controlled stepped-sine testing

4.2.3 Control Fin Actuation Mechanism of a Real Missile

The control fin actuation mechanism of a real missile was previously studied in Section 4.1.4 to validate the nonlinear modal identification technique proposed in Chapter 2. In this study, the same test rig (see Figure 4-31) is used to validate the Describing Surface Method (DSM) proposed in Chapter 3.

In this application, the real and imaginary parts of the relative describing surface are calculated by taking the receptances measured at displacement amplitude levels of D8 and D15 as reference values, respectively, as shown in Figure 4-52. Cross-sections of the real and imaginary parts of the relative describing surface at different frequencies are also given in Figure 4-53.

In Figure 4-52 and Figure 4-53, it is observed that the real part of the relative describing surface, which represents the nonlinear stiffness, first decreases up to D8 amplitude level where it is equal to zero and then increases again. On the other hand, the imaginary part of the relative describing surface, which represents the nonlinear damping, decreases as the vibration level increases. The most important observation that can be made in Figure 4-53 is that although the nonlinear damping depends on frequency considerably, the frequency dependence of the nonlinear stiffness is negligible.

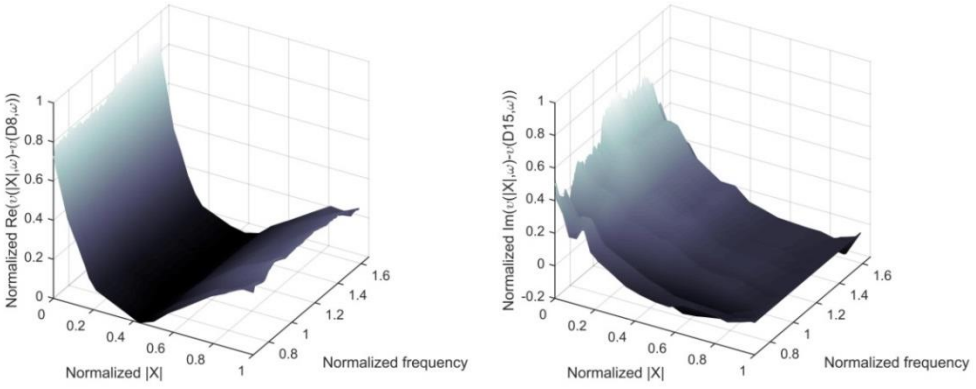

Figure 4-52. Real (left) and imaginary (right) parts of the relative describing surface of nonlinearity for the control fin actuation mechanism

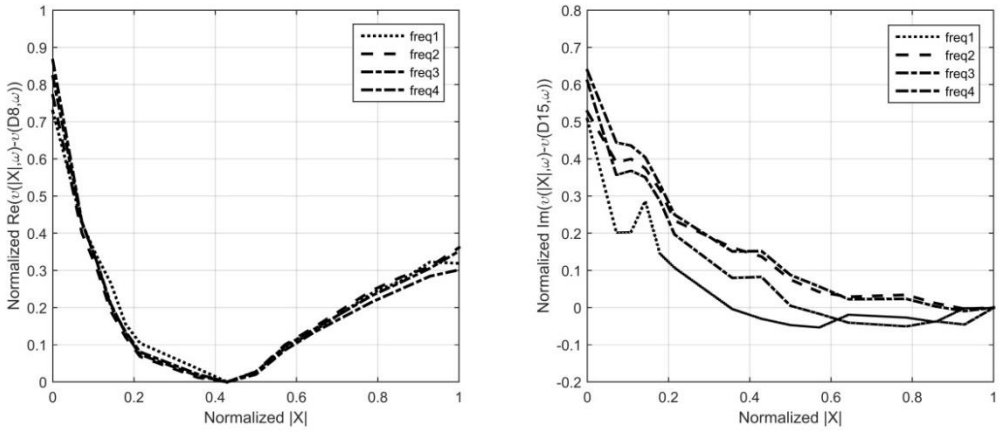

Figure 4-53. Cross-section views of the real (left) and imaginary (right) parts of the relative describing surface of nonlinearity of the control fin actuation mechanism at different frequencies

Once again, the validation of the DSM is accomplished by comparing the constant-force FRFs calculated by the DSM with the real experimental data as illustrated in Figure 4-54. As can be seen from the figure, the match between the synthesized FRFs and the ones extracted from HFS is perfect. This is something expected because the identification of the describing surface of nonlinearity and the construction of the HFS rely on the same experimental data set collected during response-controlled stepped-sine testing. On the other hand, even though the agreement between the synthesized FRFs and the ones measured from constant-force testing is quite satisfactory, there exists some discrepancy. As discussed in detail in Section 4.1.4, the main reason for the discrepancy is seemingly poor repeatability, i.e. the variability of the repeated tests.

A final note about Figure 4-54 is that contrary to the nonlinear experimental modal analysis technique used in Section 4.1.4, the unstable branches of the nonlinear receptances could not be estimated by using the DSM because Newton's Method with the arc-length continuation could not converge due to the nonsmooth characteristic of the nonparametric describing surface. It is also interesting to note that the DFM simulations do not give satisfactory results due to the difficulty in

identifying the complex nonlinear behavior of the control fin actuation mechanism parametrically; therefore they are not shown in Figure 4-54.

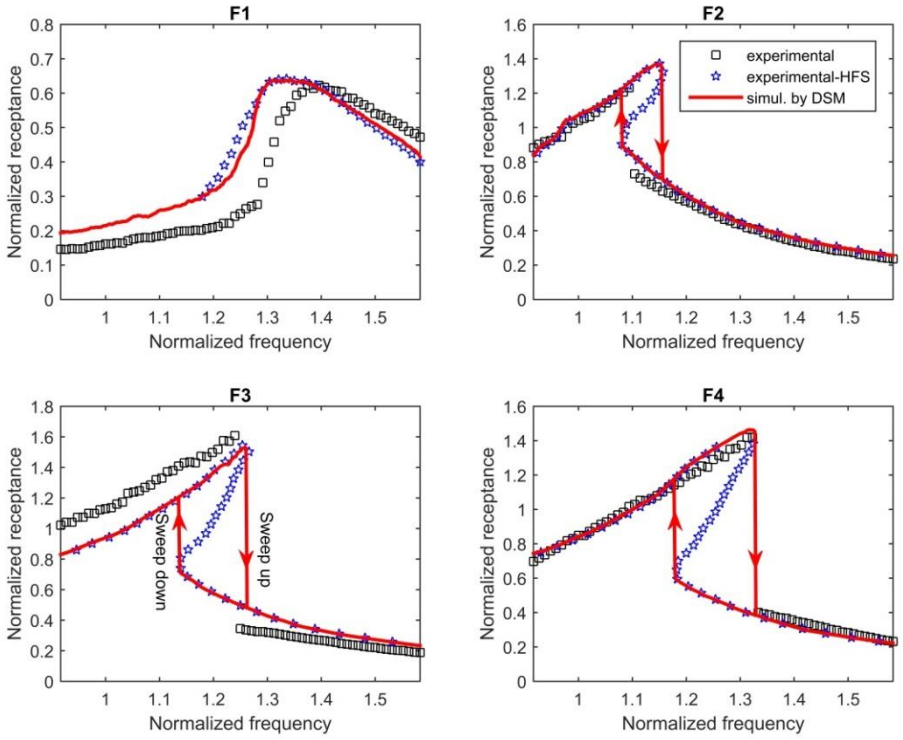

Figure 4-54. Comparison of the simulation results obtained by the DSM of the control fin actuation mechanism with the experimental data obtained from force-controlled stepped-sine testing and the HFS (response-controlled stepped-sine testing)

CHAPTER 5

SUMMARY AND CONCLUSION

Although the structural dynamics community has witnessed important developments in the field of nonlinear system identification over the last two decades, no general method applicable to a wide range of nonlinear engineering structures has been developed yet. Consequently, the current state-of-the-art still retains its toolbox philosophy.

Considering well-established nonlinear system identification techniques as well as recently proposed promising ones, it can be said that the identification of strong local nonlinearities is within reach today. However, there are still important challenging problems such as the identification of structures with multiple discrete nonlinearities at several different locations (e.g., structures with several bolted joints) and the identification of structures with continuously distributed geometrical nonlinearity due to large amplitude oscillations.

Being motivated by the challenging nonlinear system identification problems mentioned above and by the absence of a general framework applicable to a wide range of engineering structures, this thesis work introduces two novel nonlinear system identification methods proposed in the modal and spatial domains, respectively, which have the potential to build up a general framework. Both methods are based on response-controlled stepped-sine testing (RCT) where the displacement amplitude of the excitation point is kept constant throughout the frequency sweep.

The proposed modal identification method is essentially a nonlinear experimental modal analysis technique that applies to systems with several nonlinearities at different (and even unknown) locations as well as to systems with continuously distributed (geometrical) nonlinearities. This method identifies the nonlinear modal

parameters as functions of modal amplitude by applying standard linear modal analysis techniques to measured frequency response functions (FRFs) which come out in quasi-linear form by virtue of the RCT. In the case of using multiple sensors during RCT, nonlinear normal modes can also be experimentally extracted from the identified modal constants. Near-resonant constant-force FRFs including unstable branches (if there are any) can then be calculated from the identified nonlinear modal parameters by using Newton's Method with the arc-length continuation algorithm. Alternatively, the same constant-force FRFs can be extracted directly from the experiment by using a novel concept, namely, the harmonic force surface (HFS) also proposed for the first time in this thesis work. The key feature of the HFS is its ability to accurately extract the unstable branches and the turning points of constant-force FRFs, which makes it possible to extract the backbone curves of strongly nonlinear systems as well.

Within the scope of this thesis work, the proposed nonlinear experimental modal analysis method is validated with the following experimental case studies:

- A cantilever beam with a localized strong stiffening nonlinearity,
- A beam which exhibits continuously distributed strong geometrical nonlinearity due to large deformations,
- A real missile structure which exhibits considerable damping nonlinearity mostly due to several bolted joints on the structure,
- A control fin actuation mechanism which exhibits very complex and strong nonlinearity due to backlash and friction.

The diversity among all these applications clearly proves that the developed technique can be applied to a wide range of nonlinear system identification problems.

The spatial system identification method proposed in this thesis, namely the Describing Surface Method (DSM), applies to systems with a single nonlinearity localized between the excitation point and the ground where the single-degree-of-

freedom assumption can be used. The DSM identifies the describing surface of nonlinearity, real and imaginary parts of which correspond to the equivalent nonlinear stiffness and nonlinear damping at a specific location in the structure. The proposed technique essentially extends the classical describing function method to make the identification nonparametric and to include the frequency dependence of nonlinearity. Once again, constant-force FRFs, including any existing unstable branch, can be calculated iteratively by using the identified describing surface representing the nonlinearity. Similar to the nonlinear experimental modal analysis method mentioned above, the DSM also relies on FRFs measured with RCT strategy.

Within the scope of this thesis work, the DSM is validated with the following experimental case studies:

- A cantilever beam with a localized strong stiffening nonlinearity,
- A dummy mass on elastomeric vibration isolators,
- A control fin actuation mechanism which exhibits very complex and strong nonlinearity due to backlash and friction.

The prominent feature of both techniques proposed in this thesis study is that they simply rely on commercially available standard modal testing equipment (e.g., LMS SCADAS Mobile and LMS Test Lab.) and do not require sophisticated control algorithms. Furthermore, the proposed nonlinear experimental modal analysis, which simply relies on the application of standard linear modal analysis techniques (e.g. LMS PolyMAX), can be applied very easily by practicing engineers. With this approach, the identification of strongly nonlinear engineering systems by using standard equipment is now within reach. This feature has the potential to make the proposed experimental modal analysis technique very popular in the industry. The only important limitation of the proposed techniques is the assumption of no internal resonance. Possible improvements to overcome this limitation will be the subject of future projects.

The contributions of this thesis work to the literature are discussed in detail in Section 1.4 by making comparisons with the state-of-the-art. Consequently:

- By virtue of the proposed nonlinear experimental modal analysis technique based on RCT, the modal identification of a wide range of nonlinear structures including the ones that exhibit distributed nonlinearity (including geometrical nonlinearity) as well as high and nonlinear damping is within reach.
- The simple and accurate identification of mass normalized NNMs and nonlinear modal damping ratio of strongly nonlinear MDOF systems is within reach.
- The accurate identification of NNM backbone curves and unstable branches of strongly nonlinear MDOF systems directly from the experiment by using standard commercial equipment is within reach by the HFS concept.
- By virtue of the proposed DSM, the nonparametric identification of complex localized nonlinearities including the quantification of the frequency dependence of nonlinearity is within reach without the apriori knowledge of the nonlinearity type.

CHAPTER 6

FUTURE DIRECTIONS

One of the future directions would be the extension of the RCT approach to the case of internal resonance where the effects of higher harmonics cannot be neglected. This extension requires the implementation of the non-invasive control to the RCT approach.

Another future direction would be the implementation of the modal model of nonlinear structures obtained by the RCT approach in structural coupling and structural modification studies.

The nonlinear modal model and especially the nonlinear modal damping ratio obtained by RCT can very useful in the field of nonlinear aeroelasticity for the accurate prediction of limit cycle oscillation. In this context, the application of the RCT approach to determine the nonlinear modal model of a real aircraft wing would be a good start in the way of carrying aeroelastic analysis with nonlinear modal parameters.

REFERENCES

[1] D.L. Brown, R.J. Allemang, The Modern Era of Experimental Modal Analysis: One Historical Perspective, Sound and Vibration, 40th Anniversary Issue (2007) 16-25.

[2] R. W. Bunton, C. M. Denegri Jr., Limit Cycle Oscillation Characteristics of Fighter Aircraft, Journal of Aircraft, 37 (5) (2000) 916–918.

[3] C. M. Denegri Jr., Limit Cycle Oscillation Flight Test Results of a Fighter with External Stores, 37 (5) (2000) 761-769.

[4] W.J. Norton, Limit Cycle Oscillation and Flight Flutter Testing, in: Proceeds of the 21st Annual Symposium, Society of Flight Test Engineers, Lancaster, CA, 1990.

[5] R. Melville, Nonlinear Mechanisms of Aeroelastic Instability for the F-16, AIAA Paper 2002-0871, 2002.

[6] B. B. Prananta, J. C. Kok, S. P. Spekreijse, M. H. L. Hounjet, and J. J. Meijer, Simulation of Limit Cycle Oscillation of Fighter Aircraft at Moderate Angle of Attack, National Aerospace Laboratory NRL TR NRL-TP-2003-526, 2003.

[7] C. Farhat, P. Geuzaine, and G. Brown, Application of a Three-Field Nonlinear Fluid-Structure Formulation to the Prediction of the Aeroelastic Parameters of an F-16 Fighter, Computers and Fluids, 32 (1) (2003) 3-29.

[8] C. M. Denegri Jr. and J. A. Dubben, F-16 Limit Cycle Oscillation Analysis Using Transonic Small-Disturbance Theory, AIAA Paper 2005-2296, 2005.

[9] E. H. Dowell, J. P. Thomas, K. C. Hall and C. M. Denegri Jr., Theoretical Predictions of F-16 Fighter Limit Cycle Oscillations for Flight Flutter Testing, Journal of Aircraft, 46 (5) (2009) 1667–1672.

[10] P. C. Chen, Z. Zhang, A. Sengupta, and D. D. Liu, Studies of Limit-Cycle-Oscillation Mechanism of Fighter with Stores Using an Euler with Boundary Layer Solver, in: International Forum on Aeroelasticity and Structural Dynamics, IFASD Paper 2009-159, June 2009.

[11] C. M. Denegri Jr., V.K. Sharma, J.S. Northington, F-16 Limit Cycle Oscillation Analysis Using Nonlinear Damping, Journal of Aircraft, 53 (1) (2016) 243-250.

[12] P.C. Chen, Z. Zhang, Z. Zhou, X.Q. Wang, M.P. Mignolet, Limit Cycle Oscillation Prediction for Aircraft with External Stores, in: International Forum on Aeroelasticity and Structural Dynamics, IFASD-2019, Savannah, GA, USA, 2019.

[13] G. Kerschen, K. Worden, A.F. Vakakis, J.C. Golinval, Past, present and future of nonlinear system identification in structural dynamics, Mechanical Systems and Signal Processing 20 (2006) 505-592.

[14] J.P. Noël, G. Kerschen, Nonlinear system identification in structural dynamics: 10 more years of progress, Mechanical Systems Signal Processing 83 (2017) 2-35.

[15] S.F. Masri, T.K. Caughey, A nonparametric identification technique for nonlinear dynamic problems, J. Appl. Mech. 46 (1979) 433-447.

[16] E.F. Crawley, A.C. Aubert, Identification of nonlinear structural elements by force-state mapping, AIAA J. 24 (1986) 155-162.

[17] S.F. Masri, H. Sassi, T.K. Caughey, A nonparametric identification of nearly arbitrary nonlinear systems, J. Appl. Mech. 49 (1982) 619-628.

[18] K. Worden and G. R. Tomlinson. Nonlinearity in structural dynamics: Detection, identification and modeling. CRC Press, Boca Raton, 2001.

[19] Belingardi G., Campanile P., Improvement of the shock absorber dynamic simulation by the restoring force mapping method, in: Proceedings of the International Seminar in Modal Analysis and Structural Dynamics, Leuven, 1990.

[20] C. Surace, K. Worden, G.R. Tomlinson, On the nonlinear characteristics of automotive shock absorbers, J. Auto Eng. 206 (1992) 3–16.

[21] Duym S., Stiens R., Reybrouck K., Fast parametric and nonparametric identification of shock absorbers, in: Proceedings of the International Seminar on Modal Analysis (ISMA), Leuven 1996.

[22] E. Bonisoli, A. Vigliani, Identification techniques applied to a passive elasto-magnetic suspension, Mech. Syst. Signal Process. 21 (2007) 1479-1488.

[23] D. Rizos, G. Feltrin, M. Motavalli, Structural identification of a prototype pre-stressable leaf-spring based adaptive tuned mass damper: nonlinear characterization and classification, Mech. Syst. Signal Process. 25 (2011) 205-221.

[24] D. Goege, J.M. Sinapius, Experiences with dynamic load simulation by means of modal forces in the presence of structural nonlinearities, Aerosp. Sci.Technol. 10 (2006) 411-419.

[25] M.S. Allen, H. Sumali, D.S. Epp, Piecewise-linear restoring force surfaces for semi-nonparametric identification of nonlinear systems, Nonlinear Dyn. 54 (2008) 123-155.

[26] J.P. Noël, L. Renson, G. Kerschen, Complex dynamics of a nonlinear aerospace structure: experimental identification and modal interactions, J. Sound Vib. 333 (2014) 2588-2607.

[27] K. Worden, D. Hickey, M. Haroon, D.E. Adams, Nonlinear system identification of automotive dampers: a time and frequency-domain analysis, Mech. Syst. Signal Process. 23 (2009) 104-126.

[28] H. Ahmadian, H. Jalali, F. Pourahmadian, Nonlinear model identification of a frictional contact support, Mech. Syst. Signal Process. 24 (2010) 2844-2854.

[29] T. Dossogne, J.P. Noël, C. Grappasonni, G. Kerschen, B. Peeters, J. Debille, M. Vaes, J. Schoukens, Nonlinear ground vibration identification of an F-16 aircraft - Part II: Understanding nonlinear behavior in aerospace structures using sine-sweep testing, in: Proceedings of the 16th International Forum on Aeroelasticity and Structural Dynamics (IFASD), Saint Petersburg, Russia, 2015.

[30] I. J. Leontaritis and S. A. Billings, Input-output parametric models for nonlinear systems Part I: Deterministic non-linear systems. International Journal of Control, 41(2) (1985a) 303–328.

[31] I. J. Leontaritis and S. A. Billings, Input-output parametric models for non-linear systems Part II: Stochastic non-linear systems. International Journal of Control, 41(2) (1985b) 329–344.

[32] M. Korenberg, S.A. Billings, Y.P. Liu, P.J. McIlroy, An orthogonal parameter estimation algorithm for nonlinear stochastic systems, International Journal of Control 48 (1988) 193–210.

[33] S.A. Billings, S. Chen, R.J. Backhouse, Identification of linear and nonlinear models of a turbocharged automotive diesel engine, Mechanical Systems and Signal Processing 3 (1989) 123–142

[34] S. Chen, S.A. Billings, C.F.N. Cowan, P.M. Grant, Practical identification of NARMAX models using radial basis functions, International Journal of Control 52 (1990) 1327–1350.

[35] S.A. Billings, K.M. Tsang, Spectral analysis for nonlinear systems, part I: parametric non-linear spectral analysis, Mech. Syst. Signal Process 3 (1989) 319–339.

[36] S.A. Billings, K.M. Tsang, Spectral analysis for nonlinear systems, part II: interpretation of nonlinear frequency response functions, Mech. Syst. Signal Process. 3 (1989) 341–359.

[37] Q. Chen, K.Worden, P.Peng, A.Y.T.Leung, Genetic algorithm with an improved fitness function for (N)ARX modeling, Mech. Syst. Signal Process. 21 (2007) 994–1007.

[38] Z.K. Peng, Z.Q.Lang, C.Wolters, S.A.Billings, K.Worden, Feasibility study of structural damage detection using NARMAX modeling and Nonlinear Output Frequency Response Function based analysis, Mech. Syst. Signal Process. 25 (2011) 1045–1061.

[39] K. Worden, J. Barthorpe, Identification of hysteretic systems using NARX models, part I: evolutionary identification, in: Proceedings of the 30th International Modal Analysis Conference (IMAC), Jacksonville, FL, USA, 2012.

[40] K.Worden, R.J. Barthorpe, Identification of hysteretic systems using NARX models, part II:a Bayesian approach, in: Proceedings of the 30th International Modal Analysis Conference (IMAC), Jacksonville, FL, USA, 2012.

[41] M.Simon, G.R. Tomlinson, Use of the Hilbert transform in modal analysis of linear and non-linear structures, J. Sound Vib. 96(4) (1984) 421–436.

[42] G.R. Tomlinson, Developments in the use of the Hilbert transform for detecting and quantifying non-linearity associated with frequency response functions, Mech. Syst. Signal Process. (2) (1987) 151–171.

[43] M. Feldman, Nonlinear system vibration analysis using the Hilbert transform-I. Free vibration analysis method 'FREEVIB', Mech. Syst. Signal Process. 8 (1994) 119–127.

[44] M. Feldman, Nonlinear system vibration analysis using the Hilbert transform-II. Forced vibration analysis method 'FORCEVIB', Mech. Syst. Signal Process. 8 (1994) 309–318.

[45] N.E. Huang, Z. Shen, S.R. Long, M.C. Wu, H.H. Shih, Q. Zheng, N.C. Yen, C.C. Tung, H.H. Liu, The empirical mode decomposition and the Hilbert spectrum for nonlinear and non-stationary time series analysis, Proc. R. Soc. Lond. A 454 (1998) 903–995.

[46] M. Feldman, Time-varying vibration decomposition and analysis based on the Hilbert transform, J. Sound Vib. 295 (2006) 518–530.

[47] G. Kerschen, A.F. Vakakis, Y.S. Lee, D.M. McFarland, L.A. Bergman, Toward a fundamental understanding of the Hilbert–Huang transform in nonlinear dynamics, J. Vib. Control 14 (2008) 77–105.

[48] Y.S. Lee, S. Tsakirtzis, A.F. Vakakis, D.M. McFarland, L.A. Bergman, Physics-based foundation for empirical model decomposition: correspondence between intrinsic mode functions and slow flows, AIAA J. 47(2009) 2938–2963.

[49] M. Feldman, Identification of weakly nonlinearities in multiple coupled oscillators, J. Sound Vib. 303 (2007) 357–370.

[50] D. E. Newland, Random Vibrations, Spectral & Wavelet Analysis, Third Edition, Longman Publishers, 1993.

[51] W.J. Staszewski, Identification of non-linear systems using multi-scale ridges and skeletons of the wavelet transform, J. Sound Vib. 214 (1998) 639–658.

[52] L. Garibaldi, M. Ruzzene, A. Fasana, B. Piombo, Identification of non-linear damping mechanisms using the wavelet transform, Mecanique Industrielle et Materiaux 51 (1998) 92–94.

[53] Ö. Tanrıkulu, B. Kuran, H.N. Özgüven, M. Imregün, Forced harmonic response analysis of nonlinear structures using describing functions, AIAA J. 31 (7) (1993) 1313–1320.

[54] M.B. Özer, H.N. Özgüven, A new method for localization and identification of nonlinearities in structures, in: Proceedings of the ESDA 2002: Sixth Biennial Conference on Engineering Systems Design and Analysis, ASME, Istanbul, Turkey, 2002.

[55] M.B. Özer, H.N. Özgüven, T.J. Royston, Identification of structural nonlinearities using describing functions and the Sherman-Morrison method, Mech. Syst. Signal Process. 23 (2009) 30–44.

[56] M. Aykan, H.N. Özgüven, Parametric identification of nonlinearity in structural systems using describing function inversion, Mech. Syst. Signal Process. 40 (2013) 356–376.

[57] S. Marchesiello, L. Garibaldi, A time domain approach for identifying nonlinear vibrating structures by subspace methods, Mech. Syst. Signal Process. 22 (2008) 81–101.

[58] J.P. Noël, G.Kerschen, Frequency-domain subspace identification for nonlinear mechanical systems, Mech. Syst. Signal Process. 40 (2013) 701–717.

[59] S.L. Lacy, D.S. Bernstein, Subspace identification for non-linear systems with measured-input non-linearities, Int. J. Control 78 (2005) 906–926.

[60] J.P. Noël, S. Marchesiello, G.Kerschen, Subspace-based identification of a nonlinear spacecraft in the time and frequency domains, Mech. Syst. Signal Process. 43 (2014) 217–236.

[61] G. Zhang, C. Zang, M.I. Friswell, Identification of weak nonlinearities in MDOF systems based on reconstructed constant response tests, Arch. Appl. Mech. (2019) 1-22.

[62] X. Wang, G.T. Zheng, Equivalent Dynamic Stiffness Mapping technique for identifying nonlinear structural elements from frequency response functions, Mech. Syst. Signal Process. 68-69 (2016) 394-415.

[63] R.M. Rosenberg, The normal modes of nonlinear n-degree-of-freedom systems, Journal of Applied Mechanics 29 (1962) 7–14.

[64] R.M. Rosenberg, On nonlinear vibrations of systems with many degrees of freedom, Advances in Applied Mechanics 9 (1966) 155-242.

[65] W. Szemplinska-Stupnicka, The modified single mode method in the investigation of the resonant vibration of nonlinear systems, Journal of Sound and Vibration 63(4) (1979) 475-489.

[66] S. Setio, H. D. Setio and L. Jezequel, A method of nonlinear modal identification from frequency response tests, Journal of Sound and Vibration 158(3) (1992) 497–515.

[67] R.M. Lin, Identification of dynamic characteristics of nonlinear structures, Phd Thesis, Imperial College, London, (1990).

[68] C. Gibert, Fitting measured frequency responses using nonlinear modes, Mechanical Systems and Signal Processing 17(1) (2003) 211-218.

[69] F. Thouverez, Presentation of the ECL benchmark, Mechanical Systems Signal Processing 17(1) (2003) 195-202.

[70] D. Göge, U. Füllekrug, M. Sinapius, M. Link, L. Gaul, Advanced test strategy for identification and characterization of nonlinearities of aerospace structures, AIAA Journal 43(5) (2005) 974-986.

[71] Platten, M. F., Wright, J. R., Dimitriadis, G., and Cooper, J. E., Identification of multi-degree of freedom nonlinear systems using an extended modal space model, Mechanical Systems and Signal Processing 23(1) (2009) 8–29.

[72] M.F. Platten, J.R. Wright, J.E. Cooper, G. Dimitriadis, Identification of a nonlinear wing structure using an extended modal model, AIAA Journal of Aircraft 46(5) (2009) 1614-1626.

[73] U. Füllekrug, D. Göge, Identification of weak nonlinearities within complex aerospace structures, Aerosp. Sci. Technol. 23 (2012) 53-62.

[74] Ö. Arslan, H.N. Özgüven, Modal identification of nonlinear structures and the use of modal model in structural dynamic analysis, in: Proceedings of the 26th International Modal Analysis Conference (IMAC), Orlando, USA, 2008.

[75] Ö. Arslan, M. Aykan, H.N. Özgüven, Parametric identification of structural nonlinearities from measured frequency response data, Mech. Syst. Signal Process. 25 (2011) 1112–1125.

[76] M. Link, M. Boeswald, S. Laborde, M. Weiland, A. Calvi, An approach to non-linear experimental modal analysis, in: Proceedings of the 28th International Modal Analysis Conference (IMAC), Jacksonville, FL, USA, 2010.

[77] A. Carrella, D.J. Ewins, Identifying and quantifying structural nonlinearities in engineering applications from measured frequency response functions, Mechanical Systems and Signal Processing 25 (2011) 1011-1027.

[78] M. Peeters, G. Kerschen, J.C. Golinval, Dynamic testing of nonlinear vibrating structures using nonlinear normal modes, Journal of Sound Vibration 330 (2011) 486–509.

[79] M. Peeters, G.Kerschen, J.C.Golinval, Modal testing of nonlinear vibrating structures based on nonlinear normal modes: experimental demonstration, Mechanical Systems and Signal Processing 25(2011) 1227–1247.

[80] S. Peter, R.I. Leine, Excitation power quantities in phase resonance testing of nonlinear systems with phase-locked-loop excitation, Mechanical Systems and Signal Processing 96 (2017) 139-158.

[81] L. Renson, A. Gonzalez-Buelga, D.A.W. Barton, S.A. Neild, Robust identification of backbone curves using control-based continuation, Journal of Sound Vibration 367 (2016) 145-158.

[82] V. Denis, M. Jossic, C. Giraud-Audine, B. Chomette, A. Renault, O. Thomas, Identification of nonlinear modes using phase-locked-loop experimental continuation and normal form, Mechanical Systems and Signal Processing 106 (2018) 430-452.

[83] S. Peter, M. Scheel, M. Krack, R.I. Leine, Synthesis of nonlinear frequency responses with experimentally extracted nonlinear modes, Mechanical Systems and Signal Processing 101 (2018) 498-515.

[84] M. Scheel, S. Peter, R.I. Leine, M. Krack, A phase resonance approach for modal testing of structures with nonlinear dissipation, Journal of Sound Vibration 435 (2018) 56-73.

[85] T. Karaağaçlı, H.N. Özgüven, Experimental modal analysis of nonlinear systems by using response-controlled stepped-sine testing, Mechanical Systems and Signal Processing 146 (2021).

[86] T. Karaağaçlı, H.N. Özgüven, Experimental identification of backbone curves of strongly nonlinear systems by using response-controlled stepped-sine testing (RCT), Vibration 3 (3) (2020) 266-280.

[87] T. Karaağaçlı, H.N. Özgüven, A frequency domain nonparametric identification method for nonlinear structures: Describing surface method, Mechanical Systems and Signal Processing 144 (2020).

[88] M. Scheel, T. Weigele, M. Krack, Challenging an experimental nonlinear modal analysis method with a new strongly friction-damped structure, Journal of Sound and Vibration 485 (2020).

[89] J.V. Ferreira, D.J. Ewins, Algebraic nonlinear impedance equation using multi-harmonic describing function, 15th Int. Modal Anal. Conf. (1997) 1595.

[90] G.Kerschen, M. Peeters, J.C.Golinval, A.F. Vakakis, Nonlinear normal modes, part I: A useful framework for the structural dynamicist, Mechanical Systems and Signal Processing 23 (1) (2009) 170–194.

[91] E. Budak, H.N. Özgüven, A dynamic analysis method for the harmonically excited nonlinear structures, Struct. Vib. And Acous., ASME 18 (3) (1989) 23-29.

[92] E. Budak, H.N. Özgüven, Iterative receptance method for determining harmonic response of structures with symmetrical nonlinearities, Mech. Syst. Signal Process. 7 (1) (1993) 75-87.

[93] A. Gelb, W.E. Van der Velde, Multiple-input Describing Functions and Nonlinear System Design, McGraw-Hill, New York, 1968.

[94] W.H. Shin, I. Lee, Nonlinear aeroelastic analysis for a control fin with actuator, J. Aircraft 44(2) (2007) 597-605.

[95] Y. Ning, W. Nan, Z. Xin, L. Wei, Nonlinear flutter wind tunnel test and numerical analysis of folding fins with freeplay nonlinearities, Chinese Journal of Aeronautics 29(1) (2016) 144-159.

APPENDIX A

PUBLISHED PAPERS DURING PHD

Mechanical Systems and Signal Processing 146 (2021) 107023

Contents lists available at ScienceDirect

Mechanical Systems and Signal Processing

journal homepage: www.elsevier.com/locate/ymssp

Experimental modal analysis of nonlinear systems by using response-controlled stepped-sine testing

Taylan Karaağaçlı [a], H. Nevzat Özgüven [b,*]

[a] The Scientific and Technological Research Council of Turkey, Defense Industries Research and Development Institute, TÜBİTAK-SAGE, P.K. 16, 06261 Mamak, Ankara, Turkey
[b] Mechanical Engineering Department, Middle East Technical University, 06800 Ankara, Turkey

ARTICLE INFO

Article history:
Received 23 December 2019
Received in revised form 25 May 2020
Accepted 30 May 2020

Keywords:
Nonlinear experimental modal analysis
Nonlinear system identification
Response controlled stepped sine test
Nonlinear mode
Harmonic force surface
Unstable branch

ABSTRACT

Although the identification and analysis of structures with a localized nonlinearity, either weak or strong, is within reach, identification of multiple nonlinearities coexisting at different locations is still a challenge, especially if these nonlinearities are strong. In such cases, identifying each nonlinearity separately requires a tedious work or may not be possible at all in some cases. In this paper, an approach for experimental modal analysis of nonlinear systems by using *Response-Controlled stepped-sine Testing* (RCT) is proposed. The proposed approach is applicable to systems with several nonlinearities at various different locations, provided that modes are well separated and no internal resonances occur. Step-sine testing carried out by keeping the displacement amplitude of the driving point constant yields quasi-linear frequency response functions directly, from which the modal parameters can be identified as functions of modal amplitude of the mode of concern, by employing standard linear modal analysis tools. These identified modal parameters can then be used in calculating near-resonant frequency response curves, including the unstable branch if there is any, for various untested harmonic forcing cases. The proposed RCT approach makes it also possible to extract nonlinear normal modes experimentally without using sophisticated control algorithms, directly from the identified modal constants, and also to obtain near-resonant frequency response curves experimentally for untested constant-amplitude harmonic forcing cases by extracting isocurves of constant-amplitude forcing from the measured Harmonic Force Surface (HFS), a new concept proposed in this paper. The key feature of the HFS is its ability to extract unstable branches together with turning points of constant-force frequency response curves directly from experiment, accurately. The method is validated with numerical and experimental case studies. The numerical example consists of a 5 DOF lumped system with strong several conservative nonlinear elements. Experimental case studies consist of a cantilever beam supported at its free-end by two metal strips which create strong stiffening nonlinearity, and a real missile structure which exhibit moderate damping nonlinearity mostly due to several bolted joints on the structure.

* Corresponding author.
E-mail address: ozguven@metu.edu.tr (H.N. Özgüven).

https://doi.org/10.1016/j.ymssp.2020.107023
0888-3270/

1. Introduction

Structural dynamics community witnessed important developments in the field of nonlinear system identification over the last two decades [1,2]. Despite the significant progress in the state-of-the-art, there are still difficult problems such as joint nonlinearities (multiple and discrete) or geometric (i.e. continuously distributed) nonlinearities due to large deformations. Since there are generally several joints in engineering structures, it would be very difficult, if not impossible, to identify each joint nonlinearity separately. On the other hand, in case of geometric nonlinearities, the concept of discrete nonlinear elements cannot be used. Consequently, the right identification strategy in these complex problems is to quantify the resultant effect of all nonlinearities, instead of focusing on individual nonlinear elements. Fortunately, the concept of nonlinear normal modes (NNMs), which dates back to Rosenberg [3,4] (1960s), provides a rigorous theoretical framework to study the overall effect of several nonlinearities in a structure. Analogous to linear normal modes, Rosenberg defined an NNM as a *vibration in unison* of the system, i.e. synchronous periodic motion. Later, in 1979, Szemplinska-Stupnicka proposed a novel technique called the *single nonlinear mode method* [5] to study the effect of nonlinearities on the resonant vibrations of multi-degree-of-freedom (MDOF) systems. The method showed that if the modes are well separated and no pronounced modal coupling occurs in the energy range of interest, near-resonant frequency responses of a nonlinear system can be represented accurately by a single NNM and its corresponding natural frequency which are functions of modal amplitude. This pioneering work of Szemplinska-Stupnicka led to the development of various nonlinear modal identification techniques. For example, in the early 1990s, Setio et al. [6] proposed to extract nonlinear modal parameters by minimizing the error function between frequency responses measured by force-controlled sine-sweep testing and analytical frequency responses represented by superposition of NNMs, which gives satisfactory results if the modes are well separated and no internal resonances occur. The method was validated on a real cantilever beam supported at its free end by a string which creates cubic stiffness effect. Later, in the early 2000s, Gibert [7] proposed a similar modal identification algorithm based on minimization of the error function between measured and analytical frequency responses and showed that superposition of NNMs gives satisfactory results for the synthesis of frequency responses of the Ecole-Central-de-Lyon (ECL) benchmark [8] over the frequency range including the first three elastic modes.

Early 2000s witnessed other promising nonlinear modal identification strategies. For example, Göge et al. [9] proposed a novel method called the identification of nonlinearity by time-series-based linearity plots (INTL) which is based on the application of the restoring force surface (RFS) method [10] in modal space. The test strategy used in the INTL approach is the normal mode force appropriation which is also known as phase resonance testing, where the nonlinear system is harmonically excited at its resonance frequency by means of an excitation force pattern appropriated to a single mode of interest. Nonlinear modal stiffness and damping parameters can then be determined by curve fitting to the measured nonlinear restoring force in modal space. The application of the method was demonstrated on a real space structure. Platten et al. [11] also proposed another RFS-based technique called the nonlinear resonant decay method (NLRDM). This method differs from the INTL approach in that it can take also the cross-coupling of nonlinear modes into account by virtue of its excitation strategy which consists of a burst sine at the resonance frequency of the mode of interest. The NLRDM technique was validated on a wing-like structure with hardening stiffness at the pylon connections [12] and on a real transport aircraft [13].

The major difference between the new generation techniques developed in the last decade and the afore-mentioned ones is that in the new generation algorithms, computational effort is minimized at the cost of experimental effort. Most of the recently developed nonlinear modal identification methods are inspired by phase resonance testing approach and they focus on direct parameter estimation, which reduces computational effort considerably. For example, in the method proposed by Peeters et al. [14] in 2011, the phase lag quadrature criterion was generalized to nonlinear structures in order to locate a single NNM during experiment. Once the NNM appropriation is achieved, the frequency-energy dependence of that nonlinear mode can be determined by applying time-frequency analysis to the free decay response data. The proposed methodology was demonstrated on numerical examples [14] and on a real nonlinear beam structure [15]. However, an important drawback of this early version of the nonlinear phase resonance testing was the manual tuning process of the phase lag between response and excitation. By virtue of the recently proposed control algorithms [16,17], the tuning of the phase lag was automated throughout the entire NNM backbone curve. The control technique proposed by Peter and Leine in [16] is called phase-locked-loop (PLL) control which provides a robust and fast way of tracing out back-bone curves as well as of stabilizing the unstable branches of near-resonant frequency response curves. The PLL control strategy, which outputs zeroth and higher harmonics of nonlinear modes as well as the fundamental harmonic, was validated on a benchmark beam structure in [16] and on a circular plate, a chinese gong and a piezoelectric cantilever beam in [18]. In accordance with the single nonlinear mode assumption [5], synthesis of the near-resonant frequency response curve of a nonlinear cantilever beam from a single NNM measured by PLL technique was also demonstrated in [19]. Another interesting application of the PLL technique is the identification of the nonlinear dissipation at a bolted joint [20]. The control approach proposed by Renson et al. in [17], called control-based continuation (CBC), is similar to the PLL method, and also enables backbone curve identification of nonlinear structures. The application of the CBC method was demonstrated on a real single-degree-of-freedom (SDOF) oscillator in [17].

All of the nonlinear modal identification techniques mentioned above have their own advantages and limitations. Early identification methods [6,7] which rely on simple frequency response data measured by standard force-controlled sine sweep testing involve considerable computational cost. On the other hand, INLT and NLRDM require considerable effort both

in computation and experiment, and they are applicable to weakly nonlinear systems. In nonlinear phase resonance testing method [14], the computational effort is considerable reduced, but the manual tuning of the phase lag between response and excitation process requires careful and time consuming experimentation. Although recently developed PLL and CBC control strategies automated the tuning of the phase lag as well as the determination of the backbone curve, they cannot make use of the available standard equipment. Furthermore, although experimental extraction of natural frequencies and deflection shapes at resonance is straightforward in the methods based on phase resonance testing approach, determination of nonlinear modal damping is still an important issue.

In this paper, an approach for experimental modal analysis of nonlinear systems by using *response-controlled stepped-sine testing* (RCT) is proposed. The proposed approach is applicable to systems with several nonlinearities at various different locations, provided that modes are well separated and no internal resonances occur. The method is based on the single nonlinear mode assumption of Szemplinska-Stupnicka [5], where near-resonant frequency responses of a nonlinear system can be represented accurately by a single NNM and its corresponding natural frequency which are functions of a single modal amplitude. Accordingly, the proposed method hypothesizes that if the displacement (equivalently modal) amplitude is kept constant with the RCT strategy during modal testing, measured frequency response functions (FRFs) come out in quasi-linear form. That makes it possible to use standard linear modal analysis tools to extract all modal parameters as functions of modal amplitude. These identified modal parameters can then be employed to synthesize near-resonant frequency response curves including unstable branches, if there is any, for various untested harmonic forcing scenarios. Furthermore, in case of using multiple sensors during RCT, NNMs can also be experimentally extracted from identified modal constants. Therefore, the contribution of the proposed method is threefold. Firstly, it relies on standard controllers (available in commercial modal testing hardware and driven by commercial software) which makes it very attractive especially for industrial applications. Secondly, identification of modal damping and mass normalization of NNMs, which are necessary for the prediction of frequency responses of untested harmonic forcing scenarios, is straightforward with the proposed method, by applying linear modal analysis methods available in commercial software packages to measured constant-response FRFs of nonlinear structures. Finally, the proposed approach provides two different ways of determining near-resonant frequency response curves for untested constant-amplitude harmonic forcing scenarios; either computationally by using the nonlinear modal parameters identified during RCT, or experimentally by directly extracting isocurves of constant-amplitude forcing from the measured Harmonic Force Surface (HFS), a new concept proposed in this paper. It should be noted that both approaches are capable of determining unstable branches of frequency response curves, which may occur in strongly nonlinear systems. Theoretically, both approaches must give identical results, which constitutes a self-validation measure for the proposed method.

The paper is organized as follows. In Section 2, the theoretical background of the proposed approach is given. Subsequently, in Section 3 the proposed experimental methodology used to identify nonlinear modal parameters, and two different ways of determining near-resonant frequency responses corresponding to constant-amplitude harmonic forcing are explained in detail. Section 4 is dedicated to the numerical validation of the proposed approach with a lumped MDOF system with strong conservative nonlinearity. In Section 5, the method is applied on a real cantilever beam supported at its free end by thin metal strips which create cubic stiffness effect due to geometric nonlinearity, and also on a real missile structure which exhibits considerable nonlinear damping due to bolted joints. Finally, conclusions are discussed in Section 6.

2. Theory

2.1. The nonlinearity matrix concept

Equation of motion of a nonlinear n degrees-of-freedom system with structural damping subjected to a harmonic excitation force of frequency ω, neglecting all the sub- and super-harmonic terms, can be written in the form of a nonlinear complex algebraic equation in frequency domain as follows

$$-\omega^2[M]\{X\} + i[H]\{X\} + [K]\{X\} + \{F_N\} = \{F\}, \tag{1}$$

where $[M]$, $[H]$ and $[K]$ are the mass, hysteretic (structural) damping and stiffness matrices of the underlying linear system, respectively. All matrices are symmetric and positive definite, whereas $[K]$ and $[H]$ can be positive semi-definite as well. $\{X\}$, $\{F_N\}$ and $\{F\}$ are the complex vectors of displacement amplitude, nonlinear internal force amplitude and external excitation force amplitude, respectively.

According to Describing Function Method (DFM) [21], the complex vector of nonlinear internal force amplitude can be expressed as

$$\{F_N\} = [\Delta]\{X\}, \tag{2}$$

where $[\Delta]$ is the displacement level dependent complex and symmetric *nonlinearity matrix*. Real and imaginary parts of this matrix correspond to the displacement level dependent nonlinear stiffness and nonlinear damping matrices, respectively.

Substituting Eq. (2) into Eq. (1) yields

$$\left(-\omega^2[M] + i[H] + [K] + [\Delta]\right)\{X\} = \{F\}. \tag{3}$$

It should be noted that DFM is mathematically equivalent to the classical Harmonic Balance Method (HBM). The major difference between DFM and HBM relies in the expression of nonlinear internal forces. HBM expresses nonlinear internal forces as a single force vector, whereas in DFM they are written as a multiplication of the so-called Nonlinearity Matrix with displacement amplitude vector as shown in Eq. (2). The second representation allows one to treat a nonlinear system, mathematically, as a linear system at a given displacement amplitude level, which makes it possible to extend some of the methods developed for linear systems to nonlinear systems by using iterative solutions.

2.2. The nonlinear eigenvalue problem

According to the single nonlinear mode theory [5–7], NNMs are found by solving the nonlinear eigenvalue problem associated with the *conservative* part of Eq. (3) as follows

$$\left([K]+[\Delta]_{re}\right)\left\{\overline{\psi}(q_r)\right\}_r = \overline{\omega}_r^2(q_r)[M]\left\{\overline{\psi}(q_r)\right\}_r. \tag{4}$$

Here, q_r is the rth modal amplitude, $\left\{\overline{\psi}(q_r)\right\}_r$ and $\overline{\omega}_r(q_r)$ are the rth real valued NNM and its corresponding natural frequency, which are functions of q_r. $[\Delta]_{re}$ represents the real part of the nonlinearity matrix, which corresponds to the nonlinear stiffness matrix. It should be noted that $[\Delta]_{re}$ depends on the displacement response level of the system, and therefore on the product $q_r\left\{\overline{\psi}(q_r)\right\}_r$, i.e.

$$[\Delta]_{re} = \left[\Delta\left(q_r\left\{\overline{\psi}(q_r)\right\}_r\right)\right]_{re}. \tag{5}$$

Consequently, Eq. (4) is a nonlinear eigenvalue problem which requires an iterative solution procedure. Starting from the corresponding normal mode of the underlying linear system, Eq. (4) can be solved for $\left\{\overline{\psi}(q_r)\right\}_r$ and $\overline{\omega}_r(q_r)$ by using various iterative solution techniques (e.g. Newton-Raphson Method [6]).

2.3. The single nonlinear mode method

If the modes are well separated and no pronounced modal coupling occurs in the energy range of interest, near-resonant solution of Eq. (3) around an rth mode can be approximated by a single NNM calculated from Eq. (4) as follows [5–7]

$$\{X\} = q_r\left\{\overline{\psi}(q_r)\right\}_r. \tag{6}$$

Substituting Eq. (6) into Eq. (3) and premultiplying by $\left\{\overline{\psi}(q_r)\right\}_r^T$ yields

$$\left(-\omega^2\overline{m}_r(q_r)+\overline{k}_r(q_r)+i\overline{h}_r(q_r)\right)q_r = \left\{\overline{\psi}(q_r)\right\}_r^T\{F\}, \tag{7}$$

where

$$\begin{aligned}
\overline{m}_r(q_r) &= \left\{\overline{\psi}(q_r)\right\}_r^T[M]\left\{\overline{\psi}(q_r)\right\}_r,\\
\overline{k}_r(q_r) &= \left\{\overline{\psi}(q_r)\right\}_r^T\left([K]+[\Delta]_{re}\right)\left\{\overline{\psi}(q_r)\right\}_r,\\
\overline{h}_r(q_r) &= \left\{\overline{\psi}(q_r)\right\}_r^T\left([H]+[\Delta]_{im}\right)\left\{\overline{\psi}(q_r)\right\}_r.
\end{aligned} \tag{8}$$

Here, $\overline{m}_r(q_r)$, $\overline{k}_r(q_r)$ and $\overline{h}_r(q_r)$ are the modal mass, modal stiffness and modal hysteretic damping, respectively. $[\Delta]_{im}$ represents the imaginary part of the nonlinearity matrix, which corresponds to the displacement response level dependent nonlinear damping matrix.

Eq. (7) can be alternatively written as

$$\overline{m}_r(q_r)\left(-\omega^2+\overline{\omega}_r^2(q_r)+i\overline{\eta}_r(q_r)\overline{\omega}_r^2(q_r)\right)q_r = \left\{\overline{\psi}(q_r)\right\}_r^T\{F\}, \tag{9}$$

where

$$\overline{\omega}_r^2(q_r) = \frac{\overline{k}_r(q_r)}{\overline{m}_r(q_r)}, \quad \overline{\eta}_r(q_r) = \frac{\overline{h}_r(q_r)}{\overline{m}_r(q_r)\overline{\omega}_r^2(q_r)}. \tag{10}$$

Modal amplitude q_r can be solved from Eq. (9) as follows

$$q_r = \frac{\left\{\overline{\psi}(q_r)\right\}_r^T\{F\}}{\overline{m}_r(q_r)\left(\overline{\omega}_r^2(q_r)-\omega^2+i\overline{\eta}_r(q_r)\overline{\omega}_r^2(q_r)\right)}. \tag{11}$$

Inserting Eq. (11) into Eq. (6) yields

$$\{X\} = \frac{\{\overline{\psi}(q_r)\}_r \{\overline{\psi}(q_r)\}_r^T \{F\}}{\overline{m}_r(q_r)(\overline{\omega}_r^2(q_r) - \omega^2 + i\overline{\eta}_r(q_r)\overline{\omega}_r^2(q_r))}. \tag{12}$$

Here, NNM can be normalized with respect to modal mass as follows

$$\{\overline{\phi}(q_r)\}_r = \frac{\{\overline{\psi}(q_r)\}_r}{\sqrt{\overline{m}_r(q_r)}}. \tag{13}$$

Substituting Eq. (13) into Eq. (12) yields

$$\{X\} = \frac{\{\overline{\phi}(q_r)\}_r \{\overline{\phi}(q_r)\}_r^T \{F\}}{\overline{\omega}_r^2(q_r) - \omega^2 + i\overline{\eta}_r(q_r)\overline{\omega}_r^2(q_r)}. \tag{14}$$

Near-resonant receptance $\overline{\alpha}_{jk}$ at point j for a given excitation at point k can be deduced from Eq. (14) as follows

$$\overline{\alpha}_{jk}(\omega, q_r) = \frac{\overline{\phi}_{jr}(q_r)\overline{\phi}_{kr}(q_r)}{\overline{\omega}_r^2(q_r) - \omega^2 + i\overline{\eta}_r(q_r)\overline{\omega}_r^2(q_r)}. \tag{15}$$

In Eq. (15) the nonlinear hysteretic modal damping model can be replaced by an equivalent nonlinear viscous damping model as well. Accordingly, an alternative form of Eq. (15) can be written as follows

$$\overline{\alpha}_{jk}(\omega, q_r) = \frac{\overline{\phi}_{jr}(q_r)\overline{\phi}_{kr}(q_r)}{\overline{\omega}_r^2(q_r) - \omega^2 + i2\overline{\xi}_r(q_r)\omega\overline{\omega}_r(q_r)}, \tag{16}$$

where $\overline{\xi}_r(q_r)$ is the nonlinear viscous modal damping ratio.

The experimental methodology proposed to identify nonlinear modal parameters which can be used for the synthesis of near-resonant frequency response curves for untested constant-amplitude harmonic forcing scenarios is explained in the next section.

3. Proposed experimental methodology – Identification of nonlinear modal parameters and synthesis of frequency responses for constant-amplitude harmonic forcing

3.1. Measurement of constant-response FRFs in quasi-linear form

Modal parameters in Eqs. (15) and (16) are functions of a single parameter; the modal amplitude. In this paper, it is proposed to measure *constant-response* FRFs of nonlinear systems by keeping the driving point displacement amplitude constant with RCT strategy. According to the single nonlinear mode assumption, these constant-response FRFs are expected to come out in quasi-linear form. Consequently, modal parameters can be extracted from measured constant-response FRFs by using standard linear modal analysis methods available in commercial software packages. This approach essentially extends the method proposed by Arslan and Özgüven [22] which is restricted to structures where nonlinearity is localized between a single DOF and ground, to complex engineering structures with multiple nonlinearities connecting internal coordinates and spread over the structure (e.g., structures with several bolted joints).

Although single nonlinear mode theory [5] completely discards higher harmonics in the derivation of the nonlinear receptance model given in Eqs. (15) and (16), quasi-linearization of FRFs with RCT strategy can still be achieved under the effects of higher harmonics if these effects are not pronounced. In Section 4, this is demonstrated on the RCT simulation of a lumped MDOF system with strong conservative nonlinearity, where the system is excited at a single DOF and the fundamental harmonic displacement of the driving point is kept constant. Firstly, the frequency responses of the fundamental and higher harmonics as well as excitation force spectrum are calculated by using multi-harmonics version of the DFM [23]. Secondly, constant-response FRFs corresponding to the fundamental harmonic are determined by dividing the fundamental harmonic displacement with the harmonic excitation force. Eventually, it is shown that FRFs determined by using multiple harmonics are also quasi-linear.

3.2. Excitation strategy

Several experimental studies have shown that in the absence of internal resonances; single point, single harmonic excitation is sufficient to isolate nonlinear modes to a satisfying accuracy [14,19]. Furthermore, in case of a single point excitation, keeping the modal amplitude constant is equivalent to keeping the displacement amplitude of the driving point constant. Due to these practical benefits, in the proposed method, a single input stepped-sine test strategy is used to identify modal parameters. Theoretically, RCT approach can also be applied by using multi-point excitation. In that case, adjustment of the amplitude ratios of excitation signals would be necessary, as in the case of NNM force appropriation, to keep the modal amplitude at a constant level. This adjustment can be achieved with the help of a preliminary single point excitation test.

3.3. Response control strategy

Displacement amplitude of the driving point can be kept constant either directly or indirectly depending on the type of the sensor used during RCT. Since accelerometer is the most widely used sensor in experimental modal analysis, it was chosen as the control sensor in the proposed method. Acceleration profile corresponding to a constant displacement amplitude over the frequency range of interest is calculated and input to the *closed-loop* controller as a reference profile, which is an available option in standard modal testing software packages (e.g. LMS Test Lab©).

3.4. Identification of nonlinear modal parameters and experimental extraction of mass normalized NNMs

Determination of near-resonant frequency response curves for various unmeasured harmonic forcing scenarios is an important task to understand complex dynamics of engineering structures and eventually to satisfy critical design requirements. If one could experimentally extract nonlinear modal parameters used in Eqs. (15) and (16), these identified modal parameters can then be used to synthesize near-resonant frequency responses corresponding to various constant-amplitude harmonic forcing scenarios.

In the proposed method, in order to identify nonlinear modal parameters, constant-response FRFs at several different displacement amplitude levels are measured by conducting a series of modal tests with RCT strategy. Then, modal identification is achieved by fitting the following analytical model to the measured constant-response FRFs with an appropriate linear modal analysis method

$$\overline{\alpha}_{jk}(\omega, q_r) = \frac{\overline{A}_{jkr}(q_r)}{\overline{\omega}_r^2(q_r) - \omega^2 + i\overline{\eta}_r(q_r)\overline{\omega}_r^2(q_r)}, \tag{17}$$

where $A_{jkr}(q_r)$ is a complex valued modal constant. The nonlinear hysteretic modal damping model used in Eq. (17) can be replaced by an equivalent nonlinear viscous modal damping model as follows

$$\overline{\alpha}_{jk}(\omega, q_r) = \frac{\overline{A}_{jkr}(q_r)}{\overline{\omega}_r^2(q_r) - \omega^2 + i2\overline{\xi}_r(q_r)\omega\overline{\omega}_r(q_r)}. \tag{18}$$

Once $A_{jkr}(q_r)$, $\overline{\omega}_r(q_r)$ and $\overline{\xi}_r(q_r)$ (or $\overline{\eta}_r(q_r)$) are experimentally extracted, they can be plotted with respect to modal amplitude. These plots can either be used in parametric form by fitting polynomials, if possible, or directly as look-up tables in the synthesis of near-resonant frequency response curves for untested harmonic forcing scenarios.

In case of a single input and multiple outputs modal testing, mass normalized NNMs can be determined from experiment by using the following procedure.

First of all, identified modal constants can be collected into a vector as follows

$$\left\{\overline{A}(q_r)\right\}_r^T = \left\{\overline{A}_{11r}(q_r) \quad \overline{A}_{21r}(q_r) \quad \cdots \quad \overline{A}_{m1r}(q_r)\right\}^T, \tag{19}$$

where m indicates the total number of measurement points.

Comparison of Eqs. (17) and (18) with Eqs. (15) and (16) reveals that experimentally extracted modal constants are closely related to mass normalized NNMs with the following relation

$$\overline{A}_{jkr}(q_r) = \overline{\phi}_{jr}(q_r)\overline{\phi}_{kr}(q_r). \tag{20}$$

Substituting Eq. (20) into Eq. (19) yields

$$\left\{\overline{A}(q_r)\right\}_r = \left\{\overline{\phi}_{1r}(q_r)\overline{\phi}_{1r}(q_r) \quad \overline{\phi}_{1r}(q_r)\overline{\phi}_{2r}(q_r) \quad \cdots \quad \overline{\phi}_{1r}(q_r)\overline{\phi}_{mr}(q_r)\right\}^T. \tag{21}$$

It can easily be noticed that all terms of the vector given in Eq. (21) have a common multiplier which is $\overline{\phi}_{1r}(q_r)$. This multiplier can be determined by taking square root of the identified modal constant of the driving point FRF as follows

$$\overline{\phi}_{1r}(q_r) = \sqrt{\overline{A}_{11r}(q_r)}. \tag{22}$$

Finally, dividing Eq. (21) by the square root term given in Eq. (22), the NNM of interest can be identified in mass normalized form as follows

$$\left\{\overline{\phi}(q_r)\right\}_r = \frac{1}{\sqrt{\overline{A}_{11r}(q_r)}}\left\{\overline{A}(q_r)\right\}_r. \tag{23}$$

The nonlinear modal damping ratio and mass normalized NNMs are essential elements required in the synthesis of frequency response curves for untested harmonic forcing scenarios. Obviously, if one is interested in the synthesis of the frequency response curves of a single point, identification of the modal constant corresponding to that point will be sufficient.

In concluding this section, it is important to note that the NNMs used in Eqs. (15) and (16) are assumed to be the NNMs of the underlying conservative system, whereas those extracted from experimental data by using Eq. (23) are the NNMs of the

actual damped system, which may seem paradoxical. However, the damped NNMs of a nonlinear system can be approximated by the NNMs of the underlying undamped system, and vice versa, under the assumption of moderate damping as discussed in [15,24], and as also experimentally confirmed in this study. The applicability of the method for high damping will be the subject of a future work.

3.5. Synthesis of frequency responses for untested constant-amplitude harmonic forcing scenarios

The nonlinear modal parameters identified from constant-response FRFs can be employed in the following equation to calculate near-resonant frequency responses for untested constant-amplitude harmonic forcing scenarios

$$X_j(q_r) = \frac{\overline{A}_{jkr}(q_r)F_k}{\overline{\omega}_r^2(q_r) - \omega^2 + i2\overline{\zeta}_r(q_r)\omega\overline{\omega}_r(q_r)}, \tag{24}$$

where $X_j(q_r)$ is the displacement amplitude at point j for a given constant-amplitude F_k at point k.

In this study, Eq. (24) is solved iteratively by using Newton's Method with arc-length continuation algorithm which is capable of capturing any unstable branch which might occur in strongly nonlinear systems. Eq. (24) can also be solved explicitly in closed form for the excitation frequency as shown in [25].

3.6. Experimental extraction of frequency responses for untested constant-amplitude harmonic forcing scenarios by using HFS

As an alternative to the computational approach given in Eq. (24), the HFS concept is capable of deriving frequency response curves, experimentally, at constant force levels including unstable branches, if there is any, by using harmonic force spectra measured at constant vibration levels during RCT without any extra experimental effort.

3.6.1. Difficulties in frequency response measurement of nonlinear structures with standard force-control

In linear experimental modal analysis, standard closed-loop stepped sine test with force control starts with a linear system identification which determines a rough initial estimate of the plant, i.e. the transfer function of the structure under test. In case of nonlinear structures, this procedure may lead to very poor estimate of the structure's actual dynamic behavior. Consequently, controller may need to make many corrective iterations to keep the force within tolerance of the reference profile, which may become very time consuming. Furthermore, in case of nonlinear structures with strong stiffening or softening character, multiple steady-state vibration responses may co-exist for the same excitation frequency, which results in an overhanging unstable branch in the frequency response. Standard force-control algorithms available in commercial softwares can only measure nonlinear frequency responses until the turning points of the stable branches, at the cost of multiple runs with different sweep directions. When a turning point is reached, standard force-controller cannot avoid jumping from one stable branch to another, passing over the unstable region. Even worse, in some cases small corrective force perturbations of the controller to capture the reference signal in the vicinity of the turning points may lead to a *premature jump* before reaching the actual turning point. These drawbacks of standard techniques paved the way for the development of control algorithms such as PLL and CBC. The primary advantage of these control strategies over classical force-control approach is the ability of measuring backbone curves and unstable branches of nonlinear frequency responses. However, these methods were not commercialized yet, therefore available standard equipment cannot be used in these approaches. As an alternative to new generation control strategies, the Harmonic Force Surface (HFS) concept proposed in this paper can be used as described below, in order to determine unstable branches of nonlinear frequency response curves by using standard controllers available in commercial modal testing hardware and driven by commercial software together with RCT strategy.

3.6.2. HFS approach

In case of strong stiffness nonlinearity where multiple steady-state vibration responses co-exist for the same excitation frequency, response level of the structure highly depends on initial conditions. In case of force-control test strategy, there is no control over vibration response which may exhibit drastic changes around resonance even if very small frequency steps are used. Since gradual change in vibration response and eventually in initial conditions are not guaranteed, experimental continuation of the unstable branch cannot be achieved. In RCT, this problem is solved by keeping the displacement amplitude constant, which results in smooth response spectrum incorporating points on the unstable branch as well. This is somewhat different from PLL and CBC algorithms which aim tracing points on the unstable branch consecutively. In RCT, points on the unstable branch are visited at different times during stepped-sine tests carried out at different vibration amplitude levels. Then they are collected together on the HFS. Determination of the nonlinear frequency response with unstable branch by using RCT and HFS consists of the following steps:

1. An RCT is carried out by keeping the displacement amplitude of the driving point constant. The test is repeated at several different displacement amplitude levels (in general, repeating the test at 10–15 different levels may be sufficient to obtain satisfactory results), and the corresponding harmonic force spectra of the driving point are measured.
2. Harmonic Force Surface, HFS, is constructed by collecting measured harmonic force spectra and using linear interpolation.

3. The contour plot obtained by cutting the HFS with a constant force plane gives the harmonic response spectrum corresponding to that force level, including any unstable branch if there is any.

Application of the HFS procedure given above is demonstrated with numerical and experimental case studies in the subsequent sections.

4. Numerical validation

In this section, the proposed modal identification method is validated on the 5 DOF nonlinear lumped system with 5 cubic stiffness elements, which is shown in Fig. 1. Systems parameters are as follows: $m = 1kg$, $k = 10000N/m$, $c = 5Ns/m$, $k^* = 10^7 N/m^3$.

Standard force-control and RCT simulations carried out in this section are achieved by solving the following equation of motion which includes multiple harmonics [23]

$$\left(\begin{bmatrix} [Z]_{11} & 0 & \cdots & 0 \\ 0 & [Z]_{22} & \cdots & 0 \\ \vdots & \vdots & \vdots & \vdots \\ 0 & 0 & \cdots & [Z]_{hh} \end{bmatrix} + \begin{bmatrix} [\Delta]_{11} & [\Delta]_{12} & \cdots & [\Delta]_{1h} \\ [\Delta]_{21} & [\Delta]_{22} & \cdots & [\Delta]_{2h} \\ \vdots & \vdots & \vdots & \vdots \\ [\Delta]_{h1} & [\Delta]_{h2} & \cdots & [\Delta]_{hh} \end{bmatrix} \right) \begin{Bmatrix} \{X\}_1 \\ \{X\}_2 \\ \vdots \\ \{X\}_h \end{Bmatrix} = \begin{Bmatrix} \{F\} \\ 0 \\ \vdots \\ 0 \end{Bmatrix}, \tag{25}$$

where $\{X\}_h$ and $[Z]_{hh}$ are the complex displacement amplitude vector and the dynamic stiffness matrix corresponding to the hth harmonic, respectively. $\{F\}$ denotes the vector of external excitation force amplitude. $[\Delta]_{11}$,$[\Delta]_{12}$ etc. are the components of the complex nonlinearity matrix, where off-diagonal matrices represent coupling terms between different harmonics (e.g., $[\Delta]_{12}$ is the coupling matrix between 1st and 2nd harmonics). In the paper where DFM was first introduced [21], only a single harmonic was considered, which corresponds to taking $[Z]_{11}$ and $[\Delta]_{11}$ matrices into account and neglecting all other submatrices in Eq. (25). $[Z]_{hh}$ can be explicitly written as follows

$$[Z]_{hh} = -(h\omega)^2[M] + i[H] + [K]. \tag{26}$$

In the force-control simulations, a single point, single harmonic excitation force is applied to 1st DOF which is the driving point, and Eq. (25) is solved for the displacement amplitudes of the fundamental and higher harmonics by keeping the amplitude of the excitation force constant. On the other hand, in the RCT simulations, the displacement amplitude corresponding to the first harmonic of the 1st DOF is kept constant and Eq. (25) is solved for the displacement amplitudes of all other DOFs and higher harmonics as well as the amplitude of the excitation force. In both simulations, equation of motion is solved numerically by using Newton's Method with arc-length continuation algorithm. In this case study, it is found to be sufficient to consider only the first and the third harmonics in the solution. The effect of the third harmonic on the FRFs in the first mode is illustrated in Fig. 2. It should be noted that throughout the paper, FRF term is used to refer to the frequency response function between the fundamental harmonic response and the excitation forcing. Since FRFs are not invariant of the excitation forcing in nonlinear systems, normalization of the frequency response with the amplitude of the excitation forcing may seem to be unnecessary. However, normalization process, which is very commonly used even for nonlinear systems, in literature, helps to suppress the effect of excitation forcing on the amplitude of the frequency response curve and to emphasize the effect of nonlinear stiffness and damping on the shape change of the frequency response curve.

4.1. Results of the standard force-control simulation

The classical approach to measure frequency responses of a nonlinear system is to apply force-controlled stepped-sine testing by keeping the amplitude of the harmonic forcing constant throughout the frequency sweep. Accordingly, a series of force-control simulations was carried out on the 5 DOF nonlinear system shown in Fig. 1. Constant-force FRFs determined around the first mode of the system at different forcing levels ranging from 1 N to 50 N are shown in Fig. 3. Obviously, the strong stiffness nonlinearity of the system changes the shape of each FRF considerably with increasing forcing level and

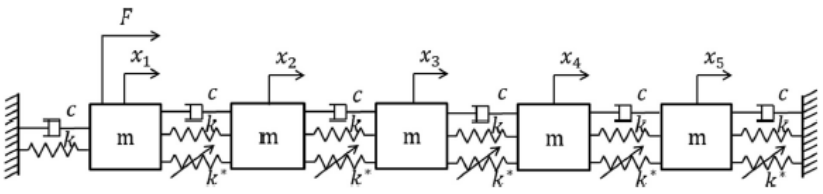

Fig. 1. 5 DOF system with cubic stiffness nonlinearity.

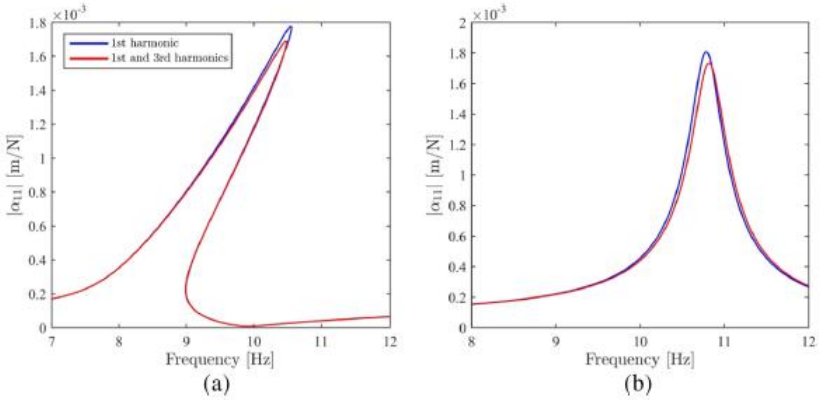

Fig. 2. Effect of the 3rd harmonic on the FRFs (a) constant-force driving point FRF at 50 N (b) constant-response driving point FRF at 0.10 m.

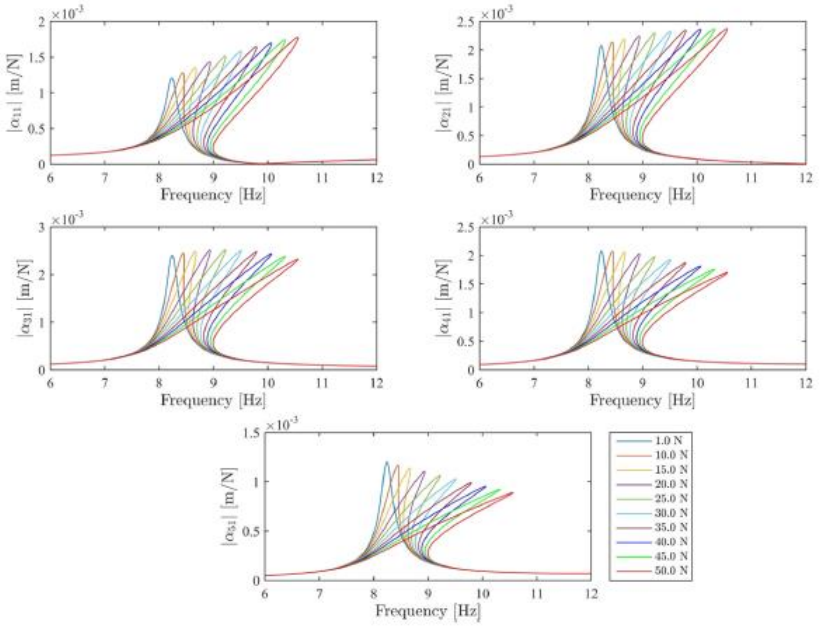

Fig. 3. Constant-force FRFs of the 5 DOF system with cubic stiffness, obtained by force-controlled stepped-sine testing simulations.

results in overhanging unstable branches. By virtue of the arc-length continuation algorithm, the computer simulation made it possible to capture these unstable branches and consequently, to determine exact locations of resonance points which constitute the NNM backbone curves. However, in real experimental applications, this cannot be achieved by using standard force control testing due to the jump phenomenon as explained in Section 3.6.1. In the following sections, it is shown that by just switching the control strategy from force control to response control, jump phenomenon can be avoided and consequently, standard equipment can still be used for modal identification of nonlinear systems.

4.2. Determination of constant-response FRFs by using the RCT simulation

Harmonic excitation force spectra of the driving point (1st DOF) determined from RCT simulations at different displacement amplitude levels are shown in Fig. 4. By dividing the displacement amplitude spectrum of each DOF with the harmonic excitation force spectrum, constant-response FRFs (corresponding to the first harmonic) were determined around the first mode of the system at different displacement amplitude levels ranging from 0.01 m to 0.1 m as shown in Fig. 5. It should be noted that not only constant-response FRFs of the 1st DOF, but also the constant-response FRFs of all other DOFs turned out to be quasi-linear. Of course, visual inspection is not sufficient, and a solid proof is given in the next section by fitting linear analytical model to constant-response FRFs. This outcome validates the fundamental hypothesis of the proposed method, i.e. if the modal amplitude is kept constant, FRFs given in Eqs. (15) and (16) turn out to be quasi-linear. It should be noted that in case of single point excitation, modal amplitude can be kept constant by just keeping the displacement amplitude of the driving point constant.

The physics behind the quasi-linearization phenomenon is essentially very simple. When the displacement amplitude of the driving point is kept constant, if the NNM of interest is well separated from the other modes and no internal resonances occur, then the near-resonant deflection shape of the system can be approximated by the product of that single NNM with the modal amplitude. If the modal amplitude is kept constant, the deflection shape and so the energy level of the system is *frozen* throughout the frequency sweep in the vicinity of the resonant region. Accordingly, if this *frozen* deflection shape is fed into the nonlinearity matrix given in Eq. (3), this matrix remains also constant, which quasi-linearizes the equation of motion. Even though the displacement level is kept constant through the frequency sweep, the resonant peaks are observed in the constant-response FRFs shown in Fig. 5. These peaks result from the dip of the excitation force spectrum at the resonant point as shown in Fig. 4.

It is important to note that quasi-linearization holds true even when the shape of the NNM strongly depends on the response level as shown in Fig. 6. The shape of the 1st NNM of the 5 DOF nonlinear system considered in this study deviates from a symmetric shape toward an asymmetric shape with increasing displacement amplitude level due to the missing cubic stiffness element between 1st DOF and ground as shown in Fig. 1. Yet, constant-response FRFs given in Fig. 5 are still quasi-linear.

A final important observation made from Fig. 5 is that constant-response FRFs do not exhibit unstable branches although they cover the excitation forcing levels (1 N to 50 N) studied in Section 4.1. As explained in Section 3.6.2, the points on the unstable branches are visited at different times during RCT carried out at different displacement amplitude levels. In other words, points on the unstable branch of a constant-force FRF given in Fig. 3 are stabilized and shared among several different constant-response FRFs given in Fig. 5. This point is explained further in Section 4.5 by using the HFS concept.

4.3. Identification of nonlinear modal parameters from quasi-linear constant-response FRFs

Once constant-response FRFs are determined by using RCT simulations as shown in Fig. 5, modal identification methods for linear systems can then be used to extract nonlinear modal parameters as a function of modal amplitude. In this study, well known peak-picking method is used to determine modal parameters at each displacement amplitude level. As an example, constant-response FRFs corresponding to the highest displacement amplitude level, i.e. 0.10 m, obtained by RCT simulation are compared with the corresponding FRFs synthesized by using modal parameters identified from peak-picking technique in Fig. 7. The good match between the results of the simulated experiment and the corresponding linear analytical models shows that constant-response FRFs are really quasi-linear.

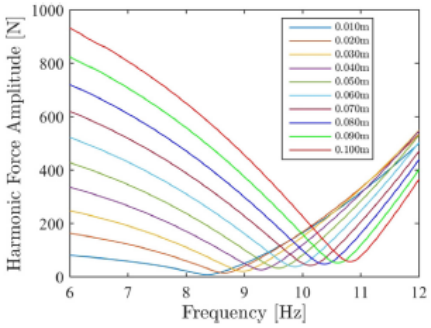

Fig. 4. Harmonic force spectra of the driving point (1st DOF) of the 5 DOF nonlinear system obtained from RCT simulations.

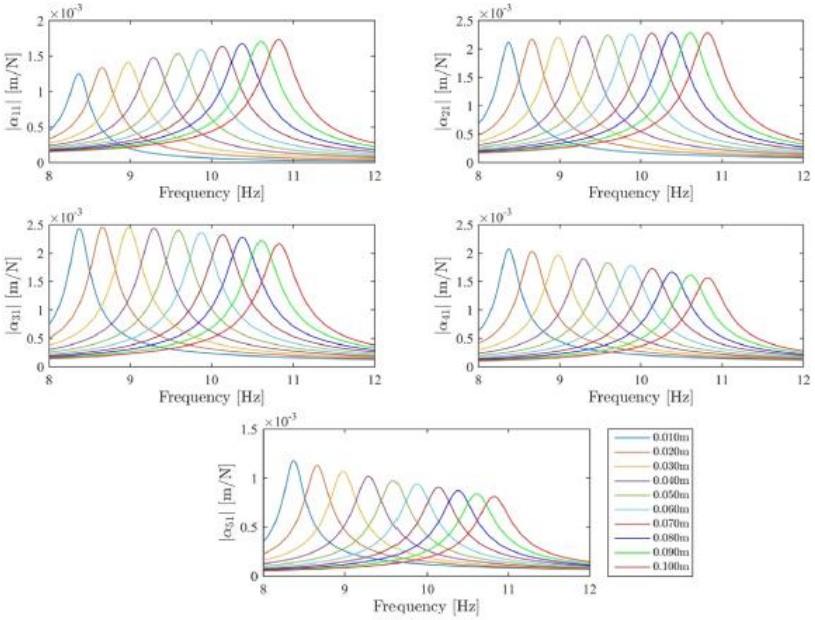

Fig. 5. Constant-response FRFs of the 5 DOF system with cubic stiffness, obtained from RCT simulations.

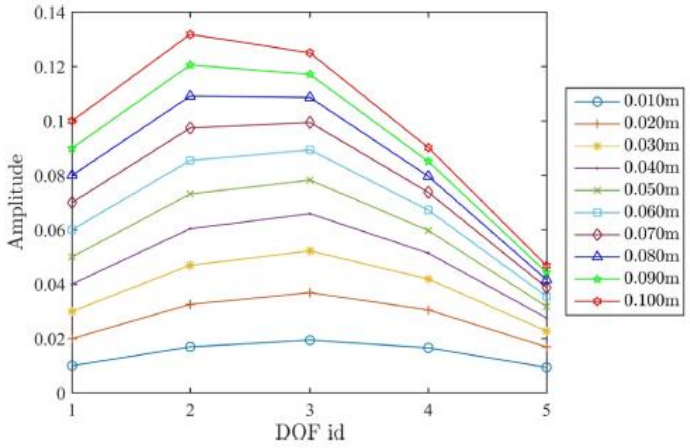

Fig. 6. The shape change of the 1st NNM of the 5 DOF nonlinear system with increasing displacement amplitude level.

By processing each set of FRFs corresponding to each displacement amplitude level (see Fig. 5) and collecting modal parameters of the 1st mode; the variations of the natural frequency, the nonlinear modal damping ratio and the modal constants with respect to modal amplitude can be determined as shown in Fig. 8 and Fig. 9. Substituting these modal parameters into Eq. (24), one can predict frequency responses of the system to various forcing scenarios without making any force con-

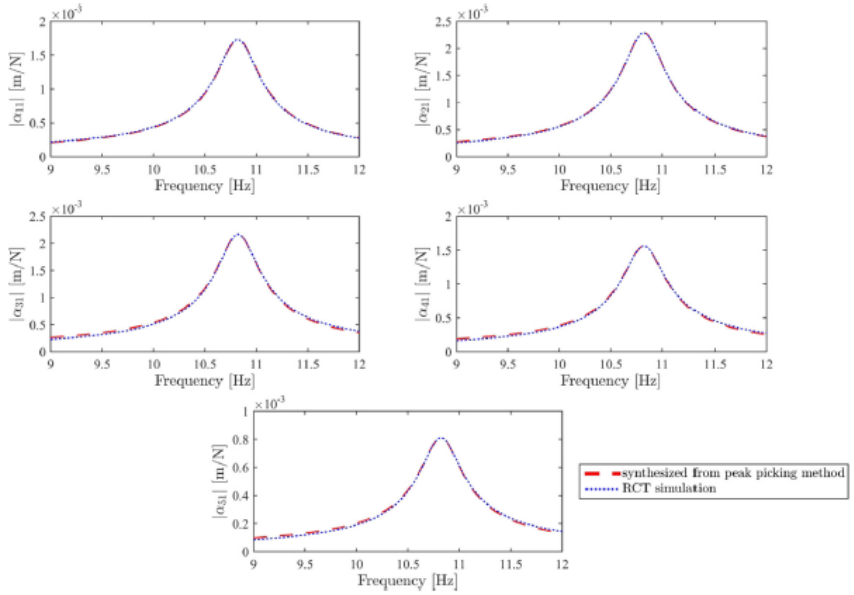

Fig. 7. Comparison of the constant-response FRFs obtained from RCT simulation, with the FRFs synthesized by using modal parameters identified from pick-peaking method at 0.10 mm amplitude level.

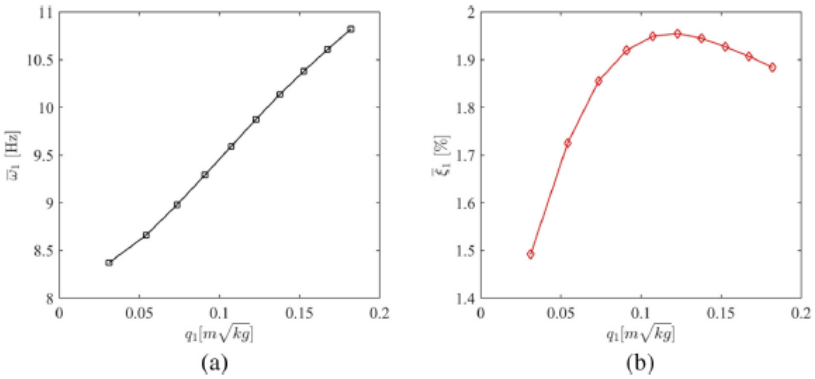

Fig. 8. Variation of the modal parameters corresponding to the 1st mode of the 5 DOF nonlinear system with modal response level (a) natural frequency (b) viscous modal damping ratio.

trolled test, which is very useful for the design and analysis of engineering structures. It should be noted that modal constants A_{jkr} given in Fig. 9 are closely related with mass normalized NNMs as shown in Eq. (23) and explained in Section 3.4. So, RCT approach makes it possible to experimentally extract mass normalized NNM from the identified modal constants given in Fig. 9.

4.4. Synthesis of constant-force FRFs by using the nonlinear modal parameters identified from RCT

Identified modal parameters given in Fig. 8 and Fig. 9 can be employed in Eq. (24) to synthesize frequency responses for various harmonic forcing scenarios. For validation, frequency responses of all 5 dofs were synthesized at 50 N using Eq. (24)

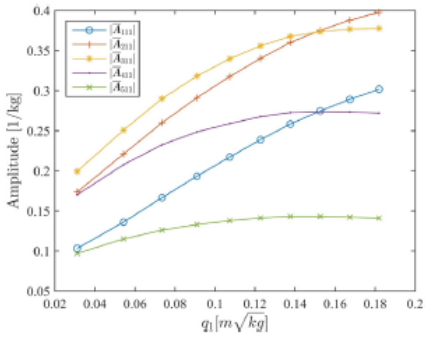

Fig. 9. Variation of the modal constants corresponding to the 1st mode of the 5 DOF nonlinear system with modal response level.

iteratively by applying Newton's Method with arc-length continuation algorithm. These frequency responses were then normalized with 50 N and were compared with the results of constant-force simulation as shown in Fig. 10. The comparison was also made at different force levels as shown in Fig. 11. The match between the computational results and the simulated experimental results is found to be satisfactory. The deviation further away from resonance peaks results from discarding the contribution of higher modes, which is the basic assumption of the single nonlinear mode theory. It is important to note that the modal parameters given in Fig. 8 and Fig. 9 were used as look-up tables without necessitating any polynomial fit.

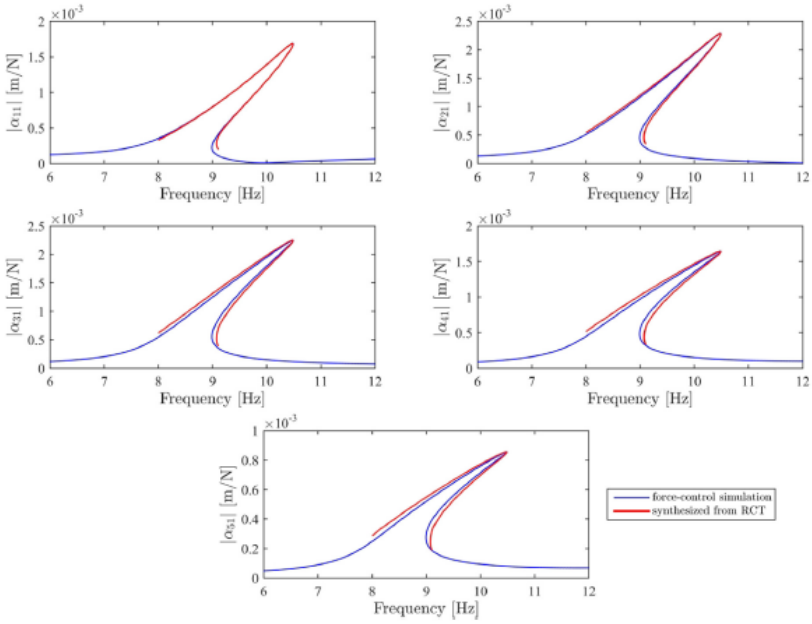

Fig. 10. Comparison of the constant-force FRFs obtained from simulated experiment, with the FRFs synthesized by using nonlinear modal parameters of the 5 DOF nonlinear system at 50 N forcing amplitude level.

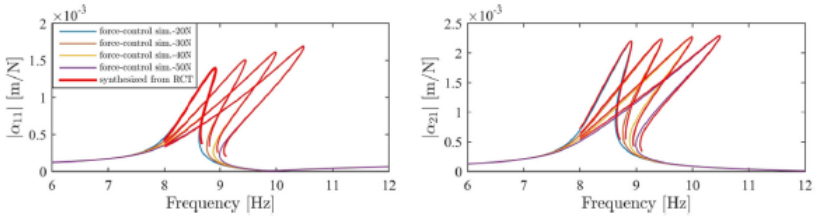

Fig. 11. Comparison of the constant-force FRFs obtained from simulated experiment, with the FRFs synthesized by using nonlinear modal parameters of the 5 DOF nonlinear system at several different forcing amplitude levels.

4.5. Experimental extraction of constant-force FRFs by using HFS

As an alternative to the analytical model based on identified modal parameters, untested constant-force FRFs can also be determined directly from experimental data by using the HFS concept. To do so, first of all, harmonic force spectra already obtained from RCT simulations at 10 different displacement amplitude levels, as shown in Fig. 4, were combined to construct the HFS given in Fig. 12(a). Then, the surface was cut with the 50 N constant-amplitude plane. The curve intersecting this plane and the HFS is nothing but the frequency response curve of the 1st DOF corresponding to 50 N forcing level. Finally, the receptance curve for the 1st DOF was obtained by normalizing the frequency response curve with the amplitude of the excitation force. Comparison of the receptances obtained from the HFS approach with the ones synthesized by using identified modal parameters, as well as with the original receptances obtained from simulated force-control experiment is shown in Fig. 12(b).

5. Experiments

5.1. T-beam

The first experimental setup used to validate the proposed method is shown in Fig. 13. The test rig consists of a cantilever beam supported at its free end by two metal strips which exhibit distributed geometric nonlinearity due to large deformations. Dimensions of the rig can be found in [26]. This experimental study focuses on the frequency response around the first nonlinear mode of the structure, where a strong stiffening nonlinearity is observed.

During experiments, the system was excited with a B&K shaker attached to its T-junction via a push-rod with a Dytran 1022V force transducer as shown in Fig. 13. The vibration response was measured by using a Dytran 3225M23 miniature accelerometer attached to the top of the T-junction. All measurements and closed loop controls were accomplished by LMS SCADAS Mobile data acquisition system and LMS Test Lab. software package. The upper and lower frequency limits of the stepped-sine tests were selected based on FRF data obtained from preliminary broadband random testing. The fre-

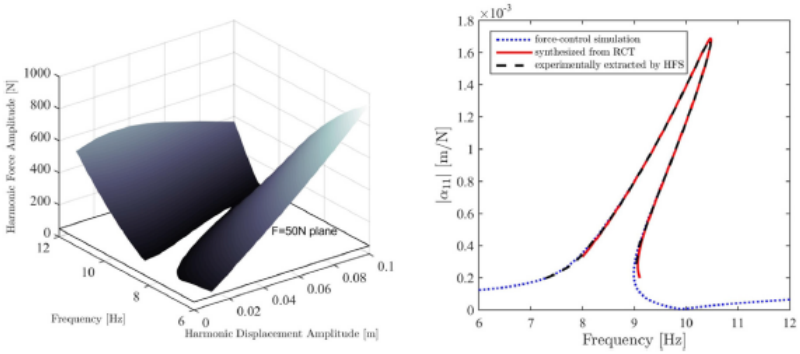

Fig. 12. (a) HFS of the 5 DOF nonlinear system (b) Comparison of the receptances extracted by using the HFS approach, with the ones synthesized by using the nonlinear modal parameters identified from RCT, and with the original receptances obtained from simulated force-control experiment at 50 N.

Fig. 13. The T-beam experimental setup.

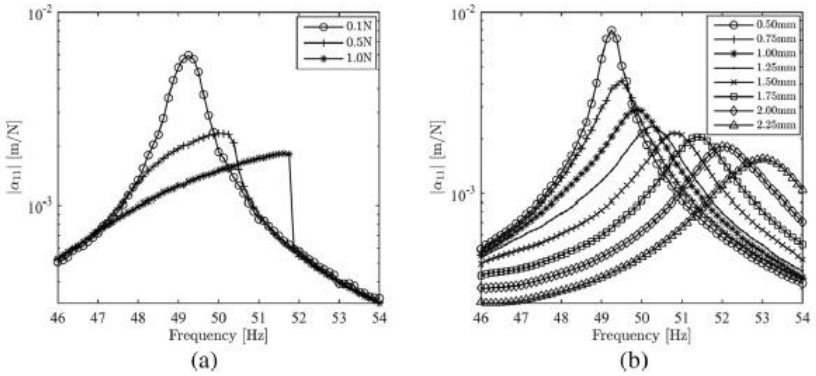

Fig. 14. (a) Constant-force FRFs of the T-beam measured by the classical force-control approach (b) constant-response FRFs of the T-beam measured by the RCT approach.

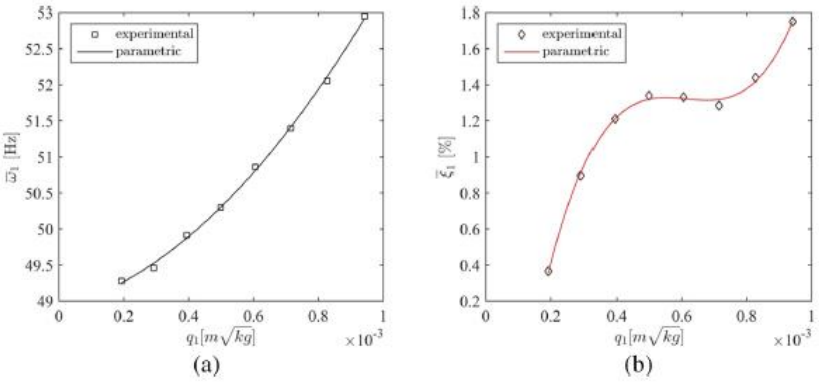

Fig. 15. Variation of the modal parameters corresponding to the 1st mode of the T-beam with modal response level (a) natural frequency (b) viscous modal damping ratio.

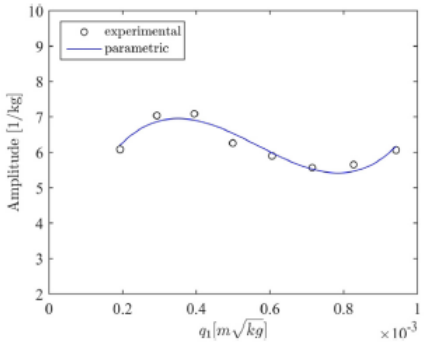

Fig. 16. Variation of the modal constant corresponding to the 1st mode of the T-beam with modal response level.

quency step was taken to be 0.125 Hz. After putting the control signal between the tolerance limits of the reference signal, the controller waits for a number of delay cycles to switch to the next frequency point.

First of all, a series of stepped-sine tests was conducted to characterize the nonlinearity by using classical force-control approach. Constant-force FRFs measured at 3 different excitation levels are shown in Fig. 14(a). The shift of the FRF-peak toward higher frequencies with increasing excitation level and the jump phenomenon observed at the highest level are clear indications of strong stiffening nonlinearity. Force-control tests were followed by a series of stepped-sine tests with RCT strategy. Constant-response FRFs of the T-beam measured at 8 different constant displacement amplitude levels, ranging

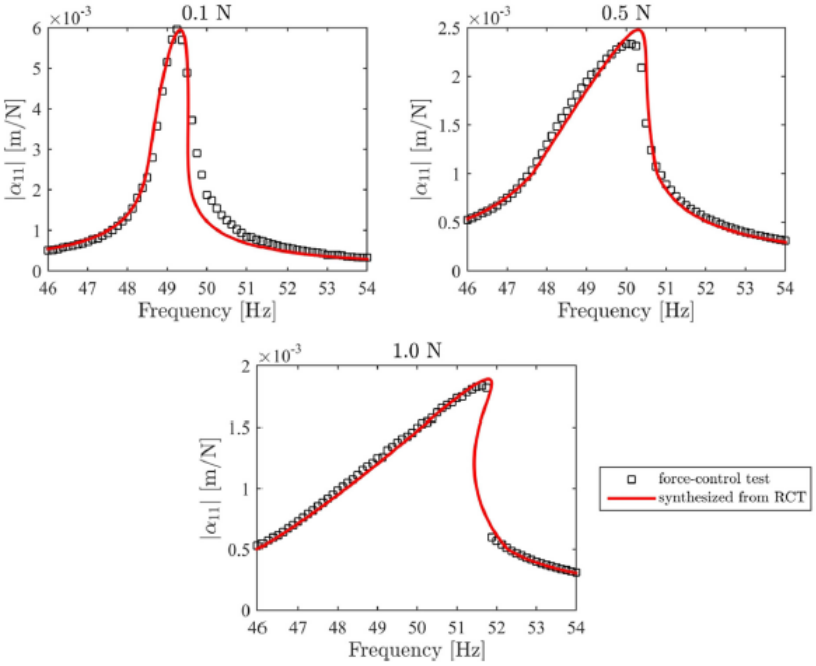

Fig. 17. Comparison of constant-force FRFs obtained from force-control test with FRFs synthesized by using nonlinear modal parameters of the T-beam.

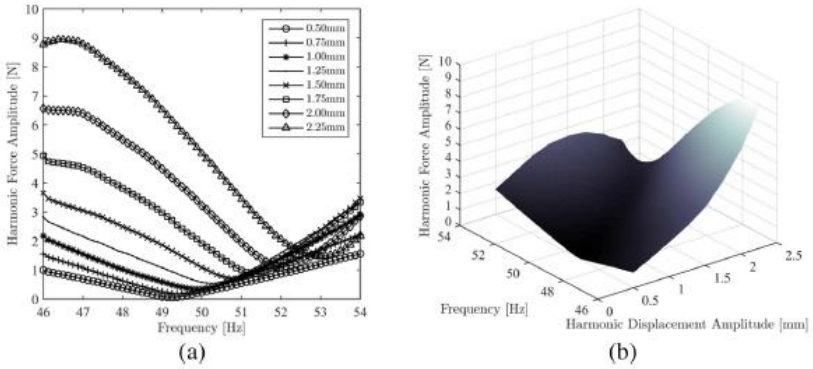

Fig. 18. (a) Harmonic force spectra of the T-beam measured during RCT (b) HFS of the T-beam constructed by collecting harmonic force spectra and using linear interpolation.

from 0.50 mm to 2.25 mm, are shown in Fig. 14(b). Although the proposed method requires collecting more data compared to some other approaches, since response control is easier than force control due to more predictable (quasi-linear) behavior of the system, the response-controlled testing is much faster. For example, in the T-beam experiments, a single response-controlled testing is about 3 times faster than a single force-controlled testing. Therefore, total experimental effort does not increase, at least compared to force-control testing.

Fig. 15 and Fig. 16 show variations of the nonlinear modal parameters corresponding to the 1st mode of the T-beam with respect to modal amplitude. These parameters were extracted from constant-response FRFs given in Fig. 14(b) by using linear modal analysis module of the LMS Test Lab., which is called PolyMAX. Fig. 15 and Fig. 16 show also parametric models of the nonlinear modal parameters obtained by polynomial curve fitting.

Fig. 17 compares the constant-force FRFs synthesized by employing response level dependent values of the identified modal parameters in Eq. (24), with the ones directly measured from force-controlled stepped sine testing. The agreement between the computational and experimental results is found to be quite satisfactory. Furthermore, although the force-control testing cannot capture the unstable branch, it is computationally obtained by using the theoretical model based on identified modal parameters, by employing the arc-length continuation algorithm in solving Eq. (24).

Harmonic force spectra measured at different displacement amplitude levels during RCT are illustrated in Fig. 18(a). The HFS of the T-beam is constructed by collecting these force spectra together and using linear interpolation as shown in Fig. 18 (b). The frequency response curve corresponding to 1 N excitation force level is obtained by cutting the HFS with 1 N constant-amplitude plane as demonstrated in Fig. 19(a). The frequency response curve obtained from the HFS is compared

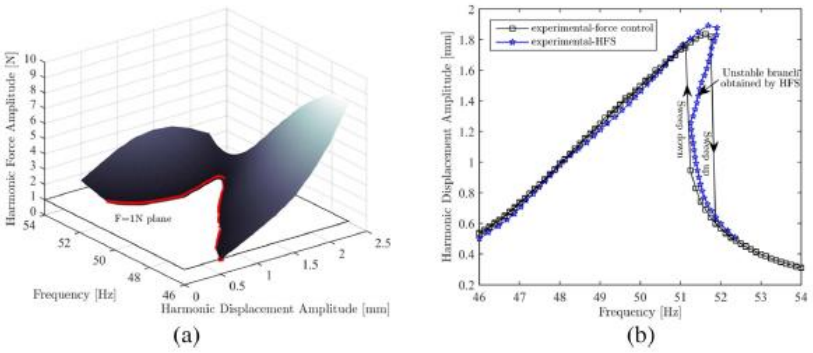

Fig. 19. (a) Determination of the harmonic response spectrum with any existing unstable branch by cutting HFS with a constant force plane (b) Comparison of the response spectrum obtained by HFS with the one obtained by force controlled testing.

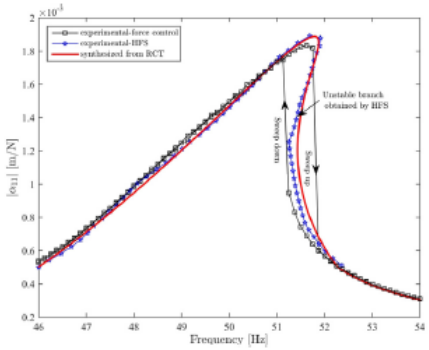

Fig. 20. Comparison of the receptances of the T-beam extracted by using the HFS approach with the ones synthesized by using nonlinear modal parameters identified from RCT, and with the original receptances obtained from force-control experiment at 1 N.

with the one directly obtained from the force-controlled stepped-sine testing is given in Fig. 19(b). Although the HFS is capable of capturing the unstable branch completely, classical force-controlled testing can only capture it until the turning points at the cost of multiple runs with different sweep directions. The unstable branches of constant-force frequency response curves can also be determined by using the CBC method, where a set of curves are obtained fixing the frequency and varying the response level. Then theses curves, which require considerable time to obtain experimentally as reported by the authors, are processed with Gaussian process regression [17].

To conclude this section, constant-force FRFs determined from the proposed method for 1 N excitation level are compared to the one obtained from classical force-controlled stepped-sine testing in Fig. 20. The agreement between all three approaches is found to be satisfactory.

5.2. Real missile

5.2.1. Identification of nonlinear modal parameters and synthesis of constant-force FRFs

The test setup of the real missile structure is shown in Fig. 21. Modal tests were conducted with free-free boundary conditions by using bungee-chords, lengths of which were adjusted such that rigid body mode frequencies of the missile struc-

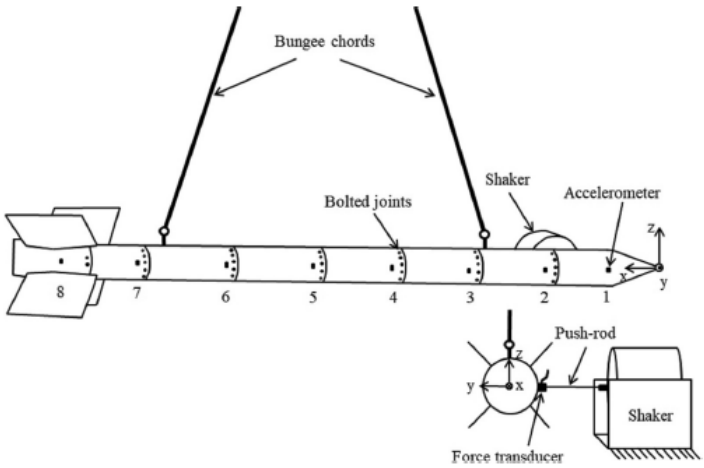

Fig. 21. Sketch of the experimental setup of the real missile.

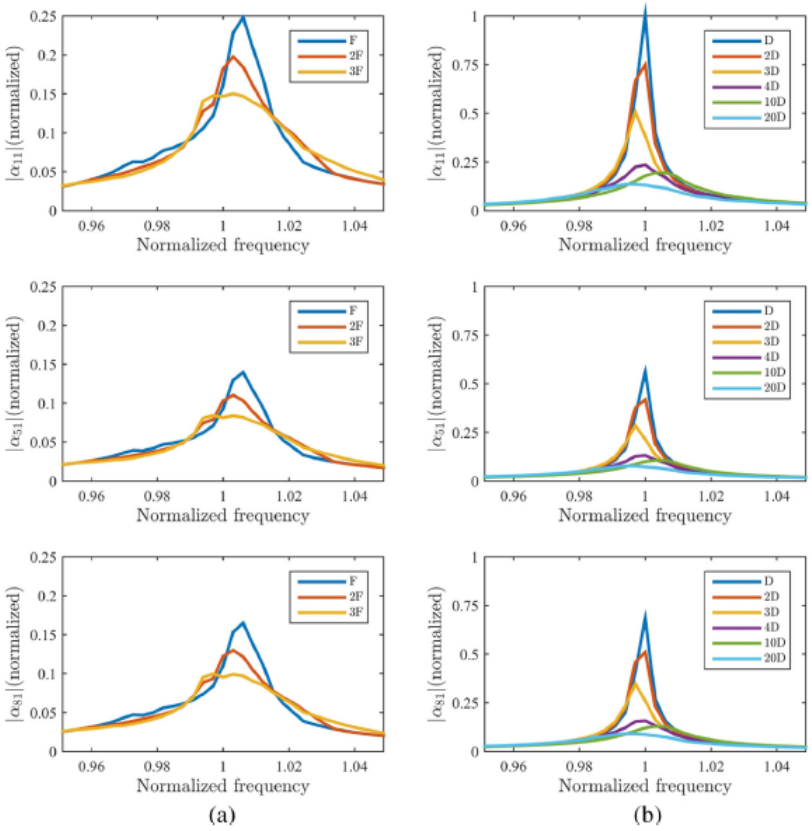

Fig. 22. (a) Constant-force FRFs of the missile structure measured by the classical force-control approach (b) constant-response FRFs of the missile structure measured by the RCT approach.

ture were kept far below its first elastic mode. In total, 8 Dytran 3225M23 miniature accelerometers were attached along the centerline of the missile and they were enumerated from 1 to 8, as shown in Fig. 21. In this study, the focus was on the first elastic mode of the system, so the structure was excited with a single shaker in y-direction. An MB Dynamics Modal 110 shaker was attached to the structure via a push-rod with a Dytran 1051V4 force transducer at point 1. All measurements and closed loop controls were accomplished by LMS SCADAS Mobile data acquisition system and LMS Test Lab. software package.

The locations of the bolted joints, connecting different parts of the missile are also shown in Fig. 21. All bolts are identical and have the same preload which was applied by a torque wrench during the assembly process.

The missile structure was first subjected to a series of stepped-sine tests by using classical force-control approach. The constant-force FRFs measured at three different excitation levels (F, 2F and 3F), and corresponding to three different accelerometer locations are illustrated in Fig. 22(a). The shift of the FRF-peak toward lower frequencies and the decrease in the FRF peak amplitude with increasing excitation level indicate softening nonlinear behavior with increasing nonlinear damping. The test campaign continued with a series of stepped-sine tests conducted at 14 different displacement amplitude levels (ranging from D to 20D) with RCT strategy. For the sake of readability, constant-response FRFs corresponding to 6 selected displacement amplitude levels are illustrated in Fig. 22(b).

Variation of modal parameters identified from constant-response FRFs are shown in Fig. 23 and Fig. 24. Confidence intervals were obtained by repeating each test several times during the test campaign. The first important observation made from

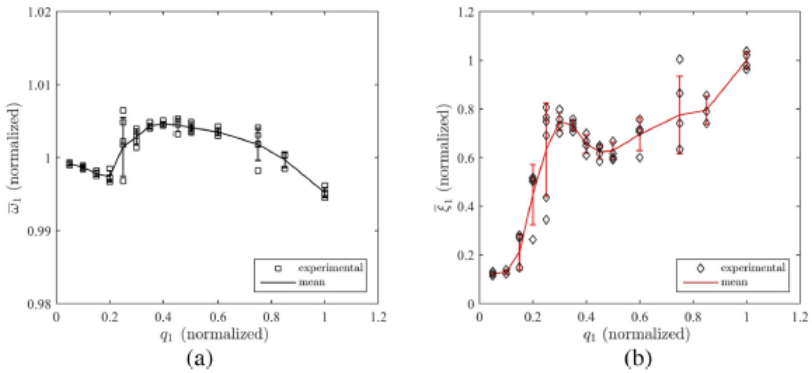

Fig. 23. Variation of the modal parameters corresponding to the 1st mode of the missile structure with modal response level (a) natural frequency (b) viscous modal damping ratio.

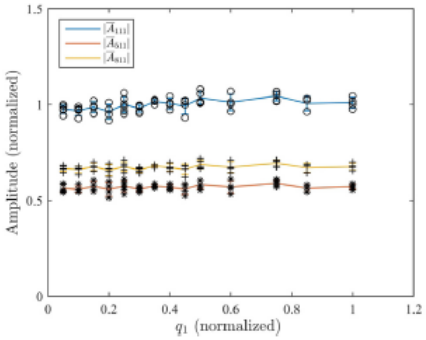

Fig. 24. Variation of modal constants corresponding to the 1st mode of the missile structure with modal response level.

Fig. 23 is the order of magnitude change in the nonlinear modal damping ratio and a very small change in the natural frequency, which indicate that the system exhibits considerable damping nonlinearity but weak stiffness nonlinearity. Another observation worth mentioning is the transition region (between 0.2 and 0.4), where nominal damping increases drastically,

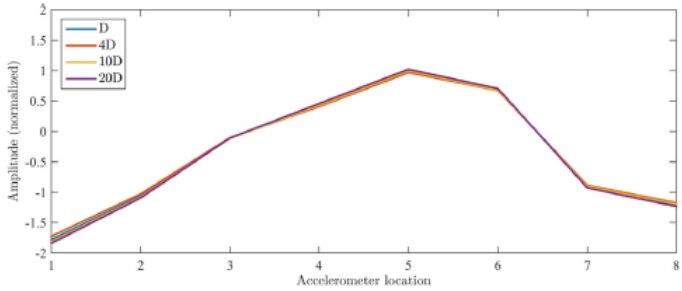

Fig. 25. 1st NNM of the missile structure experimentally extracted by using the modal constants identified from RCT.

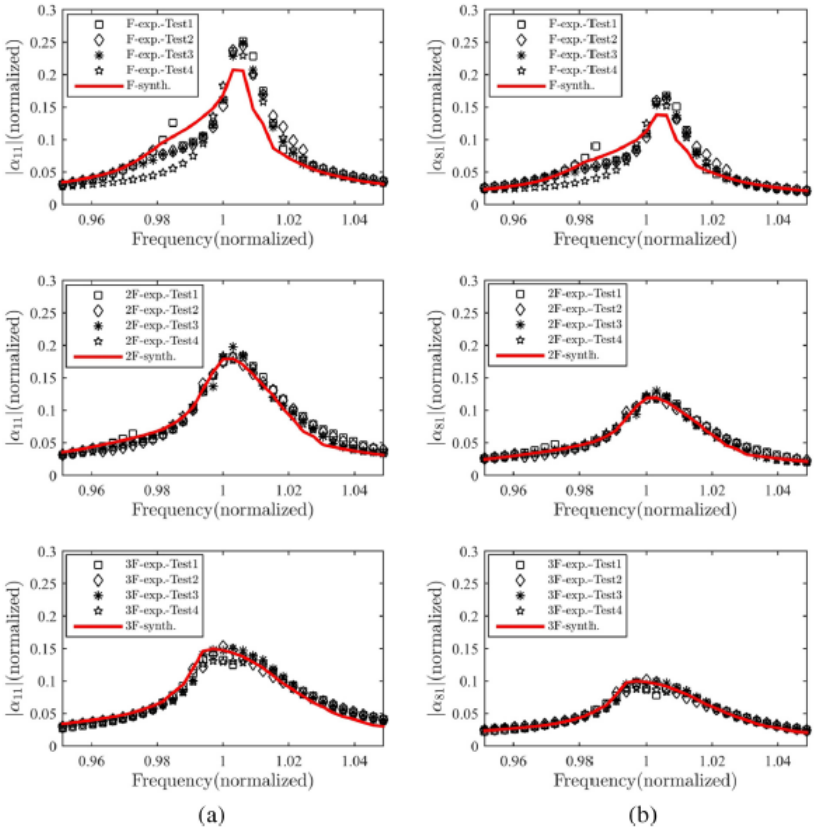

Fig. 26. Comparison of the constant-force FRFs obtained from force-controlled test, with FRFs synthesized by using nonlinear modal parameters of the missile: (a) driving point FRF (point1 in Fig. 21) (b) FRF between tail point (point 8 in Fig. 21) and driving point.

and the considerably large confidence intervals in this region. This transition region may be an indication of the stick to slip transition (slipping means more friction and damping). On the other hand, large confidence intervals may result from combined effects of several different environmental conditions such as temperature change and changes of contact conditions due to vibration at the joint interfaces.

Due to the negligible change in the identified modal constants with response level, as illustrated in Fig. 24, it can be concluded that the shape changes in the NNM with vibration response level are also negligible, as can be seen in Fig. 25.

This section is concluded with the comparison of the constant-force FRFs synthesized by employing response level dependent values of the identified modal parameter (see Fig. 23 and Fig. 24) in Eq. (24), with the ones directly measured from force-controlled stepped sine testing, which is shown in Fig. 26. The agreement between the computational and experimental results is found to be quite satisfactory at moderate and high excitation levels (i.e. at 2F and 3F). At the lowest excitation level, repeatability of the measured constant-force FRFs is poor, which is the cause of large confidence intervals observed in the nonlinear damping ratio shown in Fig. 23(b). Consequently, the agreement between the computational and experimental FRFs at the lowest excitation level is not as good as that obtained at moderate and high excitation levels.

5.2.2. Effect of bolt preload on modal parameters

The modal parameters given in Fig. 23 were obtained for the bolt tightening torque of T1 which is the design torque level of the bolts shown in Fig. 21. In order to determine the effects of bolt preload on the modal parameters, RCTs were repeated

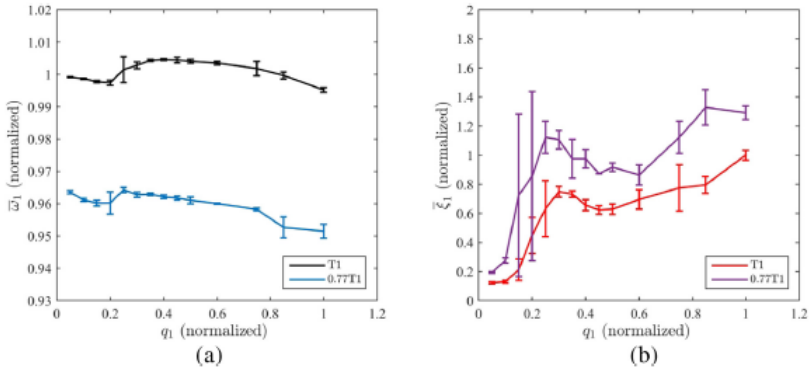

Fig. 27. Effect of bolt preload on the modal parameters (a) natural frequency (b) viscous modal damping ratio.

for a lower torque level of 0.77 T1. The modal parameters obtained at these two different torque levels are compared in Fig. 27.

It can be observed from Fig. 27(a) that when the bolt preload is reduced, the natural frequency decreases, i.e. the structure becomes more flexible. Furthermore, since less preload means more sliding (i.e. more friction and damping), nonlinear damping at the joints is enhanced when the preload is reduced as shown in Fig. 27(b). Another interesting observation relevant to Fig. 27 is that the percentage increase in the modal damping ratio exceeds 50% at various displacement levels, while the decrease in the natural frequency is limited to 3–5%. Therefore, it is concluded that modal damping, compared to natural frequency, is much more sensitive to bolt preload. In other words, stiffness is affected much less than damping. To know the amount of increase that can be achieved in modal damping by decreasing bold preload may be an important parameter in designing such structures from an aeroelastic perspective.

6. Conclusions

This paper proposes a nonlinear experimental modal analysis approach based on response-controlled stepped sine testing (RCT). The proposed approach is applicable to systems with several nonlinearities at various different locations, provided that modes are well separated and no internal resonances occur. In this approach, a series of modal tests is conducted by using RCT strategy. In each test, the displacement amplitude of the driving point is kept at a constant level, as a result of which measured *constant-response* FRFs come out in quasi-linear form. Subsequently, by applying standard linear modal analysis techniques to these constant-response FRFs, modal parameters corresponding to a specific nonlinear mode are experimentally extracted as functions of the modal amplitude. The identified response dependent modal parameters are used to synthesize near-resonant frequency response curves, even with unstable branches if there is any, for unmeasured harmonic forcing cases without any extra experimental effort. As the experimentally extracted nonlinear modal parameters are response level dependent, the computation of frequency response curves require an iterative solution. In this work, Newton's Methods and arc-length continuation algorithm is used which makes it possible to calculate any unstable branch as well. The proposed approach provides also an alternative way of determining frequency response curves (once again without any extra experimental effort) by directly extracting isocurves of constant-amplitude forcing from the Harmonic Force Surface measured during RCT, which is a novel concept proposed in this paper. Furthermore, by using multiple sensors during RCT, mass normalized NNMs can also be experimentally extracted from the identified modal constants.

Considering state-of-the-art techniques, the proposed method has several contributions. Firstly, it relies on standard controllers (available in commercial modal testing hardware and driven by commercial software), which makes it very attractive especially for industrial applications. Secondly, identification of modal damping and mass normalization of NNMs is straightforward with the proposed method, by applying linear modal analysis methods available in commercial software packages to constant-response FRFs measured during RCT. Finally, in case of strongly nonlinear systems, the method is capable of capturing unstable branches of frequency response curves either computationally by using identified modal parameters or experimentally by using the HFS concept. However, it should be noted that the proposed method is limited to systems which have well separated modes and which do not exhibit internal resonances within the energy range of interest. An investigation on the applicability of the proposed method to the case of internal resonances is in our future work program.

In this study, the application and validation of the approach proposed are demonstrated on numerical and experimental case studies. In the numerical example, the method is successfully applied to a 5 DOF lumped system with strong conservative nonlinearity. A very good match is obtained between the computational results and the simulated experimental

results, even for high forcing cases where very strong nonlinear effects with unstable branches are observed. Next, the method is validated on a cantilever beam supported at its free end by thin metal strips which exhibit geometric nonlinearity due to large deformations. Frequency response curves for constant amplitude harmonic forcing are accurately predicted (including the unstable branch which appears at the highest excitation level due to strong stiffening nonlinearity) both computationally from the identified nonlinear modal parameters, and experimentally from the HFS whose prominent feature is the experimental extraction of the unstable branches together with accurate determination of the turning points of frequency response curves at constant excitation level. Finally, the method is applied to a real missile structure which exhibit moderate damping nonlinearity. In this case study, standard force-controlled modal test approach leads to nonlinear FRFs, and linear modal analysis fails to predict even an approximate value for structural damping. However, by using the measured constant-response FRFs, the proposed method accurately predicts modal damping ratio as a function of modal amplitude, which has an important role in the accuracy of aeroelastic analyses. Missile example also shows that bolt preload has a considerable effect on the nonlinear modal damping, which makes it an important design parameter from an aeroelastic perspective.

CRediT authorship contribution statement

Taylan Karaağaçlı: Conceptualization, Methodology, Software, Validation, Formal analysis, Investigation, Writing - original draft. **H. Nevzat Özgüven:** Supervision, Conceptualization, Methodology, Writing - review & editing.

Declaration of Competing Interest

The authors declare that they have no known competing financial interests or personal relationships that could have appeared to influence the work reported in this paper.

Acknowledgment

The provision of TÜBİTAK-SAGE for modal testing and analysis capabilities is gratefully acknowledged.

References

[1] G. Kerschen, K. Worden, A.F. Vakakis, J.C. Golinval, Past, present and future of nonlinear system identification in structural dynamics, Mech. Syst. Sig. Process. 20 (2006) 505–592.
[2] J.P. Noël, G. Kerschen, Nonlinear system identification in structural dynamics: 10 more years of progress, Mech. Syst. Signal Process. 83 (2017) 2–35.
[3] R.M. Rosenberg, The normal modes of nonlinear n-degree-of-freedom systems, J. Appl. Mech. 29 (1962) 7–14.
[4] R.M. Rosenberg, On nonlinear vibrations of systems with many degrees of freedom, Adv. Appl. Mech. 9 (1966) 155–242.
[5] W. Szemplinska-Stupnicka, The modified single mode method in the investigations of the resonant vibrations of nonlinear systems, J. Sound Vib. 63 (4) (1979) 475–489.
[6] S. Setio, H.D. Setio, L. Jezequel, A method of nonlinear modal identification from frequency response tests, J. Sound Vib. 158 (3) (1992) 497–515.
[7] C. Gibert, Fitting measured frequency response using nonlinear modes, Mech. Syst. Sig. Process. 17 (1) (2003) 211–218.
[8] F. Thouverez, Presentation of the ECL benchmark, Mech. Syst. Sig. Process. 17 (1) (2003) 195–202.
[9] D. Göge, U. Füllekrug, M. Sinapius, M. Link, L. Gaul, Advanced test strategy for identification and characterization of nonlinearities of aerospace structures, AIAA J. 43 (5) (2005) 974–986.
[10] S.F. Masri, T.K. Caughey, A nonparametric identification technique for nonlinear dynamic problems, J. Appl. Mech. 46 (1979) 433–447.
[11] M.F. Platten, J.R. Wright, G. Dimitriadis, J.E. Cooper, Identification of multi-degree of freedom nonlinear systems using an extended modal space model, Mech. Syst. Sig. Process. 23 (1) (2009) 8–29.
[12] M.F. Platten, J.R. Wright, J.E. Cooper, G. Dimitriadis, Identification of a nonlinear wing structure using an extended modal model, AIAA J. Aircraft 46 (5) (2009) 1614–1626.
[13] U. Fuellekrug, D. Goege, Identification of weak nonlinearities within complex aerospace structures, Aerosp. Sci. Technol. 23 (2012) 53–62.
[14] M. Peeters, G. Kerschen, J.C. Golinval, Dynamic testing of nonlinear vibrating structures using nonlinear normal modes, J. Sound Vib. 330 (2011) 486–509.
[15] M. Peeters, G. Kerschen, J.C. Golinval, Modal testing of nonlinear vibrating structures based on nonlinear normal modes: experimental demonstration, Mech. Syst. Sig. Process. 25 (2011) 1227–1247.
[16] S. Peter, R.I. Leine, Excitation power quantities in phase resonance testing of nonlinear systems with phase-locked-loop excitation, Mech. Syst. Sig. Process. 96 (2017) 139–158.
[17] L. Renson, A. Gonzalez-Buelga, D.A.W. Barton, S.A. Neild, Robust identification of backbone curves using control-based continuation, J. Sound Vib. 367 (2016) 145–158.
[18] V. Denis, M. Jossic, C. Giraud-Audine, B. Chomette, A. Renault, O. Thomas, Identification of nonlinear modes using phase-locked-loop experimental continuation and normal form, Mech. Syst. Sig. Process. 106 (2018) 430–452.
[19] S. Peter, M. Scheel, M. Krack, R.I. Leine, Synthesis of nonlinear frequency responses with experimentally extracted nonlinear modes, Mech. Syst. Sig. Process. 101 (2018) 498–515.
[20] M. Scheel, S. Peter, R.I. Leine, M. Krack, A phase resonance approach for modal testing of structures with nonlinear dissipation, J. Sound Vib. 435 (2018) 56–73.
[21] Ö. Tannkulu, B. Kuran, H.N. Özgüven, M. İmregün, Forced harmonic response analysis of nonlinear structures using describing functions, AIAA J. 31 (7) (1993) 1313–1320.
[22] Arslan Ö., Özgüven, H.N., Modal identification of nonlinear structures and the use of modal model in structural dynamic analysis, in: Proceedings of the 26th International Modal Analysis Conference (IMAC), Orlando, USA, 2008.
[23] Ferreira J.V. , Ewins D.J., Algebraic nonlinear impedance equation using multi-harmonic describing function, 15th , Int. Modal Anal. Conf. (1997) 1595.
[24] G. Kerschen, M. Peeters, J.C. Golinval, A.F. Vakakis, Nonlinear normal modes, part I: a useful framework for the structural dynamicist, Mech. Syst. Sig. Process. 23 (1) (2009) 170–194.

[25] S. Schwarz, L. Kohlmann, A. Hartung, J. Gross, M. Scheel, M. Krack, Validation of a turbine blade component test with frictional contacts by phase-locked-loop and force-controlled measurements, J. Eng. Gas Turbines Power 142 (5) (2020), https://doi.org/10.1115/1.4044772.
[26] Ö. Arslan, M. Aykan, H.N. Özgüven, Parametric identification of structural nonlinearities from measured frequency response data, Mech. Syst. Signal Process. 25 (2011) 1112–1125.

Mechanical Systems and Signal Processing 144 (2020) 106872

Contents lists available at ScienceDirect

Mechanical Systems and Signal Processing

journal homepage: www.elsevier.com/locate/ymssp

A frequency domain nonparametric identification method for nonlinear structures: Describing surface method

Taylan Karaağaçlı [a,b], H. Nevzat Özgüven [b,*]

[a] The Scientific and Technological Research Council of Turkey, Defense Industries Research and Development Institute, TÜBİTAK-SAGE, P.K. 16, 06261 Mamak, Ankara, Turkey
[b] Mechanical Engineering Department, Middle East Technical University, 06531 Ankara, Turkey

ARTICLE INFO

Article history:
Received 4 August 2019
Received in revised form 28 March 2020
Accepted 3 April 2020

Keywords:
Nonlinear structural dynamics
Nonlinear system identification
Frequency dependent nonlinearity
Nonparametric identification of nonlinearity
Response controlled stepped sine test

ABSTRACT

In this paper a new method called 'Describing Surface Method' (DSM) is developed for nonparametric identification of a localized nonlinearity in structural dynamics. The method makes use of the Nonlinearity Matrix concept developed in the past by using classical describing function theory, which assumes that nonlinearity depends mainly on the response amplitude and frequency dependence is negligible for almost all of the standard nonlinear elements. However, this may not always be the case for complex nonlinearities. With the method proposed in this study, nonlinearities which are functions of both frequency and displacement amplitude can be identified by using response-controlled stepped-sine testing. Furthermore, the nonlinearity does not need to be mathematically expressible in terms of response amplitude and frequency, which allows us to identify more complex nonlinearities nonparametrically. The method is applicable to real engineering structures with local nonlinearity affecting the boundary conditions, where modes are not closely spaced, and sub- and super-harmonics are assumed to be negligible compared to the fundamental harmonic. Multiple nonlinearities may coexist at the same location and a priori knowledge of nonlinearity type is not necessary. The method yields the describing surface of nonlinearity, real and imaginary parts of which correspond to the equivalent nonlinear stiffness and nonlinear damping at that location in the structure. Harmonic response of a nonlinear system to any force, including any existing unstable branch, can be calculated iteratively by using the describing surface representing the nonlinearity. Unstable branches captured by using Newton's Method with arc-length continuation algorithm can be validated experimentally by using Harmonic Force Surface (HFS) concept. The validation of DSM is demonstrated with three experimental case studies: a cantilever beam with cubic stiffness at its tip point, a dummy mass on elastomeric vibration isolators, and a control fin actuation mechanism of a real missile structure which exhibits very complex (due to backlash and friction) and strong nonlinearity causing jump phenomenon in the frequency response. In each case, nonlinear FRFs calculated by using identified describing surface agree with measured FRFs at various force levels much better than FRFs calculated by using classical describing function method. It is observed in the experimental case studies that frequency dependence of nonlinearity occurs mostly in the imaginary part of the describing surface which represents nonlinear damping.

* Corresponding author.
E-mail address: ozguven@metu.edu.tr (H.N. Özgüven).

https://doi.org/10.1016/j.ymssp.2020.106872
0888-3270/

1. Introduction

By virtue of the important theoretical and technological advances over the last 40 years, linear system identification in structural dynamics is a mature research field today. Linear experimental modal analysis is widely used in industry, and is applicable to almost all types of engineering structures including very complex ones (e.g. aircrafts, satellites). On the other hand, the massive increase in computational power and the demand for higher performance in aircrafts, turbomachinery and satellites in terms of weight, speed and durability are encouraging industry more than ever to take into account nonlinear effects and include nonlinearities in the design and analysis of complex engineering structures.

The maturity of linear system identification and the increasing interest of industry in structural nonlinearities attracted also the attention of academia towards nonlinear system identification, which can be clearly seen by the exponential growth in the number of academic work in this field during the last two decades. The interested reader may refer to review papers [1,2] to gain some insight in the vast and rich literature of nonlinear system identification. Unfortunately, among many different techniques developed so far, there is no general method applicable to all nonlinear structures easily. Some of the techniques suffer from complicated mathematics; some others require tedious test procedures and most of them are applicable to simple structures with localized nonlinearities. In this section, a brief review of the well-established methods as well as some recently developed promising techniques will be given.

One of the earliest nonlinear identification methodologies in structural dynamics is the restoring force surface (RFS) method [3] which is also referred to as force-state mapping method [4]. This nonparametric time domain method basically plots internal restoring force of a nonlinear element as a function of displacement and velocity amplitudes. This way, elastic and dissipative forces can be visualized by cutting the restoring force surface with a vertical plane where either the velocity or displacement is equal to zero, respectively. Its simple formulation which is based on Newton's second law, and its nonparametric nature made the RFS method one of the most widely used nonlinear system identification approaches in structural dynamics over the years. Although the extension of the RFS method to multi-degree-of-freedom (MDOF) systems was theoretically shown [5], due to its computational burden, the application of the method in practice remained restricted to simple structures with few degrees of freedom and with localized nonlinearity. An early application of the RFS method was a study of space structure joints [6]. In the early 1990s, the RFS technique was also applied in several other works [e.g., see 7–9] for the characterization and identification of automobile shock absorbers. In a more recent study [10] the frequency dependence of nonlinearity, other than the displacement amplitude dependence, is also considered. In that work, the dynamic elastic modulus of elastomeric cylinder mounts was expressed by a restoring force model which is a nonlinear differential equation whose parameters are determined by force–deflection loops measured at various displacement amplitudes and frequencies. Although the model takes into account the frequency dependence of nonlinearity, its formulation is mathematically complex and is restricted to elastomers. Some other recent applications of the RFS method focusing primarily on the identification of nonlinear stiffness mechanisms include [11–15]. There are also several important studies investigating complex damping nonlinearities. For example, an automotive damper is identified by the RFS in [16]. In that work, the inability of the RFS method to capture the frequency dependence of nonlinear damping is reported as an important drawback. In another interesting study [17], hysteretic behavior of the frictional contact support of a cantilever beam was identified by force-state mapping approach. Due to its simplicity and efficiency, the RFS method is also preferred for qualitative identification of nonlinearity in complex MDOF engineering structures. For example, stiffness and damping nonlinearities at the mounting interface of a payload in an F-16 fighter aircraft are characterized by the RFS method in [18].

Preference of the RFS method in so many applications, the most of them being very recent, is a clear indication of the scarcity of alternative identification techniques as simple and effective as the RFS method. However, there are several important attempts. For example, two promising nonlinear identification techniques are the nonlinear resonant decay method (NLRDM) and identification of nonlinearity by time series based linearity (INTL) plots method. Both techniques essentially consist of the implementation of the RFS method in modal space. The test procedure involves exciting a mode of interest with a burst of a sine excitation at resonance. Parametrization of the nonlinear stiffness and damping of that mode could be achieved by fitting polynomial functions to the measured restoring force in modal space. INTL was applied to a real spacecraft component in [19]. NLRDM is an extension of INTL which takes cross-coupling of nonlinear modes into account. Two important applications of NLRDM are the identification of hardening nonlinear stiffness at the pylon connections of a wing-like structure [20] and nonlinear modal analysis of a complete transport aircraft [21]. For the identification of a single nonlinear element, NLRDM and INTL algorithms are equivalent to the restoring force surface method. The main advantage of these methods appears when applied to large structures with multiple nonlinearities. In such cases, instead of identifying individual nonlinear elements separately, their overall effect on a specific vibration mode is determined.

Two very recent and promising nonlinear system identification approaches are an extension of nonlinear phase resonance testing proposed in [22] and a novel approach called the Response Controlled stepped-sine Test (RCT) method proposed by the authors of this paper in [23]. The former method relies on a phase-controlled tracking of the backbone curve around a specific resonance to experimentally extract corresponding nonlinear normal mode. On the other hand, RCT method is based on quasi-linearization of nonlinear structures by keeping response amplitude constant during stepped-sine testing and yields modal parameters as a function of modal amplitude. In both approaches identified modal parameters are used to synthesize nonlinear frequency response of structures to near-resonant harmonic forcing including unstable branches. These

branches can also be extracted directly from experiment by using phase-locked-loop (PLL) control strategy in [22] or by using RCT and HFS concepts proposed in [23]. The method proposed in [22] is validated on a cantilever beam attached to a leaf spring and the RCT method is successfully applied to a real missile structure with nonlinearities due to bolted joints [23]. Another recently developed approach is the so-called Control Based Continuation (CBC) [24,25], which is also capable of tracking the backbone curve and of determining unstable points of nonlinear frequency responses by combining the response-amplitude control with phase quadrature condition and by processing the collected experimental data with Gaussian process regression, respectively. In [25], CBC is validated on a nonlinear beam with harmonically coupled modes, where the possibility to make the control non-invasive is also investigated. However, CBC and PLL approaches cannot make use of the standard equipment, and therefore require design of sophisticated controllers, unlike RCT approach. Similar to NLRDM and INTL, these three approaches essentially fall in the category of modal-domain nonlinear system identification and are suitable to study the overall effect of distributed nonlinearities on a specific vibration mode rather than focusing on localized nonlinearity.

Finally, two recently proposed techniques [26,27] worth mentioning fall in the category of frequency-domain nonlinear system identification and are conceptually more close to DSM than afore-mentioned approaches. The method proposed in [26] achieves parametric identification of a localized nonlinearity by using constant-response FRFs regenerated from a series of open-loop, constant-frequency and variable-excitation sinusoidal tests. The other technique proposed in [27] relies on nonlinear FRFs measured during open-loop stepped-sine testing and yields mathematical model of a nonlinear structural element as functions of frequency and response amplitude by using equivalent dynamic stiffness concept.

Each of the state-of-the-art techniques revised so far has its own advantages and limitations. However, no general method applicable to a wide range of nonlinear problems is available yet. In this paper, a frequency domain nonparametric identification method for nonlinear structures, namely the Describing Surface Method, is proposed. By using this method, many of the limitations of the aforementioned state-of-the-art identification techniques are eliminated. First of all, the method relies on the FRFs measured by response-controlled stepped-sine testing which can be obtained by using a standard data acquisition hardware and software (e.g. LMS SCADAS Mobile and LMS Test Lab.). Consequently, it can easily be used by practicing engineers. More importantly, the method determines nonlinearity as a function of not only the displacement amplitude but also the frequency, which is not addressed by many of the state-of-the-art techniques. Furthermore, the identification is purely non-parametric in the sense that it determines a describing surface of nonlinearity which can be used as a look-up table without necessitating any surface fitting. Last but not least, unstable branches of nonlinear FRFs can be obtained by using Newton's Method and arc-length continuation algorithm. The proposed method is validated by using three experimental case studies: a cantilever beam with cubic stiffness at its tip point, a dummy mass on elastomeric vibration isolators, and a control fin actuation mechanism of a real missile structure. In each case, nonlinear frequency response functions (FRFs) calculated by using identified describing surface agree very well with the measured FRFs at various force levels.

The paper is organized as follows. In Section 2, the theory is explained in detail. Section 3 is dedicated to the validation of the method with experimental case studies. Finally, important conclusions of the present study are summarized in Section 4.

2. Theory

The theory of DSM is based on the Describing Function Method (DFM) [28] proposed for harmonic vibration analysis of nonlinear systems by using describing functions. It is mathematically equivalent to the classical Harmonic Balance Method (HBM). The major difference between DFM and HBM relies in the interpretation of nonlinear internal forces. HBM expresses nonlinear internal forces as a single force vector, whereas in DFM they are written as a multiplication of displacement vector with the so-called Nonlinearity Matrix which has an important physical meaning. The real and imaginary parts of this matrix essentially correspond to equivalent nonlinear stiffness and damping matrices at a given response level, respectively. This simple but innovative idea was first prosed by Budak and Özgüven [29,30] in their studies investigating harmonic vibration response of nonlinear MDOF systems. Later, the method was generalized for any type of nonlinearity by Tanrıkulu et al. [28] by using describing functions [31], after which this approach is named DFM.

The initial motivation of the DFM method was to calculate harmonic vibration response of nonlinear MDOF systems. The concept of using nonlinearity matrix approach in nonlinear system identification was first suggested by Özer and Özgüven [32], and a method was developed to identify type and parametric values of a nonlinear element between ground and a single coordinate in a MDOF system, which is later extended to identify a single nonlinear element between any two coordinates of the system [33]. It was further improved by Aykan and Özgüven [34] by using incomplete FRF data which makes the method applicable to large systems with localized nonlinearity. These parametric identification methods based on classical DFM are restricted to the cases where nonlinearity is not a function of frequency. In this paper, the proposed DSM extends these methods to the identification of nonlinearities which can be functions of both the displacement amplitude and frequency. Moreover, since nonlinearity does not need to be mathematically expressible in terms of response amplitude and frequency, in the DSM complex nonlinearities can easily be identified nonparametrically contrary to the DFM-based identification methods which are restricted to parametric representation of nonlinearity.

For the sake of completeness, the theoretical bases of the DFM [28] and nonlinearity matrix concept are briefly summarized below before the derivation of the DSM.

2.1. Nonlinearity matrix and DFM

The equation of motion for a nonlinear MDOF system under harmonic excitation can be written as

$$[M]\{\ddot{x}\} + [C]\{\dot{x}\} + [K]\{x\} + \{N(x,\dot{x})\} = \{f\} \tag{1}$$

where $[M]$, $[C]$ and $[K]$ are the mass, viscous damping and stiffness matrices of the underlying linear system, respectively. Here, the vectors $\{x\}$ and $\{f\}$ represent the response of the system and the external force applied on it, respectively. $\{N\}$ is the nonlinear internal force in the system.

Consider a harmonic excitation of

$$\{f\} = \{F\}e^{i\omega t} \tag{2}$$

where $\{F\}$ denotes the amplitude of forcing, ω represents the excitation frequency. "i" shows the unit imaginary number. The response is assumed to be harmonic with a response amplitude of $\{X\}$. The internal nonlinear forces can then be written as

$$\{N\} = \{G\}e^{i\omega t} \tag{3}$$

where the amplitude of the internal nonlinear forcing vector can be expressed [28] as

$$\{G\} = [\Delta]\{X\} \tag{4}$$

Here $[\Delta]$ is called nonlinearity matrix, and it is response level dependent.

Tannkulu et al. [28] proposed the use of describing functions for the evaluation of the nonlinearity matrix, $[\Delta]$. The elements of $[\Delta]$ are obtained as follows

$$\Delta_{rr} = \upsilon_{rr} + \sum_{\substack{s=1 \\ s\neq r}}^{n} \upsilon_{rs}, \tag{5}$$

$$\Delta_{rs} = -\upsilon_{rs} \tag{6}$$

Here, n is the total degrees of freedom of the system and υ_{rs} is the harmonic describing function representation of the nonlinear internal force which can be obtained as

$$\upsilon_{rs} = \frac{i}{\pi Y_{rs}} \int_0^{2\pi} N_{rs} e^{i\psi} d\psi, \tag{7}$$

where N_{rs} and Y_{rs} are, respectively, the amplitudes of the nonlinear internal force and the relative displacement between coordinates r and s for $r \neq s$, and between rth coordinate and the ground for $r = s$.

$$Y_{rs} = \begin{Bmatrix} if\ r \neq s, & X_r - X_s \\ if\ r = s, & X_r \end{Bmatrix} \tag{8}$$

and

$$\psi = \omega t \tag{9}$$

Then, the response vector $\{X\}$ can be written as

$$\{X\} = \left[H^{NL}\right]\{F\} \tag{10}$$

where $\left[H^{NL}\right]$ is the nonlinear receptance matrix and it can be evaluated as

$$\left[H^{NL}\right] = \left(-\omega^2[M] + i\omega[C] + [K] + [\Delta]\right)^{-1} \tag{11}$$

As the elements of the nonlinearity matrix $[\Delta]$ are functions of the response itself, an iterative procedure is to be applied to calculate response amplitude $\{X\}$ from Eq. (10). Details of the DFM can be found in [28].

2.2. Describing surface method

Inverting the nonlinear receptance matrix given by Eq. (11) yields

$$-\omega^2[M] + i\omega[C] + [K] + [\Delta] = \left[H^{NL}\right]^{-1} \tag{12}$$

Similarly, inverse of the receptance matrix of the underlying linear system can be written as

$$-\omega^2[M]+i\omega[C]+[K]=\left[H^L\right]^{-1} \tag{13}$$

Subtracting Eq. (13) from Eq. (12) yields

$$[\Delta]=\left[H^{NL}\right]^{-1}-\left[H^L\right]^{-1} \tag{14}$$

Consider a MDOF system with localized nonlinearity at a single coordinate, say a nonlinear element between coordinate p and ground. Then the nonlinearity matrix $[\Delta]$ will include only a single nonzero element Δ_{pp} as follows

$$[\Delta]=\begin{bmatrix}0 & \cdots & 0\\ \vdots & \Delta_{pp} & \vdots\\ 0 & \cdots & 0\end{bmatrix} \tag{15}$$

Since there is single nonlinear element in the system, Eqn. (5) yields

$$\Delta_{pp}=\upsilon_{pp} \tag{16}$$

where υ_{pp} is the describing function of nonlinearity between coordinate p and ground.

Substituting Eqs. (15) and (16) into Eq. (14) and using single degree of freedom (SDOF) assumption at coordinate p yields

$$\upsilon_{pp}\left(|X_p|,\omega\right)=1/H^{NL}_{pp}-1/H^{L}_{pp}. \tag{17}$$

where $|X_p|$ denotes the displacement amplitude at coordinate p and ω is the excitation frequency. Here, H^{L}_{pp} and H^{NL}_{pp} represent point FRFs of the underlying linear and nonlinear MDOF systems at p^{th} coordinate, respectively.

For the sake of simplicity, subscript p will be dropped out hereafter. Displacement amplitudes $|X_p|$ will be referred to generically by $|X|$. Similarly, the H^{L}_{pp} and H^{NL}_{pp} terms will be represented generically by H^L and H^{NL}, respectively.

If the nonlinear system has multiple nonlinearities at the same location (with potentially hysteretic terms), nonlinear internal forces may not be negligible at very low or very high vibration levels. Consequently, receptance of the underlying linear system H^L may not be measured accurately. An alternative solution could be to eliminate H^L from Eq. (17) as explained below.

Consider that stepped-sine tests were conducted successively by keeping the displacement amplitude constant at levels $\left|X^k\right|$ and $\left|X^{k+1}\right|$ with a closed-loop control. Then, describing function of nonlinearity at these vibration levels can be written as

$$\upsilon\left(\left|X^k\right|,\omega\right)=1/H^{NL}_{|X^k|}-1/H^{L}, \tag{18}$$

$$\upsilon\left(\left|X^{k+1}\right|,\omega\right)=1/H^{NL}_{|X^{k+1}|}-1/H^{L}. \tag{19}$$

where superscripts k, $k+1$ denote successive amplitude levels.

Subtracting Eq. (18) from Eq. (19) yields

$$\upsilon\left(\left|X^{k+1}\right|,\omega\right)-\upsilon\left(\left|X^k\right|,\omega\right)=1/H^{NL}_{|X^{k+1}|}-1/H^{NL}_{|X^k|}. \tag{20}$$

Dividing Eq. (20) by $\delta X=\left|X^{k+1}\right|-\left|X^k\right|$ yields a finite difference approximation to the partial derivative of $\upsilon(|X|,\omega)$ with respect to $|X|$ within the interval $\left[\left|X^k\right|,\left|X^{k+1}\right|\right]$ as follows:

$$\partial\upsilon/\partial|X|\approx\left(1/H^{NL}_{|X^{k+1}|}-1/H^{NL}_{|X^k|}\right)/\left(\left|X^{k+1}\right|-\left|X^k\right|\right)|X|\in\left[\left|X^k\right|,\left|X^{k+1}\right|\right]. \tag{21}$$

By using the above formulation, the main algorithm of the DSM can be given as follows:

1. A stepped-sine test is conducted at a constant displacement amplitude level $\left|X^1\right|$ and the corresponding nonlinear receptance H^{NL} is measured (within the frequency range of interest). The same procedure is repeated at successive vibration levels $\left|X^2\right|,\cdots,\left|X^k\right|,\left|X^{k+1}\right|,\cdots|X^m|$.
2. Right hand side of Eq. (21) is calculated as a nonparametric function of $|X|$ at each interval $[|X_k|,|X_{k+1}|]$ by using the measured nonlinear FRFs.
3. Differential Eq. (21) is solved numerically for $\upsilon(|X|,\omega_1),\upsilon(|X|,\omega_2)$, etc., i.e. for each frequency point separately. Then describing functions determined at all frequency points are combined together to construct the describing function surface $\upsilon(|X|,\omega)$. In this study, Eq. (21) is solved by using the finite element method.
4. Estimate of the FRF of the underlying linear system, then, can be obtained as follows

$$H^L = 1/\left(1/H^{NL}_{|X^k|} - \upsilon\left(\left|X^k\right|,\omega\right)\right). \tag{22}$$

Since H^L is unique, $\left|X^k\right|$ can be any of the constant displacement amplitude levels tested, i.e. $\left|X^1\right|$ or $\left|X^2\right|$, etc.

5. Finally, response of the nonlinear system to any harmonic forcing can be determined iteratively by applying Newton's Method and arc-length continuation algorithm to the following equation

$$X = F/\left(1/H^L + \upsilon(|X|,\omega)\right). \tag{23}$$

Important clues for a successful application of the DSM are as follows:

- Describing surface of nonlinearity $\upsilon(|X|,\omega)$ is actually a complex function. Its real and imaginary parts stand for the equivalent nonlinear stiffness and nonlinear damping terms, respectively. Consequently, Eq. (21) has to be evaluated for the real and imaginary parts separately.
- Eq. (21) is a first order differential equation and needs a specific boundary value for a unique solution. If the measured FRF converges to a linear FRF at a low vibration level, then the appropriate boundary values for the real and imaginary parts of $\upsilon(|X|,\omega)$ are $Re(\upsilon(0,\omega)) = 0$ and $Im(\upsilon(0,\omega)) = 0$, respectively. On the other hand, if the measured FRF converges to a linear FRF at high vibration levels, then the appropriate boundary values for the real and imaginary parts of $\upsilon(|X|,\omega)$ are $Re(\upsilon(\infty,\omega)) = 0$ and $Im(\upsilon(\infty,\omega)) = 0$, respectively.
- As another example, if a structure includes cubic stiffness and Coulomb friction, the appropriate boundary values for the real and imaginary parts of $\upsilon(|X|,\omega)$ would be $Re(\upsilon(0,\omega)) = 0$ and $Im(\upsilon(\infty,\omega)) = 0$, respectively.
- In structures with complex nonlinear behavior, decision of the appropriate boundary value and consequently determining the absolute value of the describing surface of the nonlinearity may be difficult. In such cases, Eq. (18) can be substituted into Eq. (23) to obtain

$$X = F/\left(1/H^{NL}_{|X^s|} + \upsilon(|X|,\omega) - \upsilon\left(\left|X^s\right|,\omega\right)\right). \tag{24}$$

which is an alternative form of Eq. (23), and it takes the nonlinear FRF measured at displacement level $|X^s|$ as the reference, instead of the linear FRF.

- In the most general case, different displacement levels can be chosen as the reference values for the real and imaginary parts of the complex dynamic stiffness, which puts Eq. (24) into the following form

$$X = F/\left(Re\left(1/H^{NL}_{|X^s|} + \upsilon(|X|,\omega) - \upsilon\left(\left|X^s\right|,\omega\right)\right) + Im\left(1/H^{NL}_{|X^r|} + \upsilon(|X|,\omega) - \upsilon\left(\left|X^r\right|,\omega\right)\right)\right). \tag{25}$$

$$|X^s| \neq |X^r|$$

- In solving Eq. (21) numerically, it is usually a good practice to start with the assumption that $\upsilon(|X|,\omega)$ is C^o continuous, which means that the partial derivative value calculated using the right-hand side of Eq. (21) is assumed to be constant for each interval $\left[\left|X^k\right|,\left|X^{k+1}\right|\right]$. In all of the experimental case studies given in Section 3, $\upsilon(|X|,\omega)$ is assumed to be C^o continuous.
- Since the nonlinear FRF at absolute zero vibration level cannot be measured, the partial derivative within the interval $\left[0,\left|X^1\right|\right]$ cannot be obtained directly from measurements. For instance, the missing information can be obtained by linear extrapolation. So, if $\upsilon(|X|,\omega)$ is assumed to be C^o continuous, linear extrapolation corresponds to taking the partial derivative within the interval $\left[0,\left|X^1\right|\right]$ to be equal to the one calculated in the interval $\left[\left|X^1\right|,\left|X^2\right|\right]$.

The DSM presented in this study is applicable to systems with multiple nonlinearities as long as these nonlinearities are not continuously distributed, but concentrated at discrete locations so that they affect local vibration modes for which SDOF assumption can be made. Mounting interfaces of control surfaces and pylons of aircraft structures are good examples of concentrated nonlinearities which affect local vibration modes of these components. Since SDOF assumption can be made for each local mode, nonlinearity in each interface can theoretically be identified separately by using the DSM method. On the other hand, main wings of aircrafts which include many riveted and bolted connections as well as wide contacting surfaces are examples of structures with continuously distributed nonlinearities. Application of the DSM to such continuously distributed nonlinearities requires direct implementation of Eq. (14) which is not so straightforward as there are several

critical issues such as missing elements of the linear and nonlinear receptance matrices which may not be measured due to physical limitations, and sensitivity of matrix inversions to measurement error.

3. Experimental studies

3.1. T-beam

The proposed method was first validated by using the T-beam experimental setup shown in Fig. 1. The test rig consists of a cantilever beam whose free end is held between two metal strips which create hardening cubic stiffness effect. Dimensions and other technical details of the setup can be found in [35].

In this study, T-beam was excited with a B&K shaker attached to its T-junction via a push-rod with a Dytran 1022 V force transducer as shown in Fig. 1. The vibration response was measured by using a Dytran 3225M23 miniature accelerometer attached to the top of the T-junction.

All measurements and closed loop controls were accomplished by LMS SCADAS Mobile data acquisition and control hardware driven by LMS Test Lab. software package. In all the force-controlled and response-controlled stepped-sine tests conducted during the experiments in this work, the control strategy was the closed-loop amplitude control (the excitation force amplitude or the response amplitude, respectively) corresponding to the fundamental harmonic.

To be able to start the stepped-sine testing (force or displacement controlled), LMS Test Lab. requires a preliminary system identification to estimate the system FRF, which can be determined from a broadband random test or preliminary sine sweep testing. Furthermore, during the actual stepped sine testing, if the measured control channel has a value outside the upper or lower tolerance of the target amplitude, the controller updates the system FRF at the current frequency by dividing current control channel value with the source control channel value, which provides a real-time control.

A series of response-controlled stepped sine tests were conducted at frequencies around the first elastic mode of the T-beam which can be modelled as a SDOF system. A frequency resolution of 0.125 Hz was used. During each response-controlled test, the displacement amplitude of the driving point was kept constant in an indirect way. The accelerometer was used as the control sensor, and a 'constant displacement amplitude' value was input to LMS Test Lab, from which the corresponding acceleration profile was calculated and followed by LMS Test Lab during stepped sine tests. Receptances of the T-beam measured at 8 different constant displacement amplitude levels, ranging from 0.50 mm to 2.25 mm, are shown in Fig. 2. It is observed that as the vibration level increases, both the nonlinear stiffness and nonlinear damping of the structure increase. As the nonlinear effects become negligible at low vibration levels in the T-beam, the appropriate boundary value in solving Eq. (21) is $\upsilon(0,\omega)=0$.

As in [27], typical fast-Fourier-transforms (FFTs) of time data samples collected during response-controlled and force-controlled stepped-sine tests of the T-beam around resonance region are illustrated in Fig. 3. As can be seen from the figure, in both cases, the fundamental harmonic is considerably dominant over the higher harmonic term, which indicates that the single harmonic assumption is valid for the T-beam application.

Substituting receptances given in Fig. 2 into Eq. (21) yields partial derivative of the describing surface of nonlinearity with respect to the displacement amplitude as shown in Fig. 4. As already mentioned, the partial derivative value between two consecutive displacement amplitude levels is taken to be constant, indicating that $\upsilon(|X|,\omega)$ is assumed to be C^0 continuous. Then, Eq. (21) is solved numerically, which yields the describing surface of nonlinearity as shown in Fig. 5. As it may not be

Fig. 1. T-beam experimental setup.

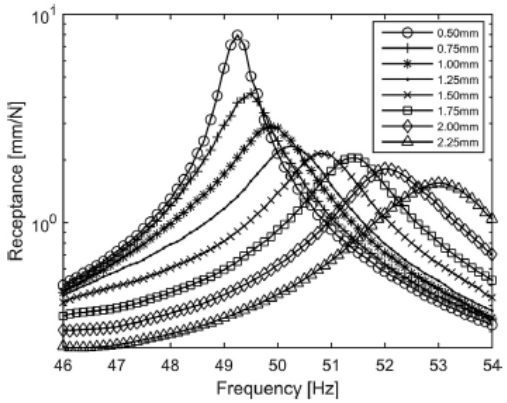

Fig. 2. Receptances of the T-beam measured by response-controlled stepped sine tests at various constant displacement amplitudes.

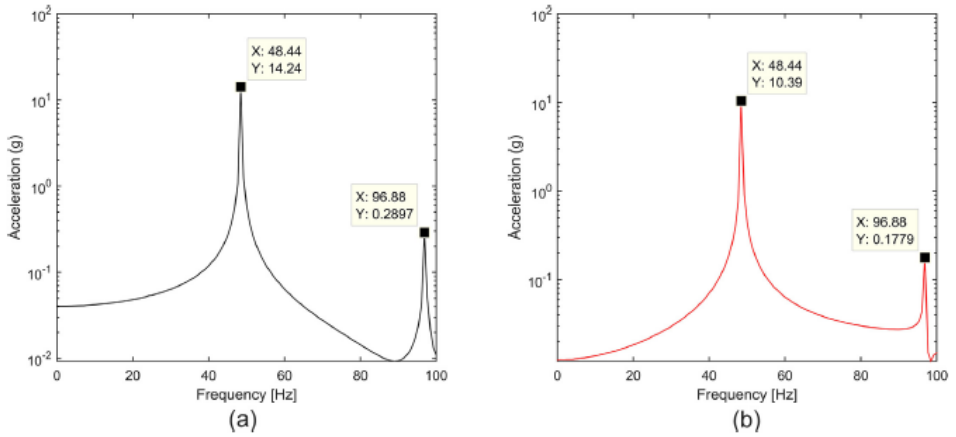

Fig. 3. Typical FFTs of time data samples collected during stepped-sine testing of the T-beam: (a) response-controlled test (1.50 mm amplitude level) (b) force-controlled test (1.0 N amplitude level).

always easy to fit a mathematical function to such surfaces, it is preferred to make a nonparametric identification, and use the surface obtained as a look-up table. However, if required, it is always possible to fit a curve to the surface obtained whenever it is smooth.

As can be seen from the above discussion, the receptances measured at several different 'constant displacement amplitude' levels (see Fig. 2) are the only necessary input required for the nonlinear system identification by using the DSM. These receptances are determined through response-controlled stepped sine tests, which can be achieved with the closed-loop amplitude control corresponding to the fundamental harmonic throughout the frequency sweep. The controller is initially fed with a transfer function between drive voltage and control channel estimated from a preliminary system identification (by using broad band random or sine sweep testing), which is updated real time during the test in order to keep the control channel value within the tolerance limits of the reference profile.

In Fig. 5, cubic stiffness effect and increasing nonlinear damping effect can be clearly seen from the real and imaginary parts of the describing surface. It is interesting to note that although the frequency dependence of nonlinear stiffness is negligible, there is considerable frequency dependence in nonlinear damping, especially at higher vibration levels, which can be

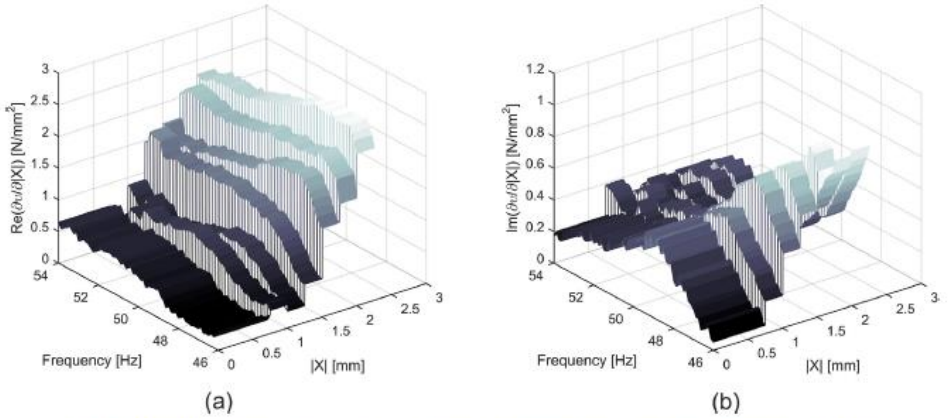

Fig. 4. Real (left) and imaginary (right) parts of the partial derivative of the describing surface of the nonlinearity for the T-beam.

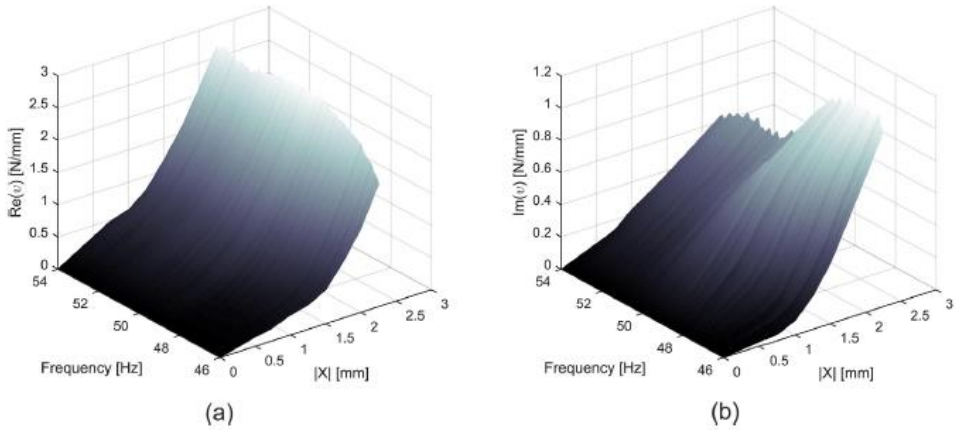

Fig. 5. Real (left) and imaginary (right) parts of the describing surface of nonlinearity for the T-beam.

seen from the imaginary part given on the right. This observation could not be made in the classical DFM or alternatively in the RFS method.

Once the describing surface of nonlinearity is determined, the FRF of the underlying linear system can be estimated by using Eq. (22). The result is shown in Fig. 6.

In order to compare the performance of the DSM with the classical DFM [34], the describing function of the nonlinearity is also calculated by using the latter approach. The describing function of nonlinearity is determined by using the receptances measured employing force-controlled stepped sine tests, results of which are shown in Fig. 7. The real and imaginary parts of the describing function values calculated at different displacement levels by using the DFM are shown in Fig. 8. Here, due to the cubic stiffness behavior of the T-beam, a second order polynomial fits the real part of the describing function best. For the imaginary part, which represents nonlinear damping term, the best fit is obtained by using a polynomial of order 5.

The primary aim of the DSM (or the DFM) is to use the describing surface (or describing function) in predicting the nonlinear response of the system to prescribed harmonic forcing. To validate the DSM and to compare its performance with that of the DFM, the point FRFs of the system at the T-junction are calculated by employing the DSM and the DFM for three dif-

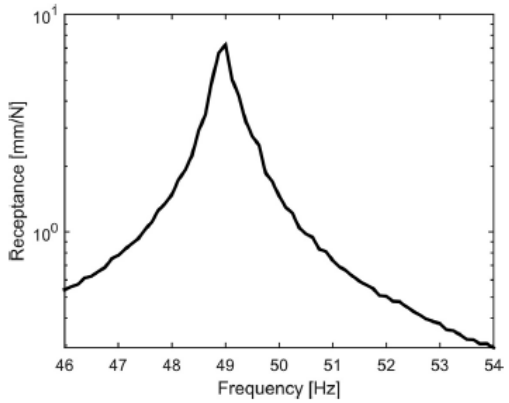

Fig. 6. Receptance of the underlying linear system of the T-beam estimated by using the DSM.

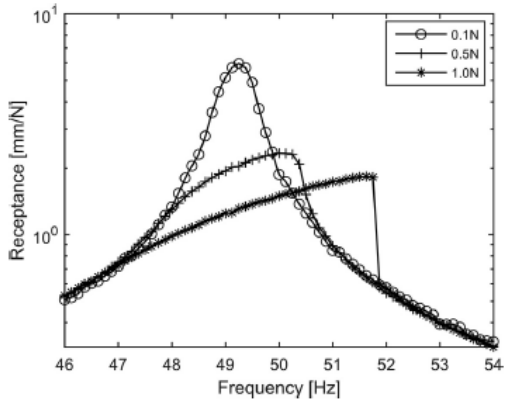

Fig. 7. Receptances of the T-beam measured by force-controlled stepped sine tests at various constant force amplitudes.

ferent forcing levels (0.1, 0.5 and 1.0 N), and the results are compared with the experimentally measured ones. The results are shown in Fig. 9. It is observed that the simulation results of the DSM match perfectly with the real experimental data, which is not the case for the DFM simulation results.

It is important to note that response-controlled test strategy adopted by the DSM has several important advantages over the force-controlled stepped-sine tests which is used in the DFM and in many other state-of-the art identification techniques. In case of a receptance measured by force-control there are at most two frequency points (before and after resonance) corresponding to a specific displacement amplitude at a given mode, which may not be sufficient for an accurate estimate of the describing function of a nonlinearity and which is definitely not sufficient for a full assessment of frequency dependence of nonlinearity. However, these limitations of the force-control approach are eliminated by the response-controlled test which collects as many data as the frequency points at a constant displacement amplitude level. Moreover, contrary to the common preconception, in testing nonlinear structures it is more difficult to keep a constant force profile within tolerance than a constant response profile. Any closed-loop stepped sine test starts with a linear system identification which determines transfer function of the nonlinear structure approximately. During a force-controlled test, switching from one frequency point to another results a drastic change in response amplitude especially around resonance which means considerable deviation from approximate transfer function due to nonlinear effects, and consequently it requires many corrective iterations by the controller to keep the force within tolerance. However, in case of the response-controlled tests, since

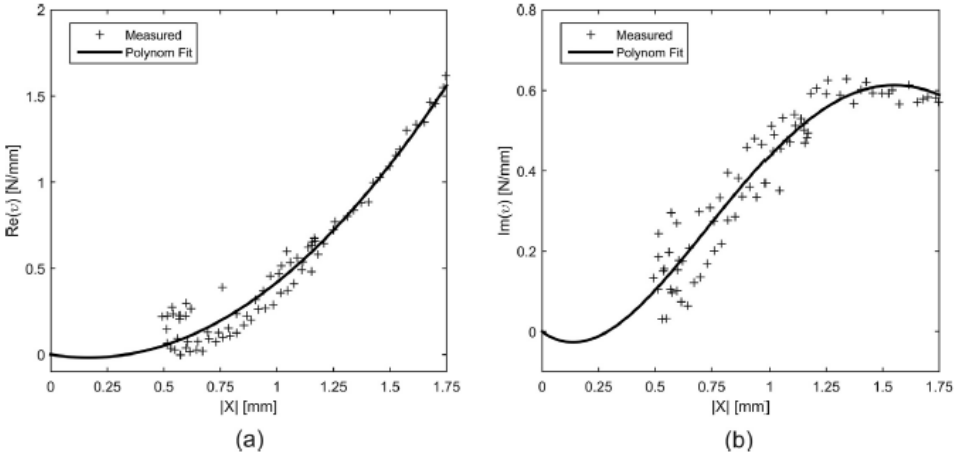

Fig. 8. Real (left) and imaginary (right) parts of the describing function of nonlinearity of the T-beam.

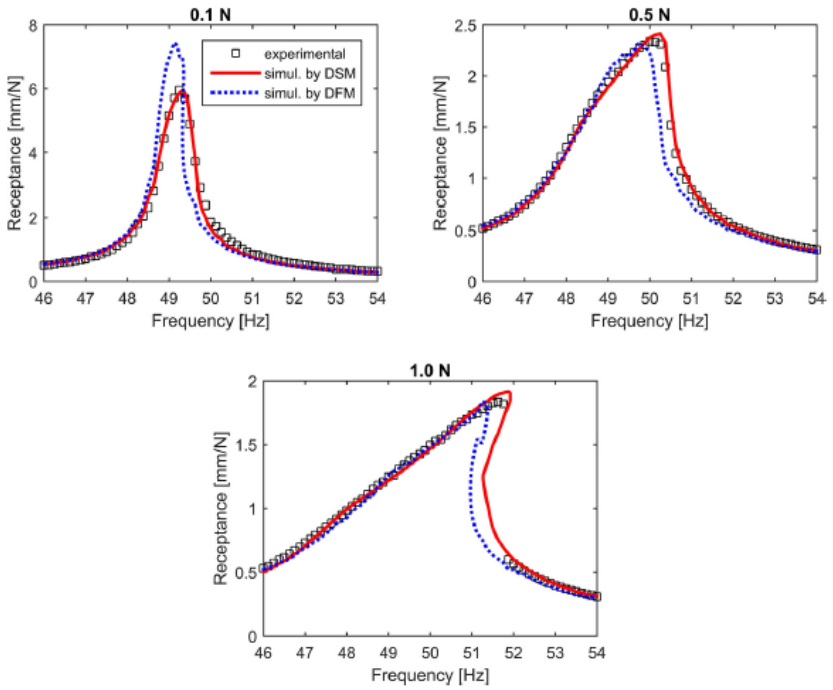

Fig. 9. Comparison of the simulation results obtained by the DSM and the DFM with the experimental data of the T-beam obtained from force-controlled stepped-sine testing.

the response amplitude (which affects the nonlinear stiffness and damping the most) is kept constant, the deviation from the approximate transfer function is minimized, which results in very fast and smooth stepped sine testing compared to force-control approach.

Last but not least, the response-controlled test strategy makes it possible to determine the *unstable branch* of a nonlinear receptance experimentally, whereas jump occurs in the force-controlled stepped sine testing. The first step in determining the unstable branch is to construct the harmonic force surface (HFS) by collecting the harmonic force spectra measured at various constant displacement amplitudes together, employing linear interpolation as shown in Fig. 10. The contour plot obtained by cutting the HFS with a constant force plane gives the harmonic response spectrum corresponding to that force level as shown in Fig. 11. The receptance plot obtained from the HFS at the constant force level of F = 1 N is compared with the receptance curve measured during force-controlled test and also with the one obtained by the DSM simulation in Fig. 12. As can be seen from Fig. 12, while the receptances measured by using classical force-controlled stepped-sine test exhibits jump at two frequencies, the receptance curve obtained by the HFS (i.e. by using response-controlled test results) captures the unstable branch, which can also be calculated employing the DSM simulation by using Newton's Method with arc-length continuation. As can be seen from the figure, the unstable branch predicted by the DSM matches perfectly with the one obtained by using response-controlled test results.

Actually, the response-controlled test follows a different path than the force-controlled test on the HFS which enables the former to capture points on the unstable branch. In case of the force-controlled test, capturing the unstable branch requires decreasing the excitation frequency during sweep up just after the resonance peak and vice versa, which is not an available option in commercial software. In this work, the HFS technique is used to experimentally validate the unstable branch calculated by the DSM method. HFS method is presented in a recent work of the authors [23], where the differences with respect to the methods such as PLL [22] in obtaining unstable branches of FRFs are also discussed in detail. In [22], it is shown that PLL control technique is also capable of tracing the unstable branch of nonlinear FRFs. Determination of the unstable branch by using HFS technique is somewhat different from the PLL algorithm which traces points on the unstable branch of a *constant-force* FRF consecutively. In the HFS method, points on the unstable branch are visited at different times during response-controlled stepped-sine tests carried out at different vibration amplitude levels. These points are then collected together on the HFS by combining harmonic excitation force spectra measured at different vibration amplitude levels. Frequency response of the system corresponding to a constant excitation forcing is then obtained by extracting isocurves of constant-amplitude forcing from the HFS. An interested reader may refer to [23] for a more detailed explanation of the HFS method.

3.2. Dummy mass on elastomeric vibration isolators

The second experimental setup used to validate the DSM consists of a dummy mass on elastomeric vibration isolators as shown in Fig. 13. The test rig consists of 4 identical AM-002-7 series LORD elastomeric vibration isolators connected to a round dummy mass of 6.4 kg. Vibration isolators are connected symmetrically with respect to the centerline of the dummy mass, so that the structure can be modeled as a SDOF system.

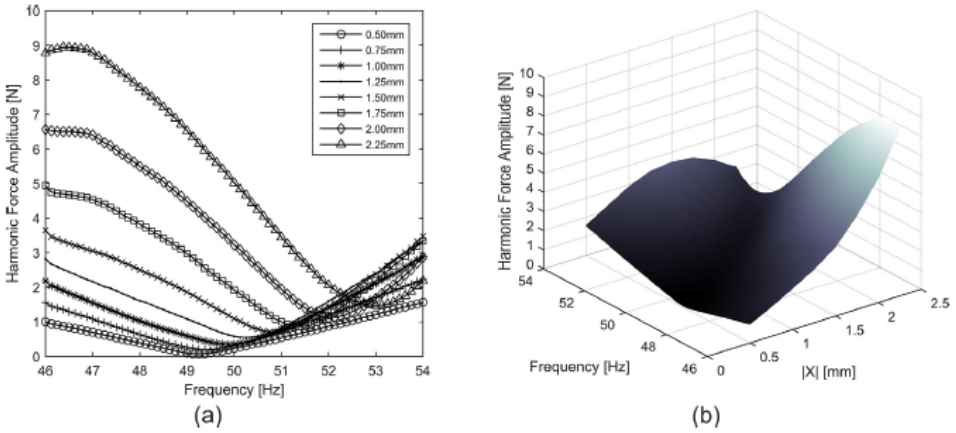

Fig. 10. HFS of the T-beam, obtained by response-controlled stepped sine test. Left: harmonic force spectra measured during the response-controlled stepped sine tests. Right: HFS constructed by collecting harmonic force spectra by using linear interpolation.

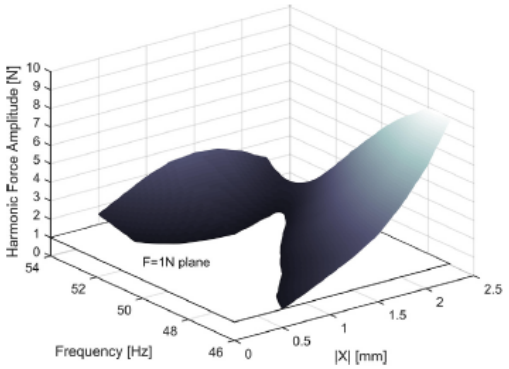

Fig. 11. HFS cut of the T-beam with constant harmonic force plane F = 1 N.

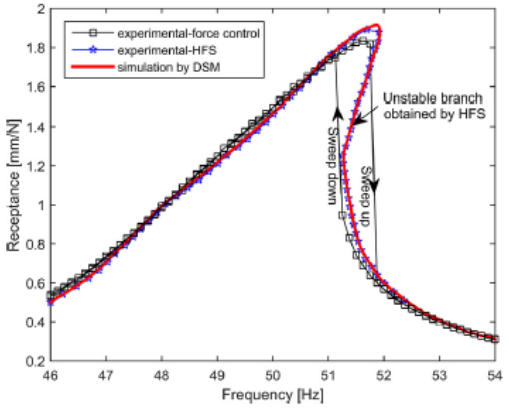

Fig. 12. Comparison of the receptances measured by the HFS of the T-beam at F = 1 N with the DSM simulation results and the receptances measured by using force-controlled stepped-sine testing.

In this study, the system was excited with a B&K shaker attached to the centerline of the dummy mass via a push-rod with a Dytran 1022 V force transducer as shown in Fig. 13. The vibration response was measured by using a Dytran 3225M23 miniature accelerometer attached to the top of the mass.

A series of response-controlled stepped sine tests were conducted at frequencies around the first elastic mode of the system. Receptances of the system measured at 8 different constant displacement amplitude levels, ranging from 0.01 mm to 0.08 mm, are shown in Fig. 14. A frequency resolution of 0.125 Hz was used. Fig. 15 illustrates typical FFTs of time data samples collected during response-controlled and force-controlled stepped-sine tests of the system. As in the previous experiment, the fundamental harmonic is observed to be considerably dominant over the higher harmonic term, which shows that the single harmonic assumption is valid for this application as well.

In case of vibration isolators, nonlinear effects diminish at high vibration levels. In this study, the relative describing surface is determined by taking the receptance measured at the highest vibration level, i.e. 0.080 mm, as the reference value, as shown in Fig. 16.

In Fig. 16 it is observed that the nonlinear damping has considerable dependence on frequency as in the case of T-beam. On the other hand, the frequency dependence of stiffness nonlinearity is, once again, negligible.

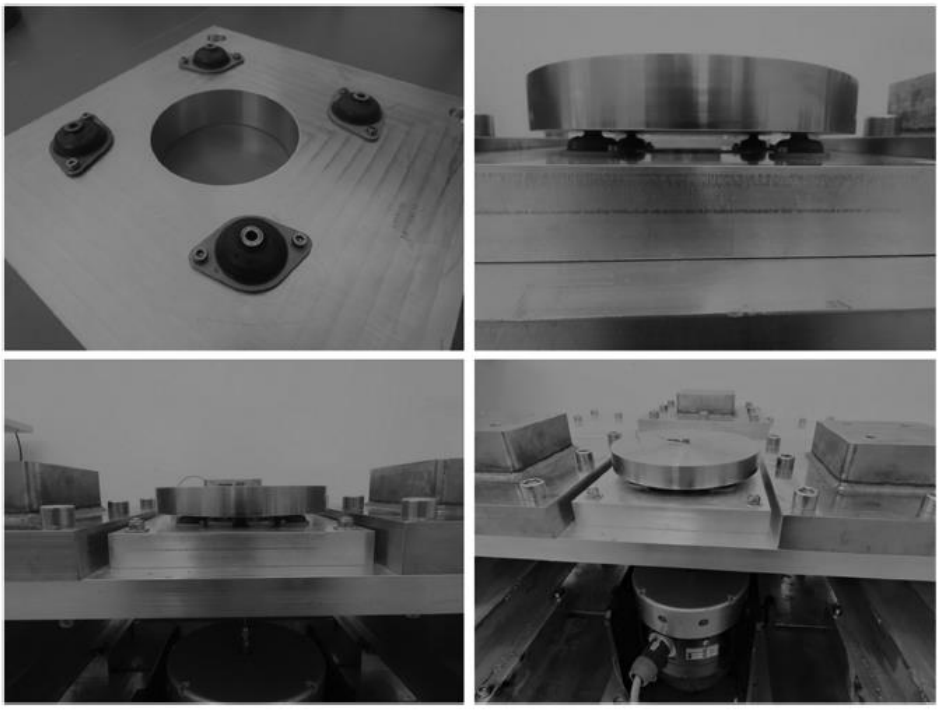

Fig. 13. Experimental setup of the dummy mass on elastomeric vibration isolators.

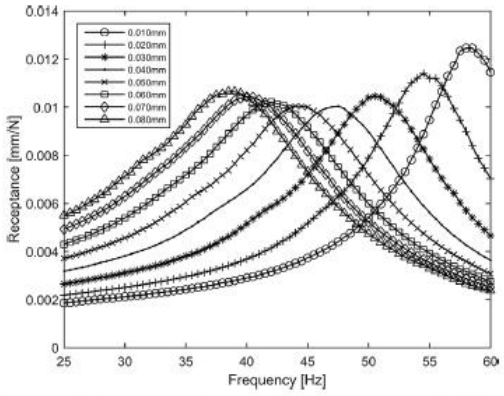

Fig. 14. Receptances of the dummy mass on elastomeric vibration isolators measured by response-controlled stepped sine tests at various constant displacement amplitudes.

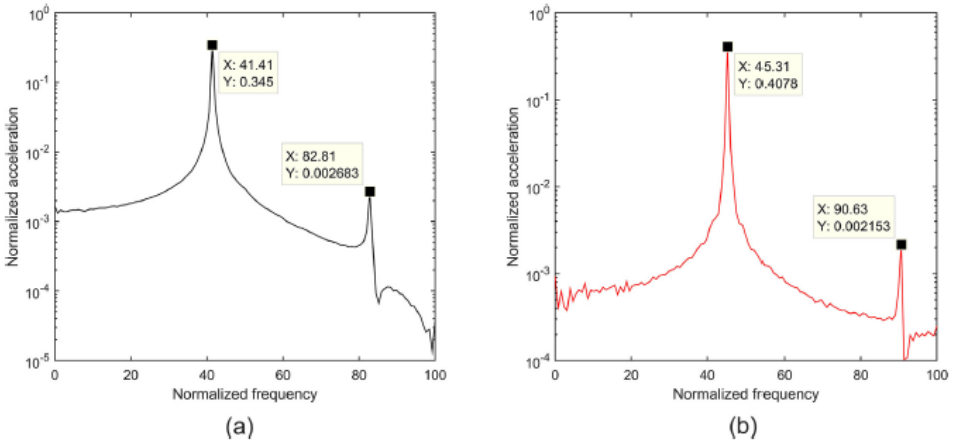

Fig. 15. Typical FFTs of time data samples collected during stepped-sine testing of the dummy mass on elastomeric vibration isolators: (a) response-controlled test (0.05 mm amplitude level) (b) force-controlled test (5.0 N amplitude level).

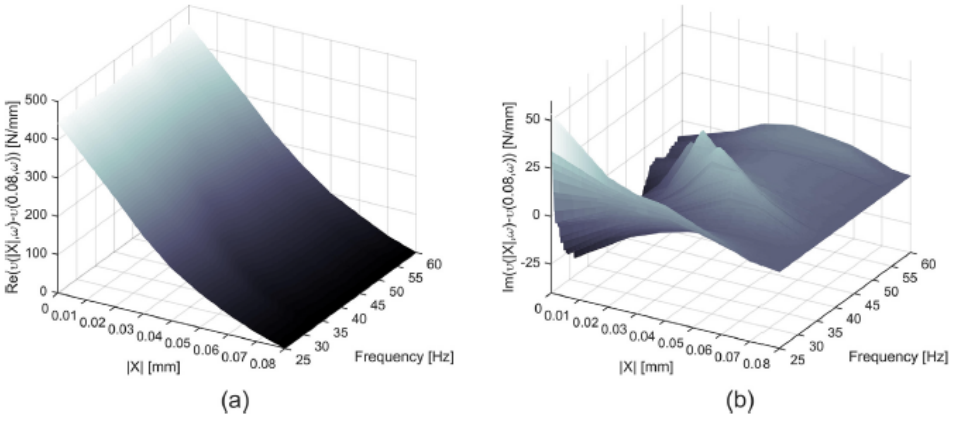

Fig. 16. Real (left) and imaginary (right) parts of the relative describing surface of the nonlinearity of the elastomeric vibration isolators.

To validate the DSM and to compare its performance with the DFM once again, results of force-controlled test simulations realized by both the DSM and the DFM were compared with experimental data. Receptances measured at 3 different constant force levels are shown in Fig. 17. By using theses receptances and taking the nonlinear receptance at the highest displacement amplitude level as reference, i.e. 0.080 mm, the relative describing function of the nonlinearity was determined as shown in Fig. 18. Comparisons of the force-controlled test simulations realized by the DSM and DFM, with experimental data are shown in Fig. 19. Simulations are achieved by using Eq. (24), which is an alternative form of Eq. (23). In this equation the relative describing surface (or describing function) is used. It is observed once again that the simulation results of the DSM match perfectly with the real experimental data and does a better job than the DFM, especially around resonance.

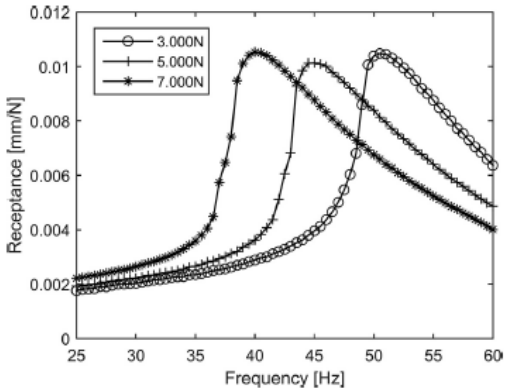

Fig. 17. Receptance curves of the dummy mass on elastomeric vibration isolators measured by force-controlled stepped sine tests at three different force amplitudes.

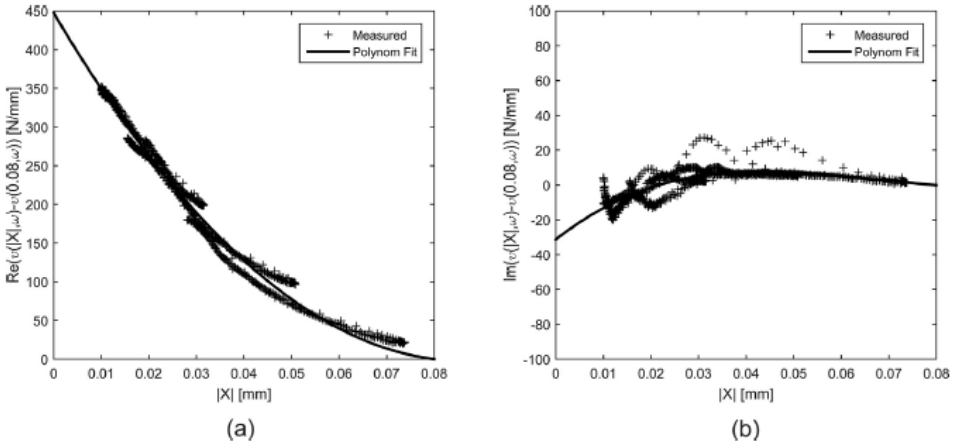

Fig. 18. Real (left) and imaginary (right) parts of the relative describing function of nonlinearity of the dummy mass on elastomeric vibration isolators.

3.3. Control fin actuation mechanism

Control fins used in guided missiles play a crucial role in aeroelastic behavior of the missile structure [36,37]. The actuation mechanism of a control fin consists of many moving parts which include multiple nonlinearities such as backlash and friction. Consequently, the first torsional mode may exhibit strongly nonlinear behavior with jump phenomenon, which is a challenging nonlinear system identification problem. In this experimental study, the DSM is successfully applied to identify nonlinearity in a real control fin actuation mechanism.

The sketch of the experimental setup is shown in Fig. 20. The casing of the mechanism is rigidly fixed to the ground. In total, 10 Dytran 3225M23 miniature accelerometers were attached on the surface of the control fin and they were enumerated from 1 to 10, as shown in Fig. 20. The system was excited, in z direction, with a B&K shaker attached to the control fin at point 1, via a push-rod with a Dytran 1022 V force transducer.

Preliminary tests indicated that the system can be treated as a rotational SDOF system. Accordingly, a series of response-controlled stepped-sine tests was conducted at frequencies around the first torsional mode of the system for a total of 15 different displacement amplitudes of the driving point, labelled D1–D15. For clarity, receptances of the system measured

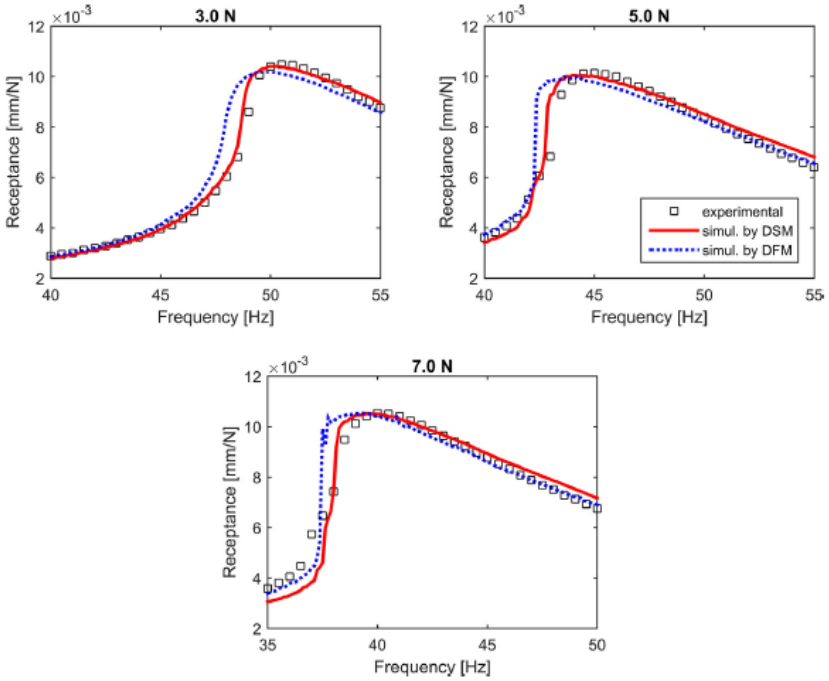

Fig. 19. Comparison of the simulation results obtained by the DSM and the DFM, with the experimental data of the dummy mass on elastomeric vibration isolators obtained from force-controlled stepped-sine testing.

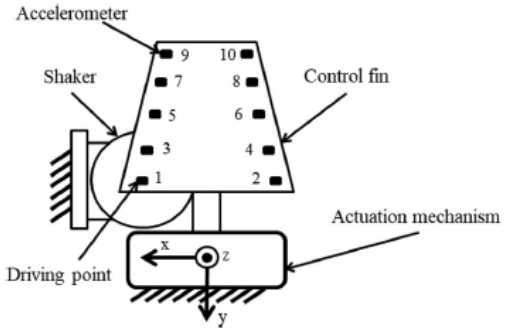

Fig. 20. Sketch of the experimental setup for the control fin actuation mechanism.

at only 10 different constant displacement amplitude levels are shown in Fig. 21. A frequency resolution of 0.125 Hz was used. Fig. 22 illustrates typical FFTs of time data samples collected during force-controlled and response-controlled stepped-sine tests of the control fin actuation mechanism. As in the previous two case studies, the fundamental harmonic is dominant over the higher harmonic term, which shows that the single harmonic assumption applies for this system as well.

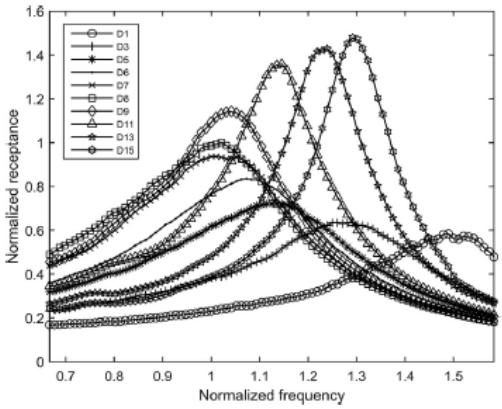

Fig. 21. Receptances of the control fin actuation mechanism measured by response-controlled stepped sine tests at various constant displacement amplitudes.

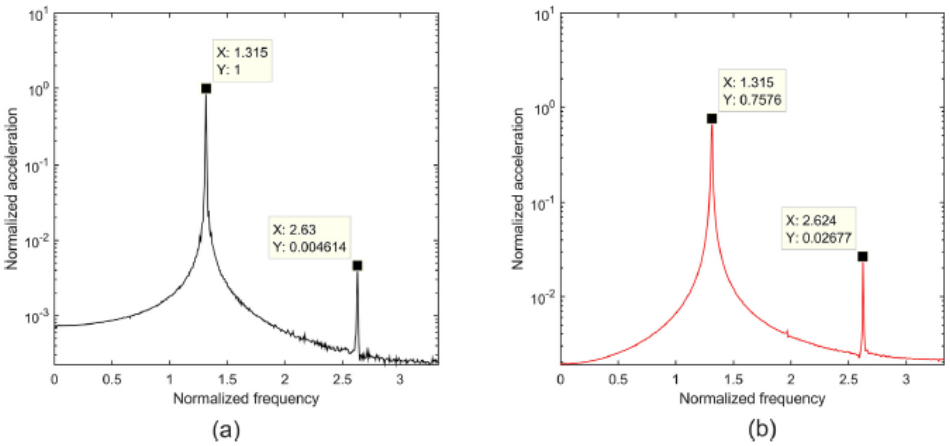

Fig. 22. Typical FFTs of time data samples collected during stepped-sine testing of the control fin actuation mechanism: (a) response-controlled test (D15 amplitude level) (b) force-controlled test (F4 amplitude level).

Fig. 21 gives important clues about the complex nonlinear behavior of the control fin actuation mechanism. The first important observation is that as the vibration level increases, the resonance frequency of the torsional mode decreases up to a certain value, after which it increases again. It is highly probable that the initial softening effect is an indication of stick to slip transition and the following hardening effect is related with the backlash. The second important observation is the gradual increase of the resonance peak as the vibration level increases, which is typically encountered in the case of friction nonlinearity.

In this study, the real and imaginary parts of the relative describing surface were calculated by taking receptances measured at displacement amplitude levels of D8 and D15 as reference values, respectively, as shown in Fig. 23. Cross sections of the real and imaginary parts of relative describing surface at different frequencies are also given in Fig. 24.

In Figs. 23 and 24, it is clearly seen that the real part of the relative describing surface, which represents the nonlinear stiffness, first decreases up to D8 amplitude level where it is equal to zero and then increases again. On the other hand, the imaginary part of the relative describing surface, which represents the nonlinear damping, decreases as the vibration

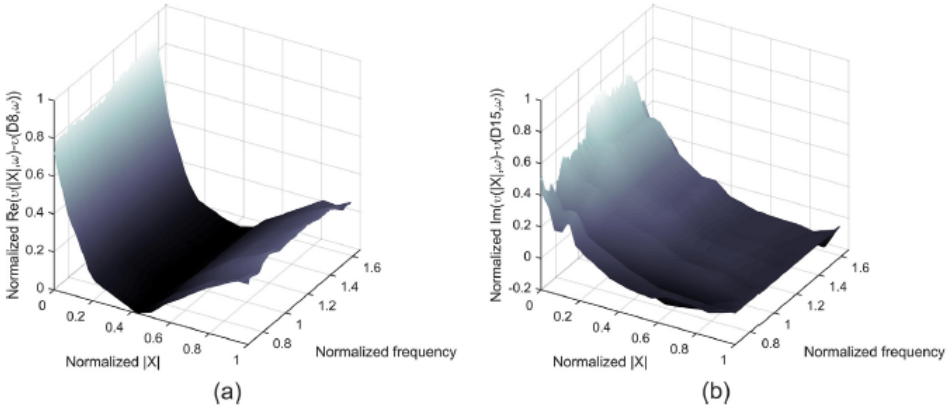

Fig. 23. Real (left) and imaginary (right) parts of the relative describing surface of nonlinearity for the control fin actuation mechanism.

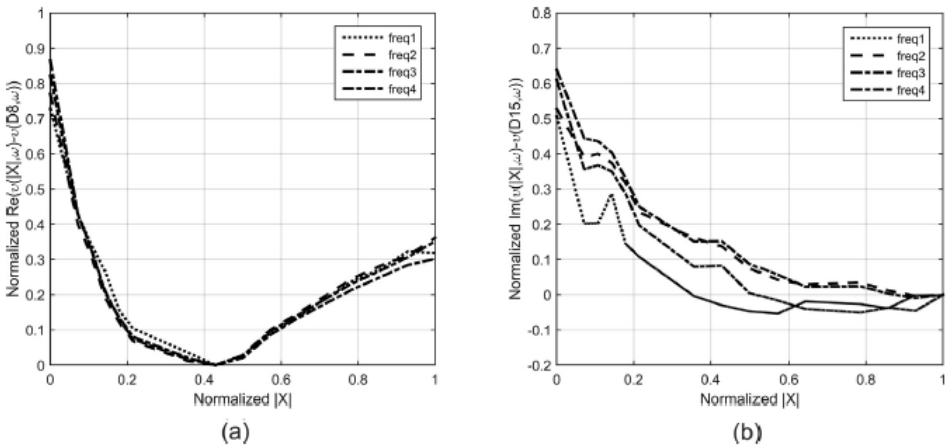

Fig. 24. Cross-section views of the real (left) and imaginary (right) parts of the relative describing surface of nonlinearity of the control fin actuation mechanism at different frequencies.

level increases. The most important observation that can be made in Fig. 24 is that although the nonlinear damping depends on frequency considerably, frequency dependence of the nonlinear stiffness is negligible.

In order to validate the DSM, a series of force-controlled stepped sine tests were conducted and receptances at 4 different constant force levels were measured. The results are shown in Fig. 25, from which the strong nonlinear behavior of the control fin actuation mechanism can easily be observed.

Comparison of the experimentally measured receptances with the simulation results obtained using the DSM is given in Fig. 26. In that figure, there are two experimental data; FRFs directly measured during force-controlled stepped sine tests and FRFs obtained by the HFS (i.e. by using response-controlled test results). Although the system is nonlinear, when it is excited at the same force amplitude and excitation frequency at different times, the response amplitude must ideally be the same. Consequently, it is expected that FRFs measured during force-controlled tests and FRFs obtained by the HFS match perfectly, which is not the case as shown in Fig. 26. As shown in Fig. 22, the effect of higher harmonics is not significant and consequently, it cannot be the main reason of the discrepancy between two types of tests. The main reason of the discrepancy is the repeatability issue. During the tests, it was observed that repeating exactly the same (response-controlled or force-

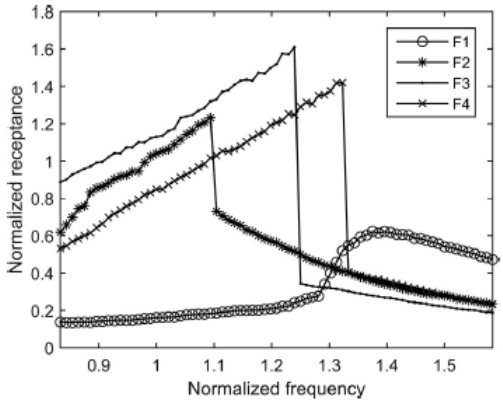

Fig. 25. Receptances of the control fin actuation mechanisms measured by force-controlled stepped sine tests at various constant force amplitudes.

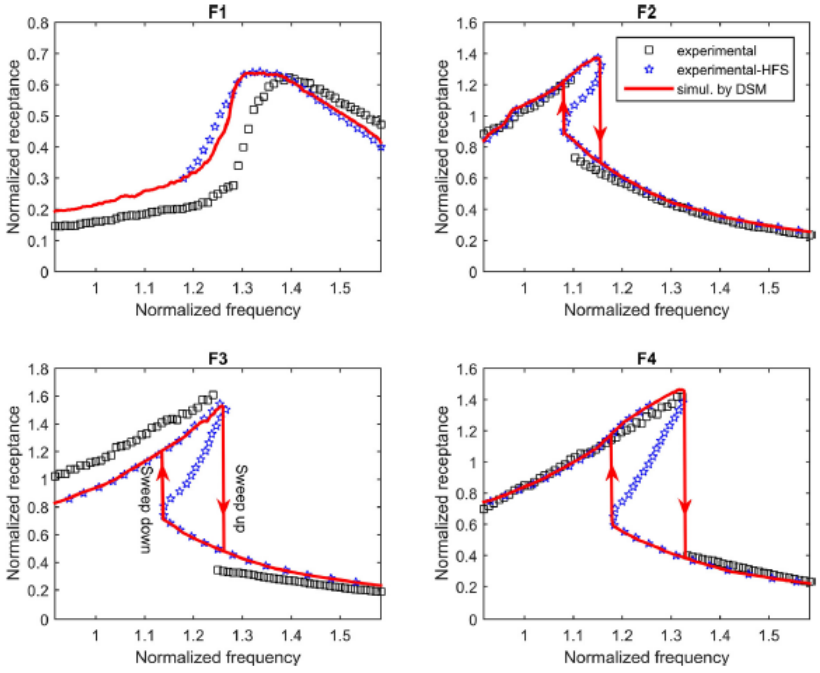

Fig. 26. Comparison of the simulation results obtained by the DSM of the control fin actuation mechanism with the experimental data obtained from force-controlled stepped-sine testing and HFS (response-controlled stepped-sine testing).

controlled) test does not give exactly the same frequency response curve. It is highly probable that the relatively poor repeatability is closely related with gaps and friction surfaces between moving parts, as well as with the sensitivity of the lubricants to the environmental conditions such as temperature. At the end of a specific test, reconfiguration of gaps and

contact surfaces in a random manner due to excessive vibration, and significant temperature change due to heat generation may result in some changes in the nonlinear dynamics of the system. From Fig. 26 it is observed that the simulation results of the DSM match perfectly with the real experimental data obtained by HFS, since HFS was obtained from the same experimental data used to compute the DSM. Although there is still a discrepancy between the DSM results and the FRFs measured with force-controlled stepped sine tests, which is assumed to be due to relatively poor repeatability of dynamic characteristic of the system as explained above, the match between these two FRF curves can be regarded sufficiently satisfactory. A final note about Fig. 26 is that the unstable branches of the nonlinear receptances are again successfully measured by the HFS approach as explained in Section 3.1; however, contrary to the T-beam example, the unstable branches in this control fin application could not be predicted by using the DSM since Newton's Method with arc-length continuation did not converge due to nonsmooth characteristic of the nonparametric describing surface. It is also interesting to note that the DFM simulations do not give satisfactory results due to the difficulty in identifying the complex nonlinear behavior of the control fin actuation mechanism parametrically; therefore they are not shown in Fig. 26.

4. Conclusions

This paper presents a new method for nonparametric identification of nonlinearity in structures. The method proposed is a frequency domain method and is suitable for the identification of complex nonlinearities which may not only be the function of response level, but also the function of the excitation frequency. The method is named as Describing Surface Method (DSM), and it can be applied to structures with local nonlinearity affecting the boundary conditions. Multiple nonlinearities may coexist at the same location and a priori knowledge of the type of the nonlinearity is not necessary. The method essentially determines the describing surface of the nonlinearity which can be used to calculate steady state harmonic response of the structure to any harmonic forcing by following an iterative solution procedure. The method is based on response-controlled stepped-sine testing from which the so-called describing surface of the nonlinearity is obtained. It is a surface giving the nonlinear stiffness and damping as a nonparametric function of both harmonic displacement amplitude and frequency. The method uses the concept of Nonlinearity Matrix proposed by Tanrıkulu et al. [28], which was employed in the parametric identification of nonlinearities for the first time by Özer et al. [33]. The method is applicable to systems where modes are not closely spaced, and sub- and super-harmonics are negligible compared to the fundamental harmonic.

The method has several important advantages over the state-of-the art nonlinear identification techniques:

- The method relies on the FRFs measured by response-controlled stepped sine testing which can be obtained by using a standard data acquisition hardware and software (e.g. LMS SCADAS Mobile and LMS Test Lab.). Consequently, it can easily be used by practicing engineers.
- The identification is nonparametric; therefore it does not require a priori knowledge of the type of the nonlinearity, and it does not require any curve fitting. All nonlinearities coexisting at the same location are represented by a resultant nonparametric describing surface, real and imaginary parts of which represent equivalent nonlinear stiffness and damping of the structure, respectively.
- The method is advantageous when the nonlinearity is a function of frequency as well. For such systems many of the state-of-the-art techniques cannot be used.
- Unstable branches of frequency response curves can be estimated by using Newton's Method and arc-length continuation algorithm together with the identified describing surface. Furthermore, these unstable branches can be experimentally validated by using the HFS concept.
- Using the DSM in a part-to-whole context may help to realize nonlinear analysis of complex engineering structures with many nonlinear elements at different locations and may pave the way for a powerful method covering a wide range of engineering structures. In a part-to-whole strategy, individual nonlinear elements of a large engineering structure may be isolated and identified separately by using the DSM. Then, the describing surfaces of nonlinearity of all identified elements may be integrated to the finite element model of the whole structure for nonlinear vibration analysis with harmonic balance method.

In this work, DSM is successfully applied to three real structures. Firstly, to a cantilever beam with cubic stiffness at its tip point, then to a dummy mass on elastomeric vibration isolators, and finally to a real control fin actuation mechanism which exhibits strong and complex nonlinear behavior with jump phenomenon due to friction and backlash. In these studies, interesting observations are made and important conclusions are obtained:

- The most important observation made in all 3 case studies is the significant frequency dependence of the nonlinear damping. However, frequency dependence of nonlinear stiffness was very limited.
- All nonlinearities in the systems are identified as describing surfaces and the method is validated by comparing force-controlled stepped sine tests results with the FRFs theoretically calculated by using DSM. In all cases a good agreement is obtained between the DSM results and the real experimental data.
- It is also observed that the DSM performs much better compared to the DFM.

- The successful application of the DSM to a real control fin actuation mechanism of a missile demonstrated that the proposed method is a powerful technique that can be applied to real engineering structures which exhibit complex and strong local nonlinearity in the boundary conditions.
- Although, in this work, it is shown that the DSM is capable of capturing unstable branches of frequency response curves in case of relatively simple nonlinear structures such as the T-beam, it may lead to a convergence problem in some complex nonlinear systems such as the control fin actuation mechanism due to its non-smooth characteristic. In such cases, it can be a good practice to apply parametric curve fitting techniques, whenever possible, to the experimentally extracted non-parametric describing surface in order to overcome the convergence issue. Alternatively, instead of the first order finite difference formula used to calculate describing surface in Eq. (21), higher order finite difference formulae may be employed, which might increase the accuracy of the DSM and thus solve the convergence problem. Higher order formulae may provide more accurate estimate of the describing surface, especially at the extreme ends, compared to the linear interpolation/extrapolation scheme used in this work.

CRediT authorship contribution statement

Taylan Karaağaçh: Conceptualization, Methodology, Software, Validation, Formal analysis, Investigation, Writing - original draft. **H. Nevzat Özgüven:** Supervision, Conceptualization, Writing - review & editing.

Declaration of Competing Interest

The authors declare that they have no known competing financial interests or personal relationships that could have appeared to influence the work reported in this paper.

Acknowledgment

The provision of TÜBİTAK-SAGE for modal testing and analysis capabilities is gratefully acknowledged.

References

[1] G. Kerschen, K. Worden, A.F. Vakakis, J.C. Golinval, Past, present and future of nonlinear system identification in structural dynamics, Mech. Syst. Signal Process. 20 (2006) 505–592, https://doi.org/10.1016/j.ymssp.2005.04.008.
[2] J.P. Noël, G. Kerschen, Nonlinear system identification in structural dynamics: 10 more years of progress, Mech. Syst. Signal Process. 83 (2017) 2–35, https://doi.org/10.1016/j.ymssp.2016.07.020.
[3] S.F. Masri, T.K. Caughey, A nonparametric identification technique for nonlinear dynamic problems, J. Appl. Mech. 46 (1979) 433–447.
[4] E.F. Crawley, A.C. Aubert, Identification of nonlinear structural elements by force-state mapping, AIAA J. 24 (1986) 155–162.
[5] S.F. Masri, H. Sassi, T.K. Caughey, A nonparametric identification of nearly arbitrary nonlinear systems, J. Appl. Mech. 49 (1982) 619–628.
[6] E.F. Crawley, K.J. O'Donnell, Identification of nonlinear system parameters in joints using the force state mapping technique, AIAA Paper 86–1013 (1986) 659–667.
[7] Belingardi G., Campanile P., Improvement of the shock absorber dynamic simulation by the restoring force mapping method, in: Proceedings of the International Seminar in Modal Analysis and Structural Dynamics, Leuven, 1990.
[8] C. Surace, K. Worden, G.R. Tomlinson, On the nonlinear characteristics of automotive shock absorbers, J. Auto Eng. 206 (1992) 3–16.
[9] Duym S., Stiens R., Reybrouck K., Fast parametric and nonparametric identification of shock absorbers, in: Proceedings of the international Seminar on Modal Analysis (ISMA), Leuven 1996.
[10] P. Saad, A. Al Majid, F. Throuverez, R. Dufour, Equivalent rheological and restoring force models for predicting the harmonic response of elastomer specimens, J. Sound Vib. 290 (2006) 619–639.
[11] E. Bonisoli, A. Vigliani, Identification techniques applied to a passive elasto-magnetic suspension, Mech. Syst. Signal Process. 21 (2007) 1479–1488.
[12] D. Rizos, G. Feltrin, M. Motavalli, Structural identification of a prototype pre-stressable leaf-spring based adaptive tuned mass damper: nonlinear characterization and classification, Mech. Syst. Signal Process. 25 (2011) 205–221.
[13] D. Goege, J.M. Sinapius, Experiences with dynamic load simulation by means of modal forces in the presence of structural nonlinearities, Aerosp. Sci. Technol. 10 (2006) 411–419.
[14] M.S. Allen, H. Sumali, D.S. Epp, Piecewise-linear restoring force surfaces for semi-nonparametric identification of nonlinear systems, Nonlinear Dyn. 54 (2008) 123–155.
[15] J.P. Noël, L. Renson, G. Kerschen, Complex dynamics of a nonlinear aerospace structure: experimental identification and modal interactions, J. Sound Vib. 333 (2014) 2588–2607.
[16] K. Worden, D. Hickey, M. Haroon, D.E. Adams, Nonlinear system identification of automotive dampers: a time and frequency-domain analysis, Mech. Syst. Signal Process. 23 (2009) 104–126.
[17] H. Ahmadian, H. Jalali, F. Pourahmadian, Nonlinear model identification of a frictional contact support, Mech. Syst. Signal Process. 24 (2010) 2844–2854.
[18] Dossogne T., Noël J.P., Grappasonni C., Kerschen G., Peeters B., Debille J., Vaes M., Schoukens J., Nonlinear ground vibration identification of an F-16 aircraft - Part II: Understanding nonlinear behavior in aerospace structures using sine-sweep testing, in: Proceedings of the 16th International Forum on Aeroelasticity and Structural Dynamics (IFASD), Saint Petersburg, Russia, 2015.
[19] D. Göge, U. Füllekrug, M. Sinapius, M. Link, L. Gaul, Advanced test strategy for identification and characterization of nonlinearities of aerospace structures, AIAA J. 43 (5) (2005) 974–986.
[20] M.F. Platten, J.R. Wright, J.E. Cooper, G. Dimitriadis, Identification of a nonlinear wing structure using an extended modal model, AIAA J. Aircraft 46 (5) (2009) 1614–1626.
[21] U. Fuellekrug, D. Goege, Identification of weak nonlinearities within complex aerospace structures, Aerosp. Sci. Technol. 23 (2012) 53–62.
[22] S. Peter, M. Scheel, M. Krack, R.I. Leine, Synthesis of nonlinear frequency responses with experimentally extracted nonlinear modes, Mech. Syst. Signal Process. 101 (2018) 498–515, https://doi.org/10.1016/j.ymssp.2017.09.014.
[23] Karaağaçlı T., Özgüven H.N., A new approach for experimental modal analysis of nonlinear systems by using response-controlled stepped-sine testing, Mech. Syst. Signal Process. (submitted).

[24] L. Renson, A. Gonzalez-Buelga, D.A.W. Barton, S.A. Neild, Robust identification of backbone curves using control-based continuation, J. Sound Vibrat. 367 (2016) 145–158.
[25] L. Renson, A.D. Shaw, D.A.W. Barton, S.A. Neild, Application of control-based continuation to a nonlinear structure with harmonically coupled modes, Mech. Syst. Signal Process. 120 (2019) 449–464.
[26] G. Zhang, C. Zang, M.I. Friswell, Identification of weak nonlinearities in MDOF systems based on reconstructed constant response tests, Arch. Appl. Mech. (2019) 1–22, https://doi.org/10.1007/s00419-019-01559-4.
[27] X. Wang, G.T. Zheng, Equivalent dynamic stiffness mapping technique for identifying nonlinear structural elements from frequency response functions, Mech. Syst. Signal Process. 68–69 (2016) 394–415.
[28] Ö. Tannkulu, B. Kuran, H.N. Özgüven, M. İmregün, Forced harmonic response analysis of nonlinear structures using describing functions, AIAA J. 31 (7) (1993) 1313–1320.
[29] E. Budak, H.N. Özgüven, A dynamic analysis method for the harmonically exited nonlinear structures, Struct. Vib. And Acous., ASME 18 (3) (1989) 23–29.
[30] E. Budak, H.N. Özgüven, Iterative receptance method for determining harmonic response of structures with symmetrical nonlinearities, Mech. Syst. Signal Process. 7 (1) (1993) 75–87.
[31] A. Gelb, W.E. Van der Velde, Multiple-input Describing Functions and Nonlinear System Design, McGraw-Hill, New York, 1968.
[32] M.B. Özer, H.N. Özgüven, A new method for localization and identification of nonlinearities in structures, in: Proceedings of the ESDA 2002: Sixth Biennial Conference on Engineering Systems Design and Analysis, ASME, İstanbul, Turkey, 2002.
[33] M.B. Özer, H.N. Özgüven, T.J. Royston, Identification of structural nonlinearities using describing functions and the Sherman-Morrison method, Mech. Syst. Signal Process. 23 (2009) 30–44.
[34] M. Aykan, H.N. Özgüven, Parametric identification of nonlinearity in structural systems using describing function inversion, Mech. Syst. Signal Process. 40 (2013) 356–376.
[35] Ö. Arslan, M. Aykan, H.N. Özgüven, Parametric identification of structural nonlinearities from measured frequency response data, Mech. Syst. Signal Process. 25 (2011) 1112–1125.
[36] W.H. Shin, I. Lee, Nonlinear aeroelastic analysis for a control fin with actuator, J. Aircraft 44 (2) (2007) 597–605.
[37] Y. Ning, W. Nan, Z. Xin, L. Wei, Nonlinear flutter wind tunnel test and numerical analysis of folding fins with freeplay nonlinearities, Chin. J. Aeronaut. 29 (1) (2016) 144–159.

vibration

MDPI

Article

Experimental Identification of Backbone Curves of Strongly Nonlinear Systems by Using Response-Controlled Stepped-Sine Testing (RCT)

Taylan Karaağaçlı [1,2] and H. Nevzat Özgüven [2,*]

[1] The Scientific and Technological Research Council of Turkey, Defense Industries Research and Development Institute, TÜBİTAK-SAGE, P.K. 16, Mamak, Ankara 06261, Turkey; taylan.karaagacli@tubitak.gov.tr
[2] Mechanical Engineering Department, Middle East Technical University, Ankara 06800, Turkey
* Correspondence: ozguven@metu.edu.tr

Received: 27 July 2020; Accepted: 2 September 2020; Published: 7 September 2020

Abstract: In stepped-sine testing of strongly nonlinear structures with the classical force-control strategy, corrective force perturbations of a standard controller used to capture the reference signal in the proximity of turning points of frequency response curves may often lead to a premature jump before reaching the actual resonance peak. Accordingly, a classical force-control approach is not suitable to identify backbone curves of strongly nonlinear structures. This paper shows that currently available commercial modal test equipment can accurately identify backbone curves of strongly nonlinear structures by using Response-Controlled stepped-sine Testing (RCT) and the Harmonic Force Surface (HFS) concept, both recently proposed by the authors. These methods can be applied to systems where there are many nonlinearities at several different (and even unknown) locations. However, these techniques are not applicable to systems where internal resonances occur. In RCT, the displacement amplitude of the driving point, rather than the amplitude of the applied force, is kept constant during the stepped-sine testing. Spectra of the harmonic excitation force measured at several different displacement amplitude levels are used to build up a smooth HFS. Isocurves of constant amplitude forcing on the HFS lead to constant-force frequency response curves with accurately measured turning points and unstable branches (if there are any), which makes it possible to identify backbone curves of strongly nonlinear structures experimentally. The validation of the proposed approach is demonstrated with numerical and experimental case studies. A five degree-of-freedom (DOF) lumped system with five cubic stiffness elements, which create strong conservative nonlinearity, is used in the numerical example. Experimental case studies consist of a cantilever beam and a control fin actuation mechanism of a real missile structure. The cantilever beam is supported at its free-end by two metal strips constrained at both ends to create strong stiffening nonlinearity. The control fin actuation mechanism exhibits very complex and strong nonlinearity due to backlash and friction.

Keywords: nonlinear experimental modal analysis; backbone curve; nonlinear system identification; response controlled stepped sine test; harmonic force surface; unstable branch

1. Introduction

By virtue of various advanced techniques developed in the field of linear experimental modal analysis over the last 40 years, the modal survey of aerospace structures, specifically named as ground vibration testing, was established as an industry standard in the new millennium. On the other hand, the increasing competition in the industry to achieve higher performance in aircraft, missiles, and satellites inevitably increased the frequency of occurrence of non-negligible structural

nonlinearities in aerospace applications (e.g., References [1–3]), which led to a shift of emphasis towards the development of nonlinear system identification techniques in structural dynamics [4,5].

The modal testing of linear structures is accomplished either by using broad band random testing or by using classical force-controlled stepped-sine testing, where the force amplitude is kept constant. Unfortunately, direct implementation of these conventional modal testing techniques to structures that exhibit strong nonlinearity does not give satisfactory results. Random testing, which requires taking many averages to increase the coherence of measured frequency response functions (FRFs), is not suitable for nonlinear system identification because averages do their best to hide nonlinearity, as stated in Reference [6]. On the other hand, constant-force sine testing often fails to capture turning points and unstable branches of nonlinear frequency response curves. The constant-force test algorithm available in commercial equipment can measure only the stable branches of the nonlinear frequency responses, which requires running multiple sine tests in opposite sweep directions. In the case of standard constant-force sine testing, the controller unavoidably jumps from one stable branch to another, as shown in Figure 1a. Moreover, in some cases, a premature jump may occur, as shown in Figure 1b. Early methods [7,8] attempted to identify amplitude-dependent nonlinear modal parameters by developing curve fitting procedures applicable to measured constant-force FRFs based on the single nonlinear mode theory [9]. However, their applications remained limited to simple benchmark structures due to the computational burden in the case of complex structures and due to the missing frequency response data caused by the jump phenomenon.

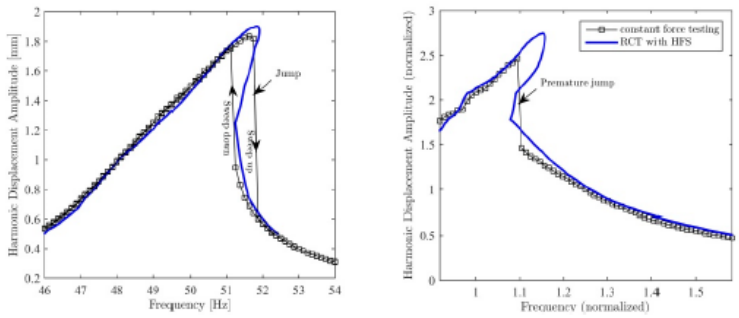

Figure 1. Frequency response curves measured in constant-force stepped-sine testing compared to the ones measured by RCT with HFS: (**a**) jump phenomenon; (**b**) premature jump.

Contrary to the early attempts based on phase separation testing mentioned above, most of the techniques proposed in succeeding years were inspired by the phased resonance testing approach. Two interesting approaches based on normal mode force appropriation and on the application of the restoring force surface in modal space were proposed in References [10,11]. Experimental application of the nonlinear resonant decay method proposed in Reference [11] to identify the backbone curve of a single degree-of-freedom oscillator was demonstrated in Reference [12]. Alternatively, the phase lag quadrature criterion was implemented in nonlinear structures in order to isolate a single nonlinear normal mode (NNM) in Reference [13]. In this approach, the NNM appropriation is succeeded by time-frequency analysis of the free-decay response data to determine the frequency-energy dependence of the nonlinear mode of interest. However, an important drawback of this method is the manual tuning of the phase lag between response and excitation, which introduces difficulty in the experiment and requires longer experimentation time. The two recently proposed experimental continuation techniques [14,15] eliminated this drawback by automating the tuning of the phase lag throughout the complete backbone curve. The phase-locked-loop (PLL) control algorithm [14] is capable of tracing

out backbone curves and also captures the unstable branches of frequency response curves, if there are any. Similarly, the control-based continuation (CBC) approach [15] relies on phase-quadrature condition to trace out the backbone curve. In CBC, unstable branches of constant-force frequency response curves are obtained by processing S-curves measured at several fixed frequencies by varying the response level. However, these two state-of-the-art techniques cannot utilize commercial modal testing equipment, and although the determination of NNMs and corresponding modal frequencies is straightforward, identification of nonlinear modal damping is still a considerable problem.

As an alternative to these experimental continuation techniques, a systematic approach called Response-Controlled stepped-sine Testing (RCT) was proposed quite recently by the authors of this paper, which constitutes the main step of a new experimental modal analysis method for nonlinear systems [16]. The method can be applied to systems where there are many nonlinearities at several different (and even unknown) locations. However, this technique is not applicable to systems with internal resonances. In other words, the effects of sub- and super-harmonics are assumed to be negligible. In the RCT strategy, the displacement amplitude of the test point (equivalently, the modal amplitude) is kept constant during stepped-sine testing, which leads to quasi-linear FRFs even in the case of strongly nonlinear structures. Accordingly, conventional linear modal analysis techniques can be employed to identify nonlinear modal parameters as functions of modal amplitude. Unmeasured constant-force FRFs, which may even have unstable branches, can then be synthesized by using these modal parameters based on the single nonlinear mode theory [9]. Alternatively, constant-force FRFs can be directly extracted from the measured Harmonic Force Surface (HFS), an innovative concept proposed in Reference [16]. The key feature of the RCT approach is that it simply uses standard equipment, which makes it very attractive especially for industrial applications. Furthermore, the identification of nonlinear modal damping and of mass normalized NNMs is straightforward via applying standard linear modal analysis methods to measured quasi-linear FRFs. The proposed HFS concept was employed as a validation tool for the constant-force FRFs synthesized by using experimentally extracted nonlinear modal parameters. The current paper is a complementary work specifically dedicated to demonstrating the performance of HFS in experimentally identifying backbone curves of strongly nonlinear systems by emphasizing its ability to accurately identify turning points of frequency response curves with unstable branches. It is important to note that in the context of this paper, *strong nonlinearity* terminology is used to refer to nonlinear systems with overhanging unstable branches in the frequency response curves which result in jump phenomenon in standard constant-force stepped-sine testing. This does not necessarily imply a significant effect of higher harmonics, as illustrated in the numerical and experimental case studies.

The paper is organized as follows. In Section 2, the RCT approach and HFS concept are briefly summarized. Section 3 is dedicated to the analytical illustration of the HFS method on a 5 DOF system with strong conservative nonlinearity. In Section 4, HFS is successfully applied to identify the backbone curves of a benchmark beam with cubic stiffness and of a control fin actuation mechanism of a real missile structure, both of which exhibit strong nonlinearity causing jump phenomenon during classical constant-force stepped-sine testing. Finally, conclusions are given in Section 5.

2. Experimental Modal Analysis with RCT and HFS

Experimental modal analysis using response-controlled stepped-sine testing was recently proposed by the authors of this paper in Reference [16], where the theoretical background is explained in full detail. Here, only a brief summary of the experimental methodology will be given, with the emphasis being on important key features.

The flow chart of the proposed experimental methodology by using RCT is shown in Figure 2. The right column of the flow chart consists of the experimental extraction of nonlinear modal parameters and of the synthesis of constant-force FRFs by using these parameters. The identification of nonlinear modal parameters is straightforward via applying standard linear modal analysis techniques to quasi-linear constant-response FRFs measured by RCT. Quasi-linearization of FRFs by keeping the

displacement of the test point (equivalently, the modal amplitude) constant is based on the Nonlinearity Matrix concept [17] and the single nonlinear mode theory [9] as explained in Reference [16]. The key formulation of the quasi-linearization concept is as follows:

$$\overline{\alpha}_{jk}(\omega, q_r) = \frac{\overline{A}_{jkr}(q_r)}{\overline{\omega}_r^2(q_r) - \omega^2 + i2\overline{\xi}_r(q_r)\omega\overline{\omega}_r(q_r)} \tag{1}$$

where $\overline{\alpha}_{jk}$ is the near-resonant receptance at point j for a given excitation at point k and ω is the excitation frequency. $\overline{A}_{jkr}(q_r)$, $\overline{\omega}_r(q_r)$ and $\overline{\xi}_r(q_r)$ are the modal constant, natural frequency, and modal damping ratio of the rth mode, respectively. These nonlinear modal parameters are functions of a single parameter; the modal amplitude q_r.

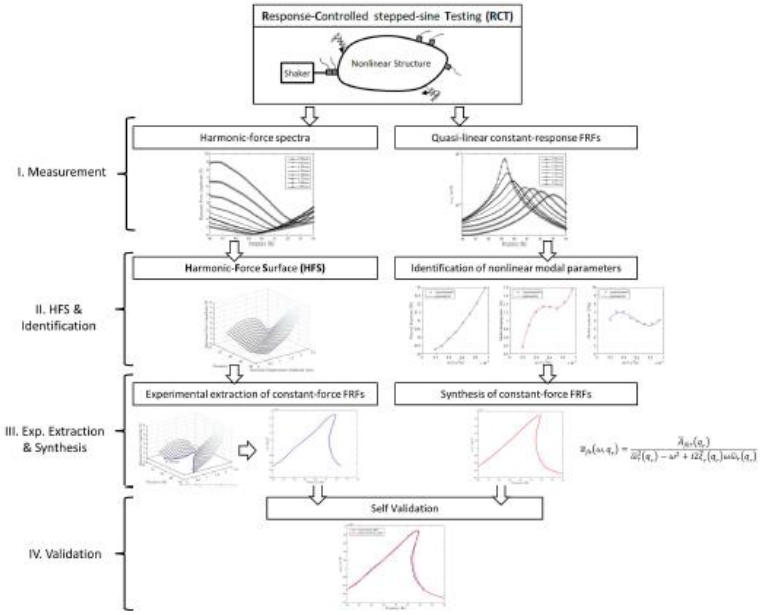

Figure 2. Experimental modal analysis with RCT and HFS.

It was shown that if the modal amplitude is kept constant during stepped-sine testing, the measured constant-response FRFs turn out to be quasi-linear. In the case of a single input sine testing, the modal amplitude can be kept constant by just keeping the displacement amplitude of the driving point constant. In References [13,16,18], it was shown that nonlinear modes can be isolated with acceptable accuracy by just using single-point single harmonic excitation under the condition that no internal resonance occurs. On the other hand, the RCT method can theoretically be employed by using multi-input sine testing, which requires careful tuning of the amplitude ratios of excitation signals to keep the modal amplitude at a constant level [16].

Due to the popularity of accelerometer in modal testing, it was preferably used as the control sensor in the applications of the proposed method. Accordingly, a constant displacement amplitude condition at the driving point over the frequency range of interest was achieved in an indirect way

by feeding the closed-loop controller with an appropriate user-defined acceleration profile, which is supported by standard modal testing software (e.g., LMS Test Lab).

The HFS concept was successfully used for the validation of constant-force FRFs synthesized from identified nonlinear modal parameters [16]. The focus of the current paper is demonstrating the performance of HFS in experimentally extracting the backbone curves of strongly nonlinear systems by emphasizing its ability to accurately extract the turning points of frequency response curves with unstable branches.

As shown in the left column of the flow chart given in Figure 2, HFS is constructed from the harmonic force spectra of the driving point measured at different constant displacement amplitude levels by using linear interpolation. A frequency response curve corresponding to a specific constant force level, which will include any existing unstable branch, is simply determined by picking up points of the HFS corresponding to that force level.

In this paper, it is proposed to determine the backbone curves of nonlinear systems by picking up resonance peaks of nonlinear frequency response curves extracted from HFS at various different constant force levels. Picking up resonance peaks requires smoothly identified turning points, which is an important issue for the state-of-the-art experimental continuation techniques. The successful application of HFS in extracting backbone curves of strongly nonlinear systems is demonstrated with numerical and experimental case studies in the subsequent sections.

3. Numerical Validation

In this section, the application of the HFS approach to identify the backbone curves is demonstrated on a 5 DOF nonlinear lumped system with 5 cubic stiffness elements. The parameters of the system (Figure 3) are as follows: $m = 1$ kg, $k = 10,000$ N/m, $c = 5$ Ns/m, $k^* = 10^7$ N/m^3. Here, k^* denotes the coefficient of cubic stiffness.

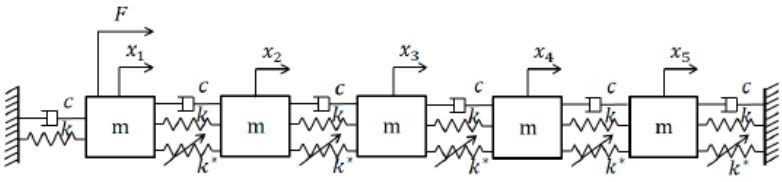

Figure 3. The 5 DOF system with cubic stiffness nonlinearity [16].

The backbone curves obtained from HFS are validated with the ones determined from constant-force simulation. Constant-force and RCT simulations used to extract backbone curves are conducted by using a multiple harmonics version of the *Describing Function Method* (DFM) details of which can be found in References [16,17,19].

3.1. Determination of Backbone Curves by Using Constant-Force Simulations

Frequency response curves of the 1st and 5th DOFs obtained from constant force simulations at force levels ranging from 10 N to 50 N and corresponding to the first mode are illustrated in Figure 4. In Reference [16], where the same simulated data is used to validate nonlinear modal parameters identified with RCT, it is shown that the effect of higher harmonics is negligible for the force and displacement levels of interest. However, stiffness nonlinearity is still strong in the sense that it leads to overhanging unstable branches, as shown in Figure 4. Although in a simulated experiment resonance peaks can accurately be determined with the help of an arc length continuation algorithm, in a real experiment this may not be possible due to a jump or, even worse, due to a premature jump, as explained in the Introduction section. In the next section, it is demonstrated that by just using RCT

and HFS concept, the inaccuracies due to the jump can be avoided, which makes it possible to identify the backbone curve more accurately with standard equipment.

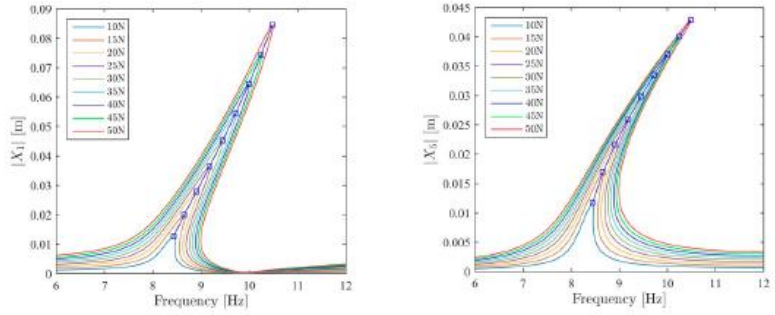

Figure 4. Determination of the backbone curves (blue square markers) of the 5 DOF system corresponding to the 1st and 5th DOFs by using constant-force stepped-sine simulations. (**a**) The backbone curve of the 1st DOF; (**b**) the backbone curve of the 5th DOF.

3.2. Determination of Backbone Curves by Using RCT with HFS

Harmonic excitation force spectra of the driving point (1st DOF) obtained from RCT simulations at several constant displacement amplitude levels ranging from 0.01 m to 0.1 m in the first mode are illustrated in Figure 5a. As explained in Section 2, the HFS corresponding to the 1st DOF is constructed by combining harmonic excitation force spectra and using linear interpolation, as shown in Figure 5b.

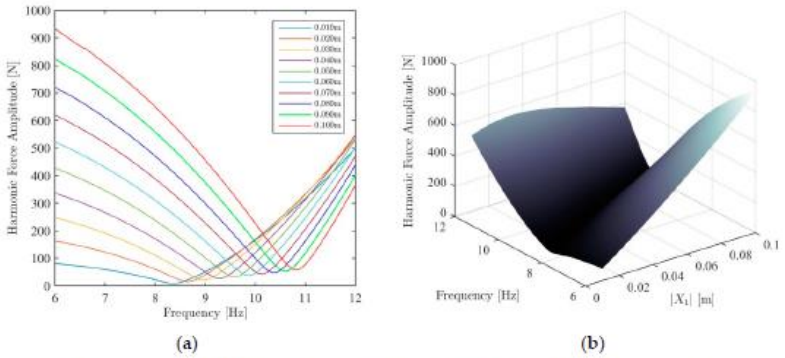

Figure 5. Construction of the HFS corresponding to the 1st DOF by combining harmonic force spectra with linear interpolation. (**a**) Harmonic excitation force spectra; (**b**) HFS of the 1st DOF [16].

By cutting the HFS with constant force planes ranging from 10 N to 50 N (with 5 N increments) as shown in Figure 6a, constant-force frequency response curves of the 1st DOF are successfully extracted with accurate resonance turning points and unstable branches as demonstrated in Figure 6b. Finally, the backbone curve of the 1st DOF is determined by combining resonance peaks of the extracted frequency response curves, as shown in the same figure.

In real experimental cases, the measurements of unstable branches together with smooth turning points shown in Figure 6b would not be possible with conventional constant-force testing due to

the jump (or even worse, premature jump) phenomenon, which eventually led the development of advanced experimental continuation techniques in the last decade to determine the backbone curves of structures exhibiting strong conservative nonlinearity. Alternatively, the RCT strategy combined with HFS concept reveals that standard equipment can still do a good job in the experimental extraction of unstable branches and backbone curves. In the RCT-HFS approach, instead of consecutively tracing out points on an unstable branch or a backbone curve, these points are measured at different times during stepped-sine tests carried out at different constant amplitude levels, and then merged into the HFS.

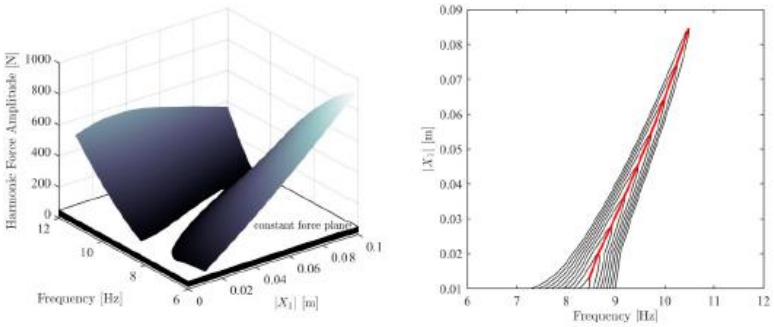

(**a**) (**b**)

Figure 6. (**a**) HFS of the 1st DOF cut with constant force planes; (**b**) extraction of constant-force frequency response curves (black—ranging from 10 N to 50 N with 5N increments) and identification of the backbone curve (red) of the 1st DOF from HFS.

It is important to note that HFS given in Figure 5b was constructed by considering the displacement amplitudes of the 1st DOF, i.e., $|X_1|$, as can be seen from the label of the displacement axis. So, this surface specifically belongs to the 1st DOF, and can only be used to obtain constant-force frequency response curves of the 1st DOF. In order to obtain frequency responses of another DOF, the HFS needs to be reconstructed by considering the displacement amplitudes of that specific DOF. As an example, the HFS corresponding to the 5th DOF is illustrated in Figure 7a. Once again, constant-force frequency response curves and the backbone curve corresponding to the 5th DOF are successfully determined, as shown in Figure 7b.

Finally, backbone curves determined from the HFS approach are compared with those obtained from constant-force simulations for the 1st and 5th DOFs, as shown in Figure 8. The excellent match indicates that HFS is a very promising concept for extracting backbone curves of strongly nonlinear systems directly from experimental measurements. It is interesting to note that, once backbone curves corresponding to several different measurement points are experimentally identified as illustrated in Figure 8, collecting the points on these backbone curves corresponding to the same resonance frequency (or equivalently energy level) into a vector gives the NNM of the structure at that energy level. This is an alternative way of obtaining the NNM of a nonlinear structure directly from experimental measurements, whereas in the earlier work of the authors [16] it is proposed to use experimental data to identify nonlinear modal constants and then to calculate NNM by using these modal constants.

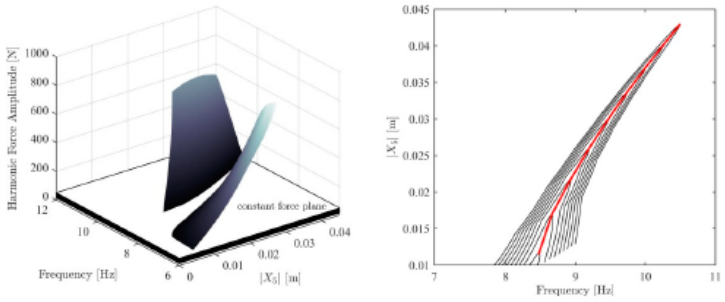

(**a**) (**b**)

Figure 7. (**a**) HFS of the 5th DOF cut with constant force planes; (**b**) extraction of the constant-force frequency response curves (black—ranging from 10 N to 50 N with 5 N increments) and the backbone curve (red) of the 5th DOF from HFS.

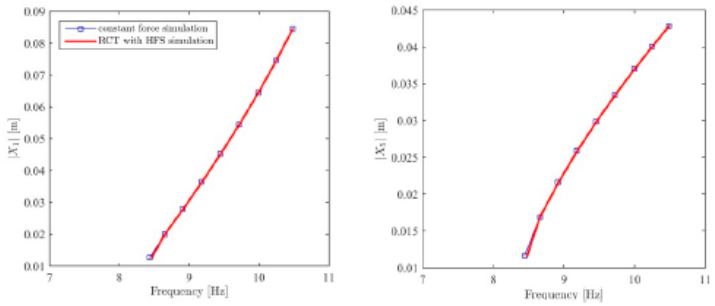

(**a**) (**b**)

Figure 8. Comparison of backbone curves obtained from RCT with HFS simulations with those obtained from constant force simulations: (**a**) the backbone curve of the 1st DOF; (**b**) the backbone curve of the 5th DOF.

4. Experimental Applications

4.1. T-Beam

The T-beam is a benchmark test setup which consists of a cantilever beam clamped at its free end by two metal strips, as shown in Figure 9. The structure exhibits geometric nonlinearity due to large deformations of the metal strips. Dimensions of the rig are given in Reference [20]. The focus of this study is the first nonlinear mode of the structure, where a strong cubic stiffness behavior is observed.

During experiments, the structure was excited with a B&K shaker at the T-junction. The excitation force was measured by using a Dytran 1022 V force transducer and vibration measurement was accomplished via a Dytran 3225M23 miniature accelerometer attached to the top of the T-junction. The frequency step was taken to be 0.125 Hz. All measurements and closed-loop controls were achieved using LMS modal test equipment (SCADAS Mobile and LMS Test Lab.).

As a first step in determining unstable branches and backbone curve, eight stepped-sine tests were conducted at constant displacement amplitude levels ranging from 0.50 mm to 2.25 mm by using the RCT approach. Even though the proposed approach requires more measured data compared to some other state-of-the-art techniques, the testing time is within reasonable limits thanks to the response

control strategy which renders the system more predictable due to quasi-linear behavior. In the case of this T-beam application, a single stepped-sine test conducted at a constant response level was 3 times faster than a single constant-force stepped-sine test.

Harmonic force spectra measured at each displacement amplitude level are shown in Figure 10a. Secondly, the HFS is built up by combining these force spectra and using linear interpolation as shown in Figure 10b. Nonlinear frequency response curves extracted by cutting the HFS with 0.5 N and 1.0 N constant force planes are validated by comparing them with constant-force test results, as shown in Figure 11. Obviously, the frequency response curve obtained from HFS incorporates the unstable branch at 1.0 N, which cannot be captured by constant-force testing. It is important to note that the negligible effect of higher harmonics around resonance for the force and displacement amplitude levels considered in this case study, which is the fundamental assumption of the proposed RCT-HFS technique, is experimentally confirmed in [21].

Figure 9. T-beam experimental setup.

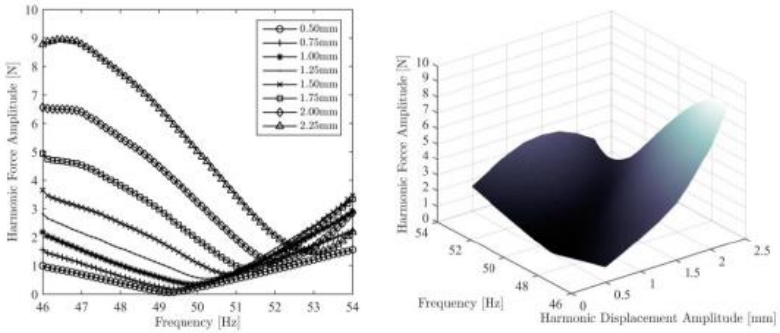

(a) (b)

Figure 10. (**a**) Harmonic force spectra of the T-beam measured by RCT; (**b**) HFS of the T-beam built up by combining harmonic force spectra with linear interpolation [16].

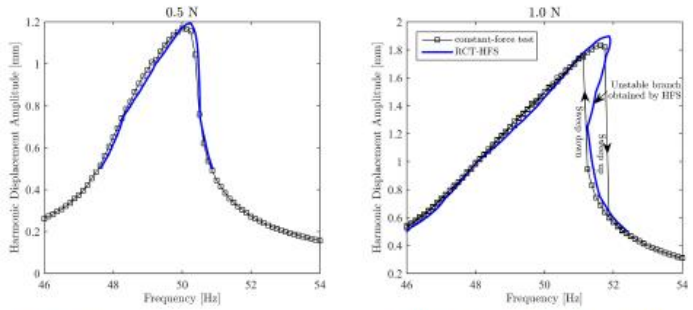

Figure 11. Validation of the frequency response curves of the T-beam extracted from HFS by using constant-force test results.

Nonlinear frequency response curves corresponding to various constant force levels ranging from 0.1 N to 1.4 N with 0.05 N increments were extracted by cutting the HFS with corresponding constant force planes, as shown in Figure 12. Finally, the backbone curve was determined by collecting resonance peaks of these frequency response curves, as shown in the same figure. It is important to note that, in this context, the resonance peak is defined as the maximum value of the imaginary part of the frequency response curve. Figure 12 clearly demonstrates that the HFS technique can successfully extract the turning points of overhanging frequency response curves, which cannot be achieved accurately by conventional constant-force testing due to the jump phenomenon and which is still a challenging issue for the state-of-the-art experimental continuation techniques.

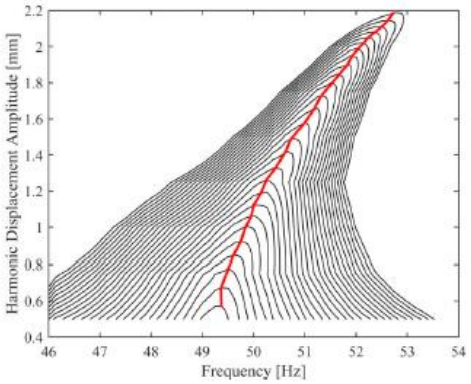

Figure 12. Constant-force frequency response curves (0.1 N–1.4 N) and backbone curve of the T-beam at the T-junction obtained by cutting the HFS with various constant force planes.

4.2. Control Fin Actuation Mechanism

Control fins of guided missiles, which play a key role in aeroelastic behavior of the missile system [22,23], may exhibit severe nonlinearity caused by backlash and friction between moving parts of the actuation mechanism. In some cases, the first torsional mode may exhibit strong nonlinearity with a jump in the frequency response, which makes it a challenging nonlinear system identification problem. In this experimental study, the HFS approach is successfully applied to identify the backbone curve of a real control fin actuation mechanism of a missile. The sketch of the test rig is shown in

Figure 13. The same experimental setup was also used in Reference [21] to validate the so-called Describing Surface Method recently proposed by the authors for nonparametric identification of structural nonlinearities in the frequency domain.

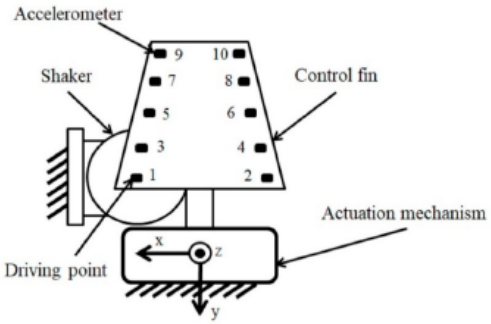

Figure 13. Sketch of the experimental setup for the real control fin actuation mechanism.

The casing of the mechanism is rigidly fixed to the ground. The response of the system was measured by using 10 accelerometers as shown in Figure 13. The system was excited, in the z-direction, with an electrodynamic shaker (B&K) at point 1. The excitation force at the driving point is measured with a Dytran 1022 V force transducer.

During the test campaign, RCT was repeated at 15 different displacement amplitude levels, which are labelled as D1, D2, . . . , D15, around the first torsional mode. The harmonic force spectra measured at only 10 different constant displacement amplitude levels are shown in Figure 14a for clarity. The HFS constructed by combining harmonic force spectra with linear interpolation is shown in Figure 14b. The frequency response curves obtained by cutting HFS with constant force planes F1, F2, and F3 are compared with constant force testing results in Figure 15a–c, respectively. Obviously, the frequency response curves measured during constant-force testing and those obtained by the HFS do not match perfectly. In Reference [21], it is experimentally confirmed that the effect of higher harmonics is not significant. Therefore, it is concluded that the contribution of higher harmonics cannot be the main reason for the discrepancy between two types of tests. The main reason seems to be the repeatability issue, which is very typical even in simple benchmark structures [24]. In the control fin problem, repeating the same test for a second time does not give exactly the same constant-force frequency response curve. This may be related to the reconfiguration of the gaps and contact surfaces due to vibration as well as a significant temperature change of lubricants due to heat generation.

Nonlinear frequency response curves corresponding to various constant force levels were extracted by cutting the HFS with corresponding constant force planes as shown in Figure 16. Finally, the backbone curve was determined by collecting resonance peaks of these frequency response curves, as shown in the same figure. This backbone curve indicates the softening–hardening nonlinear behavior of the control fin actuation mechanism, where the initial softening is probably related to the stick to slip transition and the hardening results from the backlash. This experimental case study shows that HFS can successfully determine backbone curves of real engineering structures which exhibit strong and complex nonlinear behavior, whereas the backbone curve that could be obtained from constant-force tests would be considerably inaccurate (Figure 15 for F2 indicates huge inaccuracy in resonance peak prediction due to premature jump). It is important to note that the backbone curve shown in Figure 16 was identified from a single data set, and consequently it does not reflect the variability of the repeatedly measured frequency response data which is discussed in the previous paragraph.

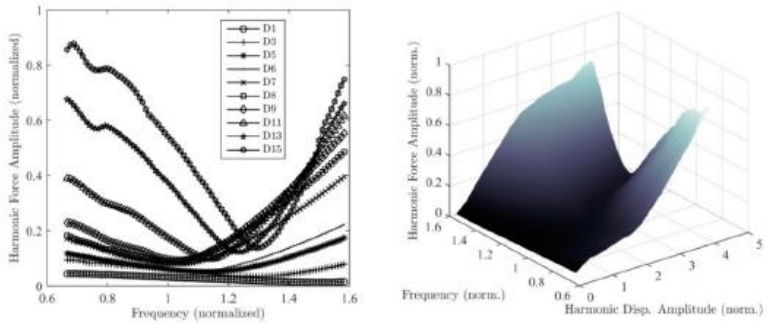

Figure 14. (**a**) Harmonic force spectra of the control fin actuation mechanism measured by RCT; (**b**) HFS of the control fin actuation mechanism at the driving point, constructed by combining harmonic force spectra.

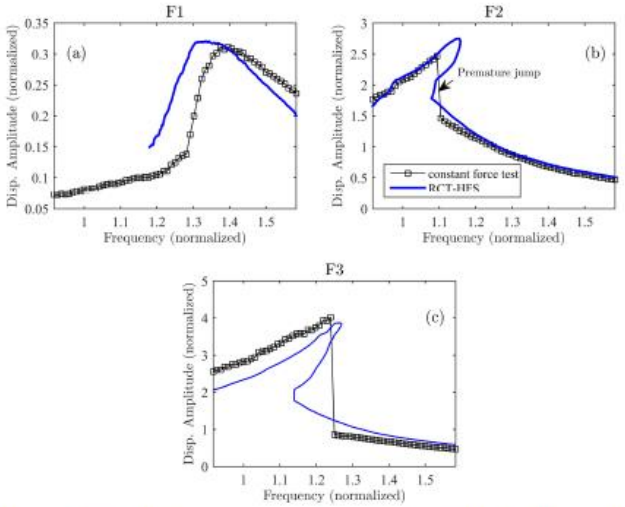

Figure 15. Comparison of the frequency response curves of the control fin actuation mechanism at the driving point, extracted from HFS with those obtained by using constant-force test results in the sweep-up direction for: (**a**) force level F1; (**b**) force level F2; (**c**) force level F3.

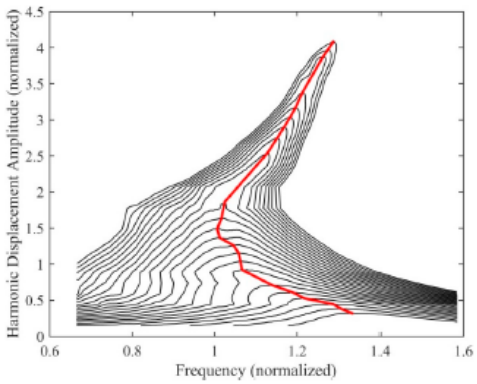

Figure 16. Constant-force frequency response curves and the backbone curve of the real control fin actuation mechanism at the driving point, obtained by cutting the HFS with various constant force planes.

5. Conclusions

Conventional constant-force sine testing is not suitable for accurately measuring turning points of frequency response curves of nonlinear structures exhibiting strong conservative nonlinearity due to the jump phenomenon. Consequently, the accuracy of backbone curves determined by constant-force testing is always questionable, which led to the development of advanced experimental continuation algorithms to extract backbone curves in the last decade. Although the current state-of-the-art provides promising control algorithms, it cannot directly make use of available modal testing equipment. This paper proposes an alternative approach that relies on standard equipment to identify backbone curves of strongly nonlinear systems directly from experimental measurements by using the Response-Controlled stepped-sine Testing (RCT) and the Harmonic Force Surface (HFS) concept recently proposed by the authors. These methods can be applied to systems where there are several nonlinearities at unknown locations. However, these techniques are not applicable to systems where internal resonances occur. So, the method is applicable to systems with strong nonlinearity in the sense that they exhibit unstable branches in the frequency response curves obtained with constant-force testing, as illustrated in the numerical and experimental case studies given in this paper, but not for nonlinearities which give rise to internal resonance.

In the proposed method, harmonic excitation force spectra measured at several different constant displacement amplitudes are collected into a smooth HFS by using linear interpolation. Next, constant-force frequency response curves with smooth turning points and unstable branches (if there is any) are extracted by cutting the HFS with constant force planes. Finally, the backbone curve is determined by connecting the resonance peaks of these frequency response curves. Points which correspond to the same resonance frequency on the backbone curves that belong to different locations build-up the NNM of the structure under test. The proposed method is numerically validated on a 5 DOF lumped system which exhibits strong conservative nonlinearity due to cubic stiffnesses. Furthermore, the method is successfully applied on a cantilever beam with a nonlinear connection and a control fin actuation mechanism of a real missile structure. The cantilever beam is supported at its free-end by two metal strips constrained at both ends to create strong stiffening nonlinearity. The control fin actuation mechanism exhibits very complex and strong nonlinearity due to backlash and friction.

Author Contributions: Conceptualization, T.K. and H.N.Ö.; methodology, T.K. and H.N.Ö.; software, T.K.; validation, T.K.; formal analysis, T.K.; investigation, T.K.; data curation, T.K.; writing—original draft preparation, T.K.; writing—review and editing, H.N.Ö.; supervision, H.N.Ö. All authors have read and agreed to the published version of the manuscript.

Funding: This research received no external funding.

Acknowledgments: The provision of TÜBİTAK-SAGE for modal testing and analysis capabilities is gratefully acknowledged.

Conflicts of Interest: The authors declare no conflict of interest.

References

1. Carney, K.; Yunis, I.; Smith, K.; Peng, C.Y. Nonlinear dynamic behavior in the Cassini spacecraft modal survey. In Proceedings of the 15th International Modal Analysis Conference (IMAC), Orlando, FL, USA, 3–6 February 1997.
2. Ahlquist, J.R.; Carreño, J.M.; Climent, H.; de Diego, R.; de Alba, J. Assessment of nonlinear structural response in A400M GVT. In Proceedings of the 28th International Modal Analysis Conference (IMAC), Jacksonville, FL, USA, 1–4 February 2010.
3. Noël, J.P.; Renson, L.; Kerschen, G. Complex dynamics of a nonlinear aerospace structure: Experimental identification and modal interactions. *J. Sound Vib.* **2014**, *333*, 2588–2607. [CrossRef]
4. Kerschen, G.; Worden, K.; Vakakis, A.F.; Golinval, J.C. Past, present and future of nonlinear system identification in structural dynamics. *Mech. Syst. Signal Process.* **2006**, *20*, 505–592. [CrossRef]
5. Noël, J.P.; Kerschen, G. Nonlinear system identification in structural dynamics: 10 more years of progress. *Mech. Syst. Signal Process.* **2017**, *83*, 2–35. [CrossRef]
6. Adams, D.E.; Allemang, R.J. Survey of nonlinear detection and identification techniques for experimental vibrations. In Proceedings of the International Conference on Noise and Vibration Engineering, Leuven, Belgium, 16–18 September 1998.
7. Setio, S.; Setio, H.D.; Jezequel, L.A. method of nonlinear modal identification from frequency response tests. *J. Sound Vib.* **1992**, *158*, 497–515. [CrossRef]
8. Gibert, C. Fitting measured frequency responses using nonlinear modes. *Mech. Syst. Signal Process.* **2003**, *17*, 211–218. [CrossRef]
9. Szemplinska-Stupnicka, W. The modified single mode method in the investigation of the resonant vibration of nonlinear systems. *J. Sound Vib.* **1979**, *63*, 475–489. [CrossRef]
10. Göge, D.; Füllekrug, U.; Sinapius, M.; Link, M.; Gaul, L. Advanced test strategy for identification and characterization of nonlinearities of aerospace structures. *AIAA J.* **2005**, *43*, 974–986. [CrossRef]
11. Platten, M.F.; Wright, J.R.; Dimitriadis, G.; Cooper, J.E. Identification of multi-degree of freedom nonlinear systems using an extended modal space model. *Mech. Syst. Signal Process.* **2009**, *23*, 8–29. [CrossRef]
12. Londono, J.M.; Neild, S.A.; Cooper, J.E. Identification of backbone curves of nonlinear systems from resonance decay responses. *J. Sound Vib.* **2015**, *348*, 224–238. [CrossRef]
13. Peeters, M.; Kerschen, G.; Golinval, J.C. Dynamic testing of nonlinear vibrating structures using nonlinear normal modes. *J. Sound Vib.* **2011**, *330*, 486–509. [CrossRef]
14. Peter, S.; Leine, R.I. Excitation power quantities in phase resonance testing of nonlinear systems with phase-locked-loop excitation. *Mech. Syst. Signal Process.* **2017**, *96*, 139–158. [CrossRef]
15. Renson, L.; Gonzalez-Buelga, A.; Barton, D.A.W.; Neild, S.A. Robust identification of backbone curves using control-based continuation. *J. Sound Vib.* **2016**, *367*, 145–158. [CrossRef]
16. Karaağaçlı, T.; Özgüven, H.N. Experimental modal analysis of nonlinear systems by using response-controlled stepped-sine testing. *Mech. Syst. Signal Process.* **2021**, *146*. [CrossRef]
17. Tanrıkulu, Ö.; Kuran, B.; Özgüven, H.N.; Imregün, M. Forced harmonic response analysis of nonlinear structures using describing functions. *AIAA J.* **1993**, *31*, 1313–1320.
18. Peter, S.; Scheel, M.; Krack, M.; Leine, R.I. Synthesis of nonlinear frequency responses with experimentally extracted nonlinear modes. *Mech. Syst. Signal Process.* **2018**, *101*, 498–515. [CrossRef]
19. Ferreira, J.V.; Ewins, D.J. Algebraic nonlinear impedance equation using multi-harmonic describing function. In Proceedings of the 15th International Modal Analysis Conference (IMAC), Orlando, FL, USA, 3–6 February 1997.

20. Arslan, Ö.; Aykan, M.; Özgüven, H.N. Parametric identification of structural nonlinearities from measured frequency response data. *Mech. Syst. Signal Process.* **2011**, *25*, 1112–1125. [CrossRef]
21. Karaağaçlı, T.; Özgüven, H.N. A frequency domain nonparametric identification method for nonlinear structures: Describing surface method. *Mech. Syst. Signal Process.* **2020**, *144*. [CrossRef]
22. Shin, W.H.; Lee, I. Nonlinear aeroelastic analysis for a control fin with actuator. *J. Aircraft* **2007**, *44*, 597–605. [CrossRef]
23. Ning, Y.; Nan, W.; Xin, Z.; Wei, L. Nonlinear flutter wind tunnel test and numerical analysis of folding fins with freeplay nonlinearities. *Chin. J. Aeronaut.* **2016**, *29*, 144–159.
24. Muller, F.; Abeloos, G.; Ferhatoglu, E.; Scheel, M.; Brake, M.R.W.; Tiso, P.; Renson, L.; Krack, M. Comparison between control-based continuation and phase-locked loop methods for the identification of backbone curves & nonlinear frequency responses. In Proceedings of the 38th International Modal Analysis Conference (IMAC), Houston, TX, USA, 10–13 February 2020.

Response-Controlled Stepped-Sine Test (RCT): A New Approach in Measuring Frequency Responses of Nonlinear Systems

Taylan Karaağaçlı[1,2], H. Nevzat Özgüven[1]

[1]Department of Mechanical Engineering, Middle East Technical University, 06800 Ankara, TURKEY

[2]The Scientific and Technological Research Council of Turkey, Defense Industries Research and Development Institute, TÜBİTAK-SAGE, P.K. 16, 06261 Mamak, Ankara, TURKEY

e-mail: taylan.karaagacli@tubitak.gov.tr, ozguven@metu.edu.tr

ABSTRACT

As a result of being widely used in linear experimental modal analysis for many years, force-controlled stepped-sine test approach is the first method that comes to mind in measuring frequency responses of nonlinear systems as well. However, in testing structures showing strong nonlinearity, force-control test strategy is not capable of capturing unstable branch of a nonlinear frequency response, which results in jump phenomenon in stepped-sine testing. On the other hand, experimental continuation methods capable of tracing unstable branches rely on sophisticated control algorithms by giving up industrial standards. Moreover, determination of nonlinear modal damping ratio is a considerable issue in these methods. This paper presents a novel approach called Response-Controlled stepped-sine Test (RCT). By combining RCT with a new concept called Harmonic Force Surface (HFS), unstable branches of frequency responses of nonlinear systems can be measured employing standard equipment, i.e. commercial hardware and software, which makes it very attractive especially for industrial applications. Furthermore, determination of nonlinear modal damping ratio in RCT is quite straightforward by making use of quasi-linearization of frequency responses of nonlinear structures. This approach has successfully been used by the authors in two recent works: In developing new methods for experimental modal analysis of nonlinear structures, and for nonparametric identification of nonlinearity. In this paper, the capability of RCT to capture unstable branches of frequency response curves in strongly nonlinear structures is demonstrated on a bench mark test setup and on a control fin actuation mechanism of a real missile.

Keywords: Response-controlled stepped-sine testing, harmonic force surface, nonlinear frequency response, unstable branch, nonlinear system identification

DIFFICULTIES IN FREQUENCY RESPONSE MEASUREMENTS OF NONLINEAR STRUCTURES

In linear experimental modal analysis, standard closed-loop stepped sine test with force control starts with a linear system identification which determines a rough initial estimate of the plant, i.e. the transfer function of the structure under test. In case of nonlinear structures, this procedure may lead to very poor estimate of the structure's actual dynamic behavior. Consequently, controller may need to make many corrective iterations to keep the force within tolerance of the reference profile, which may become very time consuming. Furthermore, in case of nonlinear structures with strong stiffening or softening character, multiple steady-state vibration responses may co-exist for the same excitation frequency, which results in an overhanging unstable branch in the frequency response. Standard force-control algorithms available in commercial softwares can only measure nonlinear frequency responses until the turning points of stable branches, at the cost of multiple runs with different sweep directions. When a turning point is reached, standard force-controller cannot avoid jumping from one stable branch to another, passing over the unstable region. Even worse, in some cases small corrective force perturbations of the controller to capture the reference signal in the vicinity of the turning points may lead to a *premature jump* before reaching the actual turning point. These drawbacks of standard techniques paved the way for the development of more sophisticated control algorithms such as control-based continuation (CBC) [1] and phase-locked-loop (PLL) [2-4] algorithms. These recently developed promising techniques are novel nonlinear extensions of the classical linear phase-resonance method, which are based on keeping the response in quadrature with excitation, i.e. in 90^{o} phase difference. Primary advantage of CBC and PLL methods over classical force-control approach is the ability of measuring backbone curves and unstable branches of nonlinear frequency responses. However, they have some drawbacks. First of all, they cannot make use of standard equipment, and therefore require design of sophisticated controllers which were not commercialized yet.

---

*T. Karaağaçlı, H.N. Özgüven, Response-Controlled Stepped-Sine Test (RCT): A New Approach in Measuring Frequency Responses of Nonlinear Systems, Extended Abstract in the 38th International Modal Analysis Conference, Houston, TX, 2020.

Furthermore, although experimental extraction of natural frequencies and deflection shapes at resonance is straightforward in these methods, measuring nonlinear modal damping requires considerable effort even in simple benchmark structures, as presented in a recent study [5].

This paper presents a novel approach with which unstable branches of nonlinear frequency responses can be measured by using standard controllers and combining this technique with a new concept called Harmonic Force Surface (HFS). The primary advantage of this method over state-of-the art experimental continuation techniques is that it relies on standard controllers available in commercial modal testing hardware and software rather than on sophisticated experimental continuation algorithms, which makes it very attractive especially for industrial applications. Moreover, the method does not require any expertise on nonlinear system identification; consequently, it can easily be applied by practicing engineers. Another important contribution is that measuring nonlinear modal damping ratio is straightforward by applying linear analysis tools to quasi-linearized frequency responses of nonlinear structures [6].

RESPONSE-CONTROLLED STEPPED-SINE TESTING AND HARMONIC FORCE SURFACE CONCEPT

In case of strong stiffness nonlinearity where multiple steady-state vibration responses co-exist for the same excitation frequency, response level of the structure highly depends on initial conditions. In case of force-control test strategy, there is no control over vibration response which may exhibit drastic changes around resonance even if very small frequency steps are used. Since gradual change in vibration response and eventually in initial conditions is not guaranteed, experimental continuation of the unstable branch cannot be achieved. In RCT, this problem is solved by keeping the displacement amplitude constant, which results in smooth response spectrum incorporating points on the unstable branch as well. This is somewhat different from experimental continuation algorithms which aim tracing points on the unstable branch consecutively. In RCT, points on the unstable branch are visited at different times during stepped-sine tests carried out at different vibration amplitude levels. Then they are collected together on the HFS. Determination of the nonlinear frequency response with unstable branch by using RCT and HFS consists of the following steps:

1. A response-controlled stepped-sine test is carried out by keeping the displacement amplitude of the driving point constant. The test is repeated at several different displacement amplitude levels (in general, repeating the test at 10-15 different levels is sufficient to obtain satisfactory results) and the corresponding harmonic force spectra of the driving point are measured as illustrated in Fig. 1(a).
2. Harmonic Force Surface, HFS, is constructed by collecting measured harmonic force spectra and using linear interpolation as shown in Fig. 1(b).
3. The contour plot obtained by cutting the HFS with a constant force plane gives the harmonic response spectrum corresponding to that force level, including any unstable branch if there is any, as shown in Fig. 2.

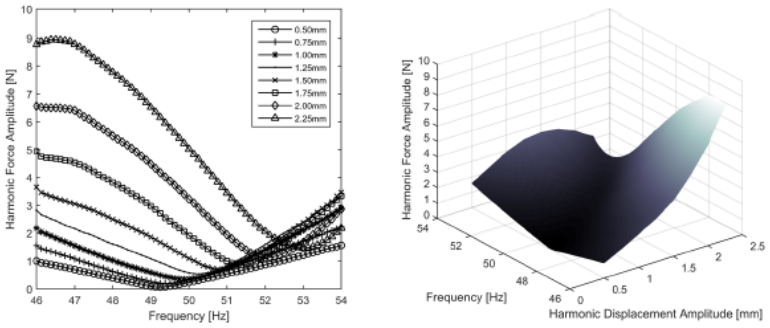

(a) (b)

Fig. 1. (a) Harmonic force spectra measured during RCT (b) HFS constructed by collecting harmonic force spectra by using linear interpolation

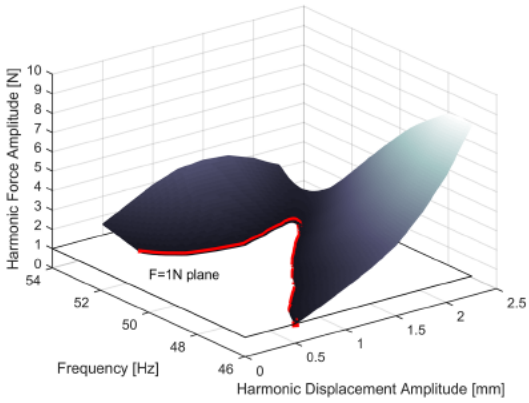

Fig. 2. Determination of the harmonic response spectrum with any existing unstable branch by cutting HFS with a constant force plane

Since accelerometer is the most widely used sensor in experimental modal analysis, it is important to note that RCT method is capable of keeping displacement amplitude of the driving point constant in an indirect way by using accelerometer as the control sensor. Acceleration profile corresponding to a constant displacement amplitude over the frequency range of interest is calculated and input to the controller as a reference profile, which is an available option in standard modal analysis softwares such as in LMS Test Lab©.

EXPERIMENTAL CASE STUDIES

RCT method with HFS concept was applied to two experimental case studies in a recent work [7]. The first case study consists of a cantilever beam whose free end is held between two metal strips which create hardening cubic stiffness effect. The test rig was excited with B&K shaker attached to its T-junction via a push-rod with a Dytran 1022V force transducer. The vibration response was measured by using a Dytran 3225M23 miniature accelerometer attached to the top of the T-junction. All measurements and closed loop controls were accomplished by LMS SCADAS Mobile data acquisition system and LMS Test Lab. software package. A series of response-controlled stepped sine tests was conducted at frequencies around the first elastic mode of the T-beam. The frequency resolution was taken to be 0.125 Hz. During each response-controlled test, the displacement amplitude of the driving point was kept constant in an indirect way by imposing an appropriate acceleration profile to the controller. Harmonic force spectra were measured at 8 different constant displacement amplitude levels ranging from 0.50 mm to 2.25 mm as shown in Fig. 1(a). HFS was obtained by collecting measured harmonic force spectra by using linear interpolation as shown in Fig. 1(b). Finally, driving point frequency response of the test rig at F = 1 N level is obtained by cutting HFS with constant force plane as shown in Fig. 2. Comparison of the nonlinear frequency response curve obtained by HFS with the one measured by force-controlled stepped-sine test is shown in Fig. 3(a). Obviously, although the frequency response measured by force control exhibits jumps during sweep up and sweep down directions, the frequency response obtained by HFS satisfactorily captures the unstable branch.

The second case study is the control fin of a real missile together with its actuation mechanism which includes strong stiffness and damping nonlinearities due to backlash and friction. The casing of the mechanism is rigidly fixed to the ground. In total, 10 Dytran 3225M23 miniature accelerometers were attached on the surface of the control fin. The system was excited in normal direction to the mid-plane of the control fin with a B&K shaker attached to its leading edge corner on the root chord via a push-rod with a Dytran 1022V force transducer. A series of response-controlled stepped sine tests was conducted at frequencies around the first elastic mode of the control fin and its actuation mechanism, which is the pitch mode (first torsional mode). Harmonic force spectra were measured at 15 different constant displacement amplitude levels of the driving point. Driving point frequency response of the control fin actuation mechanism obtained by HFS is compared with the frequency response measured by force-controlled stepped-sine test in Fig. 3(b). Once again it is observed that RCT successfully captures the unstable branch of the nonlinear frequency response.

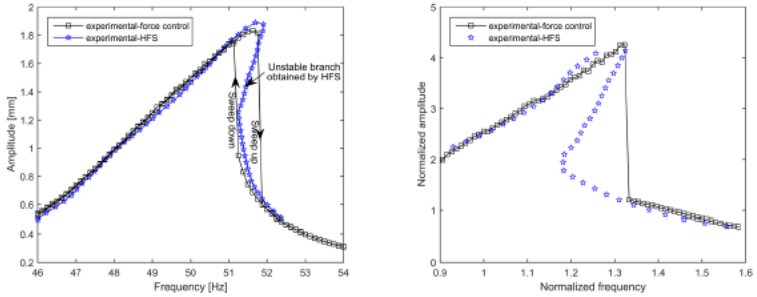

(a) (b)

Fig. 3. Comparison of nonlinear frequency responses obtained by RCT with the ones measured by classical force-control test: (a) Bench mark test structure with cubic stiffness (b) Control fin actuation mechanism of a real missile

DICUSSIONS AND CONCLUSIONS

Frequency responses provide very useful information not only for linear structures, but also for nonlinear structures. Many of the nonlinear system identification techniques rely on measuring frequency responses of nonlinear structures. In case of strong nonlinearity, measuring nonlinear frequency responses becomes a difficult task especially when there is an unstable branch. Unfortunately, classical force-control test strategy applied with standard controllers is not capable of capturing unstable branches. Consequently, more robust control algorithms capable of tracing unstable branches were developed at the cost of sophistication. Although some very recently developed controllers such as PLL gave promising results on several benchmark structures, it was reported that they require further verification on real engineering structures especially with pronounced damping nonlinearity. Sophistication of the controller is also an important issue which increases experimental effort and requires expertise. An important merit of the RCT proposed in this paper, as an experimental method, is its simplicity. The method redefines the role of standard controllers in nonlinear system identification by combining response-control test strategy together with an innovative concept called HFS to determine unstable branches. The method is validated on a benchmark test structure with cubic stiffness and on a control fin actuation mechanism of a real missile with strong stiffness and damping nonlinearities.

ACKNOWLEDGEMENTS

The provision of TÜBİTAK-SAGE for modal testing and analysis capabilities is gratefully acknowledged.

REFERENCES

[1] Renson, L., Gonzalez-Buelga, A., Barton, D.A.W., Neild, S., Robust identification of backbone curves using control based continuation, J. Sound Vib., 367, pp.145–158, 2016.

[2] Peter, S., Leine, R.I., Excitation power quantities in phase resonance testing of nonlinear systems with phase locked-loop excitation, Mech. Syst. Signal Process., 96, pp.139–158, 2017.

[3] Peter, S., Scheel, M., Krack, M., Leine, R.I., Synthesis of nonlinear frequency responses with experimentally extracted nonlinear modes, Mech. Syst. Signal Process., 101, pp. 498-515, 2018.

[4] Denis, V., Jossic, M., Giraud-Audine, C., Chomette, B., Renault, A., Thomas, O., Identification of nonlinear modes using phase-locked-loop experimental continuation and normal form, Mech. Syst. Signal Process., 106, pp. 430-452, 2018.

[5] Scheel, M., Peter, S., Leine, R.I., Krack, M., A phase resonance approach for modal testing of structures with nonlinear dissipation, Mech. Syst. Signal Process., 435, pp. 56-73, 2018.

[6] Karaağaçlı, T., Özgüven, H.N., Experimental modal analysis of nonlinear structures by using response-controlled stepped-sine testing (*in preparation*).

[7] Karaağaçlı, T., Özgüven, H.N., A frequency domain nonparametric identification method for nonlinear structures: Describing Surface Method, Mech. Syst. Signal Process. (*submitted*).

CURRICULUM VITAE

PERSONAL INFORMATION

Surname, Name: Karaağaçlı, Taylan
Nationality: Turkish (TC)
Date and Place of Birth: 17 March 1984, İstanbul
Marital Status: Married
Phone: +90 312 590 93 40
Fax: +90 312 590 91 48-49
email: taylan.karaagacli@tubitak.gov.tr

EDUCATION

Degree	Institution	Year of Graduation
MS	METU Mechanical Engineering	2010
BS	METU Mechanical Engineering	2007
High School	Saint Michel High School, İstanbul	2002

WORK EXPERIENCE

Year	Place	Enrollment
2015-Present	TÜBİTAK-SAGE	Chief Research Engineer
2010-2015	TÜBİTAK-SAGE	Senior Research Engineer
2007-2010	TÜBİTAK-SAGE	Research Engineer
2006	Roketsan	Intern Eng. Student
2005	Türk Traktör	Intern Eng. Student

FOREIGN LANGUAGES

Advanced English, Advanced French

PUBLICATIONS

1. Karaağaçlı T., Özgüven H.N. "Experimental modal analysis of nonlinear systems by using response controlled stepped sine testing", Mech. Sys. Signal Process, 146, (2021)

2. Karaağaçlı T., Özgüven H.N. "Experimental identification of backbone curves of strongly nonlinear systems by using response controlled stepped sine testing (RCT)", Vibration, 3(2), 266-280 (2020)

3. Karaağaçlı T., Özgüven H.N. "A frequency domain nonparametric identification method for nonlinear structures: Describing surface method", Mech. Sys. Signal Process, 144, (2020)

4. Karaağaçlı T., Özgüven H.N. "Response controlled stepped sine test (RCT): A new approach in measuring frequency responses of nonlinear systems", Extended Abstract in: 38th International Modal Analysis Conference (IMAC), Houston, TX, USA (2020)

5. Karaağaçlı T., Cigeroglu, E., Özgüven H.N. "Numerical computation of nonlinear normal modes (NNMs) by using response dependent nonlinear mode (RDNM) concept", Extended Abstract in: 38th International Modal Analysis Conference (IMAC), Houston, TX, USA (2020)

6. Orlando S., Brughmas M., Karaağaçlı T., Ceyhan Ü., Sümer Ö., Cerit M.E., Durak B. "A correlation study of modal parameters between flutter testing and CFD simulation", 15th International Forum on Aeroelasticity and Structural Dynamics (IFASD), St. Petersburg, Russia (2015)

7. Karaağaçlı T., Yıldız E.N., Özgüven H.N. "A new method to determine dynamically equivalent finite element models of aircraft structures from modal test data", Mech. Sys. Signal Process, 31, (2012)

8. Karaağaçlı T., Yıldız E.N., Özgüven H.N. "Determination of dynamically equivalent FE models of structures from experimental data", 28th International Modal Analysis Conference (IMAC), Jacksonville, FL, USA (2010)